

JCEEA

---

Czasopismo  
Inżynierii Lądowej,  
Środowiska  
i Architektury

---

Journal of Civil  
Engineering,  
Environment  
and Architecture

---

Kwartalnik  
tom XXXV  
zeszyt 65 (nr 2/2018)  
kwiecień-czerwiec

(e-ISSN 2300-8903)

Czasopismo Inżynierii Lądowej, Środowiska i Architektury jest kontynuacją  
Zeszytów Naukowych Politechniki Rzeszowskiej - Budownictwo i Inżynieria Środowiska.

Issued with the consent of the Rector

Editor in Chief Publishing House of Rzeszow University of Technology  
Professor Grzegorz OSTASZ, DSc, PhD

**Scientific Council**

prof. Hasan Arman (United Arab Emirates), prof. Zinoviy Blikharskyy (Ukraine)  
prof. Antonio João Carvalho de Albuquerque (Portugal), prof. Marina Ciuna (Italy)  
prof. Volodymyr V. Cherniuk (Ukraine), prof. Maurizio d'Amato (Italy)  
prof. Endre Domokos (Węgry), prof. Mohamed Eid (Francja), prof. Maria Elektorowicz (Canada),  
prof. Haritha Malladi (USA), prof. Samuel Hudson (USA), prof. Dušan Katunsky (Slovakia)  
prof. Krzysztof Knapik (Poland), prof. Ryszard L. Kowalczyk (Australia)  
prof. Jozef Kriš (Slovakia), prof. Vincent Kvočák (Slovakia), prof. Stanisław Kuś (Poland)  
prof. Mladen Radujkovic (Croatia), prof. Czesława Rosik-Dulewska (Poland)  
prof. Francesca Salvo (Italy), prof. João Antonio Saraiva Pires da Fonseca (Portugal)  
prof. Marco Simonotti (Italy), prof. Nadežda Številová (Slovakia),  
prof. Janusz A. Tomaszek (Polska), prof. David Valis (Czech Republic)  
prof. António Avelino Batista Vieira (Portugal), prof. Oksana Vovk (Ukraine)  
prof. Tomasz Winnicki (Poland), prof. Jerzy Ziółko (Poland)

*Editorial Board*

(affiliation: Poland)

*Editor-in-Chief*

Piotr KOSZELNIK, DSc, PhD, Eng., Professor

*Editorial Committee (Thematic editors)*

Bartosz MILLER, DSc, PhD, Eng., Professor

Professor Janusz RAK, DSc, PhD, Eng.

*Statistical Editor*

Szczepan WOLIŃSKI, DSc, PhD, Eng., Professor

*Editorial Assistant*

Katarzyna PIETRUCHA-URBANIK, PhD, Eng.

*Members*

Renata GRUCA-ROKOSZ, DSc, PhD, Eng., Professor;

Anna SIKORA, PhD, Arch, Eng.; Michał JUREK, PhD, Arch, Eng.;

Lucjan ŚLĘCZKA, DSc, PhD, Eng., Professor; Artur SZALACHA, MSc, Eng.

*Language Editors*

Barbara OLEKSIEWICZ, Msc

James RICHARDS, PhD – native English speaker (UK)

*Volume Editor*

Artur SZALACHA, Grzegorz RYBICKI

e-ISSN 2300-8903

p-ISSN 2300-5130

The electronic version of the Journal is an original version.

Editorial Office: Rzeszow University of Technology, Faculty of Civil and Environmental Engineering  
and Architecture, St. Poznańska, 35-084 Rzeszów, Poland, [www.oficyna.prz.edu.pl/pl/zeszyty-naukowe/czasopismo-inzynierii-ladowej-s/](http://www.oficyna.prz.edu.pl/pl/zeszyty-naukowe/czasopismo-inzynierii-ladowej-s/) (e-mail: [jceea\\_bud@prz.edu.pl](mailto:jceea_bud@prz.edu.pl))

Publisher: Publishing House of Rzeszow University of Technology, 12 Powstanców Warszawy Ave.,  
35-959 Rzeszow, [www.oficyna.prz.edu.pl](http://www.oficyna.prz.edu.pl) (e-mail: [oficyna@prz.edu.pl](mailto:oficyna@prz.edu.pl))

Additional information and an imprint – p. 233

## SPIS TREŚCI

Edyta BERNATOWSKA, Lucjan ŚLĘCZKA: Stress and Strain Concentrations in Steel Angle Tension Members Connected by One Leg .....	5
Tomasz DOMAŃSKI: Resistance of Steel Fasteners Subjected to Shear at Public Arenas in Normal and Fire Temperatures – Probabilistic Approach .....	17
Mariusz MAŚLAK, Maciej SUCHODOŁA, Piotr WOŹNICZKA: Temperature Distribution in a Steel Beam-to-Column Joint when Exposed to Fire. Part 1: End-Plate Joint.....	25
Krzysztof KUCHTA, Rafał SILEZIN, Paweł ŻWIREK: Technological Aspects of Execution of Welded Joints in Hollow Sections.....	35
Marian GWÓŹDŹ, Damian KOWALSKI: Telescopic Joints in Steel Tube Towers .....	43
Grzegorz GREMZA, Jan ZAMOROWSKI: Damage Analysis of the Blade to the Rotor Hub Connection in the Wind Turbine .....	55
Krzysztof KUCHTA, Rafał SILEZIN, Paweł ŻWIREK: Execution and Inspection of Steel Hollow Sections Welded Joints.....	69
Tomasz DOMAŃSKI, Krzysztof KMIECIK: Fire Resistance of Timber Joints with Steel Fasteners .....	81
Mariusz MAŚLAK, Michał PAZDANOWSKI, Małgorzata SNELA: Critical Temperature Evaluation for a Steel Frame with Joint Stiffness Decreasing in Fire .....	91
Mariusz MAŚLAK, Maciej SUCHODOŁA, Piotr WOŹNICZKA: Temperature Distribution in a Steel Beam-to-Column Joint when Exposed to Fire. Part 2: Flange-Plates and Web-Cleats Joint.....	103
Przemysław KRYSOSIK: Design Resistance of Welded Knees in Steel Frames .....	115

Izabela TYLEK: Shaping of Architecturally Exposed Steel Structures .....	133
Mariusz MAŚLAK, Michał PAZDANOWSKI: Influence of the End-Plate Thickness on the Steel Beam-to-Column Joint Stiffness when Subject to Bending.....	145
Tomasz SIWOWSKI, Maciej KULPA: Fatigue Tests of Welded Joints in Steel Orthotropic Bridge Deck .....	157
Piotr MILEWSKI, Mirosław BRONIEWICZ: Resistance of the Welds in CHS Joints with the Rib Plates .....	167
Jerzy K. SZLENDAK, Adrian SZPYRKA: Resistance of Tension Brace in Plug & Play N Shape RHS Truss Connection.....	177
Jan ZAMOROWSKI, Grzegorz GREMZA: On the Design of a Steel End-Plate Beam-to-Column Bolted Joint According to PN-EN 1993-1-8.....	187
Zdzisław PISAREK: Approximated Method for Determining Moment Resistance and Stiffness of Bolted Beam to Column Joints Made with Angle Web and Flange Cleats .....	197
Krzysztof OSTROWSKI, Aleksander KOZŁOWSKI: Credibility of FEM Analysis in the T-Stub Modelling.....	219

Edyta BERNATOWSKA<sup>1</sup>  
Lucjan ŚLĘCZKA<sup>2</sup>

## STRESS AND STRAIN CONCENTRATIONS IN STEEL ANGLE TENSION MEMBERS CONNECTED BY ONE LEG

The paper presents the numerical simulations results of net section failure in tensioned angles. Angles are made of structural steel with nominal grade S235. Simulation takes into account ductile fracture initiation, by application of Gurson-Tvergaard-Needleman (GTN) material model. Parametrical analysis of ultimate resistance was carried out. The finite elements analyses were conducted by ABAQUS computer program. Shear lag effect in considered joint was observed, as a non uniform tensile stress distribution in angles in the vicinity of a connection. Stress concentration areas and stress concentration factors have been predicted, both in elastic and ultimate behaviour of joint. Especially change of non-uniform stress distribution in net cross-section was observed, during increase of loading, until the ultimate resistance was reached.

**Keywords:** lap bolted connections, shear lag effect, net section fracture, numerical simulations, stress and strain concentration

### 1. Introduction

Shear lag effect is a phenomenon of non-uniform stress distribution in wide flanges due to shear deformation [1]. In European code regulations it is practically equated with uneven distribution of normal stresses in wide flanges of plated structural elements in bending. The cause of the shear lag effect in such a case is the occurrence of shear deformation along the width of flanges in their mid-planes, per both sides of the web. This results in a non-linear distribution of normal stresses in the cross-section of the profiles, which is a deviation from the linear distribution, expected during bending in accordance with the Euler-

---

<sup>1</sup> Corresponding author: Edyta Bernatowska, Rzeszow University of Technology, The Faculty of Civil and Environmental Engineering and Architecture, Poznańska 2, 35-959 Rzeszów; +48178651629; e\_bernat@prz.edu.pl

<sup>2</sup> Lucjan Ślęczka, Rzeszow University of Technology, The Faculty of Civil and Environmental Engineering and Architecture, Poznańska 2, 35-959 Rzeszów; +48178651631; sleczka@prz.edu.pl

Bernoulli assumption “plane sections remain plan”. In analysis and limit states assessments it is taken into account by using a reduced “effective” flange width.

The second source of shear lag effect in steel structures, much more common than existing in plated structural elements in bending, are connections. In this case shear lag effect is defined as non uniform tensile stress distribution in a member or connecting element in the vicinity of a connection [2]. Such non uniform stress distribution is generally produced by applying force on the joint in local manner, when tension load is transmitted to some, but not all of the cross-sectional elements (where not all parts forming section are continuous in the joint).

Such way of constructing joints is very popular for practical reasons, eg. connecting I-shape only by web (by flanges), or connecting angle by only one leg is much more easier and cheaper compared to joints in which continuity of every part of element is provided (Fig. 1).

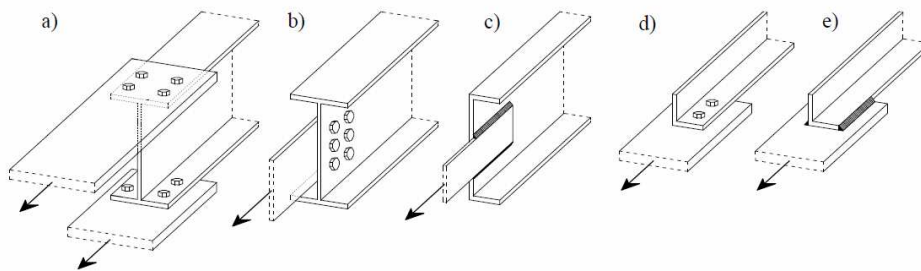


Fig. 1. Examples of joints in which shear lag effect occurs: a) I-section connected by flanges, b) I-section connected by web, c) C-section connected by web; d, e) angle connected by one leg using bolts or welds

In general case of connections, shear deformations are caused by introducing loads into a single part of cross section. In bolted shear connections stress distribution is also affected by existence of bolt holes, eccentricities and distributed pressure load in the bolt hole, close to net cross section, coming from bolt bear.

The shear lag effect in connections is known [3], [4] and included in design procedures [5], but there is a lack of detailed quantitative assessments of stress and strain concentrations which appear during gradual increase of loading. Areas of stress and strain concentration can influence the resistance of joint, where fracture of weakened cross section usually determines joint capacity. Especially value of stress concentrations factor in net cross-section can have an influence on ability of a material to deform plastically without losing its strength. The value of stress concentration can also influence initiation of fatigue crack in case of variable actions.

The paper presents a numerical simulation of net section failure of tensioned angles made of structural steel grade S235, connected by one bolt, with application of material model, taking into account ductile fracture initiation. Stress and strain concentrations areas both in elastic and ultimate behaviour of joint have been predicted as well as the stress concentration factors in elastic range. Also change of non-uniform stress distribution in net cross-section was observed, during increase of loading, until the ultimate resistance was reached.

## 2. Numerical simulations and comparison with test results

### 2.1. Range of analysis

The range of analysis covers ten equal leg angles connected by one bolt to the gusset plates, as is shown in Figure 2. The joints are made of two different sizes of angles, in each of them steel with nominal grade S235 was applied, where experimentally confirmed yield strength is equal to  $f_y=310$  MPa, and ultimate strength  $f_u=445$  MPa (using engineering stress measures). Bolts with diameters within the range from M18 to M22 were placed with different distance  $e_2$  from the edge. Bolts were fully threaded class 8.8. In the vicinity of the connection where the angle was supposed to rupture bolt hole was 2 mm larger than its diameter. Full description of analysed joints is given in Table 1.

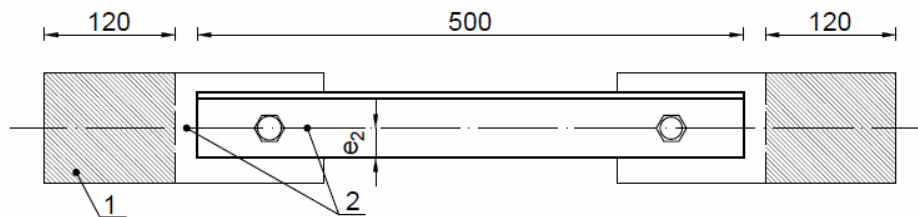


Fig. 2. Geometry of considered joints; 1) clamping area; 2) reference points to measure displacements

Table 1. Description of numerical models

Specimen	Cross-section	Bolt	Edge distance $e_2$ [mm]	Edge distance $e_1$ [mm]	$N_{FEA}$ [kN]	$N_{EXP}$ [kN]
J60/18/24	L60x6	M18	23.5	60.3	86.4	93.0
J60/20/27	L60x6	M20	25.6	65.1	87.8	83.8
J60/20/31	L60x6	M20	30.3	64.9	116.4	130.9
J60/22/27	L60x6	M22	25.5	74.0	93.4	105.6
J80/22/29	L80x6	M22	28.4	74.5	113.2	133.6
J80/22/32	L80x6	M22	30.7	74.3	122.4	132.1
J80/22/33*	L80x6	M22	33.0	74.3	131.0	-
J80/22/36	L80x6	M22	34.6	74.4	139.6	149.3
J80/22/37*	L80x6	M22	37.0	74.3	148.4	-
J80/22/39	L80x6	M22	38.9	74.3	157.5	177.6

## 2.2. Description of FE models

Finite elements models consisted of four element groups: angle, gusset plate, bolt with nut (modelled as a whole) and washers. The basis for the models were experimental tests, which are described in [6]. Generally ten specimens were analysed. Eight of them had exactly the same dimension as real specimens, two marked with asterisk (“\*”) were created for the needs of numerical investigation (see Table 1). Only half of the whole specimen was modelled, (Fig. 3).

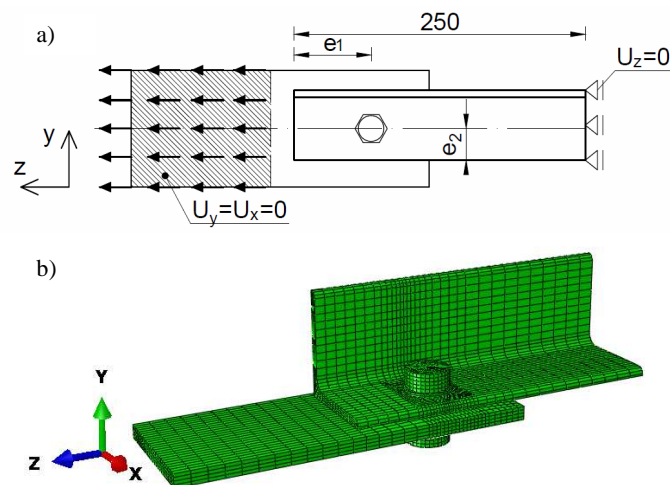


Fig. 3. Numerical models; a) schematic diagram; b) model made of finite elements

The load in  $z$ -direction has form of velocity, applied to the gusset plate. The hatched area (Fig. 3a) could not move in the direction of the  $x$  and  $y$  axes. The end of angle was blocked in  $z$ -direction. The bolt diameter was equal to the nominal value. Both washers and bolt were located concentrically with holes in angle and gusset plate.

The finite element mesh was adequately dense in the vicinity of the bolt hole in angle and gusset plate. The sides of cubic elements had similar length. Near the openings they were equal to 25% of angle thickness.

Elements of hierarchical validation were used during finite element modelling. At the beginning, choice of appropriate material model was made to simulate failure process of elements. Model's predictive capability was assessed by comparing calculations with experiments, what was described in publication [7].

Generally two types of material were implemented in models. For gusset plate, washers and bolt elastic-plastic material were used. Its behaviour was represented by a multi-linear stress-strain curve in terms of true stress and true plastic strain. They were evaluated from the standard tensile tests. The elastic behaviour was defined by Young's modulus and Poisson's ratio, equalling  $E = 210\,000\text{ MPa}$  and  $\nu = 0.3$ .

For angles porous metal plasticity characteristics were introduced. This corresponds to the description of Gurson-Tvergaard-Needleman (GTN) material, which more properly controls the fracture process. Exact description of this material model can be found in [8]. Table 2 gives values of material parameters introduced to EF analysis.

Table 2. GTN material model parameter introduced to numerical simulation

$f_0$	Tvergaard parameters $q_i$	$f_N$	$\varepsilon_N$	$s_N$	$f_c$	$f_F$
0.001	$q_1=1.5; q_2=1.0; q_3=2.25$	0.02	0.3	0.1	0.06	0.2

For angles, gusset plates and washers C3D8R type of elements were employed. To apply a porous material in computer program, dynamic explicit analysis was chosen. Because of bolt pretensioning, which was modelled by means of temperature change in bolt shank, C3D8T and C3D6T elements were used. Relatively small clamping force was applied due to A category of joints according to EN 1993-1-8 [5].

Contact between components was defined using general contact option. The frictional effects between surfaces were included by incorporating the classical isotropic Coulomb friction model in the contact definition, with a friction coefficient  $\mu$  equal to 0.2.

### 2.3. Global results and observations

Global behaviour of joints, described by force-displacements curves, is shown in Figure 4. They are divided into two groups depending on angle size. Maximum values of resistance ultimate capacity obtained from FE modelling –  $N_{FEA}$  are slightly lower in most cases in comparison to those from test results –  $N_{EXP}$  (from 2% to 18%). Only in one specimen resistance obtained from FE modelling is 5% higher in comparison to the test (Table 1). Deformation capacity of joints, measured at two reference points (see Fig. 2), obtained from FE models is noticeably shorter when compared to real joints. But qualitative comparison of behaviour obtained from FE modelling to the one measured during the tests shows high degree of accuracy, especially in terms of deformations and fracture character, (Fig. 5). Detailed comparison FE results with tests is given in [7].

The edge distance  $e_2$  has the greatest impact on behaviour of modelled joints. The greater edge distance is, the greater resistance of specimens is observed. Looking at Table 1 and Figure 4, it can be seen that specimens J80/22/32 and J60/20/31 have almost the same edge distance  $e_2$ . Although they vary in angle and bolt size, they reached very similar tensile capacity and elongation.

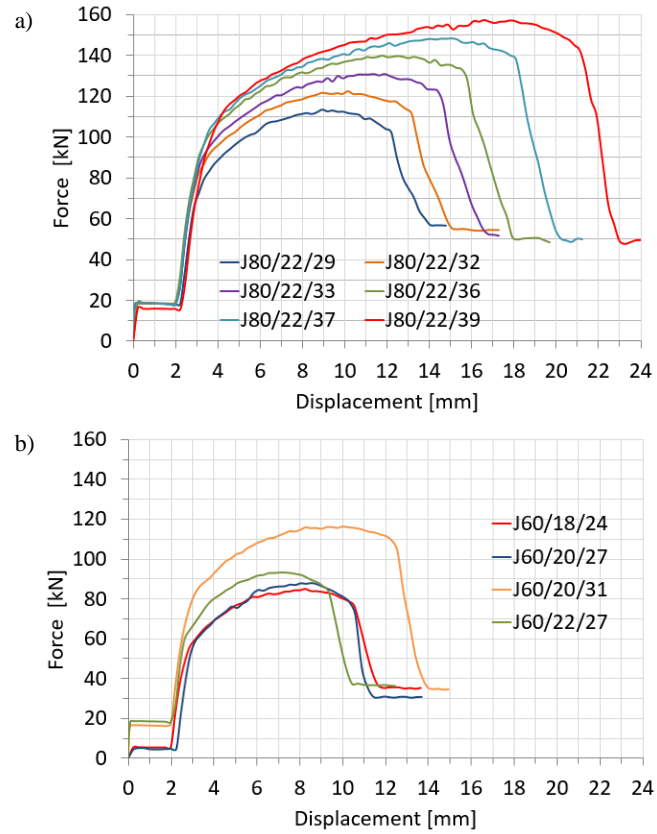


Fig. 4. Force - displacement curves from FE simulations; a) group made of L80x6, b) made of L60x6

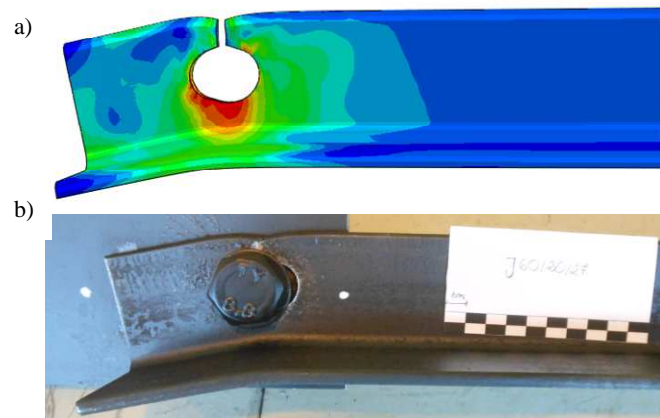


Fig. 5. Specimen J60/20/27; a) deformation and fracture mode obtained in FEA; b) obtained from test

It can be also observed that bolt diameter influences elongation of joints in a small extent. Specimens J60/20/27 and J60/22/27 (Fig. 4b) have the same edge distance  $e_2$  and they differ in bolt diameter. Ultimate resistance is slightly higher and elongation is smaller for specimen with larger bolts diameter despite the fact that net cross-section in this specimen is smaller.

### 3. Stress concentration factors in joints

One of the aims of this paper is to describe non-uniform stress distribution in net cross-section. Such description is possible so far only for welded angles and tees [9].

In elastic range the most convenient parameter which shows the stresses uniformity across considered element is the stress concentration factor  $k_t$ . Such factor is a ratio of maximum stress value to nominal ones. Within this work longitudinal stresses  $\sigma_{zz}$  were considered and nominal value of stress was calculated using tension force loading on angle and its net cross-section.

For all considered specimens stress concentration factors were calculated from equations (1) and (2).

$$k_t = \frac{\sigma_{max}}{\sigma_{nom}} \quad (1)$$

$$\sigma_{nom} = \frac{N}{A_{net}} \quad (2)$$

where:  $\sigma_{max}$  – maximum value of longitudinal stress ( $\sigma_{max} = \sigma_{zz}$ ) in steel angle,  
 $N$  – global force acting on joint equal to  $0.3N_{FEA}$ ,  
 $A_{net}$  – net cross-section.

The maximum values of longitudinal stresses were obtained from FE models for relatively small level of load (about 30% of  $N_{FEA}$ ), which on the one hand is greater from numerical slip resistance (Fig. 4), and on the other hand is enough small to longitudinal stress would be in elastic range of material characteristics.

For all specimens maximum values of  $\sigma_{zz}$  in elastic range appear in the vicinity of bolt hole (Fig. 6), not in net cross-section. So, two types of stress concentration factors were predicted. First one  $k_{t1}$  describes the largest value of concentration factor observed in specimen at all. Second one,  $k_{t2}$  describes stress concentration in net cross-section only, taking into account maximum stress in net cross-section.

Obtained values of  $k_{t1}$  and  $k_{t2}$  are given in the Table 3. It can be seen that difference between  $k_{t1}$  and  $k_{t2}$  changes in small extent (from 18 to 26%). Computed results of stress concentration factors are significantly larger compared with results for infinitive sheet in tension with circular hole, where  $k_t=3.0$  [10]. Obtained values are the results of additional bending caused by eccentricities and bearing stress created in the angle by the bolt.

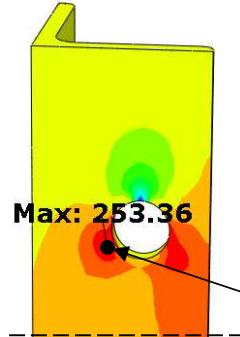


Fig. 6. Location of maximum value of  $\sigma_{zz}$  for J60/18/24 specimen

Table 3. Stress concentration factors

Specimen	$k_{t1}$	$k_{t2}$	$k_{t1}/k_{t2}$	$E_{FEA}$
J60/18/24	6.64	5.50	1.21	0.32
J60/20/27	5.86	4.74	1.24	0.35
J60/20/31	5.83	4.74	1.23	0.46
J60/22/27	5.08	4.03	1.26	0.37
J80/22/29	8.33	7.03	1.18	0.30
J80/22/32	6.86	5.78	1.19	0.33
J80/22/33	6.69	5.65	1.18	0.35
J80/22/36	6.33	5.33	1.19	0.37
J80/22/37	5.16	4.35	1.19	0.40
J80/22/39	5.16	4.35	1.19	0.42

To check correlation between predicted stress concentrations factors and ultimate resistance of joints additional parameter has been introduced. It is joint efficiency parameter  $E_{FEA}$ , which is defined as the ratio of finite element capacity (ultimate loading  $N_{FEA}$ ) over calculated nominal capacity of the net cross-section  $A_{net}$ :

$$E_{FEA} = \frac{N_{FEA}}{f_u A_{net}} \quad (3)$$

where:  $f_u$  – is ultimate strength of the steel.

Such joint efficiency parameter indicates cross-section utilization in tension members [9]. It can be observed that stress concentration factors  $k_{t1}$  and  $k_{t2}$  are inversely proportional to efficiency parameter  $E_{FEA}$ , especially in J80 group, in which edge distance  $e_1$  was constant. For this group also proportion  $k_{t1}/k_{t2}$  is nearly constant (1.18÷1.19).

#### 4. Process of stress redistribution under increasing load

Distribution of normal stress across the net cross-section in elastic range (Fig. 7) shows only area where yielding will start.

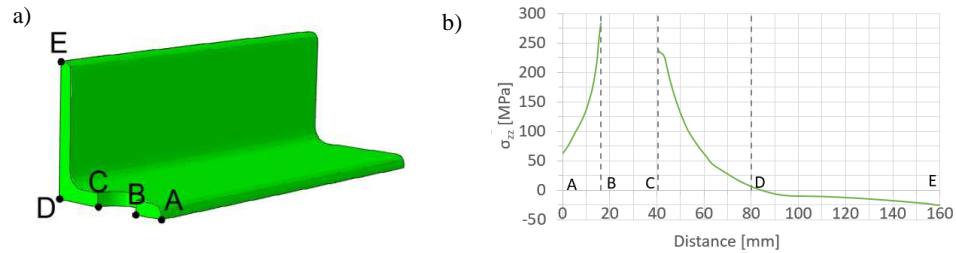


Fig. 7. Net cross-section; a) characteristic points, b) distribution of  $\sigma_{zz}$  in elastic range across net cross-section for specimen J80/22/29 for  $N=0.3N_{FEA}$

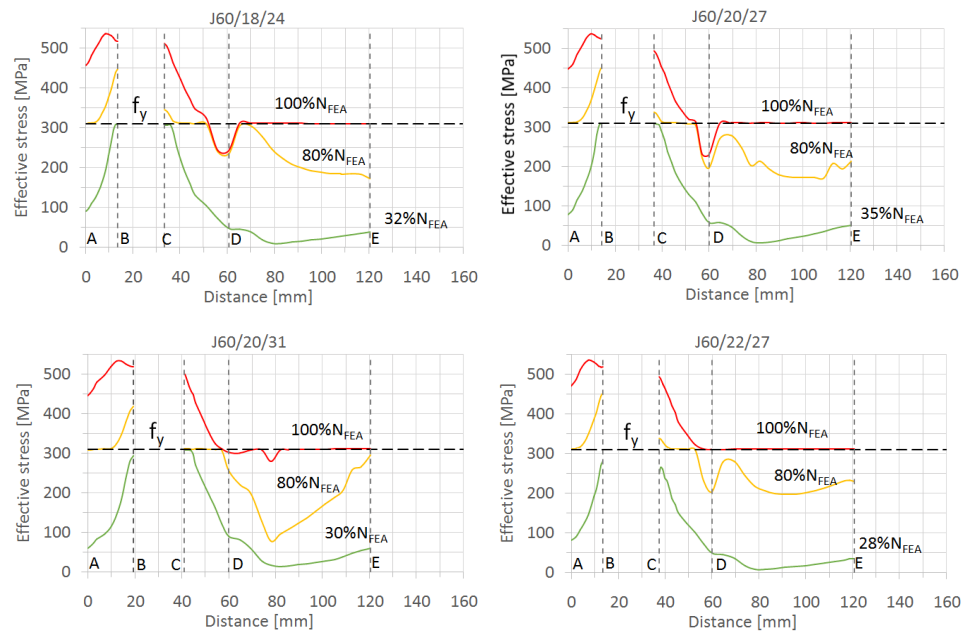


Fig. 8. Effective stress distribution in net cross-section (path A-E according to Fig. 7a) in three load levels, L60x6 angles

The change of stress distribution according to increasing level of loading is shown in Figure 8 and 9. Figures show distribution of effective stress along net cross-section (path which is defined in Fig. 7a) in three different load levels:

- $N=(0.28-0.35) N_{FEA}$ ,

- $N=0.80 N_{FEA}$ ,
- $N=N_{FEA}$ ,

where  $N_{FEA}$  is ultimate loading obtained in FE analysis.

Distance A-D refers to the width of connected leg, D-E to unconnected leg and B-C to the bolt hole.

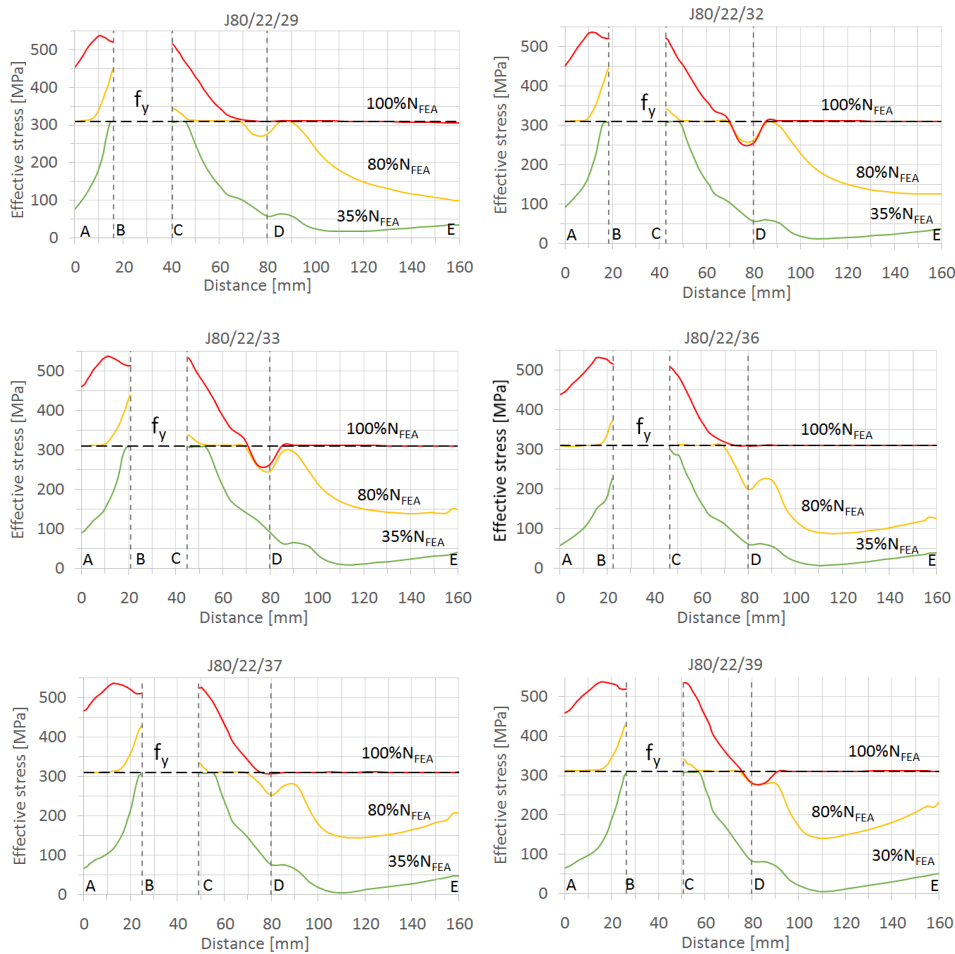


Fig. 9. Effective stress distribution in net cross-section (path A-E according to Fig. 7a) in three load levels, L80x6 angles

Presented diagrams were grouped according to the size of angles. They differ from each other in distance  $e_2$ . Dashed lines shows yield stress. To estimate effective stress, true stresses were used as a stress measures according to FE analysis type.

In all specimens it was observed that first material yielding started from area near the bolt hole in connected leg, and then spread over cross section. Stress in connected leg, in ultimate limit state, reached ultimate strength of steel, especially in section A-B in the vicinity of the bolt hole. Due to steel ductility, stress redistribution was observed before a final fracture, allowing yielding of unconnected leg D-E. However effective stress value across unconnected leg of angle does not exceed yield strength of the steel.

The sequence of initiation and propagation of fracture obtained during FE analyses was the same as during the test. Fracture initiation occurs with significant plastic deformation of the connected leg fragment, between bolt hole and adjacent edge. Concentration of longitudinal true strain  $\epsilon_{zz}$  is observed on the bolt hole edge (Fig. 10).

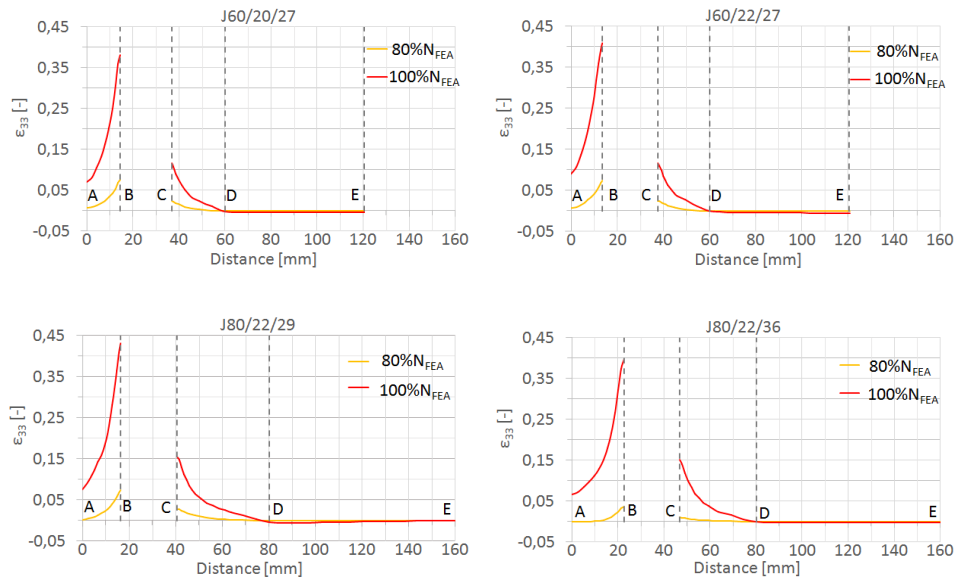


Fig. 10. True strain  $\epsilon_{zz}$  distribution in net cross-section (path A-E according to Fig. 7a) in two loading levels in selected specimens

## 5. Summary and conclusion

Results of numerical investigation on the shear lag effect of steel tension angles, connected by one bolt, are reported in this paper.

Conducted analyses show non uniform tensile stress distribution in angles, in the vicinity of a connection, both in elastic range and at the stage of reaching the ultimate load capacity. In elastic range stress concentration factors predicted for analyzed joints have clearly larger values than in other bolted lap connections.

Ductile nature of structural steel can lead to total yielding of net cross-section, but in order to obtain ultimate resistance of net cross-section, only part of connected leg area is utilized.

Analyses gave better insight into process of redistribution of stress along net cross section during increasing loading, which can be use in further work.

## References

- [1] EN 1993-1-1 Eurocode 3: Design of steel structures – Part 1-1: General rules and rules for buildings. European Committee for Standardization, Brussels, 2005.
- [2] ANSI/AISC 360-10 An American National Standard. Specification for Structural Steel Buildings. American Institute of Steel Construction, 2010.
- [3] Kulak G.L., Wu Y.: Shear lag in bolted angle tension members, *Journal of Structural Engineering*, vol. 123(9), 1997, pp. 1144–1152.
- [4] Može P.: Angles connected by one leg in tension, Eurosteel 2017, September 13-15, 2017, Copenhagen, Denmark, [onlinelibrary.wiley.com/doi/10.1002/cepa.433](https://onlinelibrary.wiley.com/doi/10.1002/cepa.433).
- [5] EN 1993-1-8 Eurocode 3: Design of steel structures – Part 1-8: Design of joints, European Committee for Standardization, Brussels, 2005.
- [6] Błyskal E., Ślęczka L.: Experimental tests of angle tension members connected by one bolt (in Polish), *Czasopismo Inżynierii Lądowej, Środowiska i Architektury – Journal of Civil Engineering, Environment and Architecture, JCEEA*; t. XXXIII, z. 63 (1/I/16), 2016, pp. 323–330, DOI:10.7862/rb.2016.38.
- [7] Bernatowska E., Ślęczka L.: Net section fracture assessment of steel bolted joints with shear lag effect. 64 Konferencja Naukowa KILiW PAN oraz KN PZITB, Krynica 2018 (paper accepted for publication).
- [8] Kossakowski P.: Application of damage mechanics in the analysis of pre-failure states of metal structures (in Polish), *Zeszyty Naukowe Politechniki Rzeszowskiej Budownictwo i Inżynieria Środowiska*, no. 59 (3/12/II), 2012, pp. 177–184.
- [9] Fang Ch., Lam A.C.C., Yam M.C.H.: Influence of shear lag on ultimate tensile capacity of angles and tees. *Journal of Constructional Steel Research* 84 (2013) pp. 49–61.
- [10] Schijve J.: *Fatigue of structures and materials*. Springer 2009.

*Przesłano do redakcji: 01.05.2018 r.*

*Przyjęto do druku: 15.06.2018 r.*

Tomasz DOMAŃSKI<sup>1</sup>

## RESISTANCE OF STEEL FASTENERS SUBJECTED TO SHEAR AT PUBLIC ARENAS IN NORMAL AND FIRE TEMPERATURES – PROBABILISTIC APPROACH

The buildings with great grandstands are the public places where consequences of failure are very high. For this reason, according to EN 1990 they belong to CC3 class consequence of failure. The reliability class RC3 is associated with the consequences class CC3 [7, 8] and is defined by the  $\beta = 4.3$  reliability index with probability of failure  $p_f \approx 8.54 \cdot 10^{-6}$ . Shear connections have to transfer forces between structural members – steel body and bolts with adequate degree of safety. The load-carrying mechanism of bolted shear connections is complex and analytical methods for predicting the shear resistance are not applicable. Instead the resistance of the connections may be determined using empirical formulas. The distributions of horizontal and shear resistance within steel body – bolts will be described depending on material characteristics of steel body and bolts components. The characteristic resistance of steel shear connection is obtained as minimum of two variables: bolts resistance and steel body resistance. Probability function of this minima will be defined and described in this paper. Laboratory tests provide the only practicable basis for specifying safety margins for ultimate strength connections. The determination of partial safety factors within shear connections will be presented according to EN1990. Design value of such resistance is specified as suitable fractile of log- normal probability distribution, calculated with the assumption that the acceptable probability of down-crossing is not greater than  $p_{f,ult} \approx 2.91 \cdot 10^{-4}$ . It means that the target reliability index, defined for the resistance, is taken as  $\beta_{R,req} = 3.44$ , in accordance with the European recommendations (EN 1990).

**Keywords:** steel structures, structural safety, steel bolt connections, fire safety

### 1. Introduction

The empirical formulas related to bolted steel connection resistance are presented in EN1993-1-8 [2], [5]. The design shear resistance bearing type A;  $F_{Rd}$  per bolt should be determined as minimum of:

---

<sup>1</sup> Corresponding author: Tomasz Domański, Cracow University of Technology, Chair of Metal Structures, ul. Warszawska 24, 31-155 Kraków; doman@pk.edu.pl

$$F_{Rd} = \min(F_{v,Rd}, F_{b,Rd}) \quad (1)$$

Where  $F_{v,Rd}$  is the design steel bolt resistance per shear plane and  $F_{b,Rd}$  is the design bearing resistance of the steel body defined for reliability class RC3, as follows [9]:

$$F_{v,Rd} = \frac{\alpha_v f_{ub} A}{\gamma_{M2} K_{FI}} \quad F_{b,Rd} = \frac{k_1 a_b f_u d t}{\gamma_{M2} K_{FI}} \quad (2)$$

where:

$\alpha_v, k_1, a_b, d, t$  – design parameters,

$f_{ub}$  – characteristic strength of the steel bolts,

$f_u$  – characteristic strength of the steel body,

$\gamma_{M2} = 1.25$  partial safety factor for connections,

$K_{FI} = 1.10$  for RC3 - partial safety factor usually associated with actions.

Partial safety factor for connections in structures of reliability class RC3 according to EN1990 is equal:

$$\gamma_{MRC3,EC} = \gamma_{M2} K_{FI} = 1.375 \quad (3)$$

## 2. Probabilistic analysis of shear bolted connection resistance

Let's assume that  $X = F_{v,Rd}$  is the random variable of steel bolt shear resistance,  $Y = F_{b,Rd}$  - random variable of bearing resistance of the steel body and define new random variable of bolted capacity  $Z = F_R$

$$Z = \min(X, Y) \quad (4)$$

Cumulative distribution function of variable  $Z$  bolted shear resistance  $F_Z(z)$  is defined as [1],[2],[3], [4]:

$$\begin{aligned} F_Z(z) &= P(Z \leq z) = P[\min(X, Y) \leq z] = 1 - P[\min(X, Y) > z] = \\ &= 1 - \int_z^\infty \int_z^\infty f_{XY}(x, y) dx dy. \end{aligned} \quad (5)$$

where:  $P(x)$  and  $f(x)$  are probability and density functions of random variable  $x$ .

Assuming that random variables  $X$  and  $Y$  are independent density function  $f_Z(Z)$  of variable  $Z$  can be obtained from:

$$f_Z(z) = f_X(z) + f_Y(z) - f_X(z)F_Y(z) - f_Y(z)F_X(z) \quad (6)$$

- Probabilistic moments of random variable  $Z$ .

The probability density function  $f_Z(Z)$  of shear stud resistance is known, then it is easy to obtain first two probabilistic moments of variable  $Z$  using classical methods as follows:

- Mean value  $\mu_Z = E(Z)$  as the first moment:

$$\mu_Z = \int_{-\infty}^{\infty} z f_Z(z) dz \quad (7)$$

- Variance  $\sigma_Z^2 = \text{var}(Z)$  as the second moment:

$$\sigma_Z^2 = \int_{-\infty}^{\infty} f_Z(z) (z - \mu_Z)^2 dz \quad (8)$$

### 3. Characteristic and design values of shear bolted connection resistance in normal temperatures

Safety condition is defined, for standardized random value  $Z$   $\ln(\tilde{Z}/z)/v_Z = \ln(\tilde{\mu}_Z/z)/v_Z$ , by using the following formula: ( $\tilde{Z}$  – median value,  $v_Z$  - coefficient of variation) [2], [5]:

$$\beta_R = \frac{\ln(\tilde{Z}/z)}{v_Z} \geq \beta_{R,req} = \alpha_R \beta_{req} \quad (9)$$

$\beta_R$  is a partial reliability index,  $\beta_{R,req}$  is target reliability index for resistance of shear stud connection. Index  $\beta_{R,req} = \alpha_R \beta_{req}$  is the part of global target reliability index  $\beta_{req}$  defined in EN 1990 [6]. The value  $\beta_{req} = 4,3$  for high consequence for loss of human life and considerable social, environmental consequences. According to EN1990  $\alpha_R = 0.8$  then  $\alpha_R \beta_{req} = 0.8 \cdot 4.3 = 3.44$ .

Design value of shear connection resistance is defined as:

$$Z_d = \tilde{Z} \exp(-\alpha_R \beta_{req} v_Z) = \tilde{Z} \exp\left(-3,44 v_Z - \frac{\sigma_{\ln Z}^2}{2}\right) \quad (10)$$

Characteristic value of  $Z$  is defined as 5% fractile of log-normal distribution as follows:

$$Z_k = \check{Z} \exp(-1,645v_Z) = \check{Z} \exp\left(-1,645v_Z - \frac{\sigma_{\ln Z}^2}{2}\right) \quad (11)$$

Based on the fact that  $Z_d$  and  $Z_k$  are known, we can estimate minimum partial safety coefficient for shear connection resistance  $Z$  in RC3 class as:

$$\gamma_{MRC3,\min} = \frac{Z_k}{Z_d} = \exp[(3,44 - 1,645)v_Z] = \exp(1,795v_Z) \quad (12)$$

As shown in Figure 1,  $\gamma_{MRC3,\min}$  is the variable for different value of coefficient variation  $v_Z$ . It is necessary to mention, assuming  $\gamma_{MRC3,\min} = 1,375$ , that the required level of safety can not be guaranteed for value of  $v_Z > 0,18$ .

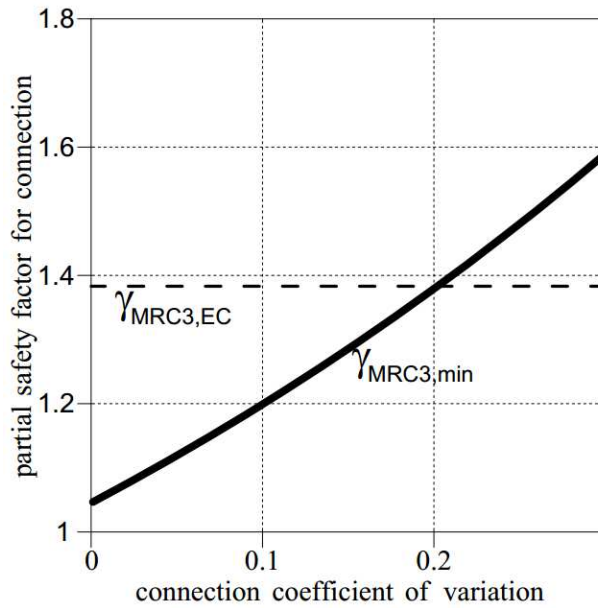


Fig. 1. Partial safety factor for steel shear connection resistance  $Z$

**Example 1.**

Let's consider the shear bolted connections with steel bolt classes 4.6, 5.6, 6.8, 8.8 with accordingly – ultimate strength of the bolts  $f_{ub}=400$  MPa, 500 MPa, 600 MPa, 800 MPa, diameter of the shank of the bolt  $d=20$  mm. The connection joins two steel plates of steel S275,  $f_u=430$  MPa, thickness  $t=7$  mm. The coefficient of variation of ultimate strength for steel body is  $v_{fu}=0.10$  and for bolt steel is  $v_{fub}=0.05$ . Table 1 presents results of calculations of connection resistance, using methods according to EC recommendations and probabilistic approach.

Table 1. Resistance for individual fasteners subjected to shear

Bolt classes	4.6	5.6	6.8	8.8
Median value of bolt ultimate strength $\check{f}_{ub}$ [MPa]	434	543	651	868
Median value of fastener resistance $\check{Z}$ [kN]	81.74	101.03	111.61	113.39
Standard deviation of fastener resistance $\sigma_Z$ [kN]	4.08	5.43	9.345	13.31
Coefficient of variation of fastener resistance $v_Z$	0.050	0.054	0.084	0.100
Design value of fastener resistance (EC) $P_{Rd}$ [kN]	54.81	68.51	70.02	70.02
Design value of fastener resistance (Probabilistic approach) $Z_d$ [kN]	68.84	83.96	83.68	80.39

**4. Steel shear connection capacity in fire temperatures****4.1. Design value of ultimate strength in fire temperatures**

The ultimate strength  $f_{u,k}$  decreases when fire temperatures  $\Theta$  grow:

$$f_{u,k,\Theta} = k_{u,\Theta} f_{u,k,20} \quad (13)$$

$$f_{y,k,20} = \check{f}_u \exp(-1.645v_{fu,20} - 0.5v_{fu,20}^2) \quad (14)$$

Where;  $\check{f}_u, v_{fu,20}$  are the median and log-normal coefficient of variation of the steel ultimate strength in temperature  $\Theta = 20^\circ C$ . It has been assumed that applied value of characteristic strength  $f_{u,k,20}$  is described in normal – room temperature  $\Theta = 20^\circ C$ . The reduction coefficient  $k_{u,\Theta} = k_{y,\Theta}$  for  $\Theta \geq 400^\circ C$ . For different fire temperatures  $\Theta$  is presented in standard EN 1993-1-2 [10]. This relation is described as:

$$Z_{k,\Theta} = k_{u,\Theta} Z_{k,20} \quad (15)$$

The  $Z_\theta$  is the random variable described by log-normal probability distribution function  $\text{LN}(\tilde{Z}_\theta, v_Z)$  – where:  $\tilde{Z}_\theta$  is the median value and  $v_Z$  is the log-normal coefficient of variation. Reduction coefficient  $k_{u,\theta}$  is defined for different fire temperatures  $\theta$ . Temperature  $\theta$  will be treated as no-random in this analysis. The relation is as follows :

$$v_{Z,\theta} = v_{Z,20} = \text{const} \quad \text{and} \quad v_{f_u,\theta} = v_{f_u,20} = \text{const} \quad (16)$$

It has been assumed that log – normal coefficient of variation  $v_R$  does not depend on temperature  $\theta$ .

#### 4.2. Standard deviation $\sigma$ and coefficient of variation $V$ of the steel ultimate strength in fire temperatures

Now, it is necessary to test hypothesis  $H_0$ - equality of variances :  $\sigma_k^2 = \text{var}(Y_k)$  in fire temperature. The null hypothesis  $H_0$  is:  $\sigma_1^2 = \sigma_2^2 = \dots = \sigma_k^2$  against alternative hypothesis  $H_1$ :  $\sigma_1^2 \neq \sigma_2^2 \neq \dots \neq \sigma_k^2$  for all fire temperatures  $\theta(k)$  and adequately  $V_k^2 = \sigma_{ln,k}^2$  the null hypothesis  $H_0$ :  $\sigma_{ln,1}^2 = \sigma_{ln,2}^2 = \dots = \sigma_{ln,k}^2$  against alternative hypothesis  $H_1$ :  $\sigma_{ln,1}^2 \neq \sigma_{ln,2}^2 \neq \dots \neq \sigma_{ln,k}^2$ .

The above hypothesis will be verified by using Bartlett's test which is based upon the following statistic[6]:

$$b = \frac{\left( \prod_{i=1}^k \sigma_i^2 \right)^{n/(N-k)}}{\sigma_p^2} \quad (17)$$

where:  $n$  – sample quantity,  $n=24$ ,  $i=1 \dots k=4$ ,  $N = k \cdot n = 96$ .

$$\sigma_p^2 = n \sum_{i=1}^k \sigma_i^2 / (N-k) \quad (18)$$

We accept hypothesis  $H_0$  at the  $\alpha$  level of significance when it's true for the following:

$$b < b_k(\alpha; n) \quad (19)$$

where:  $b_k(\alpha; n)$  – critical value for Bartlett's test , $k$  –number of populations in fire temperatures =4,  $\alpha$  – level of significance =0.01 , $n$  – sample quantity = 24.

The Bartlett's statistic  $b_{fe}$  (b) to verify hypothesis about equality of yield point standard deviation in fire temperatures  $\sigma_1^2 = \sigma_2^2 = \dots = \sigma_k^2$  was estimated as follows;

$$b_{fe}=1.171 > b_4(0.01, 24) = 0.882 \quad (20)$$

then hypothesis  $H_0 (\sigma_1^2 = \sigma_2^2 = \dots = \sigma_k^2)$  is rejected,

$\sigma_k^2$  – variance of the ultimate strength in fire temperature.

Consistently, the Bartlett's statistic  $b_{lnfe}$  to verify hypothesis about equality of ultimate tensile strength coefficient of variations in fire temperatures  $V_1^2 = V_2^2 = \dots = V_k^2$  was estimated;  
 $b_{lnfe} 0.247 < b_4(0.01, 24) = 0.882$ .

In this case we accept hypothesis  $H_0: \underline{V_1^2 = V_2^2 = \dots = V_k^2 = const}$ , and  
 $\underline{V_{fu,\theta} = V_{fu,20} = const}$ .

$V_k^2$  – coefficient of variation of the ultimate strength in fire temperatures.

## 5. Conclusions

The shear design resistance of connections in sport arena structures should be calculated as fractile (at level  $p_{f,ult} \approx 8.54 \cdot 10^{-6}$ ) of shear resistance probability density function. The shear resistance density functions can be obtained using the formulas presented in this paper. For steel fasteners it is necessary to verify the values of partial safety factors of shear connectors in fire temperatures. More research is needed on the steel ultimate variance parameters in fire temperatures assuming, that the distribution of shear resistance is lognormal.

## References

- [1] Benjamin J., R., Cornell C., A., Probability, Statistics, and Decisions for Civil Engineers. Dover Publications Inc., Mineola, New York;2014.
- [2] Ditlevsen O., Structural Reliability Methods, Wiley. New York 1996.
- [3] Domański T., Fire Safety Factors for Shear Stud Composite Beam Connections. Proc. Of 6<sup>th</sup> European Conference on Steel and Composite Structures EUROSTEEL. Budapest, Hungary, 2011.
- [4] Maślak M., Domański T., Safety factors in design of steel members for accidental fire situation, Proc of International Conference on Design, fabrication and Economy of Welded Structure. Miskolc, Hungary 24-26 April 2008. pp 563–570.
- [5] Nowak A., Collins K.,R., Reliability of Structures, Mc Graw Hill Higher Education, Boston. New York, 2000.
- [6] Walpole R.E., Myers R.H., Myers S.L., Probability & Statistics for Engineers & Scientists, Prentice Hall.N.J.2002.

- 
- [7] Woliński Sz., Global Safety Factor for Nonlinear Design of Concrete, Archives of Civil Engineering, LVII, 3, 2011.
- [8] EN 1990, Eurocode 0, Basis of structural design.
- [9] EN-1993-1-8, Eurocode 3, Design of steel structures – Design of joints.
- [10] EN-1993-1-2, Eurocode 3, Design of steel structures, General Rules, Structural fire design.

*Przesłano do redakcji: 04.05.2018 r.*

*Przyjęto do druku: 15.06.2018 r.*

Mariusz MAŚLAK<sup>1</sup>  
Maciej SUCHODOŁA<sup>2</sup>  
Piotr WOŹNICZKA<sup>3</sup>

## TEMPERATURE DISTRIBUTION IN A STEEL BEAM-TO-COLUMN JOINT WHEN EXPOSED TO FIRE. PART 1: END-PLATE JOINT

Temperature distribution usually observed in steel beam-to-column end-plate joint after 15 minutes of its standard fire exposure is presented and discussed in detail. Two types of joints are analysed for comparative purposes. The first one is a pure steel connection while the other is covered by a reinforced concrete slab. Numerical simulation of the considered joint heating scenario was performed using the 3D model in the ANSYS environment. Some results were additionally verified by simpler calculations carried out on 2D models using the SAFIR computer program. It is emphasized that due to the local accumulation of many massive steel plates the representative temperature values identified in particular joint components are significantly lower than those which at the same time are measured in beam and column outside the connection. This means that the classic assumption of even temperature over the entire length of all the structural elements of a frame load-bearing structure exposed to fire at any time during such fire, without distinguishing in the formal model any cooler nodal elements, is always safe but very conservative. In addition, as the fire develops the differentiation between the temperature values relating to the beam web and to the beam flanges becomes more visible. This effect is particularly significant in the presence of a massive floor slab adjacent the upper flange of a frame I-beam which effectively cools it.

**Keywords:** beam-to-column steel end-plate joint, fire, temperature distribution, joint components, numerical simulation

---

<sup>1</sup> Corresponding author: Mariusz Maślak, Cracow University of Technology, Faculty of Civil Engineering, Chair on Metal Structures, Warszawska 24, 31-155 Cracow, phone: 126282033, e-mail: mmaslak@pk.edu.pl

<sup>2</sup> Maciej Suchodoła, Cracow University of Technology, Faculty of Civil Engineering, Chair on Metal Structures, Warszawska 24, 31-155 Cracow, phone: 126282033, e-mail: maciek.krakow@interia.pl

<sup>3</sup> Piotr Woźniczka, Cracow University of Technology, Faculty of Civil Engineering, Chair on Metal Structures, Warszawska 24, 31-155 Cracow, phone: 126282033, e-mail: pwozniczka@pk.edu.pl

## 1. Introduction

In conventional structural analysis relating to a steel frame load-bearing structure when exposed to fire it is usually assumed that at any moment of such fire the temperature in each member is aligned not only on its entire length but also in any chosen cross-section. The basic advantage of this type of a computational model is its simplicity. It is always safe but in general very conservative. In fact, even when the frame I-beam or the frame I-column is heated on all sides in a uniform manner, with the fire development the difference between the temperature of its web and the other relating to its flanges increases. This is an inevitable consequence of the fact that the web is noticeably thinner than the adjacent flanges. The higher value of the web temperature in relation to the corresponding temperature identified at the same time of the fire in the flanges of the same beam in the case of the beam I-section evenly heated on four sides is particularly well visible for the members which are relatively tall and slender. This type of variation is not so big when the member cross-sections are lower and more stocky.

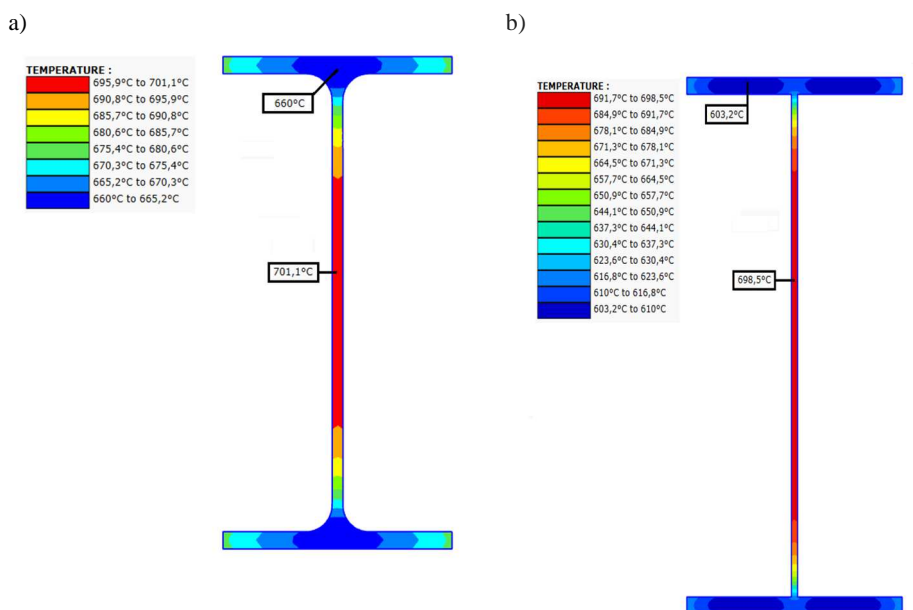


Fig. 1. Temperature distributions in the cross-sections of selected thermally non-insulated steel I-beams, heated on four sides, after 15 minutes of a numerically simulated fire exposure (simulations were performed using the SAFIR computer program [1]). In particular: a) the case of a IPE 330 frame-beam, b) the case of a 576x8x280x18 mm plate girder

It is shown here, in Fig. 1a, that after 15 minutes of a numerically simulated standard heating in a thermally non-insulated IPE 330 beam the representative web temperature turned out to be higher than that identified in the flanges by only about 40 degrees Celsius. If, however, for comparison to verify how in the same fire a relatively slim steel 576×8×280×18 mm plate girder is heated, one can see that after 15 minutes of a fire exposure the difference considered earlier will be closed to 100 degrees Celsius (Fig. 1b). Interestingly, the difference shown in Fig. 1b turns out to be particularly large in the first phase of a fire and then gradually disappears as the temperature of the exhaust gases surrounding the beam increases (Fig. 2).

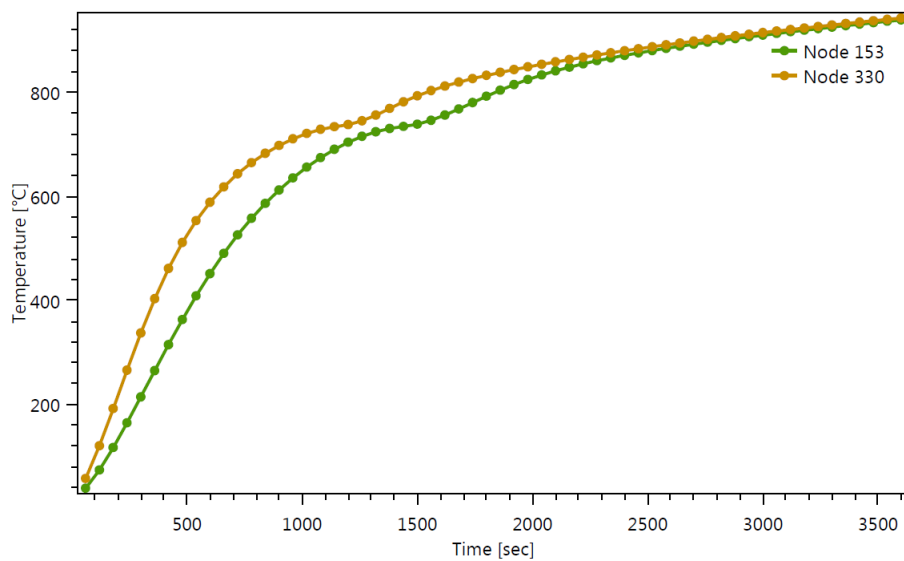


Fig. 2. Dependences between the time of a standard fire exposure and the representative temperature values identified in the I-beam web (higher) and in the same I-beam flanges (lower) for steel 576x8x280x18 mm plate girder, heated on four sides, corresponded to that shown in Fig. 1b

In the case when the upper flange of a steel I-beam is adjacent to a massive reinforced concrete floor slab with a large heat capacity, this flange is effectively cooled because the temperature in it and the temperature at the bottom of the slab strive for equalization. Consequently, the beam cross-section is heated only on three sides. Taking into account such a situation requires a significant reduction in the temperature of this upper flange both in relation to the temperature representative for the beam web and to the one representative for the lower flange. Let us note that the difference between the temperature of the beam web and the temperature of the lower flange remains significant, although not so large. Temperature distribution obtained having simulated of a 15 minutes fire exposure in the cross-section of thermally non-insulated steel IPE 330 beam, corresponding to that shown earlier in Fig. 1a but now adjacent to a massive concrete slab, is presented in detail in Fig. 3.

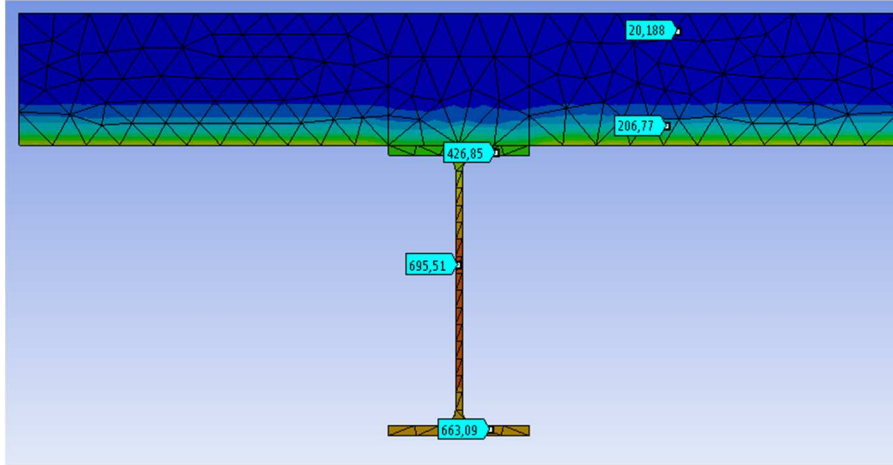


Fig. 3. Temperature distribution obtained after 15 minutes of a standard fire exposure in cross-section of a steel IPE330 frame beam, thermally non-insulated and heated on three sides due to the neighborhood with concrete slab (simulation performed using the ANSYS environment [2])

## 2. Numerical models of the pure steel end-plate joints considered in the analysis

In the introduction to this paper, it was shown that with precise modelling of any pure steel beam-to-column joint behaviour in a fire, the differentiation between the representative temperature of a beam web and the representative temperature values of beam flanges should be taken into account. The primary aim of the authors is, however, to show that the temperature identified in such a joint at any time during a fire due to a very significant increase in the effective steel thickness accumulated here will always be significantly lower than that which at the same time is measured as a representative value for the beam and for the column outside the connection. Therefore, it seems reasonable to consider whether in numerical modelling related to the fire conditions separate from a whole load-bearing frame structure the special nodal elements being colder than the neighbouring elements that they connect. In this chapter the authors want to check which elements of the considered joint are crucial for fire analysis in the sense that the precise determination of their representative temperature values determines both the bearing capacity and the stiffness of this joint under fire conditions. To do this, two steel beam-to-column end-plate joints were precisely modelled in the ANSYS environment [2], connecting a column made of the HEB 180 steel profile and a beam made of the IPE 330 steel profile. All joint components were designed as made of low carbon structural steel S235. The thickness of the end plate in both models was assumed identically, as being equal to 20 mm. The classic bolts with metric thread M20 have also been used. The difference between the joint model shown in Fig. 4a and that of Fig. 4b

consists in adding in the second case two horizontal ribs with a thickness of 10 mm stiffening the column's web. Both models were subjected to uniform heating on all sides, lasting 15 minutes, in accordance with the so-called standard fire scenario, numerically simulated in the ANSYS environment [2].

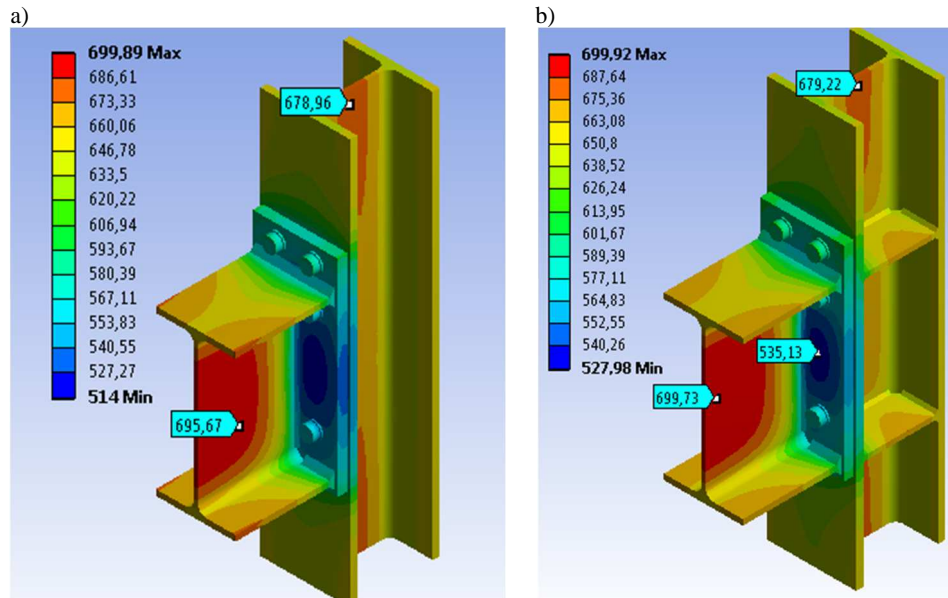


Fig. 4. Temperature distributions obtained after 15 minutes of a standard fire exposure in the models of a pure steel end-plate beam-to-column joints considered in the analysis (detailed description of such models is given in the text, simulation performed using the ANSYS environment [2]). In particular: a) model of a joint without the horizontal ribs stiffening the column's web, b) model of a joint with such the ribs

It is easy to notice that after 15 minutes of a simulated fire in both models the temperature value representative for a joint end-plate turned out to be lower, even by 150 degrees Celsius, compared to the other temperature value, representative for the beam web. This is due to the fact that in this joint zone the effective thickness of the heated steel plate is extremely high, because it is in fact the sum of the end-plate thickness and the thickness of the column's flange ( $20\text{ mm} + 14\text{ mm} = 34\text{ mm}$ ). The addition of two horizontal ribs in this case facilitates the removal of heat from the joint end-plate giving an additional surface for radiating. As a consequence in the model presented in Fig. 4b the cooler zone in the joint end-plate was clearly smaller than that observed in the model shown in detail in Fig. 4a. Generally, it can be stated that the highest steel temperature in particular joint components is always identified in those plate zones where the distance from the adjacent walls increasing the heat dissipation is large enough and its value is the higher for the lower thickness of the heated plate. Comparative analysis of the model of an analogous steel end-plate joint

with reduced end-plate thickness (from 20 mm to 14 mm), which meant a reduction in the total thickness of the heated plate (from 34 mm to 28 mm, i.e. about 17%), resulted in an increase in the end-plate temperature by approximately 30 degrees Celsius, which is a roughly 5% change. Temperature differences identified at the bolts length are negligible, as shown in Fig. 5.

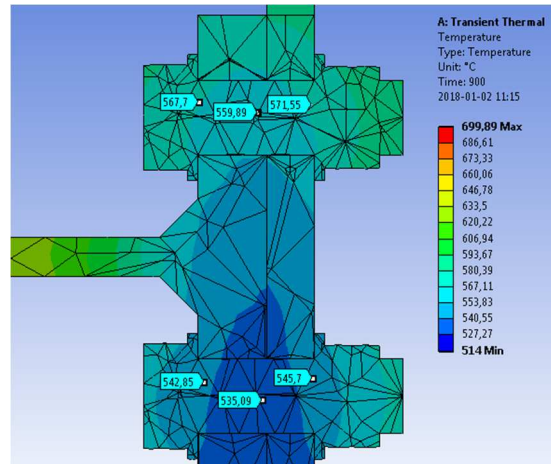


Fig. 5. Temperature distribution obtained after 15 minutes of a standard fire exposure for the joint model shown in detail in Fig. 4a in the cross section through the bolts axes. Only the bolts from the upper row, located above the top beam flange (shown on the left) as well as those from the intermediate row (located just below this flange) are visible (simulation performed using the ANSYS environment [2])

A detailed analysis of the temperature distribution in the pure steel end-plate joints presented in Fig. 4 allows to conclude that in the formal model describing their behaviour in a fire four basic groups of the joint components should be distinguished due to the different heating rate as is shown in Fig. 6. The I-beam web heats up by far the fastest among other joint components due to its low thickness. This is especially the case for beams made of the high plate girders, when the distance of the central area of the web plate from the much thicker beam flanges that cool such web in its edge areas is sufficiently large. It should also be noted that the relatively thick beam flanges in general heat up much faster than the joint end-plate. The effective heating of the joint end-plate, usually quite thick, is conditioned by the necessity of simultaneously heating the column flange adhering directly to it and generally no less thick. Differentiation in the heating rate was also observed between the particular rows of bolts. Those of bolts, which were located on the edge of the joint end-plate, outside the outline of the upper beam flange, heated up a bit faster than those located between the beam flanges, in the part shading such bolts from the direct exposure of a fire. Let us note that the difference between the temperature of the bolt and the temperature of the joint end-plate in its immediate vicinity is negligible.

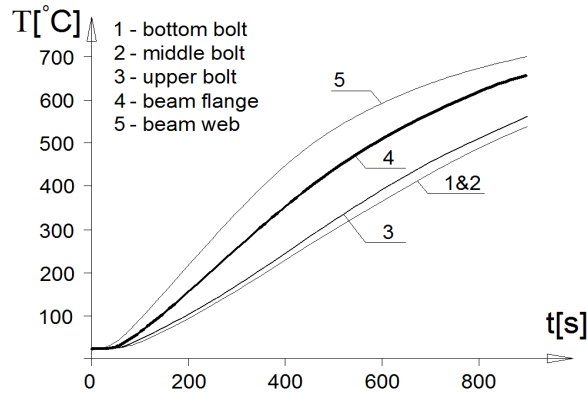


Fig. 6. Different heating rates in the numerically simulated fire of individual joint components in the case of the joint considered in the example and shown in detail in Fig. 4a (simulation performed using the ANSYS environment [2])

### 3. Heating of the beam-to-column steel end-plate joints covered by a reinforced concrete floor slab

Beam-to-column joints considered in the presented paper are usually covered from above by a massive floor slab made of the reinforced concrete with a large thermal capacity. As a consequence of such joint's configuration the joint components adjacent to this plate are usually much colder during a fire than those more distant from it. To verify this effect and to evaluate its importance for the global fire safety assessment a new model of the end-plate joint was developed, corresponding to the joint from Fig. 4a but with an added 150 mm thick reinforced concrete slab, composite with a steel frame beam (Fig. 7). It was assumed that this slab was made of concrete on a regular aggregate and with a density of 2,300 kg/m<sup>3</sup>. In the fire conditions, the steel I-beam was heated on three sides and the floor slab absorbed the heat only from below. The temperature distribution obtained at the tested model after 15 minutes of a numerically simulated standard fire exposure is shown in detail in Fig. 7. As one can see, the cooling effect of the floor slab turned out to be very important and the difference between the steel temperature representative for the lower beam flange and the one observed in the upper beam flange was close to 250 degrees Celsius.

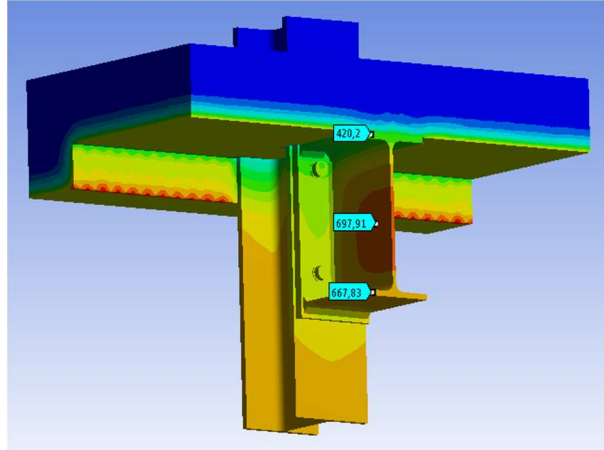


Fig. 7. Temperature distribution obtained after 15 minutes of a numerically simulated standard fire exposure in the end-plate joint covered from above by a massive reinforced concrete slab (simulation performed using the ANSYS environment [2])

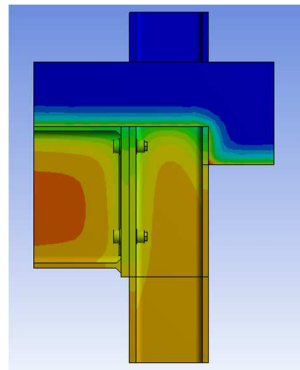


Fig. 8. Temperature distribution taken from Fig. 7 but visible in 2D side view of the joint (simulation performed using the ANSYS environment [2])

The influence of cooling a steel beam in the zone adjacent to the reinforced concrete slab is clearly visible in Fig. 8, where a side view of the considered joint after its 15 minutes fire exposure is shown in detail. In this figure, however, one can notice another interesting difference in the way of heating the neighbouring I-profiles of the beam and of the column. Under the same fire conditions, the column web does not heat up as intensely as the beam web, and as a result, as the fire develops, it becomes more and more clearly cooler. It is not only the effect of the slight difference in the thickness of both webs but also the fact that the considered column is made of a wide-flange profile. When describing the temperature development in the joint shown in Fig. 7, it is worth paying attention to the uneven temperature increase in the particular layers of a reinforced concrete floor slab. As can be seen in Fig. 9, concrete used in this

slab proved to be a heat insulator good enough that the effect of heating from the bottom is poorly noticeable in the upper layers of such a slab.

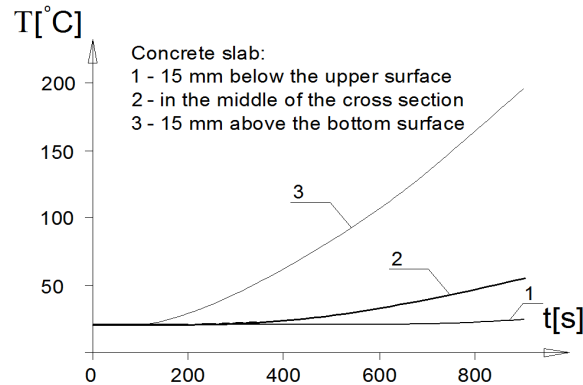


Fig. 9. Differences in the heating intensity in a simulated fire conditions of selected layers of reinforced concrete floor slab covering the considered joint (the results of the simulation performed using the ANSYS environment [2])

#### 4. Concluding remarks

The redistribution of internal forces in the members of a load-bearing steel frame structure subjected to fire is largely dependent on the real load capacity and the real stiffness of the joints connecting these members, which are changing with an increasing steel temperature [3, 4]. In order to predict it in a sufficiently reliable way, it is necessary first to define, and then to calibrate and finally to verify experimentally a suitably complex formal model that takes into account uneven temperature distribution in particular joint components, mainly in those joints that connect the frame beams and the frame columns. The assumption that the steel temperature in all the frame joints is fully evenly distributed and does not differ in value from the temperature identified in the same heating conditions outside these joints, commonly used so far in the fire safety analysis, in the opinion of the authors seems to be too simplistic and too conservative though it is always safe. For this reason, the authors recommend the use for this type of the structural analysis of specially specified nodal elements with precisely calibrated characteristics. Such characteristics could be selected on the basis of the appropriate numerical analysis, or, for example, in an analytical manner, using the procedures of the classical component method generalised for the fire case.

**References**

- [1] Franssen J.-M., Gernay T.: Modelling structures in fire with SAFIR®: Theoretical background and capabilities, *Journal of Structural Fire Engineering*, 8(3), 2017, pp. 300–323.
- [2] Kohnke P. (Ed.): ANSYS®: Theory reference. Release 5.6. Canonsburg, PA, USA, November 1999.
- [3] Maślak M., Pazdanowski M., Snela M.: Redistribution of internal forces generated in a steel frame structure with flexible joints when exposed to a fire, in: Giżejowski M., Kozłowski A., Marcinowski J., Ziółko J. (Eds.) – Recent progress in steel and composite structures, *Proceedings of the 13th International Conference on Metal Structures (ICMS 2016)*, Zielona Góra, Poland, June 15-17, 2016, CRC Press/Balkema, Leiden, The Netherlands, abstract pp. 136-137, paper CD, pp. 315–322.
- [4] Maślak M., Pazdanowski M., Woźniczka P.: Influence of joint stiffness on the behaviour of steel bearing frame under fire conditions, *Ce/Papers, The Online Collection for Conference Papers in Civil Engineering*, Ernst & Sohn, A Wiley Brand, 1 (2017), No. 2 & 3, pp. 2811–2820.

*Przesłano do redakcji: 04.05.2018 r.*

*Przyjęto do druku: 15.06.2018 r.*

Krzysztof KUCHTA<sup>1</sup>  
Rafał SILEZIN<sup>2</sup>  
Paweł ŻWIREK<sup>3</sup>

## TECHNOLOGICAL ASPECTS OF EXECUTION OF WELDED JOINTS IN HOLLOW SECTIONS

Steel structures designed according to Eurocode 3 are executed in accordance with the provisions of the standard PN-EN 1090-2, which is referred to in Eurocode 3. In addition, the standard PN-EN 1090-2 refers to in its content a number of welding standards, e.g. PN-EN ISO 9692-1. These standards provide guidelines for welded connections, which should be applied in the case of joints connecting steel hollow sections. Analysis of above-mentioned provisions revealed that for fillet welds they are simultaneously fulfilled only if the inclination angles of the elements are in the range of 70°–100°. According to recommendations of PN-EN 1993-1-8 and EN 1090-2, the same weld type around the perimeter of the element connected to the chord of lattice structure is possible to execute only for inclination angle lower than 60°. Discrepancies between these standards also exist with regard to the interpretation of the dimension of the flare groove welds in connections of rectangular hollow sections with the same width. In addition, analyses of the recommendations for welding in cold-formed zones indicate that, for steel grades currently used for the production of cold-formed rectangular hollow sections, welding in these zones is not permitted only for profiles with wall thickness equal to 12.5 and 16 mm. The above-mentioned issues point out the need for mutual unification of standards for the design and execution of steel joints in hollow sections.

**Keywords:** steel structures, lattice structures, welded joints, hollow sections

### 1. Introduction

Exactly 30 years ago, in Europe came into force the Construction Product Directive (CPD) 89/106/EEC [2]. The purpose of the CPD was to harmonise the production process of construction products and to ensure the free movement of construction products and unlimited use of these products in the European Union. Additionally, on 1st of July 2013 came into force the Regulation (EU)

---

<sup>1</sup> Corresponding author: Krzysztof Kuchta, Cracow University of Technology, Chair of Metal Structures, ul. Warszawska 24, 31-155 Kraków, +48 12 6282033, pzwi@op.pl

<sup>2</sup> Rafał Silezin, NDT SERWIS, ul. Niska 12, 31-306 Kraków, biuro@ndtserwis.pl

<sup>3</sup> Paweł Żwirek, Cracow University of Technology, Chair of Metal Structures

No 305/2011 of the European Parliament and of the Council of 9 March 2011 laying down harmonised conditions for the marketing of construction products and repealing Council Directive 89/106/EEC [13]. The regulation applies to all construction products covered by harmonised European standards or European Technical Assessments. It includes both products, which are manufactured in series and placed on the market for sale to the general public, as well as products produced on individual order to be built in the specified structure. In accordance with article 5 of the Regulation [13] the manufacturer may refrain from drawing up a declaration of performance when placing a product covered by a harmonised standard on the market, where the construction product is individually manufactured or custom-made in a non-series process in response to a specific order, and installed in a single identified construction work – as usually in the case of steel building structures. In this situation, the manufacturer shall provide for executed structure a statement of conformity with project documentation and PN-EN 1090-2 [7] for steel structures or PN-EN 1090-3 [8] for aluminium structures. Building metal structures designed according to the Eurocodes have to be manufactured by the producers having a certified system of factory production control according to PN-EN 1090-1 [6]. These issues were further described in [3]. The authors of this publication had the opportunity to participate in the process of steel workshop adaptation to the requirements of the current regulations, and as a result had a chance to confront assumptions and provisions included in European design standards for welded connections in steel hollow sections with the provisions of the standards relating to steel structure execution, including welding technology. In this paper technological and metallurgical aspects of welded joints execution in steel hollow sections are discussed.

## 2. Welding in cold-formed zones

In the case of cold-formed sections, the standard PN-EN 1993-1-8 [11] allows for welding in the cold-formed zone provided that the cold-formed zones are normalized after cold-forming but before welding or the ratio of corner inner radius  $r_i$  to profile wall thickness  $t$  fulfils appropriate condition. The standard defines above-mentioned parameters for general case, distinguishing between predominantly static loading and situations where fatigue predominates, it also specifies the case of fully killed steel (see Table 1). As can be seen from Table 1, in the case of fully killed steels welding in cold-formed zones is permitted in the wider range than in the general case. Seamed cold-formed steel hollow made of non-alloy and fine grain steels are manufactured in accordance with PN-EN 10219 [4, 5]. This standard was officially referred to in the design standard of joints in steel structures [11]. The first part of PN-EN 10219 [4] specifies the technical delivery conditions. According to its provisions sections are made of following non-alloy quality steels: S275J0H, S275J2H, S355J0H, S235JRH, S355J2H, S355K2H and fine grain steel grades: S275NH, S275NLH,

Table 1. Conditions for welding cold-formed zones and adjacent material [11] and corner geometry for steel cold-formed sections manufactured according to [5]

Conditions for welding cold-formed zones and adjacent material [11]				Cross-section parameters according to PN-EN 10219-2 [5]						
ri/t	Generally		Fully killed steel							
	Predominantly static loading	Where fatigue predominates								
	max t [mm]	max t [mm]	max t [mm]							
$\geq 25$	any	any	any							
$\geq 10$	any	16	any	t [mm]	assumed		tolerance			
$\geq 3,0$	24	12	24		ri/t	re/t	re/t			
$\geq 2,0$	12	10	12	> 10	2.0	3.0	2.4–3.6			
$\geq 1,5$	8	8	10	$6 < t \leq 10$	1.5	2.5	2–3			
$\geq 1,0$	4	4	6	$\leq 6$	1.0	2.0	1.6–2.4			

S355NH, S355LNH, S460NH, S460NLH. Both in the case of non-alloy and fine grain steels fully killed steels are used. For non-alloyed steels deoxidation method is designated as FF, it means that steel contains nitrogen binding elements in amount sufficient to bind available nitrogen (e.g. min. 0.020% total Al, or 0.015% soluble Al). For fine grain steels deoxidation method is designated as GF – steel contains nitrogen binding elements in amount sufficient to bind available nitrogen and have fine grain structure.

The second part of PN-EN 10219 [5] specifies tolerances, dimensions and sectional properties. The depth, width, and wall thickness of the profiles are specified in Tables C.2 and C.3 of PN-EN 10219-2 [5], but the values of the corner inner and outer radii can be found only as assumed values in the calculation of geometrical characteristics. It can be noticed that for cold-formed sections with wall thickness not exceeding 12 mm made of fully killed steel, welding in cold-formed zone is permitted. In the case of square and rectangular hollow sections with wall thickness  $t$  equal to 12.5 mm and 16 mm listed in Tables C.2 and C.3 of PN-EN 10219-2 [5], welds should be located at a distance of  $5t$  from the cold-formed zone. In engineering practice, the designers often use a very popular in Poland publication [1] where for both square and rectangular hollow sections – manufactured according to [4, 5] – instead of the values of corner inner radius, as marked on the figure, corner external radius is given – Fig. 1. The error described above may affect invalid geometry shaping in the joints between hollow section members committed at the design stage.

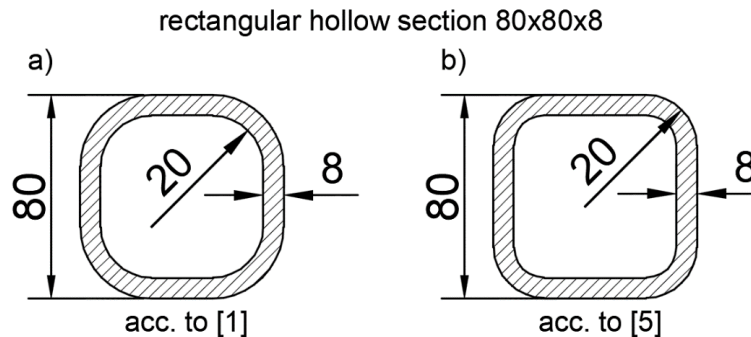


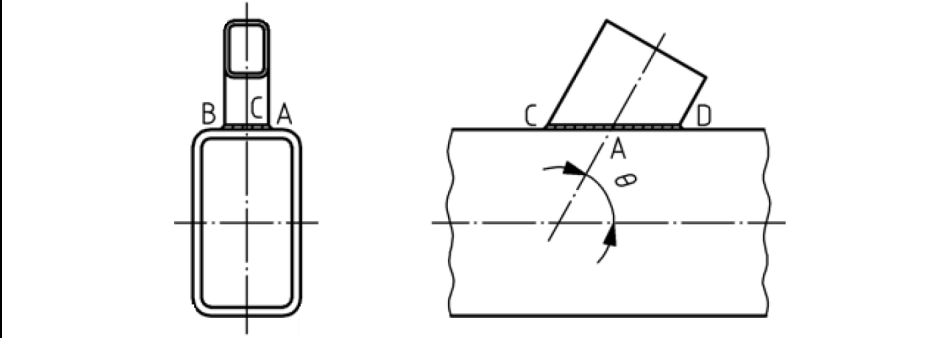
Fig. 1. Comparison of square hollow section geometry according to a) publication [1] and b) standard PN-EN 10219-2 [5]

### 3. Welded joints in hollow sections

Welded joints in steel hollow sections are contemporary designed in accordance with [11]. This standard restricts possibility to use fillet welds to the case of connected parts where the fusion faces form an angle of between  $60^\circ$  and  $120^\circ$ . In the case of inclination angles lower than  $60^\circ$ , the welds should be treated as partial penetration butt welds. For angles greater than  $120^\circ$ , fillet welds resistance should be determined by testing according to provisions of Annex D of PN-EN 1990 [9]. With regard to the fillet welds all round, the standard [11] additionally states that they may only be used to transmit shear. In respect of butt welds the standard [11] does not introduce restrictions about the connected parts inclination angle. It should be noted that, in accordance with the provisions of [10], Eurocode 3 is intended to be used together with [7] concerning the execution of steel structures. This standard introduces geometrical limitations, in the form of the inclination angle between axes of connected members, concerning the possibility of using fillet and butt welds. Conditions for the use of butt and fillet welds in joints connecting rectangular or circular hollow sections according to [7], depending on the location of the weld, are presented in Table 2 and 3.

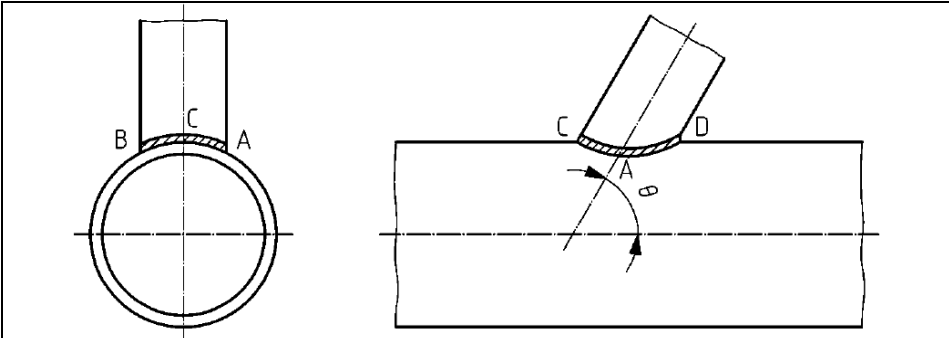
In addition, standard [7] refers to [12] that specifies how to prepare steel joints for welding. In the case of fillet welds, this last standard limits the inclination angle between walls of connected elements to the range from  $70^\circ$  to  $100^\circ$ . Figure 2 shows the conditions of applicability of fillet and butt welds in steel hollow sections joints, depending on the shape of the profile cross section and the location of the weld. Well known limitation of the minimum slope of the brace to the value of  $30^\circ$  is also taken into account on presented drawings. If one wants to meet all restrictions, given in above-mentioned standards, the possibility of using fillet welds on whole perimeter of the section is limited to the members with the inclination angle not less than  $80^\circ$ . In the case of fillet welds all round, the minimum value of the inclination angle for which the standard provision about the joint geometry are met is  $60^\circ$ .

Table 2. Geometrical limitations according to [7] on using butt and fillet welds in welded joints between rectangular hollow sections



Option I				
Weld location				
	A, B	C	D	
Weld type	butt	butt	$\theta < 60^\circ$	$60^\circ \leq \theta < 90^\circ$
			fillet	fillet
Option II				
Weld location				
	A, B	C	D	
Weld type	fillet	$\theta < 60^\circ$	$60^\circ \leq \theta < 90^\circ$	fillet
		butt	fillet	

Table 3. Geometrical limitations according to [7] on using butt and fillet welds in welded joints between circular hollow sections



Option I				
Weld location				
	A, B	C	D	
Weld type	butt	$60^\circ \leq \theta < 90^\circ$	$\theta < 60^\circ$	$60^\circ \leq \theta < 90^\circ$
		butt	fillet	butt
Option II				
Weld location				
	A, B	C	D	
Weld type	fillet	$\theta < 60^\circ$	$60^\circ \leq \theta < 90^\circ$	fillet
		butt	fillet	

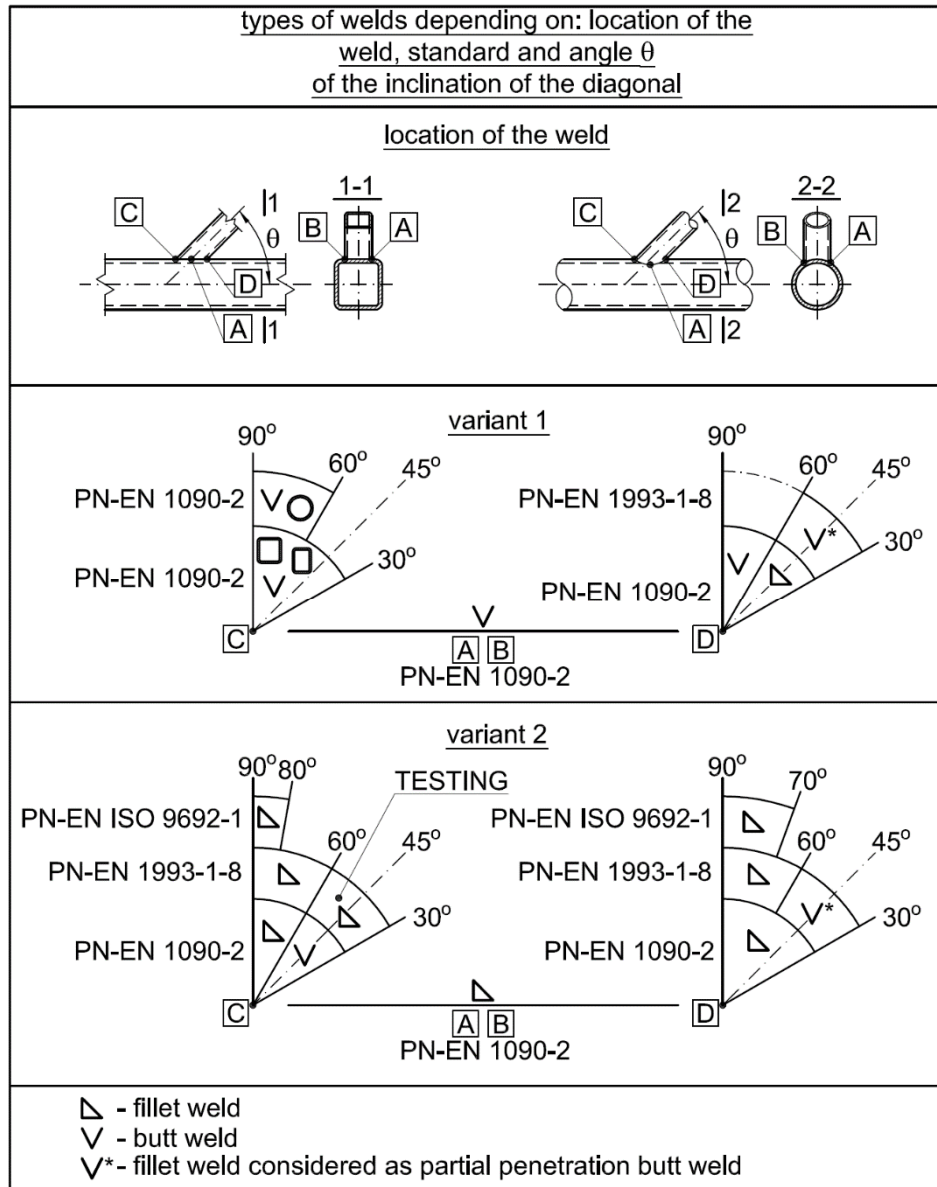


Fig. 2. The conditions of applicability of fillet and butt welds in steel hollow sections joints

#### 4. Welds in cold-formed zone of hollow sections

In the joints between rectangular hollow sections flare groove welds are used. The standard [11] specifies the thickness of this weld type as shown on Fig. 3a. Whereas according to [7], the thickness of the weld shall be determined

on the basis of the interfacial angle inscribed in the groove weld, and its value should not be smaller than  $60^\circ$ . In addition, the standard [11] refers to the design thickness, while the standard [7] to effective thickness.

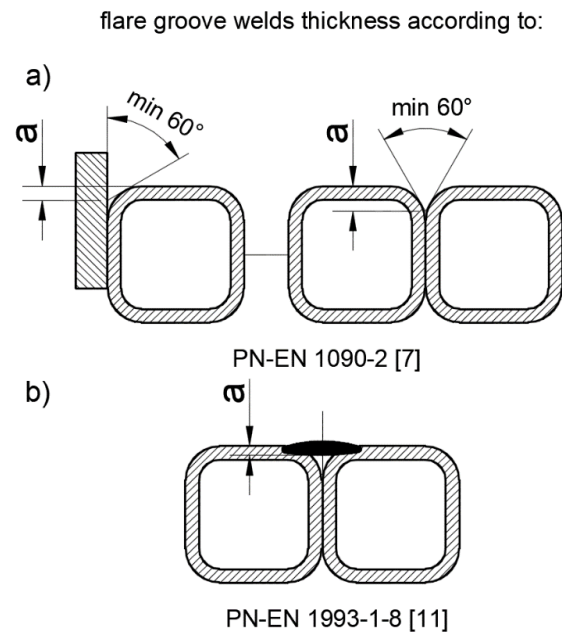


Fig. 3. Interpretation of flare groove welds thickness according to: a) standard PN-EN 1090-2 [7] and b) standard PN-EN 1993-1-8 [11]

## 5. Conclusions

Welded joints in steel hollow sections designed according to PN-EN 1993-1-8 [11] should be executed in accordance with PN-EN 1090-2. [7]. This last standard refers to PN-EN ISO 9692-1 [12] which includes recommendations for the preparation of welded joints. The first two of the above mentioned standards, apart from general provisions for welded joints, also provide detailed requirements for joints in hollow sections. It may seem that the provisions of mentioned standards should be consistent with each other. However, it appears that in many areas are mutually contradictory, and it is not possible to simultaneously meet the provisions of all above-mentioned standards. This may mean that welded joint designed in accordance with the provisions of PN-EN 1993-1-8 [11] is not possible to execute.

Analysis of aforementioned provisions revealed that for fillet welds they are simultaneously fulfilled only if the inclination angles of the elements are in the range of  $70^\circ$ – $100^\circ$ . According to recommendations of PN-EN 1993-1-8 and EN 1090-2, the same weld type around the perimeter of the element connected

to the chord of lattice structure is possible to execute only for inclination angle not lower than  $60^\circ$ . Discrepancies between these standards also exist with regard to the interpretation of the dimension of the flare groove welds in connections of rectangular hollow sections with the same width. In addition, analyses of the recommendations for welding in cold-formed zones of indicate that, for steel grades currently used for the production of cold-formed rectangular hollow sections, welding in these zones is not permitted only for profiles with wall thickness equal to 12.5 and 16 mm. The above-mentioned issues point out the need for mutual unification of Standards for the design and execution of steel joints in hollow sections.

## References

- [1] Bogucki W., Żyburtowicz M., Tablice do projektowania konstrukcji metalowych, Arkady, Warszawa 2007.
- [2] Council Directive 89/106/EEC of 21 December 1988 on the approximation of laws, regulations and administrative provisions of the Member States relating to construction products OJ No L 40 of 11 February 1989.
- [3] A. Czechowski, J. Łaguna, Elementy konstrukcji jako wyroby budowlane w świetle przepisów, Inżynier budownictwa, 5/2014.
- [4] PN-EN 10219-1 Cold formed welded structural hollow sections of non-alloy and fine grain steels. Technical delivery requirements.
- [5] PN-EN 10219-2 Cold formed welded structural hollow sections of non-alloy and fine grain steels. Tolerances, dimensions and sectional properties.
- [6] PN-EN 1090-1 Execution of steel structures and aluminium structures. Part 1 - Requirements for conformity assessment of structural components.
- [7] PN-EN 1090-2 Execution of steel structures and aluminium structures. Part 2 - Technical requirements for steel structures.
- [8] PN-EN 1090-3 Execution of steel structures and aluminium structures. Part 3 - Technical requirements for aluminium structures.
- [9] PN-EN 1990 Eurocode 0. Basis of structural design.
- [10] PN-EN 1993-1-1 Eurocode 3. Design of steel structures. General rules and rules for buildings.
- [11] PN-EN 1993-1-8 Eurocode 3. Design of steel structures. Design of joints.
- [12] PN-EN ISO 9692-1 Welding and allied processes. Types of joint preparation. Manual metal arc welding, gas-shielded metal arc welding, gas welding, TIG welding and beam welding of steels.
- [13] Regulation (EU) No 305/2011 of the European Parliament and of the Council of 9 March 2011 laying down harmonised conditions for the marketing of construction products and repealing Council Directive 89/106/EEC.

*Przesłano do redakcji: 01.05.2018 r.*

*Przyjęto do druku: 15.06.2018 r.*

Marian GWÓZDŹ<sup>1</sup>  
Damian KOWALSKI<sup>2</sup>

## TELESCOPIC JOINTS IN STEEL TUBE TOWERS

Modeling problems of new generation of steel shell towers supporting overhead power transmission lines and having telescopic joints are presented in this paper. The towers of such structure, designed according to the European standard EN 50341 [8], ensure high reliability even when subjected to high technological and climate loads. In this paper elements of differentiated reliability requirements are verified, and special attention is paid to the values of variable loads coefficients for different reliability classes of the considered structure. Using computer modeling tools and linear, elastic shell theory, the modeling error of telescopic joints in a sample tower supporting overhead power transmission line rated at 110 kV is estimated.

**Keywords:** columns, shells, power lines, bearing capacity, reliability, telescopic joint

### 1. Introduction

#### 1.1. Types of towers supporting overhead power transmission lines

Overhead power transmission lines, rated for the voltage of 110 kV and up to 400 kV, are usually supported by transmission towers having lattice structure. The precise shape of the supporting structure depends on the parameters of the supported line, including the spacing of the phase conductors and grounding wires, economic considerations and the requirements of environmental protection. The lattice supporting structures are often characterized by large dimensions, and especially built up horizontal size, due to the required stiffness of the whole structure.

In the urbanized areas, as well as in the areas with difficult access, such as near shore and on steep slopes the steel tube supporting towers characterized by compact contour, much smaller than the contour of lattice towers, seem to be a much better solution. Regarding the purpose and specific application the towers of both types may be divided into the following groups: tangent (P),

---

<sup>1</sup> Corresponding author: Marian Gwóźdź, Cracow University of Technology, 31-155 Cracow, 24 Warszawska St., tel. 12 6282033, e-mail: margwozdz@interia.pl

<sup>2</sup> Damian Kowalski, Eurocoles Kroniss Sp. z o.o., 32-500 Chrzanów, 38F Krocymiech St., tel. 784610080, e-mail: dkowalski@eurocoles-kroniss.pl

angle (N), tangent strain (O), angle strain (ON), dead end (K), branching (R) and crossover (S). The functions of all tower types are described in detail, among others, in monograph [3].

The steel shell towers offered in Poland cover typical structures, designed to support overhead power transmission lines rated for the voltage of 110 kV (cf. the catalogue [2]). An assortment of towers supporting one or two circuits and belonging to various series is listed in this catalogue. Depending on the foreseen application, the following two types have been designed: tangent (P) and strong (M2), (M4), (M6), (M9), (K) and (KG). With the catalogue heights of 15.00 m to 25.00 m and span lengths of 250.00 m to 400.00 m in the 1<sup>st</sup> wind and icing climate zone these towers satisfy the reliability requirements of the Eurocode PN-EN 1990 [4], including the specification of load and bearing capacity coefficients listed in the code PN-EN 50341-2-22:2016 [8]. The fitting elements of these towers, exceeding the commercially available sheet metal lengths, are assembled on site with telescopic joints (cf. fig. 1).



Fig. 1. Assembly of the steel shell tower trunk

The steel shell towers supporting overhead power transmission lines, in spite of modern structural solutions and warranted durability, should not be treated as competition of the lattice towers, but rather as an important supplement of the commercial offer available in Poland.

## 1.2. Reliability elements of steel supporting structures

Elements of reliability for the steel structures supporting overhead power transmission lines, including the partial components of: loads  $\gamma_F$  and bearing capacity  $\gamma_M$  present in the version of limit state method adopted in Eurocodes may

be found in several codes. Especially the general rules specified in Eurocode PN-EN 1990 and the following parts of Eurocode 3: PN-EN 1993-1-1 [5], PN-EN 1993-1-6 [6], PN-EN 1993-3-1 [7] (lattice supporting structures) and PN-EN 1993-3-2 (shell supporting structures) are to be reckoned with. In addition the European standard PN-EN 50341-2-22:2016 [8] deals with the operating conditions of overhead power transmission lines, specifying the reliability components corrected with respect to the general requirements, and oriented exclusively on this group of steel structures. Analysis of the requirements listed in the codes enumerated above indicates that the system of load and bearing capacity coefficients based on Eurocode 3 and European standard PN-EN 50341-2-22:2016 is incoherent. This is documented in Table 1 and Table 2.

Table 1. Partial coefficients for permanent G and variable: wind W and ice I actions

Result of Actions (1)	Reliability Class RC (2)	Permanent Actions G (3)	Variable Actions	
			Wind W (4)	Icing I (5)
coefficients $\gamma_f$ according to PN-EN 1993-3/1 and 1993-3/2				
disadvantageous	3	1.2	1.6	
	<b>2</b>	<b>1.1</b>	<b>1.4</b>	
	1	1.0	1.2	
advantageous	1, 2 i 3	1.0	0	
coefficients $\gamma_f$ according to PN-EN 50341-2-22:2016				
disadvantageous	3	1.0	1.4	1.5
	2	1.0	1.2	1.25
	1	1.0	1.0	1.0
advantageous	1,2 i 3	1.0	0	0
coefficients $\gamma_f$ according to own research				
disadvantageous	3	1.1	1.5	
	<b>2</b>	<b>1.1</b>	<b>1.4</b>	
	1	1.1	1.3	
advantageous	1,2 i 3	1.0	0	

The partial coefficients of limit state method according to the Eurocode PN-EN 1990 are expressed as product of two components covering the random influences (coefficients  $\gamma_f$  for loads and  $\gamma_m$  for bearing capacity) and modeling errors (coefficients  $\gamma_{sd}$  for loads and  $\gamma_{rd}$  for bearing capacity):

$$\gamma_f = \gamma_f \gamma_{sd}, \quad \gamma_M = \gamma_m \gamma_{rd} \quad (1)$$

Initial specifications regarding the range of values the load coefficients may assume may be found in PN-EN 1993-3/1 and 1993-3/2 for the reliability class RC 2, these values are listed in bold in the Table 1. The values assumed in the abovementioned codes may be derived from the specifications listed in PN-EN

1990 [4], Table A1.2(B), when smaller modeling errors  $\gamma_{sd}$  of constant and variable loads acting on supporting structures of overhead power transmission lines, with respect to other building structures, are accounted for. Such interpretation is doubtful in the case when load coefficients are specified for RC 2 class structures according to the code PN-EN 50341-2-22:2016 (reduction of coefficients:  $\gamma_G$  from 1.15 to 1.00 and  $\gamma_Q$  from 1.50 to 1.20÷1.25 is not justified).

Differentiation of reliability in both standard approaches raises serious doubts. The value of load coefficient may not be assumed arbitrarily, but has to be justified statistically, with proper analytical formulae (cf. [1]). In the basic case the reliability condition for each structure describes the relationship, in which computational values of bearing capacity  $R_d$  and load effects  $E_d$  are compared:

$$R_d = \bar{R} - \beta_R \mu_R \geq E_d = \bar{E} + \beta_E \mu_E \quad (2)$$

Specifications of partial coefficients attributed to the bearing capacity  $\gamma_M$  for reliability classes other than RC 2 may be derived by application of correctional factor  $K_R$ , having the form:

$$\bar{R} - 0.8 \beta_{RC2} \mu_R = K_R (\bar{R} - 0.8 \beta_{RC} \mu_R) \quad (3)$$

to the left hand side of the formula (2), and thus

$$K_R = \frac{1 - 0.8 \beta_{RC2} v_R}{1 - 0.8 \beta_{RC} v_R} \quad (4)$$

where  $v_R = \mu_R / \bar{R}$  – variable random material strength coefficient.

Analogous explanation may be made for variable loads  $Q$  (characterized by the average value of  $\bar{Q}$  and standard deviation  $\mu_Q$ ), considered at the right hand side of formula (2), by introduction of the correctional factor  $K_{Fi}$ :

$$K_{Fi} (\bar{Q} + 0.7 \beta_{RC2} \mu_Q) = \bar{Q} + 0.7 \beta_{RC} \mu_Q \quad (5)$$

$$K_{Fi} = \frac{1 + 0.7 \beta_{RC} v_Q}{1 + 0.7 \beta_{RC2} v_Q} \quad (6)$$

where  $v_Q = \mu_Q / \bar{Q}$  – random load  $Q$  variability coefficient.

For the structures belonging to RC 3 class, designed for the sample reference period of  $T = 50$  years, the reliability coefficients according to the Table B2 of the code [4] are equal to:  $\beta_{RC2} = 3.8$  and  $\beta_{RC} = 4.3$ , respectively; thus the formulas (4) and (6) for bearing capacity and load reduction coefficients depend only on corresponding variability coefficients:

$$K_R = \frac{1 - 0.8 \cdot 3.8 v_R}{1 - 0.8 \cdot 4.3 v_R} = \frac{1 - 3.04 v_R}{1 - 3.44 v_R}, \quad (7)$$

$$K_{Fi} = \frac{1 + 0.7 \cdot 4.3 v_Q}{1 + 0.7 \cdot 3.8 v_Q} = \frac{1 + 3.01 v_Q}{1 + 2.66 v_Q}. \quad (8)$$

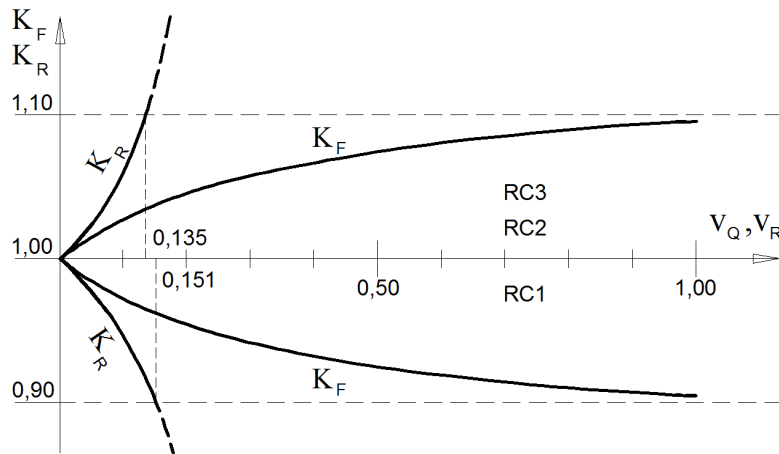


Fig. 2. Graphs of reduction coefficients  $K_R$  and  $K_{Fi}$  according to the formulas (7)-(10), cf. [1]

For the RC 1 class, the reliability coefficient, according to the Table B2, is equal to  $\beta_{RC} = 3.3$ ; thus the formulae (4) and (6) for reduction coefficients have the following form:

$$K_R = \frac{1 - 0.8 \cdot 3.8 v_R}{1 - 0.8 \cdot 3.3 v_R} = \frac{1 - 3.04 v_R}{1 - 2.64 v_R} \quad (9)$$

$$K_{Fi} = \frac{1 + 0.7 \cdot 3.3 v_Q}{1 + 0.7 \cdot 3.8 v_Q} = \frac{1 + 2.31 v_Q}{1 + 2.66 v_Q} \quad (10)$$

The graphs of reduction coefficients as a function of material strength variability coefficient  $v_R$  and variable load variability coefficient  $v_Q$  are depicted in fig. 2. In view of the above results, the differentiation of the reliability requirements set for building structures according to the recommendations of the code PN-EN 1990 is fully justified and safe ( $K_R = 1$  for RC 2 class and correction of the load coefficients  $\gamma_Q$  for classes RC 1 and RC 2 by the correction factors  $K_{Fi}$  having the values listed in Table 2).

Supporting structures of the power transmission lines are designed to be made using unified range of the rolled products: angle irons or plates, which are

characterized by small negative thickness tolerances. Safe estimation of constant loads  $G$  is a result of designing for nominal dimensions, this justifies the simplifications in formulas (8) and (9):  $v_G = v_Q = 0$ , as well as  $K_{FG} = 1.0$ . Icing and wind are characterized by substantial variability, thus a correction of the load coefficients for variable loads according to the Table 2 is justified.

Table 2. Values of the  $K_{Fi}$  coefficients for actions according to PN-EN 1990 [4]

Correction coefficient	Reliability class		
	RC1	RC2	RC3
(1)	(2)	(3)	(4)
$K_{Fi}$	0.9	1.0	1.1

Analyzing the data presented in the Table 1 one may observe, that the ratio of wind and icing load coefficients  $\gamma$  for various reliability classes is not preserved, both for recommendations contained in the code PN-EN 50341-2-22:2016 as well as codes PN-EN 1993-3/1 and 1993-3/2. Graphs depicted in fig. 2 show the limiting values  $0.9 \leq K_{Fi} \leq 1.1$ . Our own specifications, rounded down to 0.1 are in perfect agreement with analytical results.

### 1.3. Numerical analysis of bearing capacity for shells with telescopic joints

Shell model is usually assumed to analyze the bearing capacity of steel towers with telescopic joints.

Static linear (LA) analysis is the simplest method of analysis available, with simple linearly elastic material model and contact phenomena accounted for. The interaction between two independent, but adjoining shells is ensured by the tools available in the FEM computational environment. Contact is defined on the common boundary of the shells. The displacements in all three directions of the orthogonal coordinate system are restricted at the bottom edge of the joint. The nodes located at the top edge of the upper shell assembly are usually connected with rigid elements. This approach does not perfectly correspond to the real behavior of the structure, but if proper care is taken when the length of the modeled section is determined the errors induced may be limited. The same applies to the fixing of the lower shell assembly.

The numerical simulations performed allow for easy determination of the correct tower section length, at which it is possible to obtain reliable results of calculations. Quadrilateral shell elements are selected for analysis, as these elements are very convenient in modeling the regular geometry of a shell having polygonal cross-section and shall correctly model the performance of the shell subjected to loads. Two finite elements of this type, namely CQUAD4 and CQUAD8 are available in NASTRAN solver. These are isoparametric elements, taking into account the interaction of membrane and bending stiffnesses, but differing in the number of nodes in each element. According to experience, with

the same number of nodes in the whole structure the CQUAD8 elements yield better quality results in static analysis.

The contact between touching surfaces in the linear analysis is accomplished via contact surfaces, and in the nonlinear analysis – via linear gap elements. Static and dynamic friction coefficients may be defined. Finite elements of the CGAP type generate three possible states on the boundary between two touching surfaces:

- relative sliding of the surfaces, when the friction coefficient is equal to zero,
- static pressure between the surfaces, when the tangent force between the surfaces is lower than the maximum static friction force,
- relative sliding of the surfaces, when the tangent force between the contacting surfaces exceeds the maximum value of the static friction  $F_{\max}$ :

$$F_{\max} = \mu F_N, \quad (11)$$

where:  $\mu$  – static friction coefficient,

$F_N$  – force normal to the contacting surfaces.

Friction coefficient for steel surfaces subjected to hot dip galvanization is assumed to be in the range of 0.1÷0.3, depending on whether the structure is loaded primarily in a static or a dynamic manner. The loads acting on the supporting structures of overhead power transmission lines are predominantly of static character, thus the upper bound of the range may be assumed. This increases the bearing capacity of the telescopic assembly joint.

## 2. An example of telescopic joint modeling

### 2.1. Assumptions for numerical calculations

The numerical analysis results are presented for a telescopic joint in a sample strong tube tower designed as a part of a 110 kV overhead power transmission line Munina-Lubaczów construction project to the designed 110/15 kV transformer station Korczowa. The analyzed section is a two circuit one, with span lengths of 240 to 360 m. Single spans, or occasionally pairs of adjacent spans constitute a strain section.

The tube tower of the type Orc M2+32, designated M2/47, designed for the considered line functions as tangent strain and angle strain tower. The routing angle at the locations of this tower is between 160 and 180 degrees. Total height of the tower is equal to 57 meters. The structure comprises of 6 tapered sections having hexadecagonal cross-section. The taper is equal to 21 mm per one meter of section height. The diameter of circle inscribed into the contour is equal to 2.20 m at the support and 1.00 m at the top of the tower. The tower is fitted with six working cross beams and two grounding ones. The conducting and grounding wires are suspended in a strain mode at all 8 supporting points. The steel-aluminum wires AFL 6–240 mm<sup>2</sup> are used as conductors, while steel-aluminum wires AFL 1–750 mm<sup>2</sup> are used as grounding wires.

The following design assumptions have been made regarding the supporting structure:

1. The tension in the conductor wires at  $+10^{\circ}\text{C}$  is equal to 8.00 kN and 16.32 kN in the spans adjacent to the considered tower, while the tension in the grounding wires is equal to 2.94 kN and 6.93 kN, respectively.
2. The primary stress, i.e. the stress existing in the wires at the ambient temperature of  $-5^{\circ}\text{C}$ , when the standard icing occurs. In the conductors this stress is equal to  $\sigma = 55 \text{ MN/m}^2$  and  $\sigma = 100 \text{ MN/m}^2$ , while in the grounding wires it is equal to  $\sigma = 100 \text{ MN/m}^2$  and  $\sigma = 180 \text{ MN/m}^2$ .

The telescopic connection of the two middle tower sections is analyzed numerically. Both segments are made of 14 mm thick steel plate. Segment lengths are equal to 11.4 m and 12.0 m, respectively, and the sleeve length in the joint is equal to 2.70 m, (cf. fig. 3). Both segments are made of S355J2 steel.

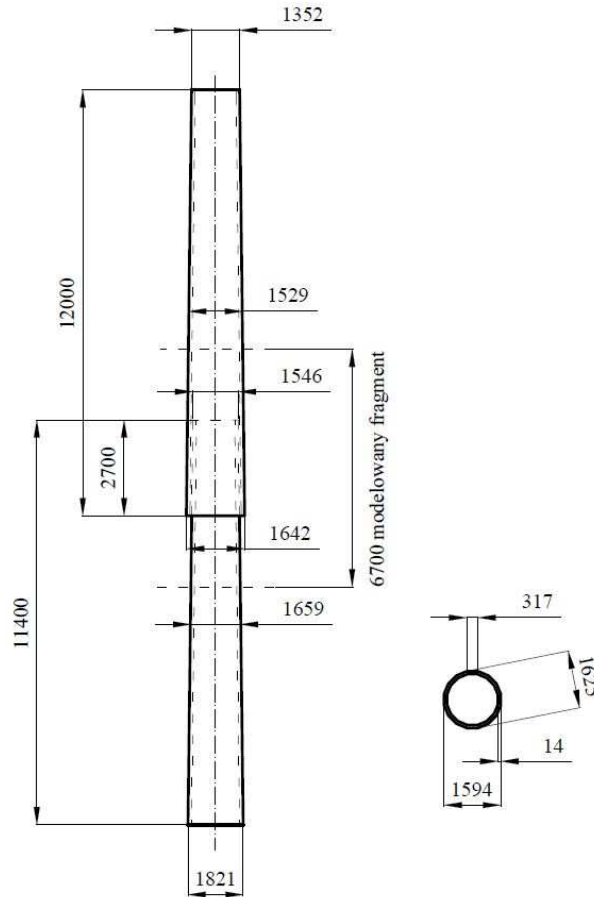


Fig. 3. Basic dimensions of the analyzed assembly sections in the telescopic joint

## 2.2. Numerical model of the joint

Numerical model of the tower segment has been built, having the length of 6.70 m, comprising of a section 2.70 m long, where the two connecting shell sections overlap, and two additional segments having the length of 2.00 m each, located above and below the overlapping zone. A fragment of the shell model of the joint is depicted in fig. 4.

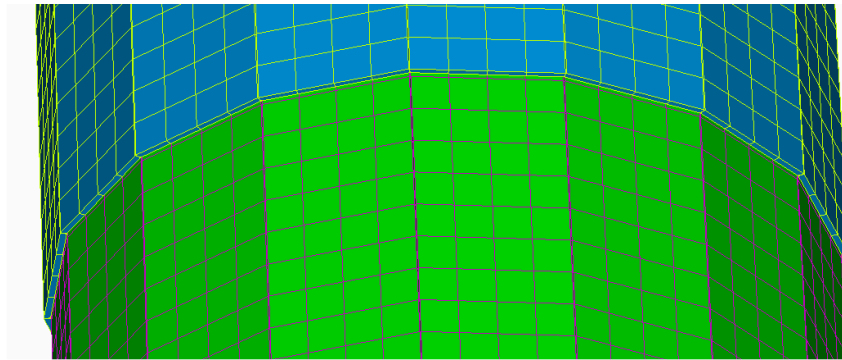


Fig. 4. Fragment of the shell model of the joint with 8x8 cm finite element mesh

The model has been loaded with a set of sectional forces:  $M_{ED} = 3,166.0$  kNm,  $N_{ED} = 190$  kN and  $V_{ED} = 157$  kN, which were computed during the global statical analysis for authoritative combination of loads acting on the tower. The numerically nonlinear analysis including the contact between elements required several simplifying assumptions, which do affect the final precision of results, especially when the model undergoes large deformations. In particular the load is applied to the shell in single step, and the interaction mode of the contacting elements is set at the beginning of the analysis. Each pair of finite elements may at any moment during the analysis be in one of three mutually exclusive states: separation (no contact), compression (tangent forces lower than the maximum static friction force) or slip (tangent forces exceed the maximum static friction force). The linear analysis leads to the results, which are strongly dependent on the assumed finite element mesh size, but the increase in mesh density usually leads to the results, which are in better agreement with the results of nonlinear analysis.

The influence of finite element mesh size on the final results expressed as the equivalent stresses in the joint area is depicted in fig. 5. In fig. 5a), for the  $8 \times 8$  cm element size, the maximum equivalent stress value is  $\sigma = 275$  MN/m<sup>2</sup> and occurs in isolated points at the bottom edge of the upper section, while in fig. 5b) for the  $4 \times 4$  cm element size the maximum equivalent stress value is  $\sigma = 241$  MN/m<sup>2</sup>.

According to the analyses performed by the authors, the finite element mesh composed of  $16 \times 16$  cm elements yields the extreme equivalent stresses  $\sigma = 175 \text{ MN/m}^2$ , thus the obtained results are ambiguous. Taking the results depicted in fig. 5a) as binding, one may state that the limit state condition, taking into account the plastic bearing capacity factor  $\gamma_M = 1.1$  is satisfied, as:  $\sigma = 241 \text{ MN/m}^2 < 355/1,1 = 323 \text{ MPa}$ .

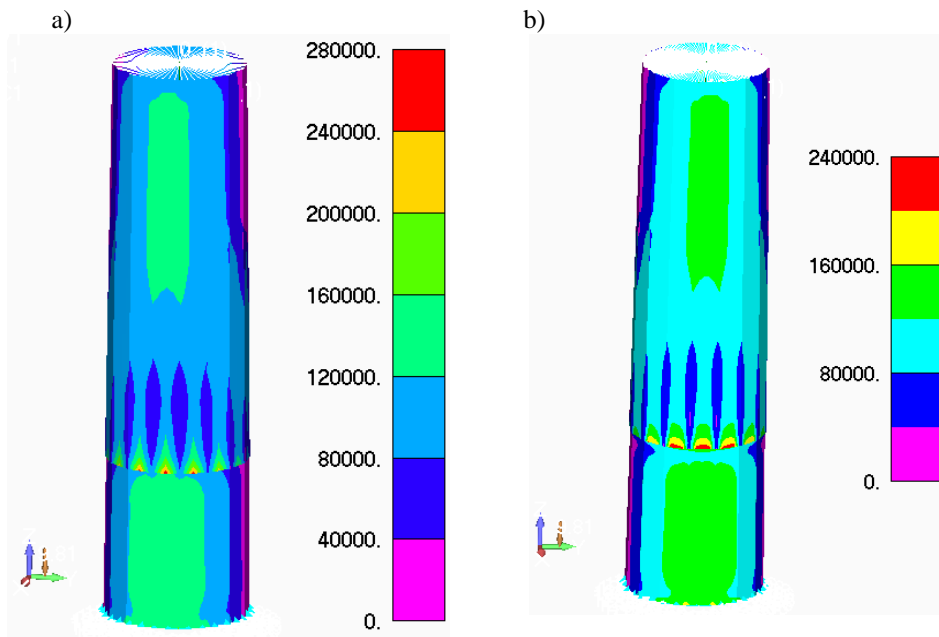


Fig. 5. Map of equivalent stresses for: a)  $8 \times 8$  cm, b)  $4 \times 4$  cm finite element mesh sizes

### 3. Summary

A comparative analysis of load coefficients for variable wind and icing actions has been performed in this paper with respect to the supporting structures of the overhead power transmission lines according to the Eurocode 3 and European code PN-EN 50341-2-22:2016 [8], for various reliability classes of such structures. The results of the analysis indicate, that the specifications present in these codes raise doubts, as they do not satisfy the analytical criteria resulting from the functional relationships between reliability classes of building structures. In addition, the coefficients mentioned above, and listed in the code PN-EN 50341-2-22:2016 according to the national recommendations are underestimated with respect to the specifications assumed for the structures of this type in the Eurocode PN-EN 1993-3. The load factor calibration errors demonstrated here are combined with modeling errors due to the application of linear analysis of telescopic joints in the tubular towers supporting overhead

power transmission lines. Using computer modeling tools and linear, elastic shell theory, the modeling error of telescopic joints in a sample tower supporting overhead power transmission line rated at 110 kV is estimated. It should be noted, that modeling of a telescopic joint, based on the linear analysis leads to computational errors due to the simplifying assumptions and arbitrarily assumed dimensions of finite elements in the finite element mesh. In the example considered here the error is equal to  $\gamma_{sd} = 275/241 = 1.14$ .

## References

- [1] Gwózdź M.: Reliability Component Differentiation in Building Structures Made of Timber. Technical Transactions 2/2018, Civil Engineering, Kraków 2018.
- [2] Eurocoles Kromiss, Energoprojekt Cracow: Catalogue of typical designs for pipe columns supporting 110 kV overhead power transmission lines.
- [3] Mendera Z., Szojda L., Wandzik G.: Steel supporting structures of high voltage overhead power transmission lines, Scientific Publishers PWN, Warsaw 2012 (in Polish).
- [4] PN-EN 1990. Eurocode. Basics of structural design. PKN, Warsaw 2004.
- [5] PN-EN 1993-1-1. Design of steel structures. Part 1-1: General rules and rules for buildings. PKN Warsaw 2006.
- [6] PN-EN 1993-1-6. Design of steel structures. Part 1-6: Reliability and stability of shell structures. PKN Warsaw 2009.
- [7] PN-EN 1993-3-1. Eurocode 3. Design of steel structures. Towers, masts and chimneys. . Part 3-1: Towers and masts. . Part 3-2: Chimneys. PKN, Warsaw 2008.
- [8] 50341-2-22:2016. Overhead electric al lines exceeding AC 1 kV. Part 2-22: National Normative Aspects (NNA) for Poland (based on EN 50341-1:2012). CEN-CENELEC Brussels 2016, PKN Warszawa 2016.

*Przesłano do redakcji: 01.05.2018 r.*

*Przyjęto do druku: 15.06.2018 r.*



Grzegorz GREMZA<sup>1</sup>  
Jan ZAMOROWSKI<sup>2</sup>

## DAMAGE ANALYSIS OF THE BLADE TO THE ROTOR HUB CONNECTION IN THE WIND TURBINE

The paper analyzes possible causes of bolts fracture in the connection of the blade to the hub of the wind turbine rotor. This failure has been growth shortly after the wind turbine was started, a few days after the storm. During the storm, electric power was turned off in the whole surrounding area for many hours, therefore it was impossible to control the device. After an initial analysis of failure modes in other wind turbines, it was found, that the bolts failure in the analysed case may be regarded as quite rare. Due to the fact that a significant part of bolts was broken brittle (flat fracture surfaces and lack of permanent elongation), it was decided to analyse the structure of the material in the direction of stress corrosion and hydrogen embrittlement. Among others, microscope analysis of fracture surfaces after their proper cleaning from corrosion products was carried out. The broken bolts were made as undersized, what is mainly used in fasteners intended for hot-dip galvanizing. On the basis of the purchase documentation analysis, it was presumed that the bolts were not galvanized by their manufacturer, which is obliged to perform the routine inspection in production process preventing the introduction of the hydrogenated bolts into the market. Besides the bolts examination, the scenarios of connection loads in extreme situations, in particular the impact of wind with high energy in the most unfavourable direction relative to the blade and nacelle, as well as the force resulting from the impact of the rotating blade on the tower that preceded the collapse of the whole structure, were considered. Conclusions from the performed tests and calculations by use of two calculation models of the connection were presented.

**Keywords:** undersized bolts, mechanical properties of bolts, wind turbine, blade failure, model of joint

### 1. Introduction

In recent years, reuse of second-hand structures of wind turbines in Poland has become frequent. In these turbines, failures consisting in the loss or failure of blade fragments due to progressive fatigue process or production defects [1] as well as excessive rotor speed, are quite common. Less common is a detachment of

---

<sup>1</sup> Corresponding author: Grzegorz Gremza, Silesian University of Technology in Gliwice, Department of Building Structures, ul. Akademicka 5, 44-100 Gliwice; tel. 322372224; ggre@interia.pl

<sup>2</sup> Jan Zamorowski, University of Bielsko-Biala, Faculty of Materials, Civil and Environmental Engineering, ul. Willowa 2, 35-959 Bielsko-Biala; zamski@interia.pl

blade from the rotor or the entire rotor from the nacelle due to the failure of bolted connections. This paper discusses the case of the bolted connection between blade and hub, which failure was accompanied by the collapse of the tower of a typical wind power plant. The power plant consisted of a steel tower, a nacelle and a 58 m in diameter rotor with an axis at 71 m above the ground (Fig. 1a).

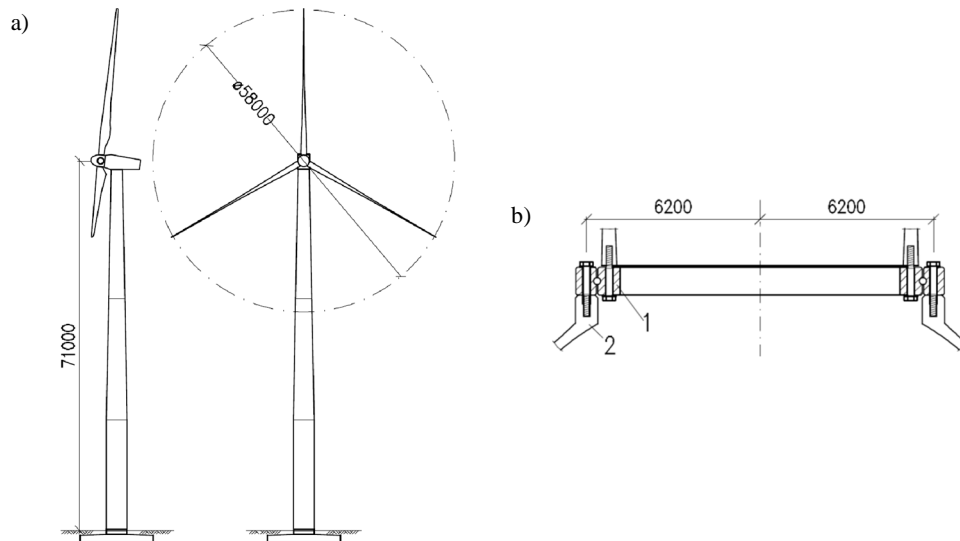


Fig. 1. Wind turbine: a) general view, b) joint between blade and hub, 1–bearing, 2–hub

## 2. Joint between blade and hub

In the connection of the blade to the hub four-point contact bearings, bolted on one side to the hub and on the other side of the blade, were used (Fig. 1b). The hub was made of nodular cast iron in a spherical form and fixed to the main shaft bearing. In the hub, threaded holes were made and in the blade, threading inserts were placed. To connect the bearing to the hub, 52 bolts M24 class 10.9 with the mark W of the manufacturer and with the additional marking U (10.9U) i.e. with undersized thread were used (Fig. 2). Such a thread is sometimes executed to maintain the required minimum clearance for the threaded connection after applying a thick layer of zinc coating in the hot dip galvanizing process.

As a result of undersize threading, the effective cross-section of the bolt decreases slightly. Moreover, bolts with an undersized thread should not be combined with nuts with oversized thread. In a given case it is difficult to prove whether the thread in the threaded hole was oversized. On the other hand, it was much longer than a thread in a typical nut, which should compensate for its likely weakening due to oversizing. In the connection of bearings to the blade, bolt class 10.9 with normal clearance and probably made by another manufacturer were used. Only 10.9U bolts in the connection of the bearing to the hub have been destroyed.



Fig. 2. Bolts in analysed joint: 1–old bolt, 2–new bolt bought in Poland

An important issue related to hot-dip galvanizing is the hydrogen embrittlement of bolts class 10.9. Regardless of the method of threading, these bolts must be galvanized under the manufacturer's control and tested in a proper way for hydrogen embrittlement at the production stage. During the in-situ inspection, it was found that the M24 bolts class 10.9, that was used in a bearing-to-hub connection of the blade detached during the disaster, were galvanized, while on the invoice there is a marking of these bolts "Bolt M24x180 DIN 931 class 10.9 g. 70 ", without any information on the coating of these bolts with a zinc coating. The certificate also does not contain any information about galvanizing these bolts. Therefore it can be assumed that these bolts were galvanized outside the bolt factory.

### 3. Wind turbine damage

The disaster was preceded by a period of a few days strong winds, during which the wind turbine was at least twice immobilized: for the first time automatically due to exceeding the permissible wind speed and for the second time due to lack of power supply. A few minutes after it was restarted, disaster has occurred. One of the blades crashed into the tower causing its brake-down (Fig. 3), what was observed by the windmill owner. This blade was detached from the rotor and discarded (thrown) far away from the windmill. During the in-situ inspection, it was found, that this blade's shells have been stripped off (Fig. 4a) and its supporting beam (spar) has been partly broken at the point of impact on the tower. A view on a bearing devoid of broken bolts has been shown in Fig 4b.

The thesis was made that the following causes of the disaster could have been:

- failure of the blade to the hub connection due to plasticization of a part of bolts or the brittle fracture of the remaining bolts,
- detaching the shells of the blade from its supporting beam and blocking of the blade's movement at the level of approximately + 52.7 m; this possibility is indicated by the damage of the blade and the tower occurring at this level,
- a collapse of the tower due to its kinking in the section with the most used bearing capacity.

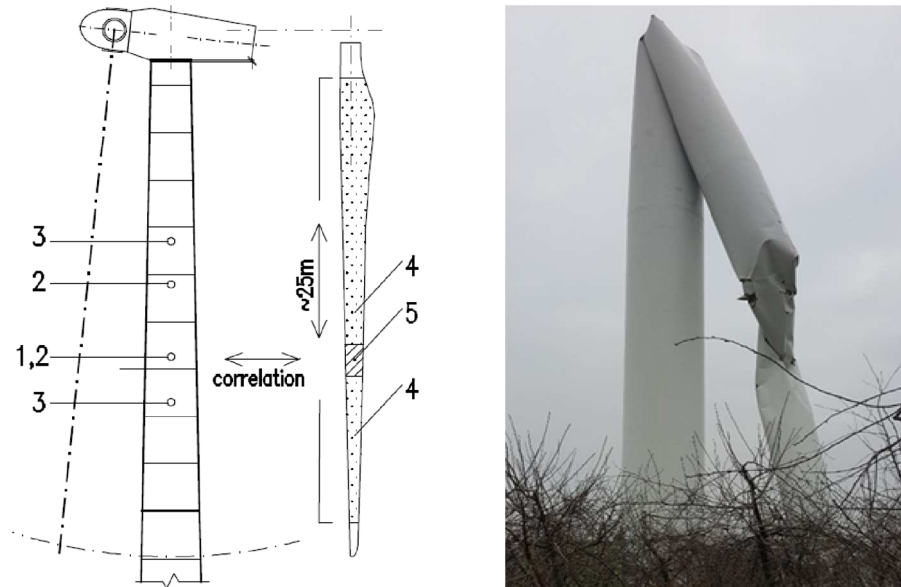


Fig. 3. Wind turbine damage: 1–point of the blade impact, 2–ends of twisted section, 3–ends of braking, 4–area of a blade without shells, 5–broken section of a blade

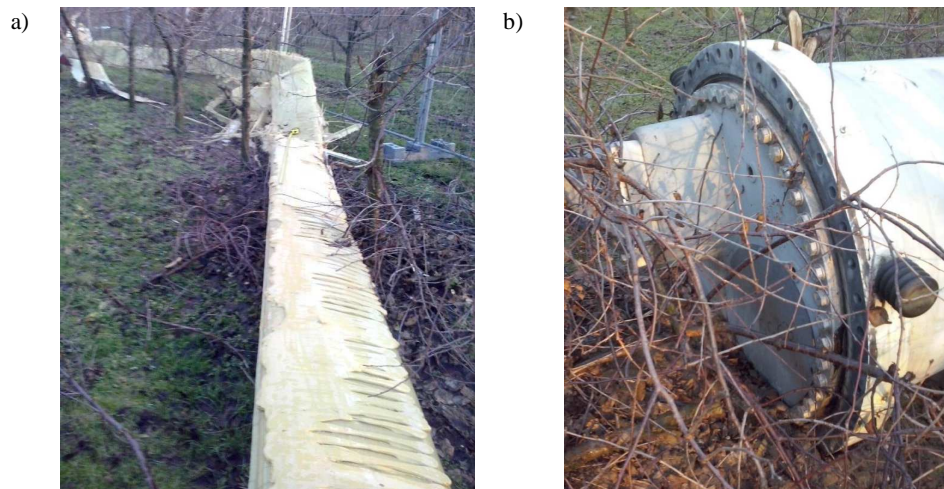


Fig. 4. Detached blade: a) supporting beam without shells, b) bearing without bolts

The shaft of the tower in the level of the blade's impact has been twisted, which may indicate a hit as a factor initiating its collapse. On the basis of calculations, the tower collapse due to its insufficient load capacity was excluded. The tower was calculated assuming that the level of its quality declared in the documentation was preserved. It was decided to carry out a wide-spread analysis of the whole structure as well as possible problems in the connection.

## 4. Bolts failures

The immediate cause of the failure of the blade-to-rotor connection was a fracture of bolts, what is rare in wind turbine failures. During the inspection it was found, that some of the bolts at about 1/3 of the circumference of the joint were destroyed with very small elongation or brittle (Fig. 5).



Fig. 5. The brittle fracture surface of bolt and a hole with end of bolt

The remaining bolts on about 2/3 of the circumference of the joint were destroyed plastically, some of them with very visible elongation and necking, which were estimated at up to 20%. The fracture surfaces of a part of bolts indicated a brittle fracture.

## 5. Bolts testing

### 5.1. Hydrogen content measurements

Bolt material was qualified as a ferritic steel. Steels of this type in bolts class 10.9 are a material that is susceptible to the adverse effects induced by possible introducing of hydrogen. For this reason, one of the bolts, with brittle fracture surface, has been examined for hydrogen content. It was obtained a hydrogen content of 7 ppm for the bolt in the condition with the coating, and after removing the coating – 1.5 ppm. The examined bolt has been used in the connection since 2015.

Atomic hydrogen can be introduced into the metal during the galvanizing process or during contact with the atmosphere due to the creation of an electric cell in a moist connection. In a case when hydrogen would get into the bolt in the hot-dip galvanizing process, the bolt usually undergoes a brittle failure in the first twenty-four hours. On the other hand, if the brittle fracture of the bolt would appear after a longer period of its exploitation, it could mean that hydrogen was

introduced into the bolt from the environment in which the bolt worked, which can also be proved by the much higher hydrogen content on the surface of the zinc coating (7 ppm) compared to the hydrogen content under the zinc coating. Hydrogen content of 1.5 ppm on the surface of the steel could not be the cause of its brittle fracture immediately before or during the disaster.

## 5.2. Analysis of fracture surfaces

The fracture surfaces of three selected bolts were examined. Tests confirmed macroscopic observations regarding the manner of their destruction. The fracture in bolt '1' was characterized with a ductile morphology with characteristic cavities (dimples) typical of this type of fracture (Fig 6a).

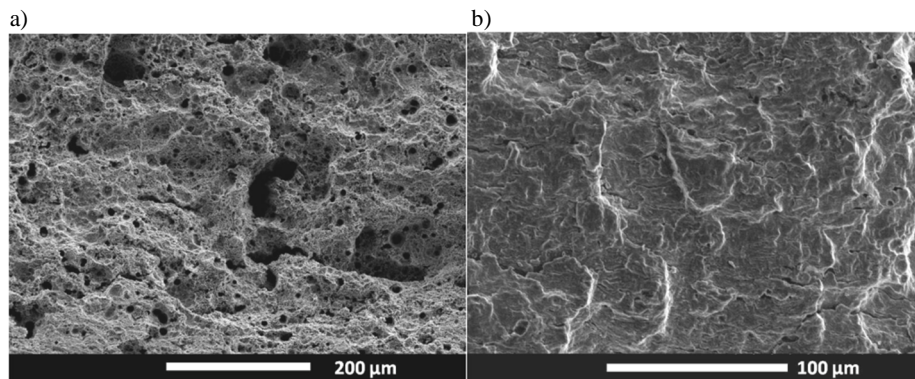


Fig. 6. Fracture surfaces of bolts: a) ductile of bolt 1, b) brittle of bolt 3

Such a fracture testifies destruction of the material after exceeding the yield point. The fracture of bolt 3 was mainly brittle (Fig. 6b) and the fracture of bolt 2 was mixed (both brittle and ductile).

Almost over the whole surface of the fracture of bolt 3, characteristic lines resembling fatigue beach marks are visible (Fig 7a). The areas between these lines are brittle. The appearance of the fracture suggests that the material was destroyed gradually, e.g. during alternating bending of the bolt. On the fragment of the fracture of the bolt 2, near its surface, characteristic lines indicating the fatigue cracking are also visible (Fig. 7b). Such a character of the fracture, at the surface, can occur not only as a result of alternating bending of the bolt but also in the case of hydrogen-induced cracking.

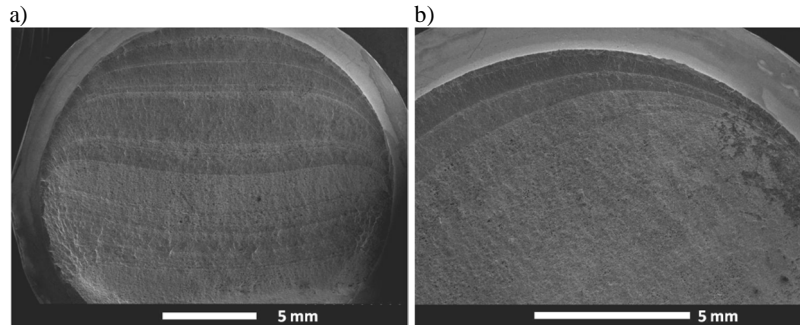


Fig. 7. Fracture surfaces of bolts: a) bolt 3, b) bolt 2

Theoretically, there should be no significant stress amplitudes in a preloaded bolt, what is reflected in the recommendation given in standard [2] allowing to adopt a reduced range of stress fluctuating for such a bolt. The brittle fracture of the bolt material characterized with symmetrical fatigue beach marks (beach lines) relative to the axis passing through the centre of the cross-section (see Fig. 7a) may indicate an alternate bending of the bolt after a separation was created in the connection of the blade with the rotor. Therefore, the hypothesis may be put forward, that the bolts in the tensioned zone had broken up first. Then, in partly damaged joint an alternate bending of bolts in compression zone and as a result their fatigue failure occurred.

### 5.3. Tensile tests of bolts

Two specimens of  $\phi 10$  in diameters with a gauge length equal to its five diameters, taken from bolts used to assemble the structure, were tested. Tensile strength ( $R_m$ ) of 954 MPa and 962 MPa, as well as the yield stress ( $R_{p,0.2}$ ) 815 MPa and 860 MPa and elongation from 15.2% to 15.8% were obtained. The strength of the bolt material was slightly smaller than declared and corresponded to the theoretical class 9.9. However, this strength was sufficient to transfer all design loads.

## 6. Joint modelling

### 6.1. Simple linear-elastic model

In the connection of the blade with the hub (Fig. 8a), a linear distribution of deformations was assumed, as in the structural members subjected to alternate actions [3]. It was assumed that the load in the compression zone is transferred by a pressure of a ring of bearing on the hub, and in the tension zone – by the bolts tension. In this model, a pressure of the ring on the hub caused by preloaded bolts is not taken into account. The effective section was determined, in which the bolts transmit tension and the flange transfers pressure (Fig. 8b). In the calculation of the connection characteristics, the nominal cross-section of the bolt has been adopted.

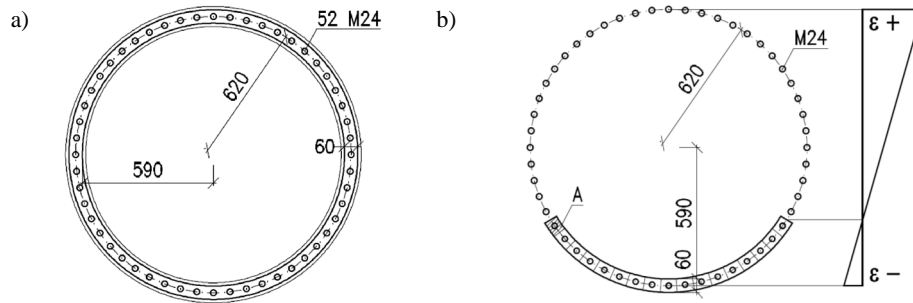


Fig. 8. Connection: a) view, b) scheme of calculation (effective cross-section)

## 6.2. Mechanical model

The connection of the rotors' blade to the hub was calculated using a mechanical model consisted of 52 basic components of the joint. The number of these components corresponds to the number of bolts. Each component was modelled as a spring (Fig. 9), whose axis coincided with the bolt axis, both in tension and compression zone. The stiffness of the spring in the compression zone was estimated based on the elastic shortening of the pre-compressed part of the ring (bearing race) and the hub with a length corresponding to 1/52 of the connection perimeter and a thickness of 15 cm – see Fig. 9. In the calculations, Young's modulus  $E = 210$  GPa and the pressure area of the ring for the hub  $A = 39.5$  cm<sup>2</sup> (see fig. 8b) were adopted. The stiffness of the spring  $k_c = EA/l = 5\,530$  kN/mm was obtained, where  $l = 150$  mm is an effective length of the spring – see fig. 9.

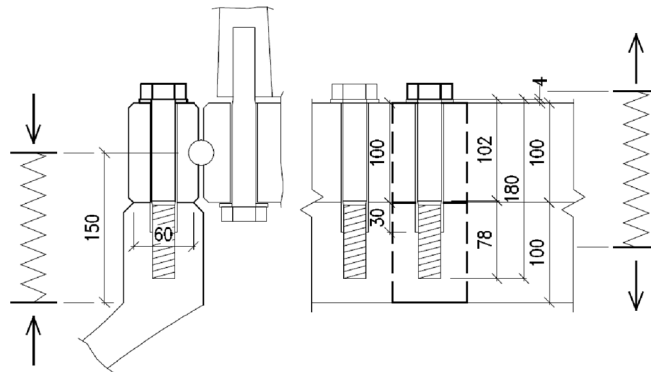


Fig. 9. Fragment of the joint and its modeling as springs in compression and tension zones

The elastic elongation of the not-tightened bolt was described by formula [4]:

$$\delta_y = \frac{F_y}{E} \left( \frac{0,4k + l_s}{A} + \frac{l_g - l_s}{0,5(A + A_s)} + \frac{l_t + 0,6}{A_s} \right) \quad (1)$$

Elongation of the preloaded bolt in the ultimate limit state depends significantly on its dimensions. In the bolts class 10.9, at the moment of their fracture, the shank deformation of the section without thread is still elastic. According to [4], the formula was adopted:

$$\delta_y = \frac{F_u}{E} \left( \frac{0,4k + l_s}{A} + \frac{l_g - l_s}{0,5(A + A_s)} + \frac{F_u}{E} \cdot \frac{l_t + 0,6 \text{ m}}{A_s} + \frac{F_u - F_y}{\alpha E} \cdot \frac{l_t + 0,6 \text{ m}}{A_s} \right) \quad (2)$$

In formulas (1) and (2):  $A$  – the gross cross-section area,  $A_s$  – the tensile stress area,  $k$  and  $m$  – head and nut height,  $l_s$  – length of unthreaded shank (body length),  $l_g - l_s$  – transition,  $l_t$  – thread length from the transition to the beginning of the nut,  $\alpha$  – coefficient equal to 0.013 for class 10.9 bolts,  $E$  – Young's modulus,  $F_y = A_s f_{yb}$ ,  $F_u = A_s f_{ub}$ .

The extension spring characteristic in the tension zone of the connection was determined under the following assumptions:

- until the separation is created, at the force equal to the preloading force magnitude  $F_{p,c} = 0.7 f_{ub} A_s = 247.1$  kN according to [5], the stiffness of parts in the tension zone is equal to the parts stiffness in the compression zone,
- ultimate elongation of the basic component of the joint is obtained by subtracting from the total elongation of the bolt defined by the formula (2) the part of its elastic elongation which was utilized during its tightening (0.473 mm) and adding the value resulting from the reducing the contact pressure between the ring and the cooperating hub fragment (0.045 mm); such assumption results from relaxation of the rigid ring under external force without essential increase of the force in the bolt – see e.g. [6–8].

The obtained characteristic of the basic part of the joint in the tension zone is shown in Figure 10b.

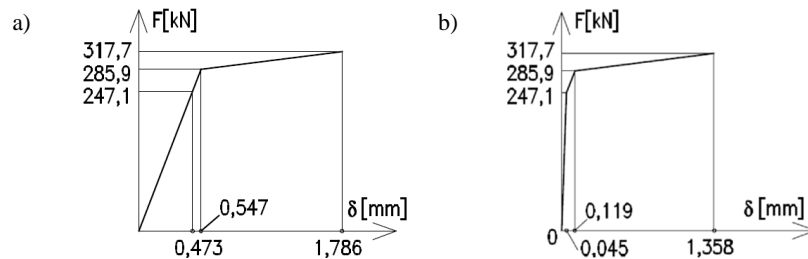


Fig. 10. Force – displacement characteristics: a) for bolt M24 class 10.9, with the actual length of its shaft and its threaded part b) for the basic component in tension in the pre-stressed connection

The bending moment in the connection was applied in the centre of gravity of the ring using fictitious finite elements with a high stiffness, connected to the basic parts.

The simple mechanical model described above could be used because there was no prying effect in the connection under consideration, and, except bolts, there was no plasticization of other parts, what was considered e.g. in [9–10].

## 7. Loads acting on the connection and the bolts effort

### 7.1. Extreme wind load

The calculations were made for the most unfavourable blade position in relation to the wind direction. Force coefficients were adopted on the basis of the data included in many publications. Due to the fact that wind turbines are automatically turned off during extreme wind, it was taken into account in the calculations, that during such wind the blades do not rotate. The estimated with this assumption bending moment in the connection of the blade to the hub will not exceed 1 423 kNm for the standard wind. In the days preceding the disaster, the speed of the wind was close to the standard wind speed, and on the day of the disaster these speed during gusts reached up to 15 m/s.

### 7.2. Load caused by the blade collision with the tower

Adopting the highest operational rotational speed of the rotor  $\Omega = 30.8$  rpm, the velocity at the point of the centre of gravity of the blade  $V = 25.65$  m/s has been obtained. It was assumed that the two upper blades stop as a result of blocking the movement by the third lower one, which acts as a brake together with the tower (similarly to a bump post e.g. in crane girders). The upper two blades (Fig. 11a) act on the axis of the system with the horizontal force  $F_{hub}$  and the moment  $M_{hub}$ :

$$M_{hub} = 2Fb, F_{hub} = 2F\cos\alpha \quad (3)$$

where:  $\alpha$  – angle of inclination of the blade to the vertical axis (60 degrees),  $b$  – distance of the centre of gravity of the blade from the axis of the hub. The force and the moment will be taken by the system consisted of the tower and the third blade that had collided with the tower. The formula based on the blade's kinetic energy is as follows:

$$0,5mV^2 = Fs \quad (4)$$

where  $s$  – distance that was made by the upper blade in period of time from the lower blade collision with the tower to the stop of the rotary motion inclusive the elastic movement of the tower and the blade itself,  $m$  – blade mass applied in its center of gravity,  $F$  – inertia force acting on the blade.

Adopting the above assumptions and calculating necessary stiffness coefficients, the bending moment in the connection of the lower (blocked) blade to the hub equal to 5 949 kNm was obtained. (Detailed formulas allowing the calculation of the bending moment in the connection together with their derivation will be presented in a separate publication.)

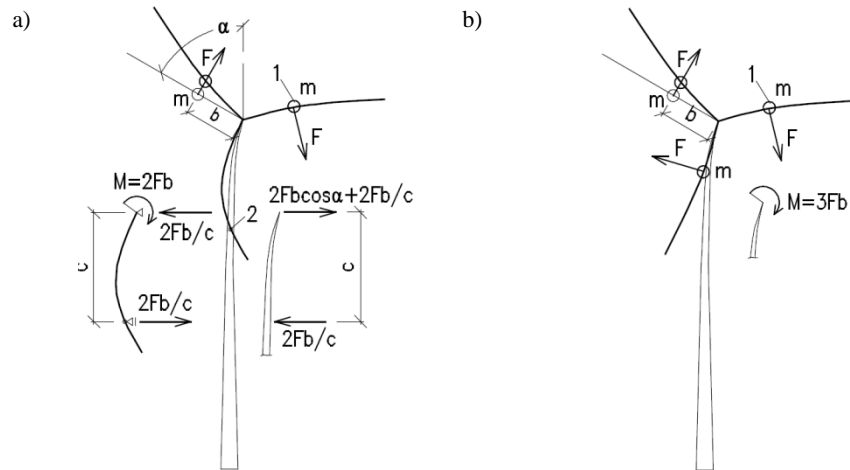


Fig. 11. Schemes of a structure work: a) blade collision with the tower, b) sudden shaft locking

### 7.3. Load caused by sudden shaft locking

The shaft locking may have occurred in a case of damage of pitch mechanism. During the disaster, one of the elements of this mechanism was broken. This could have preceded the disaster or occurred as a result of this disaster.

Similarly to the point 7.3. the greatest operational rotational speed of the rotor 30.8 rpm was adopted. It was assumed that the rotor at the moment of its sudden blockage acts on the tower with a moment (Fig. 11b):

$$M_{hub} = 3Fb \quad (5)$$

and the kinetic energy of one blade is defined by (4) – see point 7.2. Taking into account the rotation and displacement of the top of the tower resulting from the action of the concentrated moment at the hub level and taking into account the susceptibility of the blade to bending, at the root of the blade the moment 5 763 kNm was obtained.

### 7.4. The effort of the bolts depending on calculation model

Table 1 presents the estimated values of bending moments acting in the connection of the blade to the rotor hub and the values of forces in the bolts, obtained using the models described in point. 6.1 and 6.2. The obtained results in the ultimate limit state, after the separation between the ring and the hub occurred, are very similar in both models. Using the connection model described in point 6.1, the highest value of external screw load from wind load is 66.5 kN, and according to the model described in point. 6.2–88.3 kN. These values are much smaller than the preloading force in the M24 bolt 10.9.

Table 1. Values of tension external forces per bolt

Bending moment [kNm]	External tension force per bolt [kN]		Load case
	Simple model point 6.1	Numerical model point 6.2	
1 423	66.5	88.1	Design values of wind load (point 7.1)
152	7.1	9.4	Wind load at speed 15 m/s
5 949	278.3	277.2	Blockage of the blade after collision (p. 7.2)
5 763	269.5	272.9	Shaft blockage (point 7.3)
The characteristic resistance of the M24-10.9 bolt with a normal thread acc. EN 1993-1-8 is 317.7 kN; the design resistance according to PN-B-03200 is 239.0 kN, and according to EN 1993-1-8 – 254.2 kN. Considering that the thread was undersized and that the tensile strength of the bolts was at a level $R_m = 955$ MPa it was obtained $F_{t,Rk} = 285$ kN			

In the case of the load resulting from the blockage of the movement of the blades, bolts fracture would be potentially possible, because the forces acting on them would be slightly larger than their design resistances calculated in accordance with the standards.

## 8. Conclusion

The obtained results of calculation and material tests indicate that the direct cause of damage the connection of the blade to the rotor hub could have been caused by the fracture of bolts in the tensile zone due to the impact of the blade on the tower. During the windmill reassembling in Poland in 2015, there is a high probability that one of the rotor blades manufactured around 2003, was installed in the windmill that has been produced in 2008. A situation occurred, in which shells have been stripped away from the spar practically for the whole length of that blade. Resultantly the rotor movement was blocked and the connection of blade to the rotor has been broken. As a result, the tower has collapsed.

In the connection of the blade to the rotor the undersized high strength bolts, likely galvanised outside the bolt factory, were used. The strength of these bolts was slightly lower in comparison to the nominal strength. The bolts were tightened with the torque moment indicated in the technical documentation of the windmill, without carrying out own tests applying the adopted method of their lubricating. Therefore, the values of the tightening forces introduced into the connection are not known.

The presence on the market of fasteners with mechanical properties deviating from nominal values, low awareness of sellers and technical staff regarding the consequences of using high-strength galvanized bolts outside the bolt factory as well as the principles of correct tightening of high-strength bolts may be worrying.

## References

- [1] Myrent N., Adams D. E., Griffith D. T.: Wind turbine blade shear web disbond detection using rotor blade operational sensing and data analysis. Philosophical Transactions A, 2015, <http://rsta.royalsocietypublishing.org/content/373/2035/20140345>.
- [2] PN-EN 1993-1-9. Eurocode 3: Design of steel structures – Part 1-9: Fatigue.
- [3] Rykałuk K.: Konstrukcje stalowe. Kominy wieże maszty, Oficyna Wydawnicza Politechniki Wrocławskiej, Wrocław 2004.
- [4] Steurer A.: Das Tragverhalten und Rotationsvermögen geschraubter Stirnplattenverbindungen, ETH Zürich, 1999 (in German).
- [5] PN-EN 1090-2: Wykonanie konstrukcji stalowych i aluminiowych. Część 2: Wymagania techniczne dotyczące konstrukcji stalowych.
- [6] Łubiński M., Filipowicz A., Żółtowski W.: Konstrukcje metalowe. Część 1. Podstawy projektowania, Arkady, Warszawa 1986.
- [7] Bródka J., Kozłowski A., Ligocki I., Łaguna J., Ślęczka L.: Projektowanie i obliczanie połączeń i węzłów konstrukcji stalowych – tom 1. Polskie Wydawnictwo Techniczne, Rzeszów 2013.
- [8] Kulak G.L., Fisher J.W., Struik J.H.A.: Guide to Design Criteria for Bolted and Riveted Joints, American Institute of Steel Construction, Chicago 2001.
- [9] Leń D., Ślęczka L.: Efekt dźwigni w śrubowych połączeniach kołnierзовych kształtowników zamkniętych okrągłych, Konstrukcje Betonowe i Metalowe, Wyd. Uczelniane Uniwersytetu Technologiczno-Przyrodniczego w Bydgoszczy, Bydgoszcz 2015, str. 223–230.
- [10] Wojnar A., Kozłowski A.: Sztywność i nośność śrubowych połączeń kołnierзовych rur dużych średnic, Zeszyty Naukowe Politechniki Rzeszowskiej, z. 50 (256), Rzeszów 2008, str. 299–311.

*Przesłano do redakcji: 12.04.2018 r.*

*Przyjęto do druku: 15.06.2018 r.*



Krzysztof KUCHTA<sup>1</sup>  
Rafał SILEZIN<sup>2</sup>  
Paweł ŻWIREK<sup>3</sup>

## EXECUTION AND INSPECTION OF STEEL HOLLOW SECTIONS WELDED JOINTS

The hollow section welded joints require a number of actions before starting welding and appropriate supervision during this operation to achieve joints with adequate quality level, which should be confirmed by the post-completion tests. The execution of hollow section joints is associated not only with welding, but also with cutting and additional machining of edges. In some cases, weld surfacing is also applied to correct sections fit-up. Weld surfacing and thermal cutting can cause local hardening of connected elements. The welding has to be preceded by an assessment of the previous technological processes. The welded joints can be only executed on the basis of detailed Welding Procedure Specifications (WPS). It is advisable to manufacture – in accordance with previously prepared WPS – pre-production joints for testing, proving the ability of the welding personnel to execute welded joints with specified quality, using the available equipment. The quality of welded joints is proved by testing. A type of conducted tests, thus scope and type of welding defects possible to detect, depends on the weld type, wall thickness of connected elements and joint geometry. The authors' experience indicates that the proper execution of the welded joint of hollow sections is difficult task, which often requires pre-production quality testing of the joints.

**Keywords:** steel structures, lattice structures, hollow sections, welded joints, welds

### 1. Introduction

Steel structures of modern buildings or civil engineering works are treated as construction products individually manufactured or custom-made in a non-series process in response to a specific order and installed in a single identified construction work. In this situation, the manufacturer shall provide a declaration of conformity with structure design documentation and PN-EN 1090-2 [4] for steel structure or PN-EN 1090-3 [5] for aluminum structure. In compliance with

---

<sup>1</sup> Krzysztof Kuchta, Cracow University of Technology, Chair of Metal Structures

<sup>2</sup> Rafał Silezin, NDT SERWIS, ul. Niska 12, 31-306 Kraków, biuro@ndtserwis.pl

<sup>3</sup> Corresponding author: Paweł Żwirek, Cracow University of Technology, Chair of Metal Structures, ul. Warszawska 24, 31-155 Kraków, +48 12 6282033, pzwi@op.pl

the building regulations, metal structures designed according to the Eurocodes have to be executed by the manufacturers who hold Certificate of Factory Production Control according to PN-EN 1090-1 [3]. Execution of a steel structure with parameters assumed in the structural design documentation requires the contractor to take a series of actions - both prior the production process and control activities on the subsequent stages of the execution, to verify the quality of the executed work. Selected issues related to the execution and quality control of welded joints in steel hollow sections are discussed in this paper.

## 2. Preparation for welding

Steel hollow sections welded joints have to satisfy the requirements of PN-EN 1090-2 [4] concerning the execution of steel structures, necessary to ensure their adequate bearing capacity, stability, serviceability and durability. The contractor should have the necessary qualifications and use appropriate equipment and measures to achieve compliance with the requirements given in the technical specification and in PN-EN 1090-2 [4].

During the execution of welded joints in circular or rectangular hollow sections appropriate guidelines should be used which include provisions about the preparation of joint faces for welding, weather protection, preassembly for welding, welding processes, drawing of the joint, welding sequence, welding position, welding parameters (e.g. welding current, arc voltage, gas flow), heat treatment conditions, etc. To execute welded joint in hollow sections some additional information is required: start and stop positions of each weld (Fig. 1b, 2b) and – if this is the case – the manner and location on the connected section perimeter where the weld passes from fillet into the butt one. Above mentioned information should be included in Welding Procedure Specification (WPS), prepared in accordance with PN-EN ISO 15609-1 [7].

Before the execution of steel structure, the contractor shall ensure that it is able to make a joint with the parameters described in the structural design documentation. One of the elements of the system that enables to obtain welded joints with the required quality is Welding Procedure Qualification Report (WPQR). The aim of the WPQR is to confirm an ability of the steel workshop to execute a particular joint type, with a given geometry and for specify material type, using welding technique available in the workshop. The WPQR is the basis for elaboration of the WPS. Scope of tests related to welding technique qualification depends on execution class, type of parent material and welding technique. In practice, the qualification of welding technique is most commonly carried out on the basis of PN-EN ISO 15614-1 [8], which enables to qualify welding technique for execution classes EXC2, EXC3 and EXC4. Qualification of the welding technique according to PN-EN ISO 15614-1 [8] includes following stages:

- a detailed analysis of the welding production (determination of the basic variables: type of welding process, parent material group, dimensions of the elements, type of the joint – thickness, diameter, welding positions),
- choosing of joint for tests,
- elaboration of the preliminary Welding Procedure Specification (pWPS),
- execution of test specimen,
- destructive and non-destructive testing for welding techniques,
- issuance of the Welding Procedure Qualification Record (WPQR) by the notified body,
- elaboration of the Welding Procedure Specification (WPS).

If the impact testing is required, tests should be carried out at the lowest temperature at which this property has to be obtained according to appropriate Standard for grade of steel used in tests. In the case of steels manufactured according to PN-EN 10025-6 [2], microscopic test of one specimen is necessary, the picture covering the heat affected zone (HAZ), melting zone, and a filler material zone has to be taken. For elements with temporary corrosion coating, test should be performed by joining the elements with the largest acceptable thickness equal to the nominal coat thickness plus the value of tolerance.

### 3. Profiles preparation and execution of welding

Frequently in their engineering practice, the authors had to deal with documentation in which the issue of welded joint in hollow sections was treated in an imprecise way. In the design documentations, the designers very often put the graphical symbol of the circumferential weld to describe joint on the drawing. There are also structural design documentations where the weld thickness is given only in the form of description with relation to element thickness.

Structures designed according to Eurocode 3 [6] should be executed in accordance with the Standard PN-EN 1090-2 [4] – which, in the case of welded joints in hollow sections, refers to PN-EN ISO 9692-1 [14]. Each of these Standards give different ranges of butt weld application, which may cause that, from a technological point of view, type of weld assumed by the designer is impossible to execute. This issue will be further developed by the authors. For welded joint in rectangular hollow sections PN-EN 1090-2 [4] describes how to prepare profiles for welding for two variants: butt welds (Fig. 1c) and fillet welds (Fig. 1d). Preparation of faces in hollow section joint for the one-side welding should met the provisions of PN EN ISO 9692-1 [14] and PN EN ISO 9692-2 [15].

According to the information given in Figures 1 and 2, both for circular and rectangular hollow sections the same weld type around the whole perimeter can be obtained only if the angle  $\theta$  ranges from  $60^\circ$  to  $90^\circ$ .

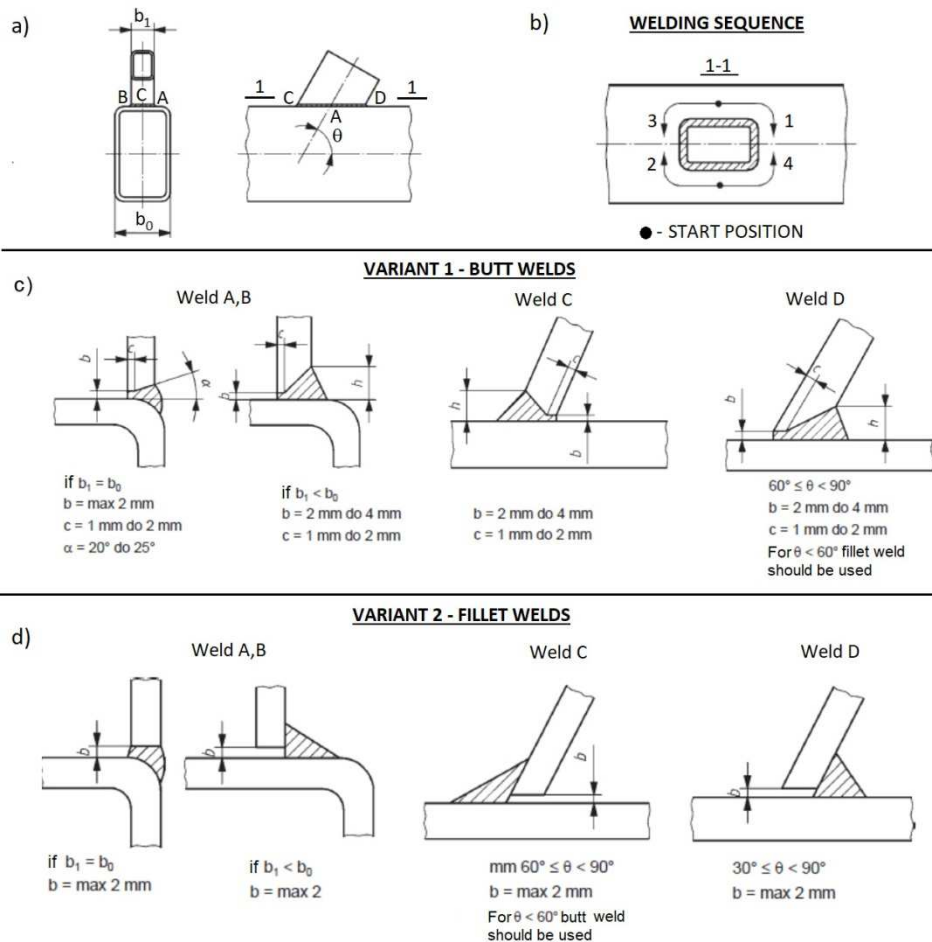


Fig. 1. Welded joints in rectangular steel hollow sections: a) description of welds and dimensions, b) start and stop positions and welding sequence, c) preparation of joint faces in the case of butt welds, d) preparation of joint faces in the case of fillet welds

When the angle  $\theta$  is lower than  $60^\circ$  the weld D (see Fig. 1a, 2a) should be executed as fillet weld, while the weld C – as butt weld. It causes that on the perimeter of the connected sections exist two types of welds – butt and fillet. According to PN-EN 1090-2 [4], welding of branch connections in hollow section with the angle  $\theta$  lower than  $60^\circ$  should be qualified on the basis of special tests.

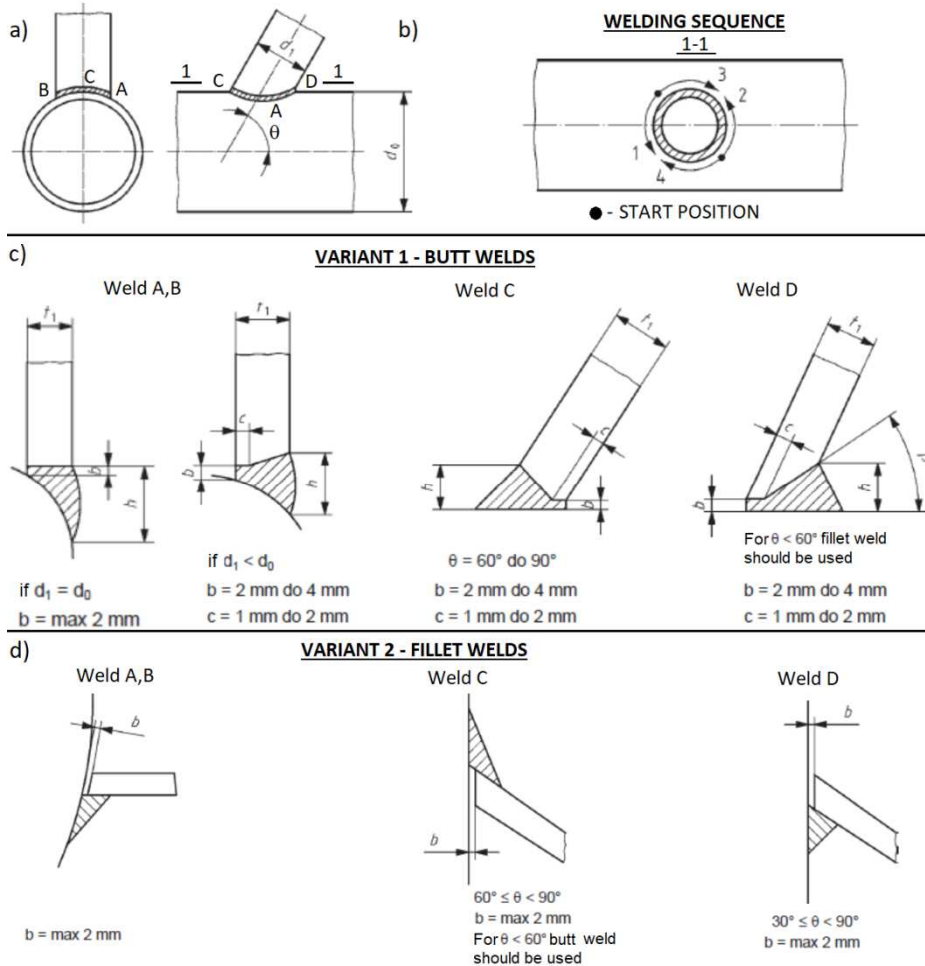


Fig. 2. Welded joints in circular steel hollow sections: a) description of welds and dimensions, b) start and stop positions and welding sequence, c) preparation of joint faces in the case of butt welds, d) preparation of joint faces in the case of fillet welds

It may be noticed that Fig. 1 and 2 give some recommendations that are worth to be taken into account during detailing the lattice structures made of rectangular hollow sections. While in the case of fillet welds it is permitted that brace fully adjoin chord, in the case of butt welds the appropriate gap between the connected elements should be ensured. This gap can be obtained by introducing in the workshop documentation appropriately shorter elements which reduces the labour consumption of the preparatory work, and thus decreases the cost of structure execution. For example, for the angle of inclination  $\theta=60^\circ$ , the element should be 4.6–9.2 mm shorter, what is much greater value than length tolerances according to PN-EN 1090-2 [4]. For circular hollow sections standard PN-EN 1090-2 [4] does not indicate the position where

welds A and B should transform from fillet to butt one. The authors propose assuming that it take place at the point where the angle between generatrix of brace external shell and tangent to the chord is equal to  $120^\circ$ .

In the case of joints of lattice structures made of rectangular hollow sections, elements are usually cut by band saw. This process that does not change the hardness of the material and therefore do not increase the risk of cracking after welding. If thermal cutting processes (e.g. laser cutting, plasma cutting) are used, their capability should be periodically checked because of their influence on steel mechanical properties, particularly hardness. The verification consists in taking of four samples from the constituent product to be cut by the process [4]:

1. a straight cut from the thickest constituent product,
2. a straight cut from the thinnest constituent product,
3. a sharp corner from a representative thickness,
4. a curved arc from a representative thickness.

The quality of cut surfaces is defined according to PN-EN ISO 9013 [12] and should fulfil provisions given in Table 9 of PN-EN 1090-2 [4]. If hardness test is required, the results should be in accordance with Table 10 of PN-EN 1090-2 [4]. In this case, capability of the processes that may cause local changes of steel hardness (thermal cutting, shearing, punching) should be checked. In order to achieve the required hardness of free edge surfaces, preheating of material may be applied. The check of the process capability is carried out as follows: four samples are taken from the structural products that are most susceptible to local hardening, four local hardness tests are done on each sample according to PN-EN ISO 6507 [11], in locations likely to be hardened. This allows to confirm the lack of influence of cutting method on steel weldability.

For joints in rectangular hollow sections with fillet welds, when the chord and brace profiles have the same width (see Fig. 1, weld A and B, the case  $b_1=b_0$ ), and the chord has a large fillet radius, the adjustments to the width of the excessive gap between the connected parts may be needed (see Fig. 3).

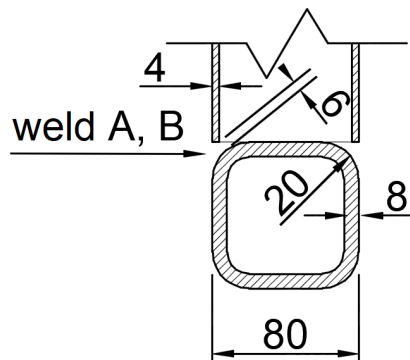


Fig. 3. Exemplary geometry of the brace to chord joint with the same section width

In this case, preparation for welding should include additional grinding of raw cut surface after cutting by band saw. However, to make this solution possible – the workshop drawings should include the appropriate length overmeasure. An alternative solution is brace weld surfacing [1]. This process should be carried out as a single-pass and, similarly as thermal cutting or welding, requires appropriate WPS. If there is a need to correct the lack of fitting of connected elements, the weld surfacing can also be used, even if braces have lower width  $b_1$  than chord  $b_0$  (Fig. 1a). In the case of joints in circular hollow sections, it is most convenient to shape element ends using computer-controlled plasma or laser cutting machine. This technology provides almost ideal surface of the groove weld edges. It is also possible to shape the groove weld edges with the use of oxyfuel gas cutting but, in this case, a significantly lower quality of surface of groove weld edges is obtained. Possibility of increased hardness of the cut surface also has to be taken into account.

Welded joints in hollow sections are executed using the following processes according to PN-EN ISO 4063 [9]:

- 111: manual metal arc welding (metal-arc welding with covered electrode),
- 135: metal active gas welding (MAG welding),
- 136: tubular-cored metal arc welding with active gas shield.

The welding methods 135 or 136 cannot be in practice applied for the execution of parts of the weld D if the angle  $\theta$  is lower than  $50^\circ$  due to the lack of appropriate access for the welding nozzle to achieve proper weld penetration. In this situation, the welding in this zone have to be carried out using the covered electrode 111 method; and the remaining part of perimeter by 135 or 136 methods. The start and stop positions (see Fig. 1b, 2b) of welds for hollow sections in the lattice structures should be given in Welding Procedure Specifications. Branch connections in hollow sections of lattice structures, containing combined welded joints (with filled and butt welds), can be welded without backings. Flat grinding of one-sided butt welds welded without backings is not permissible. This type of welds may be flat grinded to the level of parent material surface, only if they were entirely welded with backings.

#### 4. Testing of welded joints in hollow sections

The issues described in the previous paragraph cause that the execution of the welded joints in hollow sections with appropriate quality is, as practice shows, quite difficult. This follows from the fact that on section perimeter butt and fillet welds may exist alternately. Moreover, due to the geometrical limitations, the use of different welding methods (111 and 135 methods) may be needed. In addition, it may be necessary to correct the fit-up of connected elements by weld surfacing. For example, for braces leaned at an angle of  $45^\circ$  the weld D should be executed by 111 method, which requires, after formation

of each beads, proper cleaning and grinding of weld start and stop positions. Furthermore, the weld D must be finished outside the corner, as shown in Fig. 1b. As a result, at the point where the welding method is changed from 111 to 135, the type of the weld also changes from fillet to butt. This requires of welders using many different Welding Procedure Specifications.

Quality levels for imperfections in welded joints are given in PN-EN ISO 5817 [10], but the imperfections related to weld shape and micro crack fusion are not considered. The quality levels are associated with element or structure execution class EXC. For the execution class EXC1, quality level D is assumed. Execution class EXC2 is usually associated with quality level C or level D for undercuts, overlaps, stray arc and warm-holes. Execution class EXC3 corresponds to quality level B, while EXC4 to level B+ i.e. quality level B with additional requirements. It should be stressed that according to the Design Standard PN-EN 1993-1-8 [6] quality level C is usually required for steel joints. The scope of nondestructive testing (NT) methods is determined depending on the structure execution class, type and location of welds, and resistance utilization factor. For this reason, the designer should indicate in the workshop documentation if the resistance utilization factor for transversely tensioned butt welds is lower or equal to 50% or if this value is exceeded. In the case of fillet welds the information about resistance utilization factor is not required.



Fig. 4. Position of magnetic defectoscope during ultrasonic testing (UT) of brace to lower chord assembly splice

If there is a need to verify assumed quality level for certain geometry of joints (angle  $\theta < \sim 30^\circ$ ) with complete-penetration butt welds, it is not possible to use non-destructive methods, i.e. radiographic testing (RT) or ultrasonic testing (UT). In this case only magnetic particle testing (MT) or penetrant testing (PT) can be conducted – but these tests allow to detect only surface imperfections. Radiographic testing is usually not applied in the case of hollow sections. Ultrasonic testing which reveal both surface and interior of the weld, such as: cracks, lack of fusion or delaminations, can be applied only in the case of butt welds and sections with the width higher or equal to 8 mm. Ultrasonic testing is exceptionally allowed for section thickness of at least 6 mm. In this situation research program approved by the welding personnel with the third, the highest degree of qualification is required. Ultrasonic testing for weld C (Fig. 1a, 2a) may be difficult or impossible in the case of the joints where more than one brace is connected to the chord due to a need for using a magnet yoke (see Fig. 4).

The MT and PT method may be used for all types and locations of the welds, but it should be pointed out that these methods reveal only surface defects. In the case of fillet welds, using the UT is impossible.

Regardless of the test types listed in Table 1, all welds should be visually examined on entire length.

Table 1. Scope of available non-destructive testing (NDT) depending on weld type and its location on section perimeter

Type of tested weld	Weld location according to Fig. 1 and 2		
	A, B	C	D
Butt weld	UT MT, PT	UT MT, PT	UT ( $\theta > 30^\circ$ ) MT, PT
Fillet weld	MT, PT	MT, PT	MT, PT

During the examination of weld shape and surface of the branch connections in hollow sections, particular attention shall be paid to the following areas on section perimeter:

1. extreme front and rear positions, and two side positions in circular hollow section joints,
2. four corners in rectangular hollow section joints.

This means that the geometry and the type of welds indicated in the documentation affects the possibility of detecting weld imperfections. For this reason it is extremely important to manufacture so-called pre-production joints to check ability of the welders to execute this type of welded joints. The joint should be examined macroscopically, its imperfections should be indicated, and welding technique enabling to avoid possible future imperfection should be evaluated. Qualification testing of welders shall be carried out in accordance with PN-EN ISO 9606-1 [13]. In the case of hollow sections joints with element inclination angles lower than  $60^\circ$  qualification of welds shall be carried out on the basis of special tests - as defined in PN-EN 1993-1-8 [6].

Figure 5 shows the most common imperfections, detected during tests of pre-production joints in hollow sections. The lack of fusion is demonstrated in following figures: Fig. 5a (on the internal surface of the brace), Fig. 5b (between beads in the weld C) and Fig. 5d (in the weld D). Figure 5c presents improper penetration in the weld D. The authors' experience indicates that, in practice, the weld D requires the longest preproduction preparations in order to obtain properly executed welds at a given quality level. The above imperfections result from problems with appropriate access for the welding nozzle to the place of welds execution or with necessity of welding using 111 method.

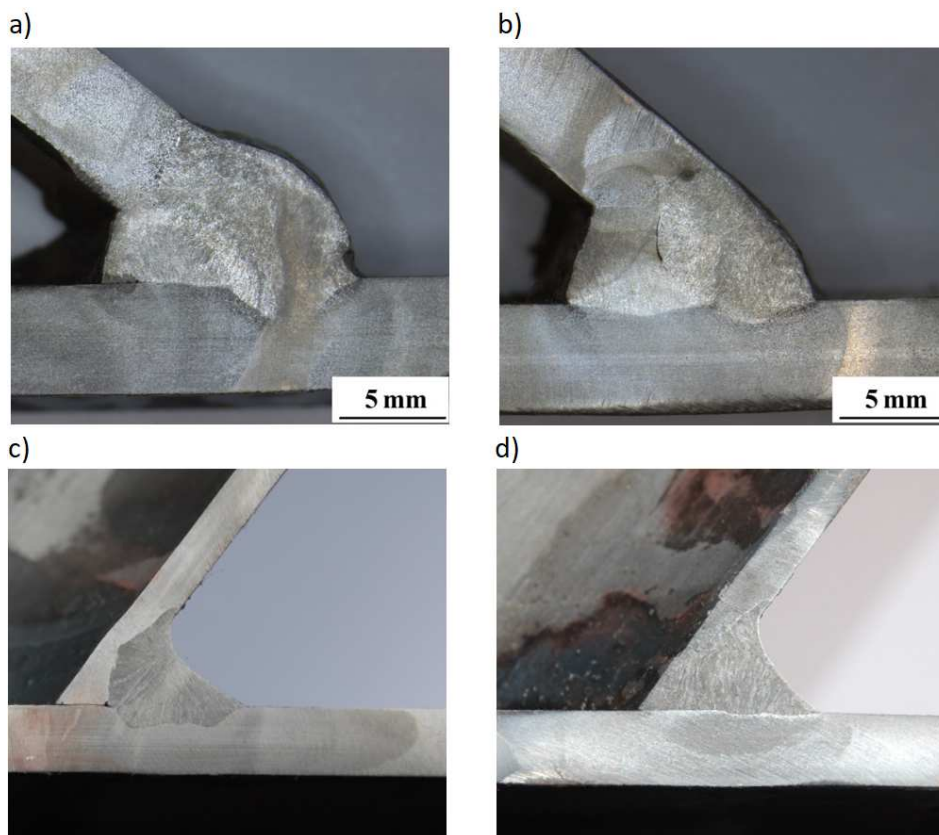


Fig. 5. Welding imperfections detected in the pre-production joints. Description in the text

## 5. Summary

The execution of welded joints in hollow sections, apart from welding works, may include cutting (also thermal cutting), additional machining of sections edges, and in some cases – weld surfacing to correct elements fit-up. As the practice shows, the execution of this joint type at appropriate quality level

is the difficult issue because in some joint geometrical configurations on the same section perimeter both fillet and butt welds have to be executed. In addition, due to the geometrical limitations, it may be necessary to use different welding techniques (111 method and 135 or 136 method). In some cases prior correction of section fit-up by weld surfacing of selected walls may be needed. These circumstances illustrate the importance of pre-production assessment to be sure that given manufacturer, using the specified equipment and personnel, is able to execute welded joints at the appropriate and consistent with design documentation quality level. Joint shape and weld type indicate possible types of quality control tests. Volumetric test methods, revealing weld internal imperfections can be used only in the case of butt welds and sections with wall thickness not smaller than 8 mm (exceptionally 6 mm). In all other cases magnetic particle (MT) or penetrant (PT) testing, detecting only surface imperfections, can be used. This shows the necessity of manufacturing and testing the pre-production joints, which can be utilized to confirm that the measures used together with the welders skills enable execution of welded joints at the appropriate quality level.

## References

- [1] Klimpel A., Napawanie i natryskiwanie cieplne, Wydawnictwo Naukowo-Techniczne, Warszawa 2000.
- [2] PN-EN 10025-6 Hot rolled products of structural steels. Technical delivery conditions for flat products of high yield strength structural steels in the quenched and tempered condition.
- [3] PN-EN 1090-1 Execution of steel structures and aluminium structures. Part 1 – Requirements for conformity assessment of structural components.
- [4] PN-EN 1090-2 Execution of steel structures and aluminium structures. Part 2 – Technical requirements for steel structures.
- [5] PN-EN 1090-3 Execution of steel structures and aluminium structures. Part 3 – Technical requirements for aluminium structures.
- [6] PN-EN 1993-1-8 Eurocode 3. Design of steel structures. Design of joints.
- [7] PN-EN ISO 15609-1 Specification and qualification of welding procedures for metallic materials. Welding procedure specification. Arc welding.
- [8] PN-EN ISO 15614-1 Specification and qualification of welding procedures for metallic materials. Welding procedure test. Arc and gas welding of steels and arc welding of nickel and nickel alloys.
- [9] PN-EN ISO 4063 Welding and allied processes. Nomenclature of processes and reference numbers.
- [10] PN-EN ISO 5817 Welding. Fusion-welded joints in steel, nickel, titanium and their alloys (beam welding excluded). Quality levels for imperfections.
- [11] PN-EN ISO 6507 Metallic materials. Vickers hardness test.
- [12] PN-EN ISO 9013 Thermal cutting. Classification of thermal cuts. Geometrical product specification and quality tolerances.

- [13] PN-EN ISO 9606-1 Qualification testing of welders. Fusion welding. Steels.
- [14] PN-EN ISO 9692-1 Welding and allied processes. Types of joint preparation. Manual metal arc welding, gas-shielded metal arc welding, gas welding, TIG welding and beam welding of steels.
- [15] PN-EN ISO 9692-2 Welding and allied processes. Joint preparation. Submerged arc welding of steels.

*Przesłano do redakcji: 04.05.2018 r.*

*Przyjęto do druku: 15.06.2018 r.*

Tomasz DOMAŃSKI<sup>1</sup>  
Kamil KMIECIK<sup>2</sup>

## FIRE RESISTANCE OF TIMBER JOINTS WITH STEEL FASTENERS

Fire safety is a major concern in the design of timber construction. Wood is combustible material. The thermal response of timber connections is usually the main factor in evaluating the overall load-bearing capacity of wood structures exposed to fire. The analysis of timber joints under fire conditions is difficult and complex. Finite element model is developed to predict the thermal behavior of bolted wood-to-wood joints exposed to fire. In fire, the material characteristic depend on the temperature. The thermal model is continuous, taking into account the thermal continuity between the joint components. Also, the thermal model is used to predict the evolution of the temperature field inside the connection.

The paper presents a summary of results from a numerical studies of the fire behavior of wood-to-wood timber connections with steel bolt. As a result of computer simulations the temperature distribution was obtained. During fire exposure, the timber section is reduced and steel bolt reduces strength. Load-carrying capacity per shear plane in fire conditions was calculated using two methods: design methods according to EN 1995-1-1 [5] and reduced load method according to EN 1995-1-2 [6]. In the first approach, the timber section loss and steel strength reduction during the fire were taken into account.

**Keywords:** thermal conductivity, fire safety, connections, elevated temperatures

### 1. Introduction

Currently, timber constructions are commonly used by designers in buildings because of their good environmental influence. High timber buildings are constructed in many countries. One of the most important technical aspects in timber constructions is the fire safety requirements. Wood is a combustible material. The resistance of timber structure depends on the thermo-mechanical behavior of the structural elements represented by the beams, the columns and the connections.

Connections are the weakest parts in timber structures in normal and fire conditions [2,3]. They determine the bearing capacity and the mechanical

---

<sup>1</sup> Corresponding author: Tomasz Domański, Cracow University of Technology, Chair of Metal Structures, ul. Warszawska 24, 31-155 Kraków; doman@pk.edu.pl

<sup>2</sup> Kamil Kmiecik, Cracow University of Technology, Chair of Metal Structures, , ul. Warszawska 24, 31-155 Kraków; kamil.kmiecik@pk.edu.pl

behavior of the structure. The analysis of the fire behavior of timber connections is complex and difficult to predict [8,11]. It depends on several parameters such as the geometry of the connection, the fastener types and different thermal properties of steel and timber.

## 2. Thermal analysis

### 2.1. Heat transfer

Timber is anisotropic material. It causes high variability of properties. In fire conditions, timber begins to pyrolyse at about 200°C and chars at about 250°C under the formation of charcoal and combustible gases. Charcoal has a lower thermal conductivity than wood and protects the inner timber members against fire. Thermal actions are given by the net heat flux  $h_{net}$  to the surface of the member. In fire conditions the net heat flux should contain heat transfer by radiation and convection [10].

$$h_{net} = h_{net,c} + h_{net,r} \quad (1)$$

where:  $h_{net}$  – net heat flux [W/m<sup>2</sup>],  
 $h_{net,c}$  – convective heat flux [W/m<sup>2</sup>],  
 $h_{net,r}$  – radiative heat flux [W/m<sup>2</sup>].

Convection is the heat transfer between a solid and a gas. The heat flux depends on the temperature of the gas in the vicinity of the fire exposed member and on the surface temperature of the member. The equation of the net convective heat flux should be defined as follows:

$$h_{net,c} = \alpha_c \cdot (\Theta_g - \Theta_m) \quad (2)$$

where:  $\alpha_c$  – coefficient of heat transfer by convection [W/(m<sup>2</sup>K)],  
 $\Theta_g$  – gas temperature in the vicinity of the fire exposed member [°C],  
 $\Theta_m$  – surface temperature of the member [°C].

Radiation depends on the temperature of the radiation source and the material properties of the surface. The equation of the net radiative heat flux should be defined as follows:

$$h_{net,r} = \Phi \cdot \varepsilon_m \cdot \varepsilon_f \cdot \sigma \cdot [(\Theta_r + 273)^4 - (\Theta_m + 273)^4] \quad (3)$$

where:  $\Phi$  – configuration factor,  
 $\varepsilon_m$  – surface emissivity of the member,  
 $\varepsilon_f$  – emissivity of fire,

- $\sigma$  – Stephan Boltzmann constant,
- $\Theta_r$  – effective radiation temperature of environment [ $^{\circ}\text{C}$ ],
- $\Theta_m$  – surface temperature of the member [ $^{\circ}\text{C}$ ].

## 2.2. Thermal Finite Element simulations

The subject of the research are the timber joints with steel fasteners. Figure 1 shows the geometry of the modeled connections. The joints consist of the solid wood C20 class, and the steel bolt M16 cl.4.6. In the first connection (I), the beams have the following dimensions:  $250 \times 150$  mm. In the other connection (II), the beams are half lower ( $250 \times 75$  mm).

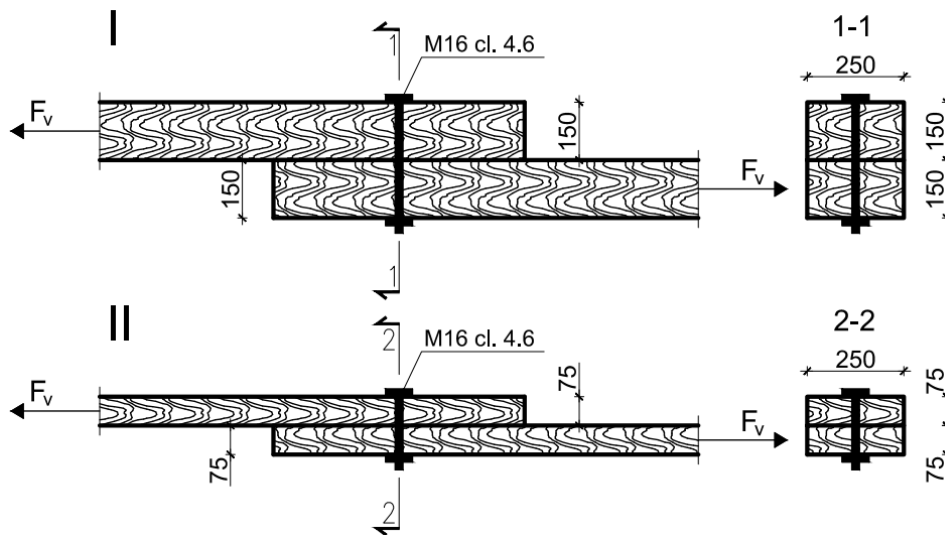


Fig. 1. Geometry of connections

The purpose of modeling the connections using the finite element method was to determine the influence of steel elements in timber connections on the temperature distribution under standard fire curve [1,9,12]. The connections were modeled in 2-dimensional pictures. Thermal radiation and convection as described in chapter 2.1 were applied on four sides. The connections were modeled using the SAFIR software [7].

Steel has high thermal conductivity [4]. The heat flux through the steel elements leads to higher temperatures of the timber interior. It causes faster reduction of the net section. The bolt temperature inside cross-section is much higher than the temperature of timber section (Figure 2).

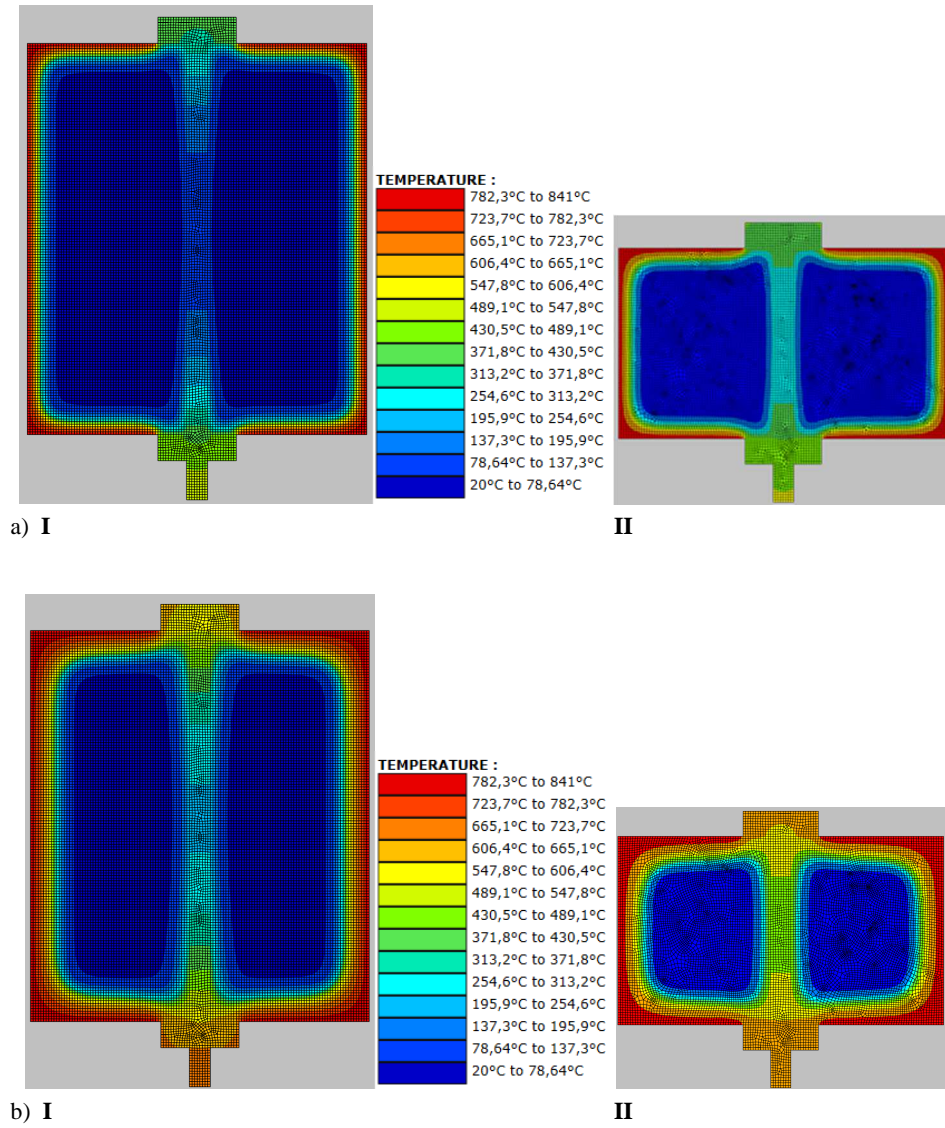


Fig. 2. Heat flux inside cross-sections 1-1 (I) and 2-2 (II) after: a) 15 min, b) 30 min

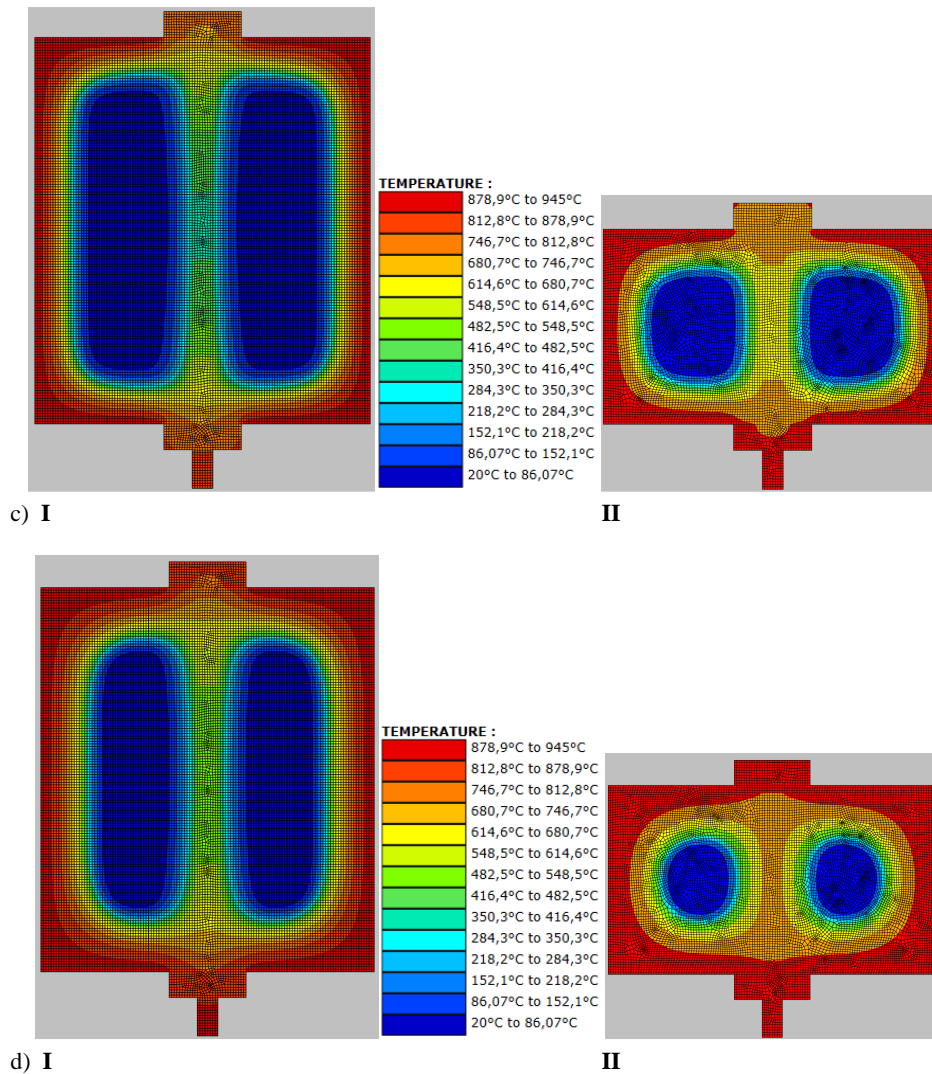


Fig. 2. (cont.) Heat flux inside cross-sections 1-1 (I) and 2-2 (II) after: c) 45 min and d) 60 min

### 3. Mechanical analysis

#### 3.1. Lateral load-carrying capacity of metal dowel-type fasteners

Metal dowel type connections have to satisfy the relevant design rules and requirements of Eurocode 5. Connection formed using metal dowel fasteners, when subjected to lateral loading, may fail in a brittle or a ductile mode. For connections in single shear, the characteristic load-carrying capacity per shear plane per fastener  $F_{v,Rk}$ , is the minimum value equation for the relevant single shear cases given in Figure 3.

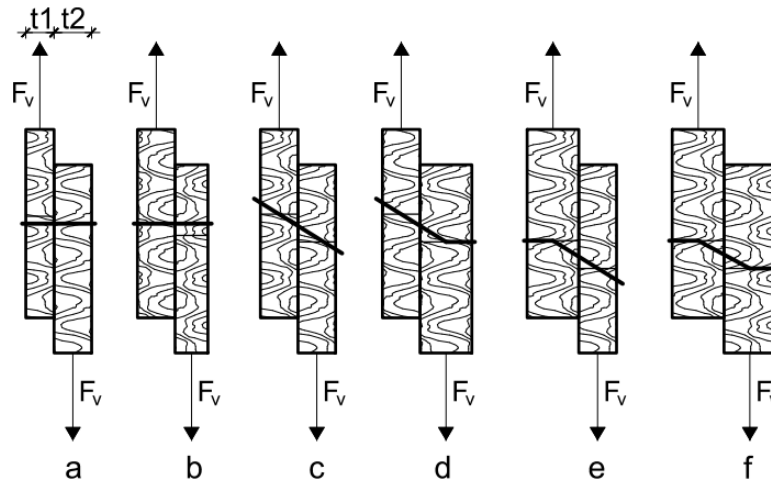


Fig 3. Failure models for timber connections, based on [5]

Because of the fact that there is only one shear plane, this value will also equate to the load-carrying capacity per fastener in the connection and the failure mode will be the mode associated with the minimum value equation. The main functions used in the strength equations are the diameter of the dowel –  $d$ , the characteristic fastener yield moment  $M_{y,Rk}$  and the characteristic embedment strength,  $f_{h,i,k}$  of the connected member  $i$ .

### 3.2. Lateral load-carrying capacity of metal dowel-type fasteners in fire

The determination of the load-carrying capacity of the connection in fire conditions is complex. It depends on the geometry of the connection, the fastener types and the different thermal properties of steel and timber. During fire exposure, the timber section is reduced and steel bolt reduces strength. Table 1 contains load-carrying capacity for the appropriate failure model in fire conditions. The reduction of the timber cross-section was taken into account using isotherm 300°C in the MES analysis. The reduction of steel strength with time was determined on the basis of EC3 (Figure 4).

Table 1. Load-carrying capacity per fastener during the fire

Duration of fire [min]	Load-carrying capacity per fastener for the failure model [kN]							
	a = b		c		d = e		f	
	I	II	I	II	I	II	I	II
0	54.5	27.3	22.6	11.3	20.2	11.7	12.5	12.5
15	50.9	23.6	21.1	9.8	18.8	10.3	11.2	11.2
30	47.3	20.0	19.6	8.3	17.4	8.6	10.1	10.1
45	43.6	16.4	18.1	6.8	16.1	7.5	9.3	9.3
60	40.1	12.7	16.6	5.3	14.7	6.3	8.1	8.1

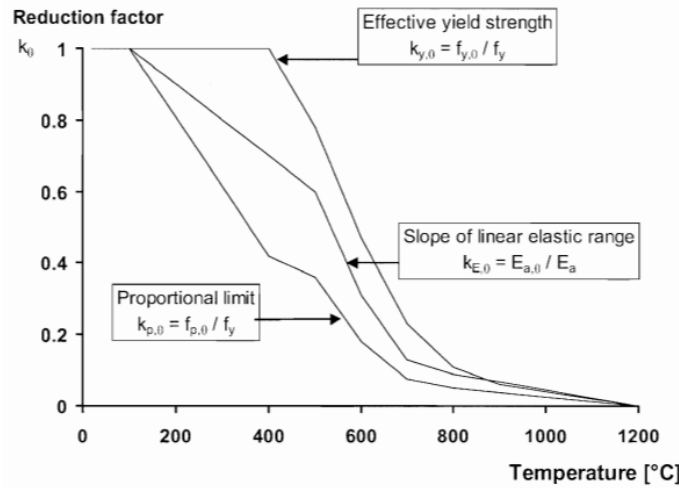


Fig 4. Reduction factors for the stress-strain relationship of carbon steel at elevated temperatures [4]

In the first connection (I), the main failure mode is a destruction of the fastener (f). This failure mode can occur when the timber side elements are very thick. In the other connection (II), the main failure mode is an elongation of fastener holes due to wood crushing and deformation of fasteners (c). This is due to the charring of timber beams and the rapid temperature increasing in steel fastener.

The load-carrying capacity for bolts per fastener should be taken as the minimum value defined by the appropriate failure models. Figure 5 shows the load-carrying capacity of the connection.

In the fire conditions, the wooden section is reduced, especially within the connection. Tensile strength is reduced. Table 2 contains the change of tensile strength during the fire.

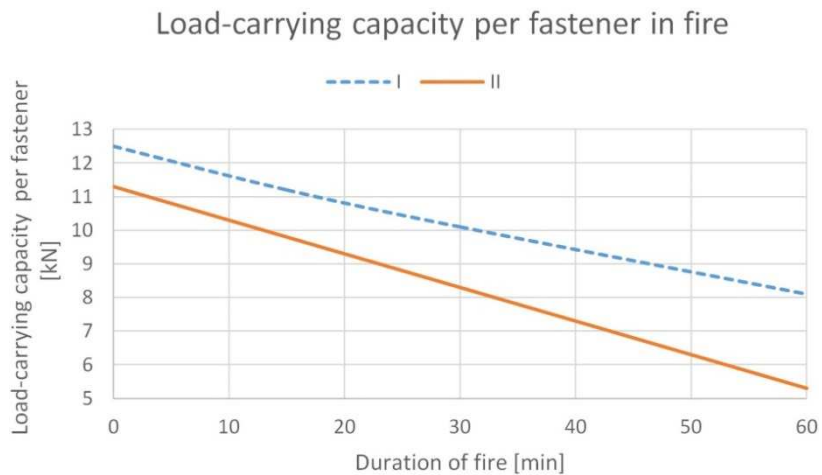


Fig. 5. Load-carrying capacity per fastener in fire

#### 4. Design methods according to EN 1995-1-2

EN 1995 1-2 [6] provides design rules for symmetrical three-member connections with various types of fasteners (nails, bolts, dowels, etc.) exposed to the ISO-standard fire. These apply to laterally loaded joints and are generally limited to fire resistances less than 60 min. The design can be approached in two ways: as the “application of simplified rules” and as the “reduced load method”.

Table 2. Load-carrying capacity per block break

Duration of fire [min]	Load-carrying capacity per block break [kN]	
	I	II
0	417.6	208.8
15	356.2	165.4
30	287.1	121.4
45	224.6	84.2
60	168.9	53.8

##### 4.1. Simplified rules

The fire resistance of unprotected wood-to-wood connections where spacings, edge and distances and side member dimensions comply with the minimum requirements given in EN 1995-1-1 [5] section 8, may be taken from table 3. If the greater fire rating is desirable, the edge distance as well as the thickness and width of the side members should be increased.

Table 3. Fire resistances of unprotected connections with side members of wood

	Time of fire resistance $t_{a,R}$ [min]	Provisions
Nails	15	$d \geq 2.8$ mm
Screws	15	$d \geq 3.5$ mm
Bolts	15	$t_1 \geq 45$ mm
Dowels	20	$t_1 \geq 45$ mm
Connectors according to EN 912	15	$t_1 \geq 45$ mm
d is the diameter of the fastener and $t_1$ is the thickness of the side member		

EN 1995-1-2 [6] provides only simplified methods that allow to calculate the load-carrying capacity of the connection in minutes.

#### 4.2. “Reduced load method”

The rules for bolts and dowels are valid where the thickness of the side plate is equal or greater than  $t_1$  in mm:

$$t_1 = \max \begin{cases} 50 \\ 50 + 1,2(d - 12) \end{cases} \quad (4)$$

where:  $d$  – diameter of bolt or dowel [mm].

According to the “reduced load method”, the load bearing capacity of the connection under fire exposure is obtained by reducing the room temperature capacity by a conversion factor  $\eta$ :

$$\eta = e^{-k \cdot t_{d,fi}} \quad (5)$$

where:  $k$  – parameter depending on the connection type,

$t_{d,fi}$  – design fire resistance of the unprotected connection in minutes.

$$t_{d,fi} = -\frac{1}{k} \ln \frac{\eta_{fi} \eta_0 k_{mod} \gamma_{M,fi}}{\gamma_M k_{fi}} \quad (6)$$

where:  $\eta_{fi}$  – reduction factor for the design load in the fire situation,

$\eta_0$  – degree of utilisation at normal temperature,

$k_{mod}$  – modification factor,

$\gamma_M$  – partial factor for the connection,

$k_{fi}$  – coefficient depending on the type of timber,

$\gamma_{M,fi}$  – partial safety factor for timber in fire,

For standard fire exposure, the characteristic load-carrying capacity of a connection with fasteners in shear should be calculated as:

$$F_{v,Rk,fi} = \eta F_{v,Rk} \quad (7)$$

where:  $\eta$  – conversion factor,

$F_{v,Rk}$  – characteristic lateral load-carrying capacity of the connection with fasteners in shear at normal temperature.

“Reduced load method” was used to calculate the load capacity of the analyzed connections. As a result of calculations, the design fire resistance of the unprotected connections were about 18 minutes. The conversion factor  $\eta$  was 0.48.

Specifications for calculations the joints resistance with axially loaded screws under elevated temperatures are also presented. The above take into consideration the configuration of the connection, the edge distance and the embedment depth of screws. Both of the above methods allow to estimate the load-carrying capacity of the connection in minutes.

## 5. Conclusions

The finite element method was used to carry out a thermal analysis in order to determine the temperature profiles within wood-to-wood timber connections with bolts exposed to fire. The thermal finite element analysis of timber members with steel bolt was carried out under ISO-fire exposure on four sides. The charring depth is the same on each side of timber members. Due to the high thermal conductivity of steel, the heat flux through the steel dowel led to higher temperatures in the interior of timber member. This approach has to be taken into consideration for the work in progress to provide a design model for the calculation of the fire resistance of shear connections with steel bolts.

## References

- [1] Audebert M., Dhima D., Taazount M., Bouchair A.: Numerical investigations on the thermo-mechanical behavior of steel-to-timber joints exposed to fire, *Engineering Structures*, no. 33, 2011, p. 3257–3268.
- [2] Barber D.: Determination of fire resistance ratings for glulam connectors within US high rise timber buildings, *Fire Safety Journal*, no. 91, 2017, p. 579–585.
- [3] Domański T.: Wybrane zagadnienia niezawodności konstrukcji drewnianych. Wydawnictwo PK, Cracow 2016.
- [4] EN 1993-1-2 Eurocode 3: Design of steel structures – Part 1-2: General rules – structural fire design, PKN, Warsaw 2007.
- [5] EN 1995-1-1 Eurocode 5: Design of timber structures – Part 1-1: General – Common rules and rules for buildings, PKN, Warsaw 2010.
- [6] EN 1995-1-2 Eurocode 5: Design of timber structures – Part 1-2: General – Structural fire design, PKN, Warsaw 2008.
- [7] Franssen J.M., Gernay T.: Modeling structures in fire with SAFIR: theoretical background and capabilities, *Journal of Structural Fire Engineering*, vol. 8, 2017, issue 3, p. 300–323.
- [8] Maraveas C., Miamis K., Matthaïou E.: Performance of timber connections exposed to fire, *Fire Technology*, no. 51, 2013, p. 1401–1432.
- [9] Moss P., Buchanan A., Fragiaco M., Austruy C.: Experimental testing and analytical prediction of the behavior of timber bolted connections subjected to fire, *Fire Technology*, no. 46, 2010, p. 129–148.
- [10] Peng L., Mehaffey J., Mohammad M.: Predicting the fire resistance of wood-steel-wood timber connections, *Fire Technology*, no. 47, 2009, p. 1101–1119.
- [11] Racher P., Laplanche K., Dhima D., Bouchair A.: Thermo-mechanical analysis of the fire performance of dowelled timber connection, *Engineering Structures*, no. 32, 2010, p. 1148–1157.
- [12] Thi V.D., Khelifa M., Oudjene M., El Ganaoui M., Rogaume Y.: Finite element analysis of heat transfer through timber elements exposed to fire, *Engineering Structures*, no. 143, 2017, p. 11–21.

*Przesłano do redakcji: 15.05.2018 r.*

*Przyjęto do druku: 15.06.2018 r.*

Mariusz MAŚLAK<sup>1</sup>  
Michał PAZDANOWSKI<sup>2</sup>  
Małgorzata SNELA<sup>3</sup>

## CRITICAL TEMPERATURE EVALUATION FOR A STEEL FRAME WITH JOINT STIFFNESS DECREASING IN FIRE

A procedure to determine the critical temperature of a selected steel frame bearing structure is presented and discussed. This temperature, in case of fully developed fire, when the temperature of the exhaust gasses enveloping the structural members is equalized within the whole fire zone, may be considered as an impartial measure of safety. The obtained result does not depend on the heating progress but only on the static scheme and the load level in the considered structure. The quantitative and qualitative evaluation of the influence the joint stiffness decreasing in fire exerts on the resultant critical temperature constitutes the basic objective of the authors. It has been shown, that proceeding according to the recommended computational procedure does not necessarily result in an estimate fully unambiguous in interpretation. The critical temperature specified in a global mode, for the whole considered frame, is usually associated with a specific component of such frame, interpreted as the so called “weakest link”. Thus local loss of bearing capacity in such element is in this approach equivalent to the total destruction of the whole bearing structure. Indication, which of the components present in the considered frame should be treated as the critical one, because of its behaviour under fire conditions, seems to be a key to the forecast safety level warranted to the users of the structure. The authors show, that this association changes depending on the selected computational method, and this in turn substantially limits the reliability of the obtained estimate.

**Keywords:** steel bearing frame, fire, critical temperature, joint stiffness, moment – rotation relationship, weakest link

---

<sup>1</sup> Corresponding author: Mariusz Maślak, Cracow University of Technology, Faculty of Civil Engineering, Chair on Metal Structures, Warszawska 24, 31-155 Cracow, phone: 126282033, e-mail: mmaslak@pk.edu.pl

<sup>2</sup> Michał Pazdanowski, Cracow University of Technology, Faculty of Civil Engineering, Institute for Computational Civil Engineering, Warszawska 24, 31-155 Cracow, phone: 126282929, e-mail: michal@15.pk.edu.pl

<sup>3</sup> Małgorzata Snela, Lublin University of Technology, Faculty of Civil Engineering and Architecture, Department of Structural Engineering, Nadbystrzycka 40, 20-618 Lublin, phone: 815384388, e-mail: m.snela@pollub.pl

## 1. Introduction

In the classical computational approach the time during which in fire conditions, and counting from the moment of initiation to fire exposure, the structure is capable of safely resisting the loads applied to it, including the internal forces induced in the structure by the restrained capability to freely yield to thermally induced deformations, is treated as the measure of fire resistance. Unfortunately, a measure of this type can hardly be treated as an impartial measure of safety. Its value determined for given frame will change with changed fire scenario, this means, that it may not be uniquely assigned to considered structure and be interpreted as one of its characteristics. Thus the authors of this paper recommend for use in its place the critical temperature calculated globally for the whole bearing structure and associated with this structure reaching the ultimate limit state in fire. However, this temperature will be reached locally in fire, in the weakest part of the structure, treated as the "weakest link". Unequivocal indication of such "weakest link" in the analyzed frame, when subjected to the forecast fire action, constitutes the basic task of an expert performing fire safety appraisal for the users of the considered building. The qualitative and quantitative verification of this influence, taking into account decreasing joint rigidity in fire exerts on the estimated critical temperature of the selected steel frame, is the basic purpose of this paper. The authors intend to show, that in the specific case selection of a single critical structural element, authoritative for the specification of critical temperature depends on the selected calculation method, and this in turn significantly undermines credibility of the obtained estimate.

## 2. Description of the frame analyzed in this case

Let us consider in detail a two-storey two-aisle steel sway frame having the dimensions and static scheme as depicted in Fig. 1a. All the structural components of this frame are made of the low carbon steel S235, with HEB 240 wide-flange I sections used for columns and IPE 400 I sections used for beams. These sections have been selected so, as to in the persistent design situation, excluding the influence of a fire, assure the safe bearing of applied loads. Both the ultimate and serviceability limit states of the considered structure have been checked. The distributions of dead and selected live loads (applied to the floors of intermediate level) are depicted in Fig. 1b. The dead weight of structural members has been accounted for automatically in the computer program. The equivalent horizontal forces modeling the influence of global sway imperfection having the magnitude prescribed by the code (without amplification) are depicted in the same figure [1].

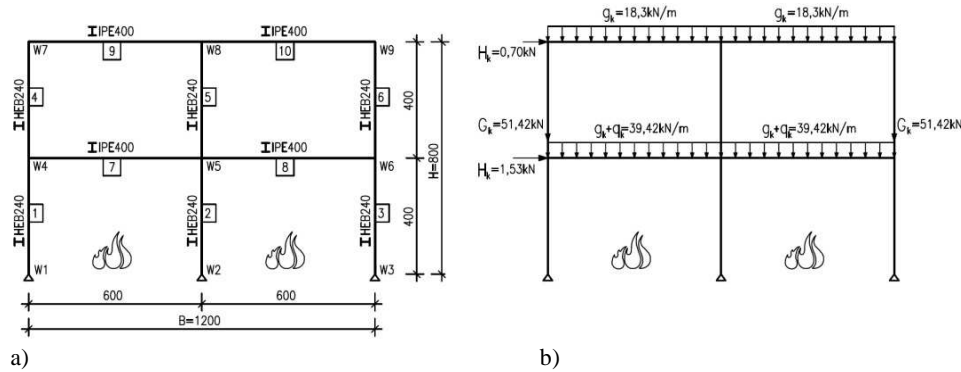


Fig. 1. Frame considered here, including: a) dimensions, static scheme and sections used, b) distribution of dead and selected live loads (combination with live load applied to both floors at the intermediate level – i.e. combination 20, authoritative for consideration of exceptional design scenario – see Table 1) and horizontal equivalent forces modeling the influence of initial sway imperfection (the force values depicted are preset for combination 20)

The static analysis and dimensioning of cross sections in the considered frame have been performed using Robot Structural Analysis computer code [2]. The following loads indicated by consecutive numbers have been declared for the purpose of this analysis:

- 1 – dead load of structural members,
- 2 – other dead loads (weight of roofing materials, floor slabs, curtain walls),
- 3 – live load applied to the flat roof (category H, top left beam),
- 4 – live load applied to the flat roof (category H, top right beam),
- 5 – live load applied to the floor (category C, left intermediate floor beam),
- 6 – live load applied to the floor (category C, right intermediate floor beam),
- 7 – snow load on the roof (determined directly in Robot Structural Analysis for selected location),
- 8 to 15 – consecutive wind load schemes (determined directly in Robot Structural Analysis for selected location).

The structural steel used to make all structural components of the considered frame has been modeled in the considered scenario as elastic perfectly plastic material. It has been also assumed, that all the joints in the frame have the same configuration depicted in detail in Fig. 2. As there are no ribs stiffening the column web at the levels of beam flanges, these joints are undoubtedly flexible. However, in the considerations pertaining to the persistent design scenario, these joints have been treated, with a certain level of simplification, as nominally rigid.

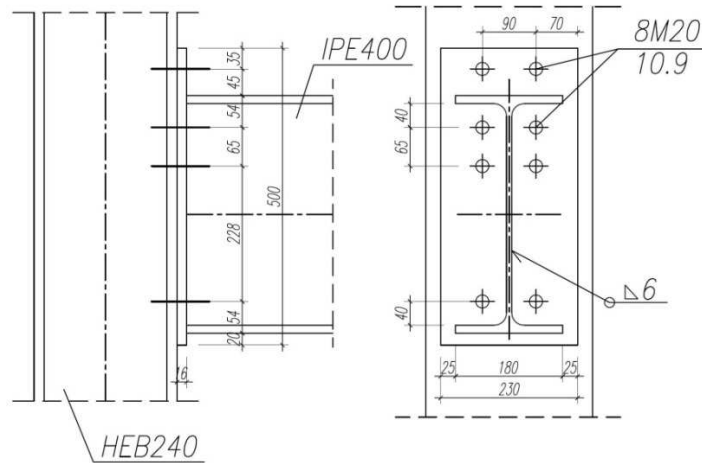


Fig. 2. Scheme of the beam to column joint used in the frame considered here

Detailed analysis of the frame described above, performed for the persistent design scenario resulted in the following selection of sections based on the "weakest links" scenario: beam denoted with No 7 and column denoted with No 3 in Fig. 1a.

### 3. Analyzed frame in the exceptional design scenario of a fully developed fire

The essential part of analysis was related to the exceptional design scenario of a fully developed fire. It was assumed, that the fire was initiated and developed in both aisles at the ground level of the considered building. This resulted in the heating of only lower columns and lower beams in the bearing structure due to the fire action (Fig. 1). It was also assumed, that top columns and top beams were perfectly insulated from the fire action and were not heated. The fire itself was modeled by the increasing temperature of structural elements indicated above, evenly distributed in their cross sections. The dependence of yield limit and longitudinal modulus of elasticity in steel used to make the considered frame on temperature has been accounted for. The standard formulae,  $f_{y,\theta} = k_{y,\theta} \cdot f_y$  and  $E_{a,\theta} = k_{a,\theta} \cdot E_a$  were used, where  $f_y$  and  $E_a$  represent the respective values specified at the room temperature, while  $k_{y,\theta}$  and  $k_{a,\theta}$  represent the respective reduction factors listed in the code EN 1993-1-2 [3] for different temperature values of steel. The uniform heating of columns 1, 2 and 3 as well as beams 7 and 8 is treated as additional exceptional loading scheme, and assigned the number 16.

Further considerations have been performed according to the rules specified for exceptional combination of actions [4]. The following combinations proved to be the most adverse (Table 1).

Table 1. Combination of actions, authoritative for verification of the ultimate limit state in fire for frame beams and columns, respectively (an excerpt of calculations protocol generated by Robot Structural Analysis [2])

Combination No.	The worst case combinations - top and bottom beams	
20	19(K)	$(1+2+16)*1.00+(5+6)*0.70$
24	56(K)	$(1+2+16)*1.00+5*0.60+7*0.20$
25	57(K)	$(1+2+16)*1.00+6*0.60+7*0.20$
Combination No.	The worst case combinations - bottom columns	
21	20(K)	$(1+2+16)*1.00+5*0.70$
22	39(K)	$(1+2+16)*1.00+5*0.60+9*0.20$
23	47(K)	$(1+2+16)*1.00+6*0.60+9*0.20$

The behaviour of the frame considered here, when subjected to fire action developing on the ground floor as described above, for comparative reasons has been analysed in detail using two approaches to model joints. In the first approach it was assumed conventionally, that all joints remain nominally rigid during the whole time of fire. In the second approach the flexibility of joints, increasing with fire development, has been accounted for (Fig. 3), and the characteristics of this flexibility have been described by a set of curves linking bending moment with increasing angle of rotation at the joint (the so called  $M-\varphi$  curves), developed based on the classical component method [5–7] generalised to the case of fire. In the case of node depicted in Fig. 2, and considered in this example, these curves had the shape depicted in detail in Fig. 4.

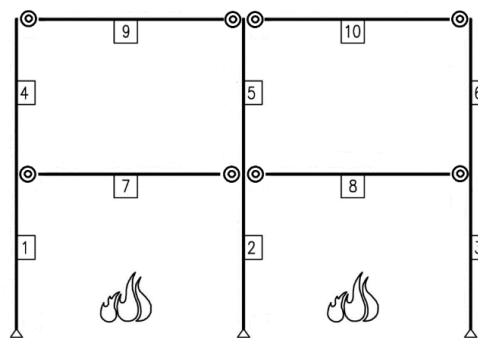


Fig. 3. Scheme of the frame considered in this example, in the case of joint flexibility increasing with the development of a fire

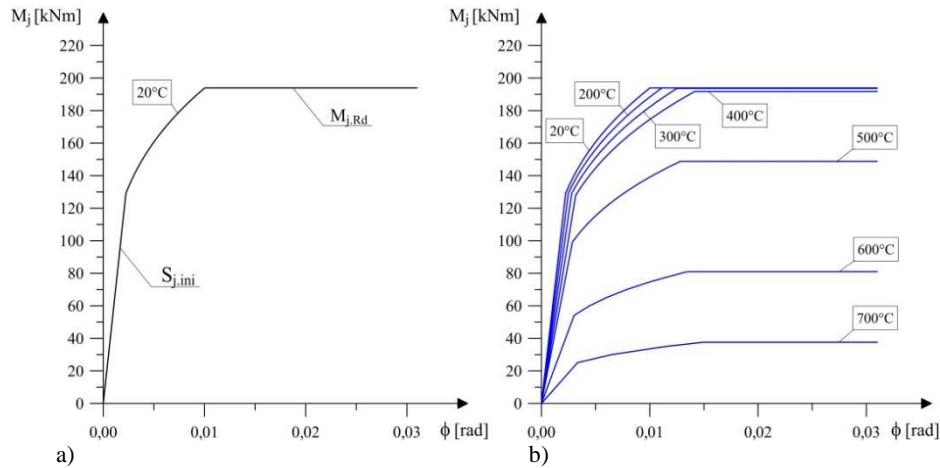


Fig. 4. Bending moment – rotation angle relationship for the joint considered in the example (based on [6]), including: a) single curve determined for room temperature, b) a set of curves developed for fire conditions

#### 4. Alternative methods of analysis

Verification of ultimate limit state for fire conditions has been performed based on two alternative computational approaches [8]. In the first approach the first order analysis using buckling length concept has been applied. For the in plane buckling the multiplier  $\lambda_{cr}$  and after that the critical load  $N_{cr,y}$  have been determined (for the first sway vibration eigenform with respect to the column, for the first symmetrical vibration eigenform with respect to the beam). For the out of plane buckling case the critical load  $N_{cr,z}$  has been determined under the assumption, that the out of plane buckling length of an element is equal to its theoretical length. In the next step the relative slendernesses  $\bar{\lambda}_y$  and  $\bar{\lambda}_z$  have been determined, and after that the buckling coefficients  $\chi_y$  and  $\chi_z$ . Independently the lateral – torsional buckling coefficient  $\chi_{LT}$  had been found. In the second computational approach the second order analysis has been applied. This analysis has been performed within the Robot Structural Analysis computational environment [2] taking into account the nonlinear phenomena specified both globally for the whole frame (of the  $P-\Delta$  type), and locally for its components (of the  $P-\delta$  type). After the internal forces had been found, the critical forces  $N_{cr,y}$  and  $N_{cr,z}$  were determined, subject to the assumption, that both in plane and out of plane buckling lengths of the structural components were equal to the theoretical lengths of these components. The remaining steps were identical to the steps taken earlier in the first approach.

After the detailed analysis it was found, that the ground floor column No 3 (cf. Fig. 1a) and the beam No7 supporting the ceiling over this floor are authoritative for the determination of critical temperature. These elements are bent and compressed at the same time, thus the sought temperature  $\theta_{cr}$  is determined by the more restrictive constraint of the two listed below (the upper index  $\Theta$  denotes in these formulae the dependence of so indexed quantity on steel temperature  $\theta_a$ ):

$$\rho_1 = \rho(\theta_{cr}) = \frac{N_{fi,Ed}^{\Theta}}{\chi_{\min,fi}^{\Theta} \cdot A \cdot k_{y,\theta}^{\Theta} \cdot \frac{f_y}{\gamma_{M,fi}}} + \frac{k_y^{\Theta} \cdot M_{y,fi,Ed}^{\Theta}}{W_y \cdot k_{y,\theta}^{\Theta} \cdot \frac{f_y}{\gamma_{M,fi}}} = 1 \quad (1)$$

$$\rho_2 = \rho(\theta_{cr}) = \frac{N_{fi,Ed}^{\Theta}}{\chi_{z,fi}^{\Theta} \cdot A \cdot k_{y,\theta}^{\Theta} \cdot \frac{f_y}{\gamma_{M,fi}}} + \frac{k_{LT}^{\Theta} \cdot M_{y,fi,Ed}^{\Theta}}{\chi_{LT,fi}^{\Theta} \cdot W_y \cdot k_{y,\theta}^{\Theta} \cdot \frac{f_y}{\gamma_{M,fi}}} = 1 \quad (2)$$

In these relationships  $N_{fi,Ed}^{\Theta}$  represents the longitudinal force identified in the structural component for the design scenario related to the developed fire, while  $M_{y,fi,Ed}^{\Theta}$  represents the bending moment correlated with this force and determined with respect to the so called strong axis of the cross section. In addition,  $\chi_{\min,fi}^{\Theta}$  is the smaller of  $\chi_{y,fi}^{\Theta}$  and  $\chi_{z,fi}^{\Theta}$ , which in turn represent the buckling coefficients determined for the fire scenario and computed with respect to strong and weak axes in the considered frame cross section,  $k_y^{\Theta}$  and  $k_{LT}^{\Theta}$  quantify the nonlinear phenomena, specific to flexural and lateral – torsional buckling, while  $\gamma_{M,fi}$  represents the partial safety factor covering the uncertainties in modeling material properties appropriate for fire scenario.

## 5. Detailed analysis of obtained results

### 5.1. Results obtained for the column No 3

The critical temperature estimates obtained by various methods for the column No 3 are depicted in Fig. 5, 6 and 7. One may easily observe, that these results are not completely unequivocal. If, for instance, the first order analysis is applied to determine the sought temperature, then the analysis yields the authoritative value of 486,8°C determined by the effort  $\rho_1$  (Fig. 5a). Interestingly, there is no difference in the graph depicted in Fig. 5a due to the changing real joint stiffness, decreasing with increasing temperature of frame components. Such difference, however relatively small, is visible on the graph depicted in Fig. 5b, where more precise model of the joint behaviour allowed for the demonstration of an additional safety margin having the magnitude of approximately 30 degrees Centigrade. This safety margin is conditioned by the effort  $\rho_2$ .

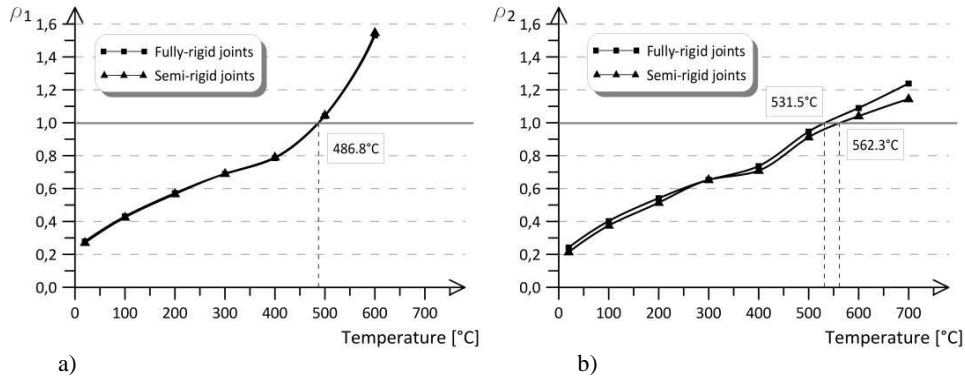


Fig. 5. Determination of the critical temperature in the case of column No 3 according to the first order theory, including: a) based on effort  $\rho_1$ , b) based on effort  $\rho_2$

Qualitatively different result has been obtained for the same column when the second order analysis has been applied. This time the effort  $\rho_2$  proved to be authoritative for the determination of critical temperature. Here, with joint flexibility increasing with temperature the critical temperature of 554.2°C has been obtained, and when this phenomenon was disregarded a more cautious value of 526.1°C was delivered (Fig. 6b). Both those estimates are significantly less restrictive, than the estimate obtained based on the Fig. 5a after application of simpler first order analysis.

Juxtaposition of the results obtained for the column No 3 after application of first and second order theories and taking into account the joint flexibility changing with the progressing fire is depicted in Fig. 7. It is clearly visible there, that equation (1) used to determine the effort  $\rho_1$  proved to be very sensitive to the type of analysis performed, as the difference in obtained estimates exceeds 120°C (Fig. 7a). Such sensitivity is not observed on the graphs depicted in Fig. 7b, related to the effort  $\rho_2$ .

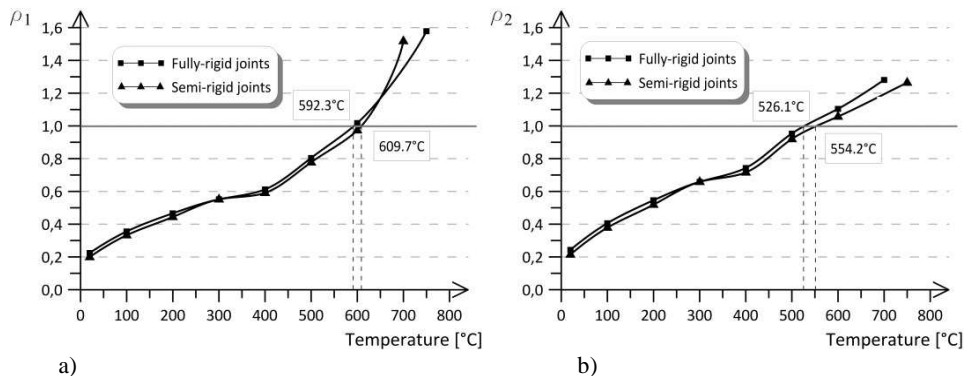


Fig. 6. Determination of the critical temperature in the case of column No 3 according to the second order theory, including: a) based on effort  $\rho_1$ , b) based on effort  $\rho_2$

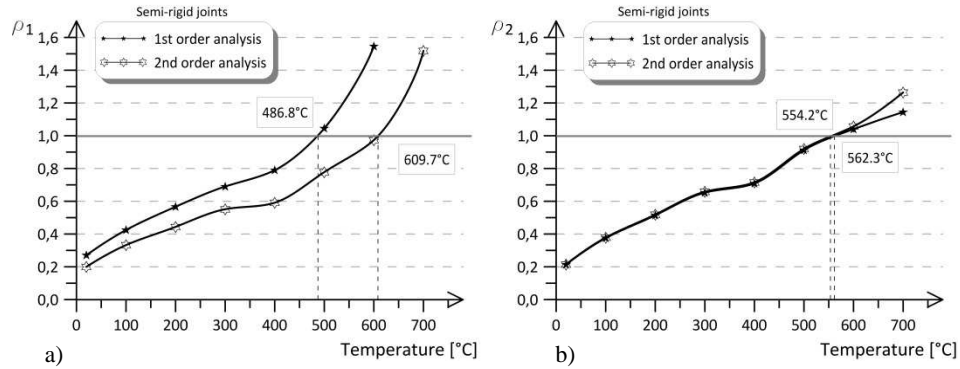


Fig. 7. Determination of the critical temperature in the case of column No 3 according to the first and second order theories, taking into account the joint flexibility changing with temperature, including: a) based on effort  $\rho_1$ , b) based on effort  $\rho_2$

**5.2. Results obtained for the beam No 7**

Analogous results obtained for the beam No 7 are depicted in Fig. 8, 9 and 10.

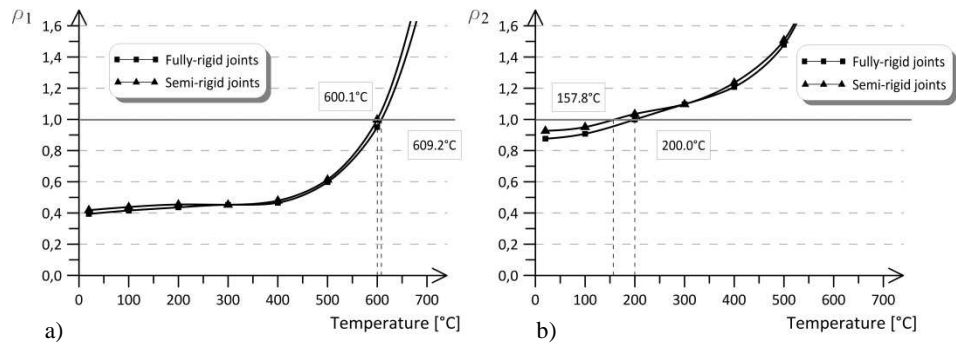


Fig. 8. Determination of critical temperature in the case of beam No 7, according to the first order theory, including: a) based on effort  $\rho_1$ , b) based on effort  $\rho_2$

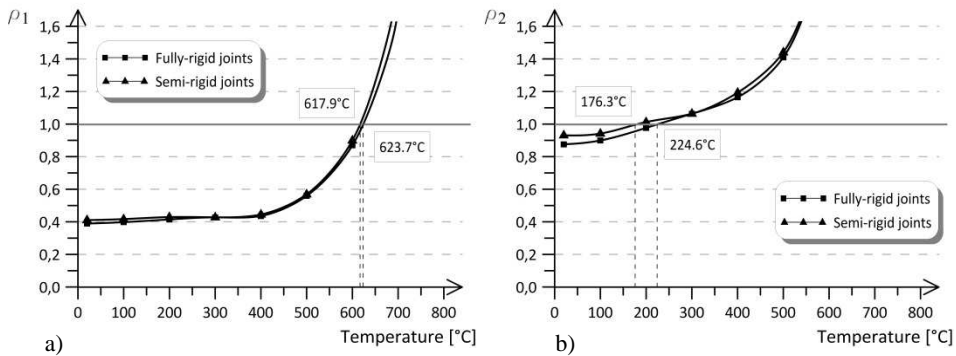


Fig. 9. Determination of critical temperature in the case of beam No 7, according to the second order theory, including: a) based on effort  $\rho_1$ , b) based on effort  $\rho_2$

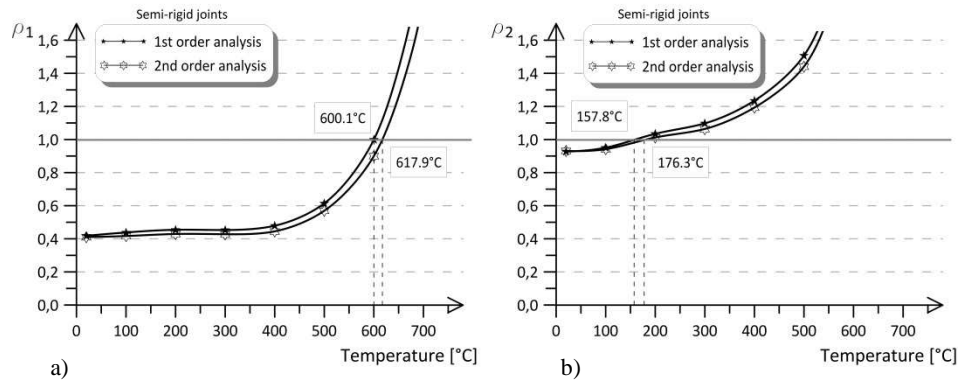


Fig. 10. Determination of critical temperature in the case of beam No 7, according to the first and second order theory, taking into account the joint stiffness changing with temperature, including: a) based on effort  $\rho_1$ , b) based on effort  $\rho_2$

This time, the far more restrictive estimates have been obtained for material effort  $\rho_2$ . However, it seems surprising, that a lower value of critical temperature is forecast in the case when the joint rigidity is decreasing with the developing fire (157.8°C related to 200.0°C when the first order theory is applied – Fig. 8a, and respectively 176.3°C related to 224.6°C when the second order theory is applied – Fig. 8b). Nevertheless, the estimates obtained with the second order theory seem to be much less restrictive than those obtained when the first order theory is applied (Fig. 10), this is analogous to the results obtained for column No 3. In addition, in the case of beam No 7 the sensitivity of the estimated effort  $\rho_1$  on the applied method of analysis is not very pronounced (Fig. 10a), this is in opposition to the phenomenon observed in the case of column No 3. This difference seems to be attributable to the fact that in the case of column compression plays the leading role in the interaction between bending moment and compressive axial force, while in the beam bending plays the dominant role.

## 6. Concluding remarks

Based on the performed analysis one may clearly foresee, that under the conditions of fully developed fire initiated at the ground floor of the considered frame, the beam denoted as the No. 7 in Fig. 1a would constitute the weakest link. The critical temperature assigned to this element, i.e. the temperature after reaching which the whole frame would lose the capability to safely support the applied loads, however, does depend on the way the calculations have been performed. It is not always true, that the application of a formal model more precisely describing the behavior of joints, i.e. taking into account the joint rigidity decreasing with increasing temperature would reveal an additional reserve of bearing capacity. In the example considered here the obtained critical

temperature estimates proved to be even more restrictive than the analogous estimates obtained earlier, with application of a simpler computational model. The estimated critical temperature also does depend on whether the first or second order theory has been used for calculations. This difference is especially pronounced in the case when the axial force starts to play a dominant role in the interaction of bending and compression.

## References

- [1] EN 1993-1-1, Eurocode 3: Design of steel structures, Part 1-1: General rules and rules for buildings.
- [2] Autodesk, Robot Structural Analysis 2010. User manual.
- [3] EN 1993-1-2, Eurocode 3: Design of steel structures, Part 1-2: General rules – Structural fire design.
- [4] EN 1990, Eurocode: Basis of structural design.
- [5] Maślak M., Snela M.: Critical temperature of steel frame with joint stiffness decreasing in fire, Scientific Papers of Rzeszów University of Technology, No 283, 2012, Series „Civil and Environmental Engineering”, Vol. 59 (3/12/II), pp. 241–248 (in Polish).
- [6] Maślak M., Snela M.: Moment – rotation relationship in fire conditions for a steel beam-to-column joint of known pliability, Building and Architecture, 12 (2), 2013, pp. 237–244 (in Polish).
- [7] Maślak M., Snela M.: Flexibility of a steel end-plate beam-to-column joint when exposed to a fire – two different, nonequivalent approaches to evaluate, Proceedings of the Eighth International Conference on Advances in Steel Structures (ICASS 2015), Lisbon, Portugal, July 21–24, 2015, paper 131, CD + pen-drive, 9 p.
- [8] Maślak M., Snela M.: Influence of increasing joint flexibility on critical temperature of steel frame in fire, Zbirek Naukowych Prac Ukrainського Instytutu Stalowych Konstrukcyj imieni W. M. Szimanowskiego, Wipusk 9/2012, Wydawnictwo “Stal”, Kiev, Ukraine, pp. 204–217.

*Przesłano do redakcji: 01.05.2018 r.*

*Przyjęto do druku: 15.06.2018 r.*



Mariusz MAŚLAK<sup>1</sup>  
Maciej SUCHODOŁA<sup>2</sup>  
Piotr WOŹNICZKA<sup>3</sup>

## TEMPERATURE DISTRIBUTION IN A STEEL BEAM-TO-COLUMN JOINT WHEN EXPOSED TO FIRE. PART 2: FLANGE-PLATES AND WEB- CLEATS JOINT

In the second part of this paper the temperature distribution is analysed for a thermally uninsulated steel beam-to-column flange-plates and web-cleats joint after 15 minutes of its exposure to a fully developed fire. Two types of such a joint are considered separately, firstly the pure steel connection with a beam and a column evenly heated on all four sides and then the analogous one, but with a massive reinforced concrete floor slab lying on the upper beam flange. In the latter case the joint beam is heated only on three sides. In addition, in each of the analysed joint the beams of two sizes are analysed independently for comparative purposes. Those that are made of the bigger I-section have a more slender web, while the smaller ones are more stocky. However, the smaller I-section heats faster than the bigger one because the section factor calculated for it has a greater value. In general, it can be concluded that in all the joints considered by the authors the steel temperature turned out to be much lower than that measured outside these joints. Moreover, a significant difference is observed in the temperature values identified in the beam web and in the beam flanges. Finally, the temperature distribution obtained from a numerical simulation and identified in the selected cross-sections of the joint beam in the case of a joint with adjacent floor slab is referred to the analogous distribution recommended for use in such circumstances in the standard EN 1993-1-2.

**Keywords:** beam-to-column joint, flange-plates joint, web-cleats joint, temperature distribution, section factor, numerical simulation

---

<sup>1</sup> Corresponding author: Mariusz Maślak, Cracow University of Technology, Faculty of Civil Engineering, Chair on Metal Structures, Warszawska 24, 31-155 Cracow, phone: 126282033, e-mail: mmaslak@pk.edu.pl

<sup>2</sup> Maciej Suchodoła, Cracow University of Technology, Faculty of Civil Engineering, Chair on Metal Structures, Warszawska 24, 31-155 Cracow, phone: 126282033, e-mail: maciej.suchodola@pk.edu.pl

<sup>3</sup> Piotr Woźniczka, Cracow University of Technology, Faculty of Civil Engineering, Chair on Metal Structures, Warszawska 24, 31-155 Cracow, phone: 126282033, e-mail: pwozniczka@pk.edu.pl

## 1. Introduction

In the first part of this paper the temperature distribution in a steel end-plate beam-to-column joint was analysed in detail, identified by a numerical analysis after 15 minutes of its simulated exposure to a fully developed fire. Two types of such a joint were considered separately, the first which was pure steel with heating the beam on all four sides and the second one, with a massive reinforced concrete floor slab lying directly on the upper beam flange, in which this beam was heated only on three sides. It has been pointed out that in fire conditions the temperature observed in individual joint components is always much lower than that recorded outside the joint. This diversity results mainly from the large accumulation of the steel sheets added in this zone that increase the effective thickness of the steel which has to be heated.

In this part of the paper, a different steel beam-to-column joint type is chosen for consideration, the one with flange plates and web cleats. Similarly as before, both a purely steel connection and a connection with an adjacent floor slab are analysed. Additionally, in each of the considered joint type it is assumed that the beams are made of the sections of two sizes, first from the IPE 330 steel section which is relatively stocky and then from the IPE 500 steel section, significantly more slender. The primary goal of the authors is now both a qualitative and a quantitative verification of the correctness of the temperature distribution recommended for use for such a joint in the standard EN 1993-1-2 [1].

## 2. The case of a pure steel joint

Let us start the detailed analysis of the temperature distribution observed in the joint under consideration after 15 minutes of its exposure to a fully developed fire from simulating the response of the numerical model of such a pure steel joint to a direct fire influence. This model is prepared using the ANSYS environment [2] and it is presented in detail in Fig. 1. As one can see the joint beam made of the IPE steel section (first of the IPE 330 and then of the IPE 500) is modelled as connected to the column made of the HEB wide-flange steel section (precisely of the HEB 180 when the beam is made of the IPE 330 and of the HEB 220 in the case when the beam is made of the IPE 500). This connection is realized by the web cleats composed of two steel angles of size L80x80x8 in the first case and L80x80x10 in the second case, set oppositely one to the other, with three rows of bolts M16. Such web cleats are attached to the column flange also by three bolts of the same size for each angle. The stiffness of the joint is ensured mainly by the flange plates of thickness 12mm in the first case when the section IPE 330 is considered and of thickness 16 mm in the second case when the section IPE 500 is assumed to the analysis, covering the beam from the bottom and from the top and attached to flanges of such the beam by four rows of bolts of size M20 with two bolts in each row. Moreover, two

double-sided horizontal ribs of thickness 10 mm (in the first case) or 16 mm (in the second case) are used in the levels defined by the upper and by the bottom beam flanges to stiffen the web of the column. There is neither a diagonal rib nor a wedge added at the bottom of the joint between the beam and the column flange.

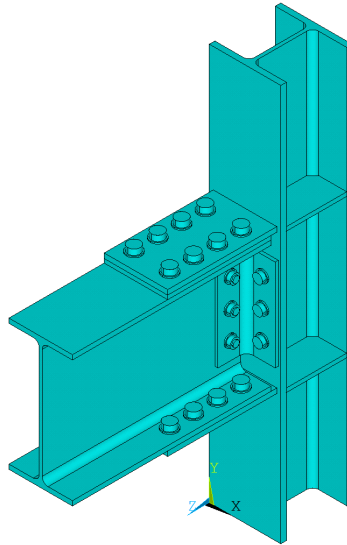


Fig. 1. Scheme of a numerical model of the pure steel joint considered in the example

The joint model presented above was evenly heated on all sides for 15 minutes by a simulated fire developing in accordance with a conventional standard scenario [3]. In Fig. 2a the temperature distribution is shown in detail identified in such a joint after this time of a fire exposure in the case when the IPE 330 steel section was assumed as a frame beam while in Fig. 2b the analogous temperature distribution but this time that related to the joint with the IPE 500 steel section used for this beam. As one can see, at any time of a fire the steel temperature observed at the joint itself is always significantly lower than that measured outside the joint. Let us note that in the first of the cases presented above the difference between the hottest and the least hot points of the joint turned out to be almost 200 degrees Celsius, however, in the second case it exceeded 250 degrees Celsius.

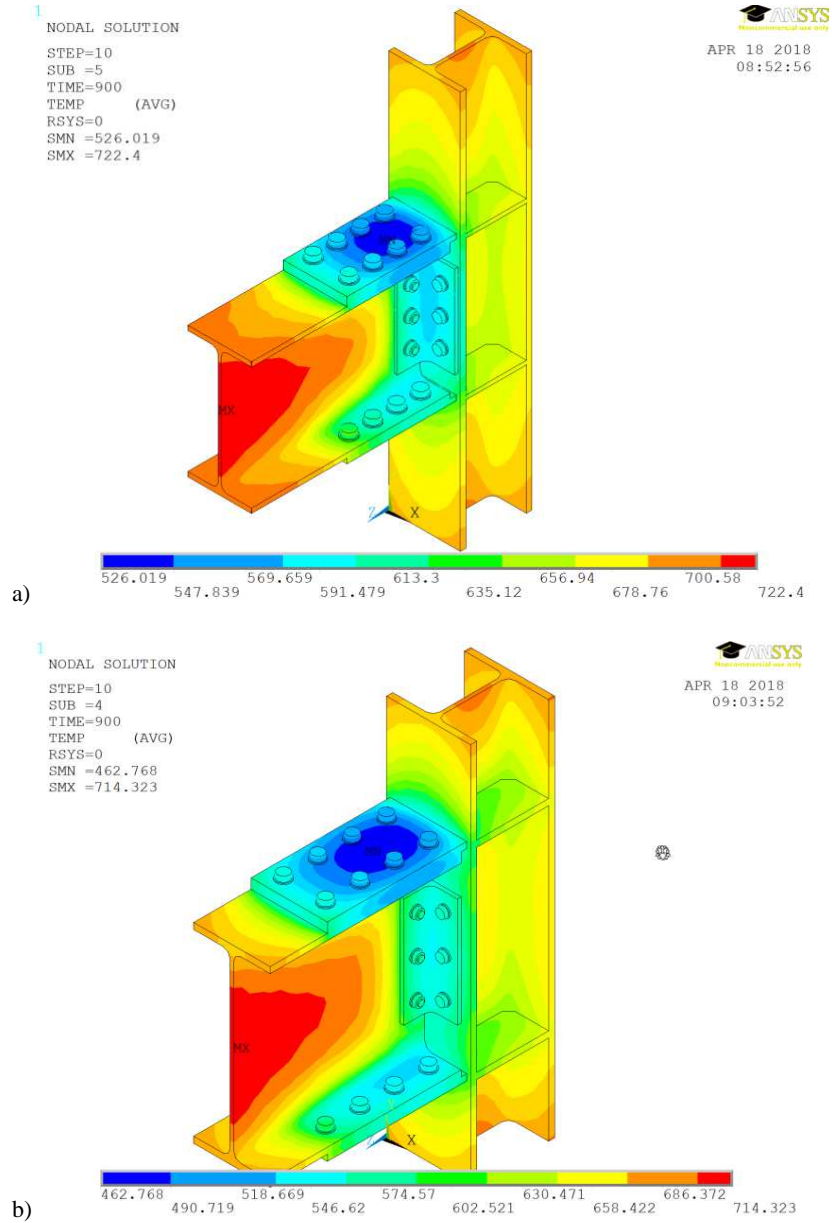


Fig. 2. Temperature distributions obtained for the evenly heated pure steel joint considered in the example after 15 minutes of its exposure to a fully developed standard fire, including:  
a) the case when the beam was made of a IPE 330 steel section, b) the case when the beam was made of the IPE 500 steel section

Details of the temperature values identified having finished the heating process in the two selected cross-sections of the considered beam, i.e. in the first section denoted by the symbol A-A which is situated in the joint itself, in place where the effective thickness of the heated steel sheet is simply the sum of the thickness of the beam web and of the thickness of two flanges belonging to the angles composed the web cleat, and in the second section denoted by the symbol B-B and localised outside the joint, are gathered in Fig. 3.

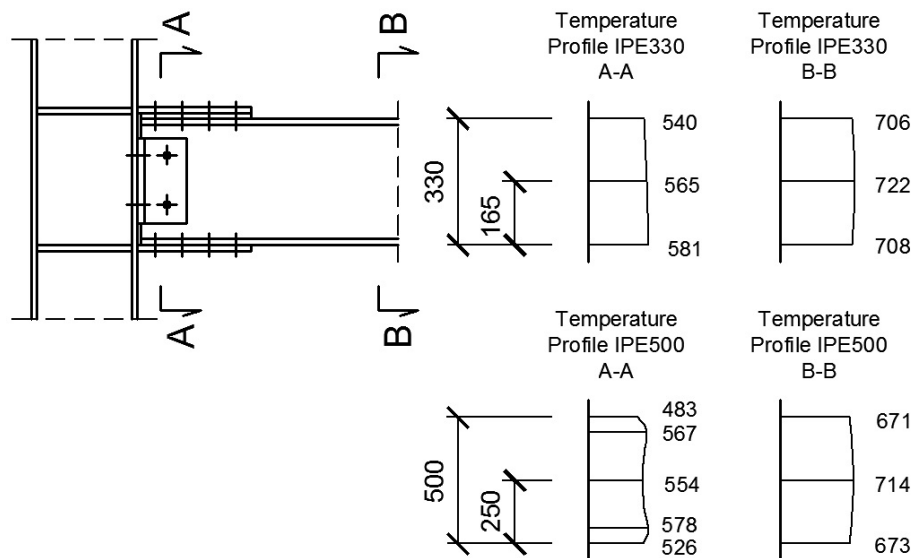


Fig. 3. Details of the steel temperature values as well as of the steel temperature distributions identified after 15 minutes of a direct fire exposure in the selected cross-sections of a beam being a part of the considered pure steel joint

Lack of symmetry in both temperature distributions presented in Fig. 3 and related to the section A-A results from the use of a horizontal steel spacer in the upper part of the joint that on the one hand facilitates the joint assembly but on the other hand increases the effective thickness of the heated beam flange. It is essential that the smaller I-section heats up much faster than the bigger one despite the fact that the latter section has more slender web. It is a result of the fact that the value of the so-called fire exposure coefficient, which is commonly named the section factor, for a smaller I-beam section ( $(U/A) = 201 \text{ m}^{-1}$ ) is significantly higher than in the case of the bigger I-beam ( $(U/A) = 151 \text{ m}^{-1}$ ). It is also worth noting that the temperature distribution in the web of beams which are respectively high is usually nonlinear while the analogous distribution observed in the beams which are not so high remains in the same conditions almost exactly linear. Let us also note that in the B-B cross-section situated outside the joint the most hot area turned out to be the web of the beam in the

place furthest from the flanges. In the section A-A the same zone was, however, much less heated due to the angles forming the web cleats and adjoining to the beam web. Therefore, the most hot in this section turned out to be some insulated web zones, those to which no additional elements are added.

### 3. The joint with a reinforced concrete floor slab lying directly on the upper beam flange

The second part of the analysis is devoted to recognition of the shape of the steel temperature distribution identified after 15 minutes of even heating under fully developed fire conditions in the steel beam-to-column joint with the floor slab lying directly on the upper beam flange. The thickness of such a floor slab was assumed in the considered example to be equal to 12 cm. The numerical model of the joint of this type with a geometry and dimensions fully analogous to the previous one described in the first part of this paper, which is prepared also in the ANSYS environment, is presented in detail in the Fig. 4. The upper horizontal rib stiffening the column web is invisible in this figure because it is fully covered with concrete.

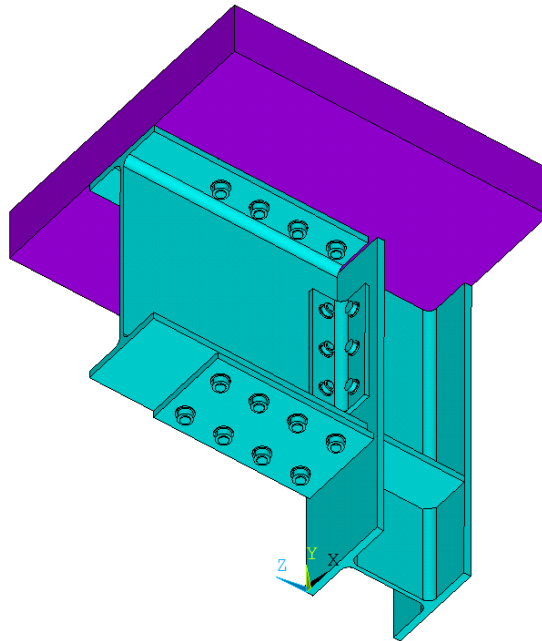


Fig. 4. Scheme of a numerically modelled steel beam-to-column joint with a reinforced concrete floor slab lying directly on the upper flange of the beam

As one can see, the beam is now heated under fire conditions only on three sides. The map of the temperature distribution identified in this joint after 15 minutes of its exposure to a fully developed fire is shown in detail in Fig. 5 for the case when the beam was made of the IPE 330 steel section.

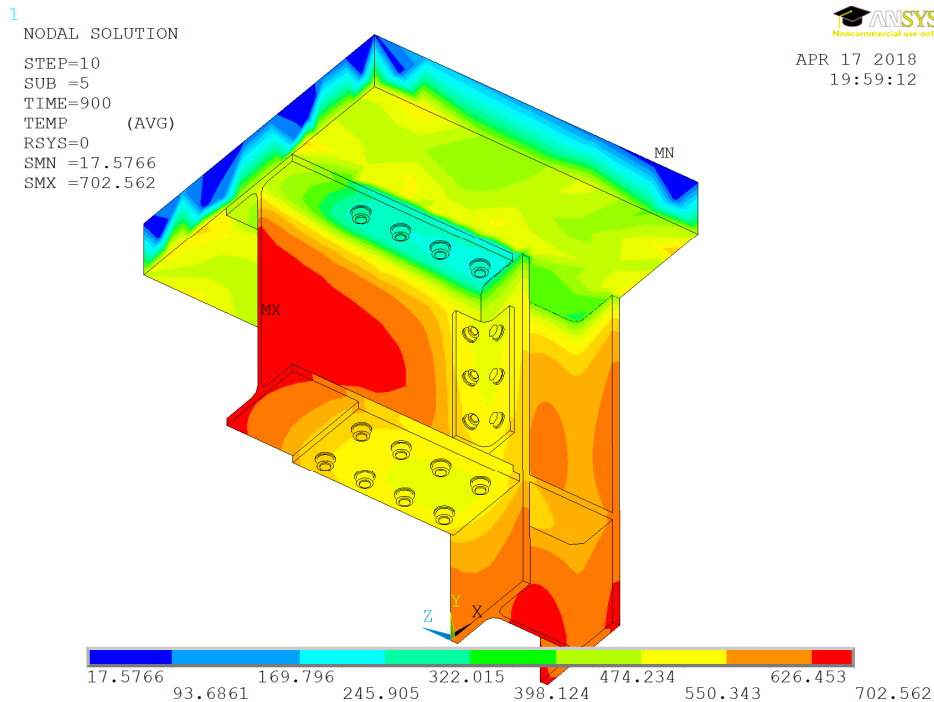


Fig. 5. Map of a steel temperature distribution obtained for a model of the joint considered in the example after 15 minutes of its simulated fire exposure (the case with the beam made of the IPE 330 steel section)

It is not a surprise now that the upper beam flange turned out to be definitely less hot than the neighbouring joint components. The heat reaching this flange is largely dissipated to a massive floor slab with a significant thermal capacity, which thus confirms good insulating properties of the concrete. This effect is well visible in the Fig. 6 in which the selected steel temperature distributions obtained for the joint considered in the example are presented in detail. Two cross-sections denoted in this figure by the symbols A-A and B-B, respectively, were chosen to conduct the suitable comparisons. As it was in the first part of the presented paper the first cross-section is now situated in the joint itself whereas the second one - outside the joint. Two pairs of the diagrams are stacked one above the other for comparative purposes. The first pair refers to a joint with a beam made of the IPE 330 steel section while the second one the analogous joint but that with a beam made of the IPE 500 steel section. In the

bigger of these two beams in the section A-A the nonlinearity of the steel temperature distribution over the entire height of the beam web is already noticed which cannot be seen in the smaller beam. In this smaller beam, only a nonlinear effect of cooling of an upper part of the beam cross-section caused by the proximity of the reinforced concrete slab is visible.

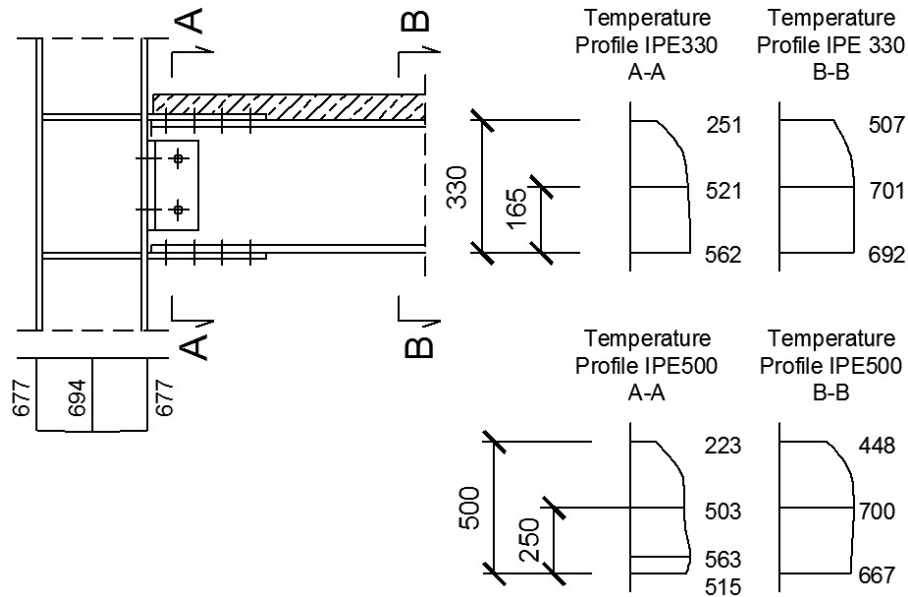


Fig. 6. Steel temperature distributions obtained in the selected beam cross-sections for the joint considered in the example after 15 minutes of a simulated fire exposure. The steel temperature distribution identified at the same time of the heating process in the cross-section related to the neighbouring column is presented on the left side of this figure

The conclusions resulting from Fig. 6 basically coincide with those formulated earlier after the presentation of Fig. 3. The smaller beam heats up faster than the bigger one and the difference between the temperature values identified in the same cross-sectional areas and at the same time points of the heating process in the sections A-A and B-B, respectively, reaches 250 degrees Celsius. In the case of the smaller of the two beams which are considered in this example, the most heated zone in the section A-A turns out to be the bottom flange, which is not true when the cross-section of the beam is higher and therefore more slender.

In addition, in Fig. 6 the temperature distribution relating to the selected cross-section of the neighbouring steel column when it is made of the HEB 180 wide-flange section is presented for comparative purposes. It is obvious that the web of such the column turned out to be more hot than the adjoining column flanges because they are significantly thicker.

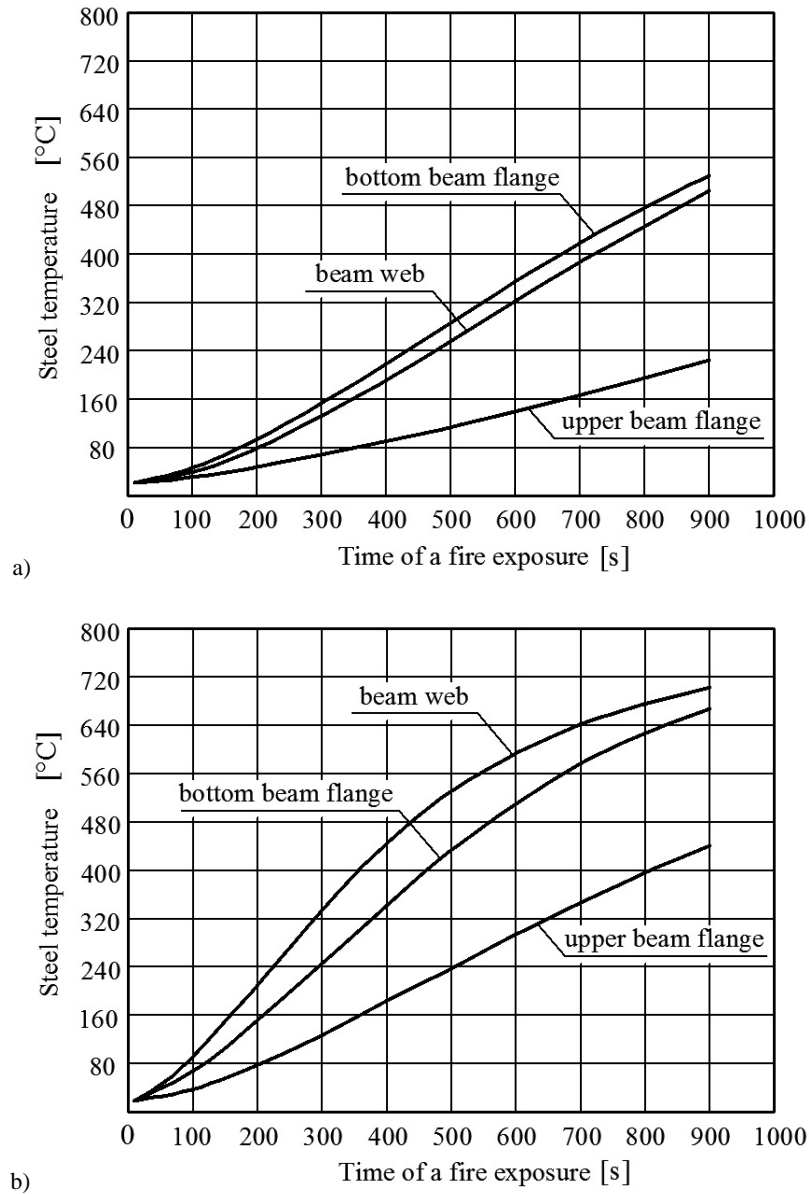


Fig. 7. Development of a steel temperature rise observed in individual beam components being a part of the joint with concrete floor slab considered in the example, during the exposure of such a joint to a standard fully developed fire, including: a) relationships identified in the section A-A, b) relationships identified in the section B-B. The localisation of such both sections is marked in Fig. 6. It is assumed that the beam was made of the IPE 330 steel section

The diagrams presented in Figs. 7a and 7b seem to be very informative. It is shown in them how, in the case of a thermally unprotected steel beam-to-column joint considered in the example with the reinforced concrete floor slab lying on the upper beam flange and with the beam made of the IPE 330 steel section, together with the fire development increased the difference between the temperature values relevant for the beam web and for the upper and bottom beam flanges, appropriately identified in the section A-A (Fig. 7a) and in the section B-B (Fig. 7b).

#### **4. Verification of the correctness of the joint temperature distribution recommended for use in the standard EN 1993-1-2**

In conventional fire safety assessment related to the steel frame load-bearing structures usually a simplifying but very conservative assumption is accepted for calculation that the steel temperature in all components of the considered joint at any given time of a fire can be treated as fully aligned and equal to the maximum temperature of such the steel measured outside this joint at the same time of this fire. For more precise estimation, however, in Annex D3 of the standard EN 1993-1-2 [1], in the case when the steel beam-to-column joint is covered by an adjacent reinforced concrete floor slab, it is recommended to use in this field the equivalent steel temperature distributions, differentiated depending on whether the height of the joint beam is greater or smaller than 400 mm. Considering that in the case of the first of beams analysed in this article, the one made of the IPE 330 steel section for which  $h < 400$  mm, the steel temperature measured in the bottom beam flange in the section B-B, i.e. outside the joint, after 15 minutes of the standard fire exposure, was identified as being equal to 692 degrees Celsius (see Fig. 6) the equivalent temperature distribution corresponding to this situation and recommended in the standard [1] has the form shown in detail in the middle of the Fig. 8. Similarly, in the case of the second beam, the one made of the IPE 500 steel section for which  $h > 400$  mm, the steel temperature measured after the same fire duration in the bottom beam flange was equal to 667 degrees Celsius (see Fig. 6), which gave an equivalent standard steel temperature distribution shown on the right side of the Fig. 8. Let us note that neither the temperature 692 degrees Celsius nor the temperature 667 degrees Celsius, both measured in section B-B in the bottom beam flange, were not the maximum temperature values identified in this section. Much hotter than the bottom beam flange in both cases turned out to be the web of the beam.

Comparison of the steel temperature distributions, those taken from the Fig. 8 with the corresponding distributions specified earlier for the A-A section of the considered steel beam-to-column joints covered by a reinforced concrete floor slab and obtained for the same beams and for the same fire exposure conditions but after the use of the more precise numerical analysis (they are

presented in Fig. 6), allows to conclude that the recommendations proposed by the standard [1] are calibrated safely but they are still very conservative.

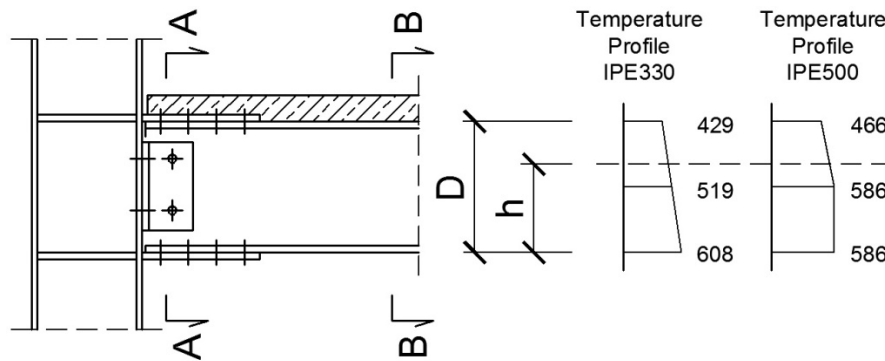


Fig. 8. Equivalent steel temperature distributions recommended in the standard EN 1993-1-2 [1] for beam-to-column joints with adjacent reinforced concrete floor slab considered in the example

## 5. Concluding remarks

The primary goal of the authors was to show in both parts of the presented paper that in a fire situation the steel temperature distribution in a steel beam – to-column joint is not homogeneous, regardless of whether it is a pure steel joint or one that is adjacent to a reinforced concrete floor slab. The fact of the heterogeneity of this type has a significant impact on the real course of the redistribution of internal forces in a fire, and thus on the guaranteed safety level [4, 5]. The uneven steel temperature distribution in the joint components determines both the effective load capacity of such a joint and its stiffness identified for the predicted scenario of a fire development. The situation is complicated by the fact that both of these parameters change with the development of a fire and they are therefore difficult to quantify.

## References

- [1] EN 1993-1-2. Eurocode 3: Design of steel structures. Part 1-2: General rules - Structural fire design.
- [2] Kohnke P. (Ed.): ANSYS®: Theory reference. Release 5.6. Canonsburg, PA, USA, November 1999.
- [3] EN 1991-1-2. Eurocode 1: Actions on structures. Part 1-2: General actions – Actions on structures exposed to fire.
- [4] Maślak M., Pazdanowski M., Snela M.: Redistribution of internal forces generated in a steel frame structure with flexible joints when exposed to a fire, in: Giżejowski M., Kozłowski A., Marcinowski J., Ziółko J. (Eds.) – Recent progress in steel and composite structures, Proceedings of the 13<sup>th</sup> International Conference on Metal Structures (ICMS 2016), Zielona Góra, Poland, June 15-17, 2016, CRC Press/Balkema, Leiden, The Netherlands, abstract pp. 136-137, paper CD pp. 315–322.

- [5] Maślak M., Pazdanowski M., Woźniczka P.: Influence of joint stiffness on the behaviour of steel bearing frame under fire conditions, Ce/Papers, The Online Collection for Conference Papers in Civil Engineering, Ernst & Sohn, A Wiley Brand, 1 (2017), No. 2 & 3, pp. 2811–2820.

*Przesłano do redakcji: 01.05.2018 r.*

*Przyjęto do druku: 15.06.2018 r.*

Przemysław KRYSOSIK<sup>1</sup>

## DESIGN RESISTANCE OF WELDED KNEES IN STEEL FRAMES

The paper presents issues related to calculations of welded knee joints, in which the interconnected load-bearing elements, beams and columns, can be made from plate girders with slender webs.

At the beginning, a typical knee joint of portal steel frame was characterized, along with presentation of calculations for the internal forces in characteristic zones of the knee, i.e. in tension, shear, and compression zone. Then, the checking procedures of resistance were presented in detail for each designated knee zone, paying particular attention to the influence of complex stresses state and loss of stability in the shear and the compression part of knee joint.

The work also presents a comprehensive calculation example, which illustrates the described method usage in practical design of welded knees of steel frames.

**Keywords:** steel frame, knee joint, transverse stiffeners, diagonal stiffeners, resistance

### 1. Introduction

Knee of steel frame, also called a knee joint (or an eaves joint), is a connection place of the load-bearing elements of the frame, i.e. the beam (rafter) and the column. Due to the kind of connected elements used, that joint can be classified as so-called, beam-to-column joints.

Designing this type of joints is quite difficult, mainly due to the complex geometry, which in turn causes a complex system of forces (stresses) acting in the knee. This mainly applies to design of bolted end-plate joints, where the need to transfer large internal forces and getting appropriate stiffness make calculations for this type of joints rather difficult [1–3].

Application of the solution in the form of welded knee joint often allows with less effort to design the joint with appropriate large resistance and stiffness, which often is also easier to manufacture. In that cases the bolted connection assembly can be located near the knee, e.g. in the beam, where there are generally smaller internal forces.

---

<sup>1</sup> Corresponding author: Przemysław Krystosik, Koszalin University of Technology, Faculty of Civil Engineering, Environmental and Geodetic Sciences, Śniadeckich 2 street, 75-453 Koszalin; tel. +48 94 34 78 577; krystosik@wbis.tu.koszalin.pl, <https://orcid.org/0000-0003-2871-8746>

Nowadays, the most commonly used method in design of steel frames joints is, a component method, recommended by Eurocode [4]. It is characterized by fairly high versatility, because the basic assumptions of that method allowed to generalize and adapt the computational algorithms so that it could be used to design welded and bolted internal joints, as well as column bases.

Despite this, application range of this method, included in the standard [4], has its own limitations. They result, among others, from the conditions of joint plates slenderness, limiting the use of Eurocode [4] to cases, where, e.g. sheared panel of column web is insensitive to instability.

This inconvenience makes it difficult to use the standard [4] when designing steel frames knees, in which the bearing elements (beams and columns) are designed from plate girders cross-sections, characterized by significant slenderness of the webs. Due to the fact that frames with plated structural elements are often used in steel construction, the procedures included in the standard [4] should be generalized in such a way that would allow to design the knee joints in that type of frames. This condition, according to the author, is met with the computational method of rectangular knees of steel frames discussed in this paper, which is partially based of information presented in [5], and also takes into account EC3 [4] provisions.

## 2. Analysis of forces acting in frame knee

Due to the complex geometry of a typical knee, the way of combining individual elements (type of welds used, technology used in performance of welded connections), as well as issues of plates instabilities cause that accurate static and strength analysis of the considered joint requires appropriate software usage (e.g. based on the finite elements method) and the use of very complex numerical models [6].

In practical design, generally, there is no need to conduct very detailed calculations of frames knees [7]. Considering the equilibrium conditions of the loaded model of knee joint (Fig. 1a), stress distribution and forces system acting on the individual components of the joint can be obtained at rough estimate (Fig. 1b and 1c). Thus, the values of the forces acting respectively in the tension zones ( $F_{bt}$  and  $F_{ct}$ ) and the compression zones ( $F_{bc}$  and  $F_{cc}$ ) of the joint can be approximately calculated from the equations:

$$F_{bt} = \frac{M_b}{b} - \frac{N_b}{2}, \quad F_{bc} = \frac{M_b}{b} + \frac{N_b}{2}, \quad F_{ct} = \frac{M_c}{c} - \frac{N_c}{2}, \quad F_{cc} = \frac{M_c}{c} + \frac{N_c}{2} \quad (1)$$

whereas, the shear forces values, corresponding to the tangential stresses in panel of the joint web can be determined with the use of expressions (Fig. 1d):

$$V_{sb} = F_{cc} - V_b = F_{ct}, \quad V_{sc} = F_{bc} - V_c = F_{bt} \quad (2)$$

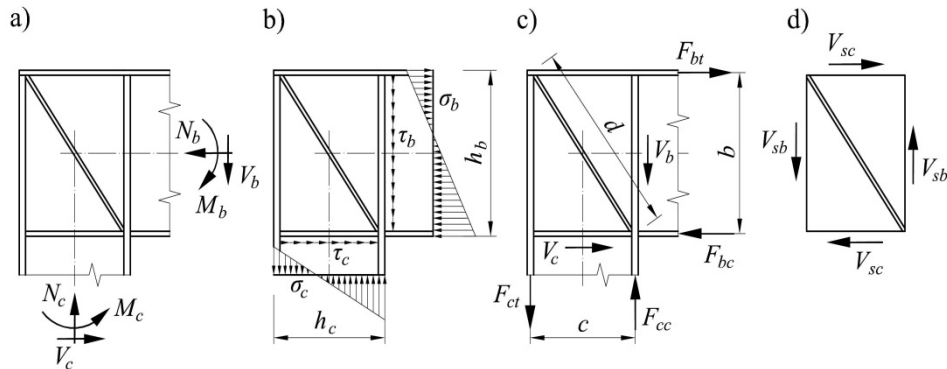


Fig. 1. Knee of frame analyzed: a) loading scheme of the knee, b) approx. stresses distribution in the knee, c) simplified system of the forces in the knee, d) scheme of the shear forces in the web panel

In case when the cross-sections of the column and the beam, as well as the welded connections have the required resistances, the calculation of the considered joint can be reduced to checking the resistance conditions in the tension, compression and shear zones.

### 3. Dimensioning of frame knee

Knowing the system and the type of forces acting in the separated zones of the joint, it is relatively easy to formulate the appropriate resistance conditions for each of mentioned zones. It gives the possibility to design the joint without having to run, often more complex calculations of resistance of the entire joint, e.g. due to bending.

#### 3.1. Resistance of tension zone

Checking the resistance condition of the tension zone can be performed according to the expression:

$$\frac{F_{bt}}{F_{t,Rd}} \leq 1 \quad (3)$$

where  $F_{t,Rd}$  is a resistance of tension zone of the welded joint, which can be obtained in accordance with point 6.2.6.3 of standards [4].

In case of knee joints of portal frames the top flange of beam is generally elongated in such a way that it could be directly connected with the exterior flange of column, thus covering the top edge of column (see Fig. 1a). In that case demonstration of the condition (3) can be presented in the form of resistance condition of the top flange cross-section of the beam, in which the tension resistance of the flange determines the equation:

$$F_{t.Rd} = \frac{b_{fb} t_{fb} f_y}{\gamma_{M0}} \quad (4)$$

where:  $b_{fb}$  and  $t_{fb}$  are respectively the beam flange width and thickness,  $f_y$  is the yield strength of steel, and  $\gamma_{M0}$  is the partial factor.

### 3.2. Resistance of shear zone

Checking of the shear zone resistance can be carried out on the basis of the condition in the form:

$$\frac{V_{sc}}{V_{wc.Rd}} \leq 1 \quad (5)$$

in which  $V_{wc.Rd}$  is the resistance of the shear zone in the form of the web panel.

The procedure of the resistance calculations should begin with sensitivity assessment of the column web panel due to the shear instability. In case, when the web panel considered is freely supported on all four edges (Fig. 2a), the sensitivity condition to instability of the web panel can be presented in the form [9]:

$$\lambda_w = \frac{c}{t_{wc}} \leq \frac{31}{\eta} \varepsilon \sqrt{k_\tau} \quad (6)$$

where:  $\eta = 1.2$  if  $f_y \leq 460$  MPa, whereas  $k_\tau$  is a coefficient taking into account boundary conditions and stresses distribution in the analyzed plate.

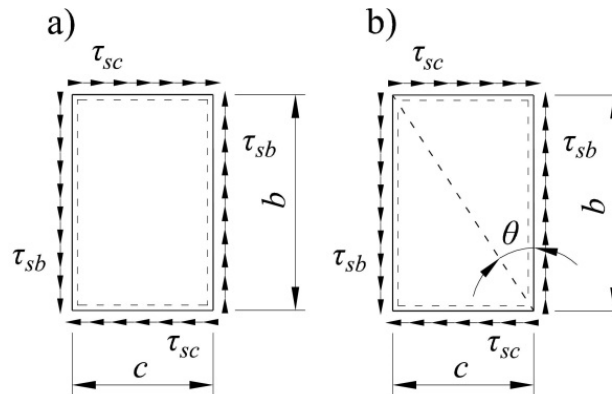


Fig. 2. Analyzed web panel of knee: a) single rectangular panel, b) system of two triangular panels

In the considered case the coefficient  $k_\tau$  can be determined with the use of expressions [9]:

$$k_r(\alpha) = 4 + \frac{5.34}{\alpha^2}, \text{ if } \alpha \leq 1 \quad (7)$$

$$k_r(\alpha) = 5.34 + \frac{4}{\alpha^2}, \text{ if } \alpha > 1$$

where  $\alpha \approx b/c$  (see Fig. 2a).

Application of additional stiffening of the shear zone in the form of diagonal stiffeners leads to the change of supporting conditions in the web panel, converting one rectangular panel into two triangular panels (Fig. 2b). In such cases, the coefficient  $k_r$  can be determined according to the relationships given in the works [10], [11]:

$$k_r(\xi) = 5.34(1 + \xi^2) + 19.3\xi, \text{ for compressed stiffeners} \quad (8)$$

$$k_r(\xi) = 5.34(1 + \xi^2) + 0.87\xi, \text{ for tensioned stiffeners}$$

which, as in case of the rectangular plate, were formulated on the assumption that the exterior edges of both panels are freely supported (Fig. 2). The graphical interpretation of coefficients value change  $k_r$ , in the angle function  $\theta$  of the stiffening ribs inclination, (see Fig. 2b) is shown in Figure 3.

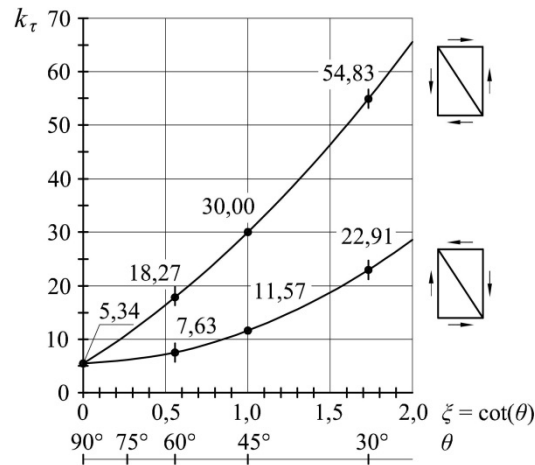


Fig. 3. Relationship of the coefficient  $k_r$  from angle  $\theta$

It can be noticed that the presented graphs of the  $k_r(\xi)$  function clearly indicate that supporting of the web panel with diagonal stiffeners reduces its sensitivity to loss of stability, especially when forces in the knee induce compression of the stiffeners.

Resistance determination of the web panel in case, when the condition (6) is met, can be determined according to the formula [12].

$$V_{wc.Rd} = \frac{A_{wc} f_y}{\sqrt{3} \gamma_{M0}} \sqrt{1 - \left( \frac{\sigma}{f_y} \right)^2} \quad (9)$$

where  $A_{wc} = h_{wc} t_{wc}$  is a shear area, while  $\sigma$  is stresses value from axial force in the column. In case, where  $\sigma$  does not exceed 50% of yield strength  $f_y$ , the resistance of sheared plate can be determined according to the equation [4]:

$$V_{wc.Rd} = 0.9 \frac{A_{wc} f_{y.wc}}{\sqrt{3} \gamma_{M0}} \quad (10)$$

If, however, the slenderness condition of stiffened web (6) is not met, then its resistance can be determined with the formula [9]:

$$V_{wc.Rd} = \chi_w \frac{A_{wc} f_y}{\sqrt{3} \gamma_{M0}} \quad (11)$$

in which  $\chi_w$  is a shear buckling factor. Assuming, in accordance with the provisions of the standard [9], that the applied web stiffeners belong to, so-called, flexible stiffeners (non-rigid end post), that the parameter value  $\chi_w$  can be determined based on the equation:

$$\chi_w = \min \left( 0.9; \frac{0.83}{\bar{\lambda}_w} \right) \quad (12)$$

where  $\bar{\lambda}_w$  is a shear panel slenderness:

$$\bar{\lambda}_w = \sqrt{\frac{f_y}{\sqrt{3} \tau_{cr}}} \quad (13)$$

Value of elastic shear buckling stresses  $\tau_{cr}$  can be calculated on the basis of formula:

$$\tau_{cr} = \frac{\pi^2 E k_\tau}{12 (1 - \nu^2) \lambda_w^2} \quad (14)$$

in which parameters  $E$  i  $\nu$  are respectively the modulus of elasticity and the Poisson's ratio.

In case of the stiffened knee with diagonal stiffeners, special attention should be paid to the fact, that the components of the shear zone – web panel and

the stiffeners can achieve resistance under the influence of significantly differing forces. In order to determine the appropriate load distribution for each of the listed components, a system of equations can be formulated in the form:

$$\begin{aligned} V_{sc} &= V_{wc} + V_{sd} \\ \delta &= \delta_{wc} = \delta_{sd} \end{aligned} \quad (15)$$

The first equation results from the equilibrium conditions of the forces in the shear zone, while the second one describes the conditions of displacements compatibility in this zone (Figure 4).

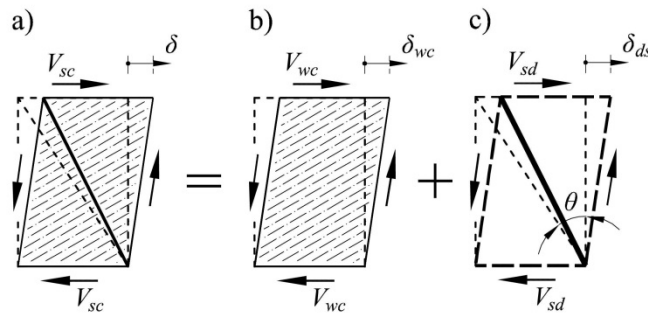


Fig. 4. Distribution of forces and deformation: a) whole shear area, b) web panel, c) stiffening ribs

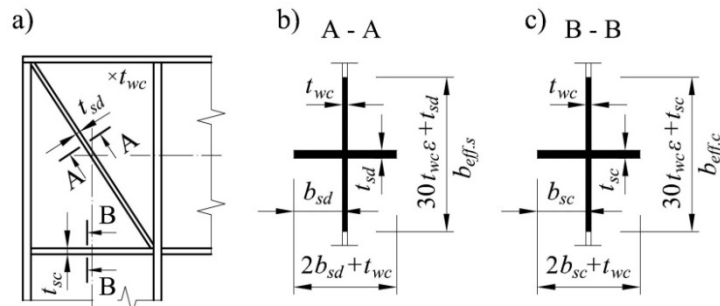


Fig. 5. Stiffeners of the knee joint: a) strengthening in the form of transverse and diagonal stiffeners, b) stiffened cross-section of the shear zone, c) stiffened cross-section of the compressed zone

Displacements caused by  $V_{wc}$  and  $V_{sd}$  forces acting on the relevant components are determined in the following equations:

$$\delta_{wc} = \frac{V_{wc} b}{A_{wc} G}, \quad \delta_{sd} = \frac{V_{sd} b}{E A_{sd} \sin^2(\theta) \cos(\theta)} \quad (16)$$

where:  $A_{sd}$  is the cross-section of the substitute compression element of the stiffened shear zone (Figure 5b). After some transformations, formulas on the values of the forces acting in each component of the shear zone can be determined:

$$V_{wc} = \left( \frac{A_{wc}}{A_{eq} + A_{wc}} \right) V_{sc}, \quad V_{ds} = \left( \frac{A_{eq}}{A_{eq} + A_{wc}} \right) V_{sc}, \quad (17)$$

where:

$$A_{eq} = A_{sd} \frac{E}{G} \sin^2(\theta) \cos(\theta) \quad (18)$$

Knowing these forces, the condition of the shear zone resistance can be formulated in the form of two inequalities:

$$V_{wc.Rd} = 0.9 \frac{A_{wc} f_y}{\sqrt{3} \gamma_{M0}} \leq V_{wc}, \quad V_{sd.Rd} = \frac{A_{sd} f_y}{\gamma_{M0}} \sin(\theta) \leq V_{sd}, \quad (19)$$

in case, when both components of the stiffened web are not sensitive to stability loss

Evaluation of the resistance of the stiffened shear zone, treated as a substitute diagonal member with a crossed cross-section (Fig 5b), which is sensitive to the loss of stability can be carried out in accordance with the algorithm used while checking resistance of compression elements [8]. For this purpose, the resistance condition of compression member, subject to the out-of-plane web buckling, should be determined using the formula:

$$V_{sd.Rd} = \chi \frac{A_{sd} f_y}{\gamma_{M1}} \sin(\theta) \leq V_{sd} \quad (20)$$

where  $\gamma_{M1}$  is the partial factor, and  $\chi$  is a reduction factor, calculated according to expression [8]:

$$\chi = \frac{1}{\phi + \sqrt{\phi^2 - \bar{\lambda}^2}} \quad (21)$$

in which:

$$\phi = \frac{1}{2} [1 + \alpha_0 (\bar{\lambda} - 0.2) + \bar{\lambda}^2] \quad (22)$$

The imperfection parameter  $\alpha_0$  can be assumed as value which equals 0.49, whereas a non-dimensional slenderness is calculated according to the formula:

$$\bar{\lambda} = \sqrt{\frac{A f_y}{N_{cr}}} = \frac{\lambda}{\lambda_1} \quad (23)$$

Slenderness of the substitutive compressed element  $\lambda$  due to the out-of-plane web buckling and a relative slenderness  $\lambda_1$  are obtained with the use of equations:

$$\lambda = \frac{\mu l}{i} \quad (24)$$

$$\lambda_1 = \pi \sqrt{\frac{E}{f_y}} = 93.9\epsilon \quad (25)$$

where:  $l$  is a length of substitutive member,  $\mu$  is a buckling length coefficient, which can be assumed with a value of 0.75, if both ends of stiffeners are fixed (e.g. in flanges of column) [9], and a radius of gyration  $i$  should be determined for the cross-section of the compression member (Fig. 5b) with respect to the vertical symmetry axis.

In the compressive resistance calculations of the stiffened components of the joint one should also take into account their sensitivity to loss of stability due to the torsional buckling. The resistance to this type of instability can be tested using the condition [9]:

$$\frac{I_t}{I_p} \geq 5.3 \frac{f_y}{E} \quad (26)$$

where  $I_t$  is the St. Venant torsional constant of the stiffener alone, while  $I_p$  is the polar second moment of area of single stiffener alone around the edge fixed to the plate. The fulfillment of this condition means that the checked stiffener is resistant to the torsional form of stability loss.

### 3.3. Resistance of compression zone

Checking the resistance of compression zone of the beam-to-column joints can be carried out according to the resistance condition in the form:

$$\frac{F_{bc}}{F_{c.Rd}} \leq 1 \quad (27)$$

in which  $F_{c.Rd}$  is the resistance of unstiffened compressed zone, which can be determined according with the standard [4] guidelines.

In case of occurrence of the diagonal stiffeners in the knee (see Fig. 5a) the resistance condition can be presented with the use of inequality:

$$\frac{F_{bc} - V_{sd}}{F_{c.Rd}} \leq 1 \quad (28)$$

However, when designing knee joints, in which the plate girders are connected together, the web panel of column is very often susceptible to stability loss, which does not guarantee the entire joint the adequate resistance. Strengthening the compressed zone with transverse stiffeners (flat ribs) greatly improves the resistance of the web to local buckling (Fig. 5a and 5c).

In case, when the value of a non-dimensional slenderness of the compression zone, treated as a substitute member with a crossed cross-section (Fig. 5c) is not larger than 0.2, and the stiffeners in the form of flat ribs are not sensitive to loss of the local stability, that resistance of that zone can be obtained from the equation:

$$F_{c.wc.Rd} = \frac{\omega k_{wc} b_{eff.c} t_{wc} f_y}{\gamma_{M0}} + \frac{2b_{sc} t_{sc} f_y}{\gamma_{M0}} \quad (29)$$

in which  $\omega$  and  $k_{wc}$  are, calculated according to point 6.2.6.2. [4], coefficients taking into account the reduction of resistance due to the complex state of stresses in the web panel, whereas  $b_{eff.c}$  is an effective width, equal  $30t_{wc} \varepsilon + t_{sc}$  (Fig. 5c).

Evaluation of the resistance of the stiffened compression zone, which is susceptible to the loss of stability ( $\bar{\lambda} > 0.2$ ) can be carried out in accordance with the algorithm used while checking resistance of compression elements [8]. For this purpose, the resistance of compression zone, sensitive to the out-of-plane web buckling, should be determined using the formula:

$$F_{c.Rd} = \chi \left( \frac{\omega k_{wc} b_{eff.c} t_{wc} f_y}{\gamma_{M1}} + \frac{2b_{sc} t_{sc} f_y}{\gamma_{M1}} \right) \quad (30)$$

Calculation of the coefficient  $\chi$  in the formula (30) should be carried out analogously to resistance checking of the stiffened shear zone case, here taking into account the geometrical and material quantities of the transverse stiffeners of the web panel. Assessment of the sensitivity to loss of stability due to the torsional buckling of transverse stiffeners also should be checked.

#### 4. Numerical example

On the basis of information presented in this paper, the knee of a certain steel frame, shown in Figure 6a), was calculated.

Using the results of static calculations in the form of forces acting on the frame knee (Fig. 6b), geometry of the cross-sections of the beam and the column



which roughly correspond to the proportions of IKS girders, was assumed. Next, taking into account the geometry of the knee (Fig. 6d), and the local equilibrium conditions (Fig. 6c), the moments  $M_b$  and  $M_c$  acting on the calculated joint were determined.

**Data:** Steel S355:  $E = 210$  GPa,  $G = 81$  GPa,  $f_y = 355$  MPa,  $\varepsilon = 0.814$ ,  $\eta = 1.2$ ; forces acting on the knee from the beam side (Fig. 6d; D – D cross-section):  $M_b = 1\,473.22$  kNm,  $N_b = 254.83$  kN,  $V_b = 330$  kN, forces acting on the knee from the column side (Fig. 6d; C – C cross-section):  $M_c = 1\,473.78$  kNm,  $N_c = 330$  kN,  $V_c = 254.83$  kN.

Geometric properties of the column: area of the cross-section  $A_c = 15 \times 10^3$  mm<sup>2</sup>, second moment of the cross-section  $I_c = 2.65 \times 10^9$  mm<sup>4</sup>.

Geometric properties of the tension zone: width of the beam flange  $b_{bf} = 250$  mm, thickness of the beam flange  $t_{bf} = 16$  mm.

Geometric properties of the shear zone: shear area:  $b_{sd} = 100$  mm,  $t_{sd} = 10$  mm,  $A_{wc} = 7 \times 10^3$  mm<sup>2</sup>, effective width of the web panel  $b_{eff.s} = 180.86$  mm, area of the cross-section  $A_{sd} = 3.27 \times 10^3$  mm<sup>2</sup>,  $I_{sd} = 5.73 \times 10^6$  mm<sup>4</sup>, radius of the cross-section gyration  $i_{sd} = 41.90$  mm.

Geometric properties of the compression zone:  $b_{sc} = 120$  mm,  $t_{sc} = 12$  mm, effective width of the web panel  $b_{eff.c} = 182.86$  mm, area of the cross-section  $A_{sc} = 4.16 \times 10^3$  mm<sup>2</sup>, second moment of the cross-section  $I_{sc} = 11.62 \times 10^6$  mm<sup>4</sup>, radius of the cross-section gyration  $i_{sc} = 52.86$  mm.

Resistance calculations of the knee were performed considering two cases:

- case I - the knee is not stiffened with diagonal stiffeners in the shear zone,
- case II - the knee is stiffened with diagonal stiffeners in the shear zone.

#### Determination of internal forces in the knee joint (acc. to 2)

$$F_{bt} = \frac{M_b}{b} - \frac{N_b}{2} = \frac{1\,473.22 \text{ kNm}}{1.316 \text{ m}} - \frac{254.83 \text{ kN}}{2} = 992.05 \text{ kN}$$

$$F_{bc} = \frac{M_b}{b} + \frac{N_b}{2} = \frac{1\,473.22 \text{ kNm}}{1.316 \text{ m}} + \frac{254.83 \text{ kN}}{2} = 1\,246.88 \text{ kN}$$

$$V_{sc} = F_{bt} = F_{bc} - V_c = 1\,246.88 \text{ kN} - 254.83 \text{ kN} = 992.05 \text{ kN}$$

#### Calculation of the tension zone (acc. to 3.1)

- Resistance of tension zone

$$F_{t.Rd} = \frac{b_{fb} t_{fb} f_y}{\gamma_{M0}} = \frac{250 \cdot 16 \cdot 355}{1.0} = 1\,420 \text{ kN}$$

- Resistance condition of the tension zone

$$\frac{F_{bt}}{F_{t.Rd}} \leq 1 \rightarrow \frac{992.05 \text{ kN}}{1420 \text{ kN}} = 0.70 - \text{condition fulfilled}$$

#### Calculation of the shear zone – case I (acc. to 3.2)

- Sensitivity assessment of the column web panel due to the shear instability

$$\alpha \approx \frac{b}{c} = \frac{1316}{1016} = 1.30 \rightarrow k_r(\alpha) = 5.34 + \frac{4}{\alpha^2} = 5.34 + \frac{4}{1.30^2} = 7.72$$

$$\lambda_w = \frac{h_{wc}}{t_{wc}} \leq \frac{31}{\eta} \varepsilon \sqrt{k_r} \rightarrow \frac{1000}{7} \leq \frac{31}{1.2} 0.814 \sqrt{7.72} \rightarrow 142.86 \geq 58.42$$

Elastic shear buckling stresses

$$\tau_{cr} = \frac{\pi^2 E k_r}{12 (1 - \nu^2) \lambda_w^2} = \frac{\pi^2 \cdot 210 \times 10^3 \cdot 7.72}{12 (1 - 0.3^2) 142.86^2} = 71.84 \text{ MPa}$$

Shear panel slenderness

$$\bar{\lambda}_w = \sqrt{\frac{f_y}{\sqrt{3} \tau_{cr}}} = \sqrt{\frac{355}{\sqrt{3} \cdot 71.84}} = 1.69$$

Shear buckling factor

$$\chi_w = \min\left(0.9; \frac{0.83}{\bar{\lambda}_w}\right) \rightarrow \chi_w = \min\left(0.9; \frac{0.83}{1.69}\right) = 0.49$$

- Resistance of the shear zone

$$V_{wc.Rd} = \chi_w \frac{A_{wc} f_y}{\sqrt{3} \gamma_{M1}} = 0.49 \cdot \frac{7 \times 10^3 \cdot 355}{\sqrt{3} \gamma_{M1}} = 704.98 \text{ kN}$$

- Resistance condition

$$\frac{V_{sc}}{V_{wc.Rd}} \leq 1 \rightarrow \frac{992.05 \text{ kN}}{704.98 \text{ kN}} = 1.41 \geq 1 - \text{condition not met}$$

**Calculation of the shear zone – case II (acc. to 3.2)**

- Determine the load distribution for each of the shear components

$$\theta = 37.70^\circ$$

$$A_{eq} = A_{sd} \frac{E}{G} \sin^2(\theta) \cos(\theta)$$

$$A_{eq} = 3.27 \cdot 10^3 \frac{210 \times 10^6}{81 \times 10^6} \sin^2(37.70) \cos(37.70) = 2.50 \times 10^3 \text{ mm}^2$$

$$V_{wc} = \left( \frac{A_{wc}}{A_{eq} + A_{wc}} \right) V_{sc} = \left( \frac{7 \cdot 10^3}{2.50 \cdot 10^3 + 7 \cdot 10^3} \right) 992.05 \text{ kN} = 730.76 \text{ kN}$$

$$V_{sd} = \left( \frac{A_{eq}}{A_{eq} + A_{wc}} \right) V_{sc} = \left( \frac{2.50 \cdot 10^3}{2.50 \cdot 10^3 + 7 \cdot 10^3} \right) 992.05 \text{ kN} = 261.30 \text{ kN}$$

- Sensitivity assessment of the column web panel due to the shear instability

$$\theta = 37.70^\circ \rightarrow \xi = \cot(\theta) = 1.30$$

$$k_\tau(\xi) = 5.34(1 + \xi^2) + 19.3\xi = 5.34(1 + 1.30^2) + 19.3 \cdot 1.30 = 39.48$$

$$\lambda_w = \frac{h_{wc}}{t_{wc}} \leq \frac{31}{\eta} \varepsilon \sqrt{k_\tau} \rightarrow \frac{1000}{7} \leq \frac{31}{1.2} 0.814 \sqrt{39.48} \rightarrow 142.86 \geq 132.07$$

Elastic shear buckling stresses

$$\tau_{cr} = \frac{\pi^2 E k_\tau}{12(1 - \nu^2) \lambda_w^2} = \frac{\pi^2 \cdot 210 \times 10^3 \cdot 39.48}{12(1 - 0.3^2) 142.86^2} = 367.19 \text{ MPa}$$

Shear panel slenderness

$$\bar{\lambda}_w = \sqrt{\frac{f_y}{\sqrt{3} \tau_{cr}}} = \sqrt{\frac{355}{\sqrt{3} \cdot 367.19}} = 0.75$$

Shear buckling factor

$$\chi_w = \min\left(0.9; \frac{0.83}{\bar{\lambda}_w}\right) \rightarrow \chi_w = \min\left(0.9; \frac{0.83}{0.75}\right) = 0.90$$

- Resistance of the shear zone –web panel

$$V_{wc.Rd} = \chi_w \frac{A_{wc} f_y}{\sqrt{3} \gamma_{M0}} = 0.90 \frac{7 \times 10^3 \cdot 355}{\sqrt{3} \cdot 1.0} = 1291.24 \text{ kN}$$

- Resistance condition

$$\frac{V_{wc}}{V_{wc.Rd}} \leq 1 \rightarrow \frac{730.76 \text{ kN}}{1291.24 \text{ kN}} = 0.57 < 1 - \text{condition fulfilled}$$

- Sensitivity assessment of the stiffened web due to the buckling instability  
Slenderness of the substitutive compressed element

$$\lambda_{sd} = \frac{d\mu}{i_{sd}} = \frac{1663 \cdot 0.75}{41.90} = 29.76$$

Relative slenderness

$$\lambda_1 = 93.9\varepsilon = 76.41$$

Non-dimensional slenderness

$$\bar{\lambda}_{sd} = \frac{\lambda_{sd}}{\lambda_1} = \frac{29.76}{76.41} = 0.39$$

Reduction factor

$$\phi_{sd} = \frac{1}{2} \left( 1 + \alpha (\bar{\lambda}_{sd} - 0.2) + \bar{\lambda}_{sd}^2 \right) = \frac{1}{2} \left( 1 + 0.49(0.39 - 0.2) + 0.39^2 \right) = 0.62$$

$$\chi_{sd} = \frac{1}{\phi_{sd} + \sqrt{\phi_{sd}^2 - \bar{\lambda}_{sd}^2}} = \frac{1}{0.62 + \sqrt{0.62^2 - 0.39^2}} = 0.90$$

- Resistance of the stiffened web

$$V_{sd.Rd} = \chi_{sd} \frac{A_{sd} f_y}{\gamma_{M1}} \sin(\theta) = 0.90 \frac{3.27 \times 10^3 \cdot 355}{1.0} \sin(37.70) = 639.73 \text{ kN}$$

- Resistance condition

$$\frac{V_{sd}}{V_{sd.Rd}} \leq 1 \rightarrow \frac{261.30 \text{ kN}}{639.73 \text{ kN}} = 0.41 < 1 - \text{condition fulfilled}$$

- Sensitivity assessment of the web stiffeners due to the torsional instability

$$I_t = \frac{b_{sd} \cdot t_{sd}^3}{3} = \frac{100 \cdot 10^3}{3} = 33.33 \times 10^3 \text{ mm}^4$$

$$I_p = \frac{b_{sd}^3 \cdot t_{sd}}{3} + \frac{b_{sd} \cdot t_{sd}^3}{12} = \frac{100^3 \cdot 10}{3} + \frac{100 \cdot 10^3}{12} = 3.34 \times 10^6 \text{ mm}^4$$

$$\frac{I_t}{I_p} \geq 5.3 \frac{f_y}{E} \rightarrow \frac{33.33 \times 10^3}{3.34 \times 10^6} \geq 5.3 \frac{355}{210 \times 10^3} \rightarrow 0.010 \geq 0.009$$

### Calculation of the compression zone - case I (acc. to 3.3)

- Coefficients taking into account the complex state of stresses in the web

$$\omega = \frac{1}{\sqrt{1 + 1.3 \left( \frac{b_{eff.c} t_{wc}}{A_{wc}} \right)^2}} = \frac{1}{\sqrt{1 + 1.3 \left( \frac{182.86 \cdot 7}{7 \cdot 10^3} \right)^2}} = 0.98$$

$$\sigma_c = \frac{N_c}{A_c} + \frac{M_c}{I_{yc}} z = \frac{330 \times 10^3}{15 \times 10^3} + \frac{1.474 \times 10^9}{2.65 \times 10^9} 500 = 300.28 \text{ MPa}$$

$$k_{wc} = 1.7 - \frac{\sigma_c}{f_y} = 1.7 - \frac{300.28}{355} = 0.85$$

- Sensitivity assessment of the web stiffeners due to the buckling instability  
Slenderness of the substitutive compressed element  $\lambda$

$$\lambda_{sc} = \frac{c\mu}{i_{sc}} = \frac{1016 \cdot 0.75}{54.46} = 14.42$$

Non-dimensional slenderness

$$\bar{\lambda}_{sc} = \frac{\lambda_{sc}}{\lambda_1} = \frac{14.42}{76.41} = 0.19 \leq 0.20 - \text{lateral buckling will not occur}$$

- Resistance of the compression zone

$$F_{c.Rd} = \frac{\omega k_{wc} b_{eff.c} t_{wc} f_y}{\gamma_{M0}} + \frac{2b_{sc} t_{sc} f_y}{\gamma_{M0}}$$

$$F_{c.Rd} = \frac{0.98 \cdot 0.85 \cdot 182.86 \cdot 7 \cdot 355}{1.0} + \frac{2 \cdot 120 \cdot 12 \cdot 355}{1.0} = 1402.36 \text{ kN}$$

- Resistance condition

$$\frac{F_{bc}}{F_{c.Rd}} \leq 1 \rightarrow \frac{1\,246.88 \text{ kN}}{1\,402.36 \text{ kN}} = 0.89 < 1$$

- Sensitivity assessment of the web stiffeners due to the torsional instability

$$I_t = \frac{b_{sc} \cdot t_{sd}^3}{3} = \frac{120 \cdot 12^3}{3} = 69.12 \times 10^3 \text{ mm}^4$$

$$I_p = \frac{b_{sc}^3 \cdot t_{sc}}{3} + \frac{b_{sc} \cdot t_{sc}^3}{12} = \frac{120^3 \cdot 10}{3} + \frac{120 \cdot 10^3}{12} = 6.93 \times 10^6 \text{ mm}^4$$

$$\frac{I_t}{I_p} \geq 5,3 \frac{f_y}{E} \rightarrow \frac{69.29 \times 10^3}{6.93 \times 10^6} \geq 5,3 \frac{355}{210 \times 10^3} \rightarrow 0.010 \geq 0.009$$

### Calculation of the compression zone - case II (acc. to 3.3)

- Resistance condition

$$\frac{F_{bc} - V_{sd}}{F_{c.Rd}} \leq 1 \rightarrow \frac{1\,246.88 \text{ kN} - 261.30 \text{ kN}}{1\,402.36 \text{ kN}} = 0.70 < 1$$

## 5. Summary

The paper presents the calculation problems of welded knees of steel frames, in which the main load-bearing elements of frames can be made of plate girders with slender webs.

The presented analysis method of joint loading state allows relatively easy to determine the forces acting in the three characteristic zones of the rectangle knee joint.

The algorithms for checking resistance have been developed in such a way as to take into account the complex state of stresses in the joint web, as well as the phenomenon of instability in the shear and the compression zone of the joint.

The proposed method of designing welded knee joints makes it possible to determine quite accurately the resistance of the individual zones of joint. This fact may in many practical cases favor more economical design of steel frames knees.

Furthermore, the method of internal forces determination and the dimensioning procedure presented in the paper were used in the calculations of certain knee joint of the portal steel frame.

Although the scope of the calculation method in this work relates directly to the design of welded knees of steel frames, the presented dimensioning

algorithms can be relatively easily adapted to calculations of knees, in which end-plate bolted connections between beams and columns appear.

The issues presented in the paper are important from the practical point of view, and therefore, they should be taken into account in the design process of frames with plate girders' cross-sections.

## References

- [1] Joint in steel construction. Moment-resisting joints to Eurocode 3. The Steel Construction Institute, The British Constructional Steelwork Association Ltd. Publication P398, 2013.
- [2] Kozłowski A., Pisarek Z.: End-plate steel joint with four bolts in the row. Proc. of Inter. Conf. of Met. Struct. (ICMS-2006), Rzeszów, Poland, 21–23 June 2006.
- [3] Ślęczka L.: Shaping and analysis of selected steel frame joints subjected to variable actions. Oficyna Wydawnicza Politechniki Rzeszowskiej, Rzeszów 2013 (in Polish).
- [4] EN 1993-1-8:2005. Eurocode 3: Design of steel structures –Part 1-8: Design of joints.
- [5] Pałkowski Sz.: Selected problems of calculation and design of steel structures (in Polish), Koszalin 1989.
- [6] Giżejowski M., Jemioło S.: Numerical modelling of the behaviour of welded, semi-rigid end plate joints (in Polish). Inżynieria i Budownictwo, no 11, 2004, pp. 623–629.
- [7] Scheer J., Pasternak H., Schween T.: Structural behavior of stiffened knee joints with thin webs. Journal of Structural Engineering, vol. 117, 1991, pp. 2600–2619.
- [8] EN 1993-1-1:2005. Eurocode 3: Design of steel structures – Part 1-1: General rules and rules for buildings.
- [9] EN 1993-1-5:2005. Eurocode 3: Design of steel structures – Part 1-5: General rules – Plated structural elements.
- [10] Wakasugi S.: Buckling of a simply supported equilateral triangular plate. Trans. Japan Soc. Mech. Eng. vol. 26, no. 164, 1960, pp. 538–544.
- [11] Wakasugi S.: Buckling of a simply supported triangular plate having inner angles of 30, 60 and 90 degrees. Trans. Japan Soc. Mech. Eng. vol. 19, no. 83, 1953, pp. 530–537.
- [12] Faella C., Piluso V., Rizzano G.: Structural Steel Semirigid Connections: Theory, Design, and Software. CRC Press, Hanover 1999.

*Przesłano do redakcji: 13.04.2018 r.*

*Przyjęto do druku: 15.06.2018 r.*

Izabela TYLEK<sup>1</sup>

## SHAPING OF ARCHITECTURALLY EXPOSED STEEL STRUCTURES

Architecturally Exposed Structural Steel (AESS) is steel that must be designed to be structurally sufficient to support the primary needs of the structure and – at the same time – remains exposed to view, being a significant part of architectural language of the building [4, 6]. The quality requirements of AESS typically exceeds the requirements of Standard Structural Steel (SSS), what increases the time and costs of the design and execution of AESS. Currently used classification of AESS distinguishes 5 categories of execution quality. This categorization has a hierarchical structure, each higher category of structure execution contains all the properties of lower category. The basis of presented classification is the degree of human visual perception of the structure. It is mainly related to the distance of the potential observer from the structure, which allows in varying degrees to see the details of structure execution. Joints and connections are the main means of architectonic expression in architecturally exposed steel structures. The principles of joints and connections shaping in AESS are the same as for SSS but additionally some requirements to the expected aesthetic are formulated. This additional requirements cause that AESS can be significantly (even a few hundred percent) more expensive than SSS with exactly the same functionality and durability. However, PN-EN 1090-2 [7] gives no provisions about AESS executions, which may impede mutual understanding between architect, structural engineer, contractor and investor.

**Keywords:** exposition of steel structure, classification of AESS, higher quality requirements, higher costs of AESS

### 1. Introduction

Exposition of steel structure in architecture of public buildings is not a new trend. Many of the 19th century buildings – built during the initial stage of steel structures development – utilize architecturally exposed structural cast iron with ornate decoration that imitated carved stone elements (Fig. 1).

High costs of cast iron elements manufacturing, particularly in the case of their reshaping, caused that their degree of repetitiveness was very large, which limits the freedom of architectural forming of the building. Additional disadvantage

---

<sup>1</sup> Corresponding author: Izabela Tylek, Cracow University of Technology, ul. Warszawska 24, 31-155 Kraków, +48126282372, itylek@pk.edu.pl



Fig. 1. Interior of the Oxford University Museum of Natural History, built 1855-1860, Oxford, England (author of photography: nz\_willowherb [10])

of cast iron – its low ductility – was the cause of a few spectacular failures of the 19th century bridges, e.g.: Dee Bridge (1847), the Tay Bridge (1879) and the Portland Road Bridge (1891). The second half of the 19th century brought the technology development, i.e. mass production of relatively cheap steel and rolling techniques of plates and profiles what increased application of steel structures in building industry. However, steel structures made of hot-rolled elements was considered to be visually heavy and aesthetically unattractive; additionally – riveted joints were very labour- and time-consuming. The above disadvantages combined with relatively fast degradation of steel element rigidity due to fire caused that for many decades steel frame structures of public buildings were hidden under the masonry or concrete cladding.

Initiated in late 1940s architectural style, later called Brutalism from the French word “brut” (“raw”), placed emphasis on the exposure of raw building materials and constructions producing expressive, minimalist forms. Built in the UK in 1954, Hunstanton Secondary Modern School in Norfolk became one of the flagship examples of this style, in which probably for the first time steel frame structure of public building was deliberately exhibited, revealing the architectural rhythm with repeated structural elements made of ordinary steel I-beams. Development of steel manufacturing and joining, which took place in the second half of the 20th century, made possible to design and execute large-area public buildings with large spans and large glazed area providing appropriate amount of natural light. Steel, because of its high strength to self-weight ratio, perfectly suited for this purpose, allowing shaping slender, visually

light structural elements with small cross section dimensions. Wide utilization of steel hollow sections and ties has become a characteristic feature of the developing from the 1970s architectural style known as high-tech architecture. Exposed structural elements are often shaped using the method called by T.M. Boake “a force-varied expression” [4]. It consists of intentional variation of cross-section dimensions of exposed steel elements, depending on the force sign and magnitude. In order to increase the architectural expression, many objects of this type have unnecessarily complex supporting system that can be replaced by simpler, but visually less impressive, one.

It should be noted that modern structural elements and their connections more often become the subject of architectural design. If the structural element performs also aesthetic function, it requires additional work effort of an architect, structural engineer, steel structure manufacturer, and erector. For this reason, architecturally exposed steel structures can even be several times more expensive than the standard steel structures.

## **2. Classification of architecturally exposed steel structures**

Popularisation of architecturally exposed steel structures in combination with a variety of applied solutions and their high costs, caused the need to create a reference document, which would be a point of reference to facilitate the understanding between investors, architects, structural engineers and contractors. The first work which introduced currently used (Table 1) classification of architecturally exposed structural steel (AESS) was the study of the Rocky Mountain Steel Construction Association and the Structural Engineers Association of Colorado published in 2003 [2]. This proposal was introduced to Canadian standard [5] in 2009, American standard [1] and Australian/New Zealand standard [3] in 2016.

Classification presented in Table 1 distinguishes 5 categories of execution quality for architecturally exposed structural steel (AESS), denoted as AESS 1 ÷ AESS 4 and AESS C, which exceed quality requirements specified in execution standards for standard structural steel (SSS). This categorization has a hierarchical structure, each higher category of structure execution contains all the properties of lower category. The exception is AESS C category, which as defined, is intended for individual requirements that can be freely selected from the properties set provided in the classification or additionally specified by the architect. The basis of presented classification is the degree of human visual perception of the structure. It is mainly related to the distance of the potential observer from the structure, which allows in varying degrees to see the details of structure execution.

According to AESS category, quality requirements for the structure execution are defined. They may concern: quality of weld and element surface finishing, geometric tolerances or the type of joints used. The specific requirement, which may optionally be formulated for category AESS 2 or higher, is performance of mock-up, usually for joint or part of the structure. Mock-ups are

Table 1. Category array for specifying AESS based on [2]

Characteristics	AESS C	AESS 4	AESS 3	AESS 2	AESS 1	SSS
1.1 Surface preparation to SSPC-SP-6 [8]		•	•	•	•	
1.2 Sharp edges ground smooth		•	•	•	•	
1.3 Continuous weld appearance		•	•	•	•	
1.4 Standard structural bolts		•	•	•	•	
1.5 Weld spatters removed		•	•	•	•	
2.1 Visual samples		optional	optional	optional		
2.2 One-half standard fabrication tolerances		•	•	•		
2.3 Fabrication marks not apparent		•	•	•		
2.4 Welds uniform and smooth		•	•	•		
3.1 Mill marks removed		•	•			
3.2 Butt and plug welds ground smooth and filled		•	•			
3.3 HSS weld seam oriented for reduced visibility		•	•			
3.4 Cross sectional abutting surface aligned		•	•			
3.5 Joint gap tolerances minimized		•	•			
3.6 All welded connections		•	•			
4.1 HSS seam not apparent		•				
4.2 Welds contoured and blended		•				
4.3 Surfaces filled and sanded		•				
4.4 Weld show-through minimized		•				
C.1						
...						
<b>Estimated cost premium [%]</b>	<b>20÷250</b>	<b>100÷250</b>	<b>60÷150</b>	<b>40÷100</b>	<b>20÷60</b>	<b>0</b>

used to carry out the arrangements and getting multilateral acceptance of the visual aspects of structure final form. They may take the form of scaled or full-scale physical mock-ups or virtual rendered 3D images, which can be relatively easy created by using computer programs for steel structures 3D detailing, e.g. Tekla Structures, Bocad, Advance Steel, etc. The necessity of mock-up execution, particularly in the case of physical full-scale mock up, must be clearly indicated in the design documentation, because it requires additional costs and time which must be included in the schedule of construction works.

The AESS 1 category includes steel structures that, despite the fact that they are visible, are not architecturally dominant elements and their distance from the observer prevents seeing structural details such as welds quality or joint gap distances. They don't focus attention within observed space, usually have the same colour as the background and are often underexposed, remains in the shadow (see Fig. 2).



Fig. 2. Stand roof structure of Cardiff City Stadium, Cardiff, Wales (author of photography: Jon Candy [10])

The AESS 2 category includes structures that can be observed from a distance of not less than 6 m, but their shaping constitutes a significant part of the architectural composition of the building. These are often a visible, well lit part of the roof structure or high-level ceilings. Similarly as in AESS 1, distance between the observer and the structure does not allow for assessing the construction details quality (Fig. 3).



Fig. 3. Roof structure of Edmonton City Hall, Edmonton, Canada (author of photography: Mack Male [10])



Fig. 4. Concourse B of O'Hare International Airport, Chicago, USA (author of photography: joevare [10])

The AESS 3 category applies to structures that can be seen from a distance of less than 6 m and even touched by the public. This allows to see details and imperfections of elements surface finishing such as grind marks. Typical structures of this category structures include terminals, airports, shopping centres, etc. (Fig. 4).

The AESS 4 category is the highest category of steel structure execution quality, it includes highly exposed elements, dominating in the architectural composition of the building. In this type of structure, the architect's intention is to present the form of structural element as its unique visually exposed geometric property (Fig. 5). In this category, structures are often composed of custom elements, manufactured on investor's individual order, e.g.: connection parts made of cast steel, tapered hollow sections, etc. Welded joints with grinded weld face are often used. The element surfaces are also grinded and then surface defects are supplementing with special synthetic filler. This labour consuming surface treatment is required for structures covered with high gloss topcoats, which due to the high light reflection coefficient, greatly reveal all geometrical imperfections of the surface.



Fig. 5. Copernicus Airport Wrocław, Wrocław, Poland (author of photography: Paweł Żwirek)

Careful steel surface preparation in combination with other treatments, makes that structure is visually deprived of any characteristics allowing to identify the material of which it was made of. The examples of two contemporary structures executed as AESS 4 are shown in Fig. 6–8.



Fig. 6. Amazon Spheres – spherical conservatories serve as employee lounge and workspace located on the headquarters campus of Amazon company in Seattle, USA, completed in January 2018: steel structure under construction (author of photography: SounderBruce [9])



Fig. 7. Amazon Spheres – spherical conservatories serve as employee lounge and workspace located on the headquarters campus of Amazon company in Seattle, USA, completed in January 2018: connections details (author of photography: Manuel Bahamondez H [10])



Fig. 8. Atrium in Brookfield Place office complex, Toronto, Canada: interior view (author of photography: Marcos Virgílio [10]) and steel column base detail (author of photography: cbrueck [10])

In one design, and even in one steel element, different AESS categories may occur. It allows reasonable selection of means and methods for increasing quality and keeping additional (premium) costs to a minimum. It is estimated that premium costs are in the range from 20% for AESS 1 to 250% for AESS 4 categories compared to the SSS.

The AESS category must be clearly specified by the architect and indicated in design and execution documentation (both in the text and on the drawings).

### **3. Shaping and execution of joints and connections**

Joints and connections are the main means of architectural expression in architecturally exposed steel structures, but they still perform their basic function that is allowing the safe transfer of loads between connected elements and enabling an efficient transport to the site and structure execution. The way of joint shaping may drastically affect the labour costs at the stage of design and detailing, manufacturing, transport, and structure execution.

The type, location and quality of joint execution should be consistent with the general aesthetic concept of the building – as a result two basic types of joint shaping may be identified: they may be displayed or hidden from the sight of the observer. Connection, and particularly splice of steel elements, is the place where the continuity of the compositional lines created by the element outlines is disturbed. These lines naturally “lead” human eye during observation of the structure and connections are the points that spontaneously focused observer’s attention. This effect can be undesirable if the essence of architectural expression are smooth lines and minimalistic forms used in different styles of modernist architecture. However, the connection may sometimes be treated as a valuable item of aesthetic effect intended by the architect, e.g. accentuating the industrial style by referring with bolts arrangement in joint to the textures of the background surfaces.

The principles of joints and connections shaping in AESS are the same as for SSS. Correctly shaped and designed joints and connections of structural elements should primarily meet the safety, serviceability and durability requirements as well as enable easy execution of the structure. Additional requirements to the expected aesthetic of the structure causes the need for reasonable methods of AESS shaping, that would allow to meet abovementioned requirements with only a little increase of costs in comparison with SSS. This can be achieved by using one of the following recommendations.

If the joint or connection is visible to the observer and harmonises with aesthetic concept of the structure, it shall be shaped in a way that refers to lines or textures of adjacent elements. If the joint or connection is meant to be “a strong point” of the composition, its elements, e.g. bolts or gusset plates, can be emphasize by increasing their number or dimensions, introducing additional holes which are unnecessary from structural point of view, designing gusset plates with more attractive geometrical shapes, e.g. curved, or manipulate colour, lighting and texture of the surface (Fig. 9).



Fig. 9. Centre Georges Pompidou, Paris, France. Visible enlarged gusset plates, additionally accentuated by the central hole (author of photography: V C [10])



Fig. 10. The joint of steel spatial structure at Heathrow airport, London, England (author of photography: Andreas Komodromos [10])

In the case of geometrically complicated joints in complex three dimensional steel structures, it often is preferable from both an aesthetic and financial point of view, to apply prefabricated cast steel elements (Fig. 10).

If the joint or connection is visible to the observer but its accentuation is inadvisable, the measures ensuring that it will minimally focus the observer's attention should be applied. These can be for example: using of welded connections instead of the bolted ones, replacing the welded shear connections with the end plate connections, replacing the intermittent fillet welds with continuous fillet welds, minimising of gaps between the connected elements, removal of welding spatters, weld grinding, surface defects supplementing with special synthetic filler, placing all bolt heads on one side of the joint, etc.

If the location of the joint in particular part of the structure is unfavourable from the aesthetic point of view, one may try to transfer it to other, less exposed place, even if for design or execution reasons it will be a worse location. The location of hollow section longitudinal seams on the side which is non-visible to the observer may be the example. If the joint cannot be transferred, one may try to hide it by appropriate shaping. In this case two approaches may be distinguished. The first one is to hide the joint by such gusset or end plates shaping that they are practically within the contour of connected profiles. The joint can be additionally enclosed by non-structural cover plates in the shape of a connected profile. The second approach involves the use of cast steel elements welded to the connected profiles. After assembly, bolt heads and nuts are hidden in hollows of the cast that are later filled in with weld deposit and ground.

If this is consistent with the aesthetic concept of the structure, some of the welded joints can be replaced by bent elements. It can be applied in the case of both connections of straight elements that form curved element and the gusset plates.

#### **4. Summary**

The high yield strength of steel makes it possible to erect building structures with slender elements, which only minimally limit the access of natural daylight to the interiors. At the same time, exposed steel structural elements became the means of the architectural expression. Joints and connections, as inherent part of steel structure, also began to be a subject of architectural design. They are an essential component of steel structure visual appearance, being within the observer's sight. Due to the fact that the fulfilment of the architect aesthetic expectations requires an increase effort, both at the stage of design and execution, AESS can be significantly (even a few hundred percent) more expensive than SSS with exactly the same functionality and durability. It should be noted that greater part of additional costs is associated with joint execution, that must meet quality requirements much higher than these for standard steel structures.

The current standard for execution of steel structures PN-EN 1090-2 [7], does not refer to execution of AESS. In the case of incorrect or incomplete specification of steel structure, it may be an obstacle to the mutual communication between the architect, engineer and contractor. This leads to misunderstandings that may sometimes have serious consequences, e.g. financial – resulting from the necessity to redesign or re-execution of structural parts, which is often associated with delays in termination of the investment. The possibility of such situation may cause that the investor will treat the realization of architecturally exposed steel structures as a venture of higher financial risk what may limit the application and development of AESS. Therefore, the demand for actions aimed at the introduction to current standard PN-EN 1090-2 [7] provisions about the execution of architecturally exposed steel structures seems to be justified.

## References

- [1] ANSI/AISC 303-16, Code of Standard Practice for Steel Buildings and Bridges, American Institute of Steel Construction, Chicago, 2016.
- [2] Architecturally Exposed Structural Steel – A supplement to Modern Steel Construction – joint publication of the Rocky Mountain Steel Construction Association and the Structural Engineers Association of Colorado, May, 2003.
- [3] AS/NZS 5131: 2016, Australian/New Zealand Standard, Structural Steelwork – Fabrication and erection.
- [4] Boake T. M., CISC Guide for Specifying Architecturally Exposed Steel, 2nd Edition, Canadian Institute of Steel Construction, 2012.
- [5] CISC Code of Standard Practice for Structural Steel – 7th Edition, Canadian Institute of Steel Construction, 2009.
- [6] CISC. Guide for Specifying Architecturally Exposed Structural Steel, <https://cisc-icca.ca/ciscwp/wp-content/uploads/2017/03/AESSGuide2E.pdf> (access: 15.03.2018 r.).
- [7] PN-EN 1090-2:2009. Wykonanie konstrukcji stalowych i aluminiowych. Część 2: Wymagania techniczne dotyczące konstrukcji stalowych.
- [8] SSPC-SP6/NACE No.3, Joint Surface Preparation Standard – Commercial Blast Cleaning, SSPC The Society for Protective Coatings, September 1, 2000.
- [9] Information materials, <https://commons.wikimedia.org> (access: 15.03.2018 r.).
- [10] Information materials, <https://www.flickr.com> (access: 15.03.2018 r.).

*Przesłano do redakcji: 13.04.2018 r.*

*Przyjęto do druku: 15.06.2018 r.*

Mariusz MAŚLAK<sup>1</sup>  
Michał PAZDANOWSKI<sup>2</sup>

## INFLUENCE OF THE END-PLATE THICKNESS ON THE STEEL BEAM-TO-COLUMN JOINT STIFFNESS WHEN SUBJECT TO BENDING

Based on the numerical simulation performed within the Abaqus computational environment for a typical end-plate beam-to-column joint the influence of the end-plate thickness on the effective joint rigidity has been verified. The initial joint rigidity at first determined for 20 mm thick end-plate has been compared with rigidity of the joint constructed with substantially more flexible end-plates 10, 8 and 6 mm thick. In all the considered cases the column was equipped with horizontal ribs stiffening the web at the height of beam top and bottom flange. No diagonal ribs were applied. In addition the column flange at the zone directly adjacent to the beam end-plate in all the analyzed cases has been set to 30 mm. This way it did not affect the computationally determined rigidity of considered joints. Juxtaposition of  $M-\varphi$  curves characterizing the considered joints and depicting the relationship between the applied bending moment and relative change of the initial angle between undeformed axes of beam and column in the analyzed frame indicates qualitatively different modes of destruction of the considered joints, and thus different computational models determining their bearing capacity. In the first case obtained parameters seem to indicate that the joint is nominally rigid but in all the remaining cases the bearing capacity seems to be exhausted by the increasing deformation of the more and more flexible end-plate.

**Keywords:** beam-to-column steel end-plate joint, end-plate thickness, joint flexibility, initial stiffness, numerical simulation

### 1. Introduction – description of the simulated research model

A typical steel beam-to-column joint of scheme, dimensions and geometry depicted in Fig. 1 is the subject of our analysis. The joint represents a connection between the cantilever column made of IPE 360 I-beam and a cantilever beam

---

<sup>1</sup> Corresponding author: Mariusz Maślak, Cracow University of Technology, Faculty of Civil Engineering, Chair on Metal Structures, Warszawska 24, 31-155 Cracow, phone: 126282033, e-mail: mmaslak@pk.edu.pl

<sup>2</sup> Michał Pazdanowski, Cracow University of Technology, Faculty of Civil Engineering, Department for Computational Civil Engineering, Warszawska 24, 31-155 Cracow, phone: 126282929, e-mail: michal@15.pk.edu.pl

made of IPE 240 I-beam at the height of 1 200 mm above the restraint level. The external load is applied as a concentrated force having the value of  $P = 60$  kN applied at the distance of  $L = 2.00$  m measured with respect to the undeformed face of the beam end plate. This results in the bending moment equal to  $M = 120$  kNm applied at the joint face, tensioning the top and compressing the bottom flange of the beam. As visible in Fig. 1, horizontal ribs stiffening the column web have been applied on both sides of the column at the height of both flanges of the beam. The rib thickness is equal to 10 mm in each considered case. No diagonal ribs have been applied.

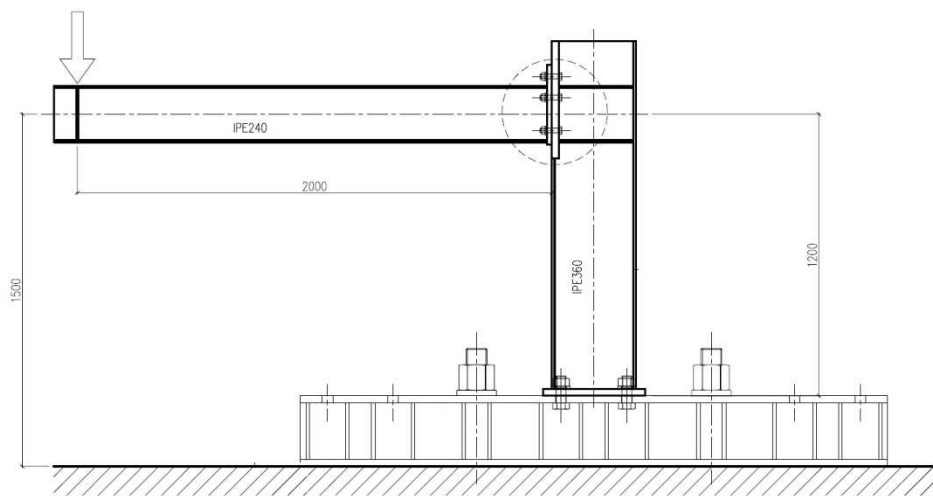


Fig. 1. Scheme, dimensions and load application for the considered joints. The presented stand has been prepared for experimental research conducted at Cracow University of Technology by another research team

In each considered case the end plate is attached to the column flange with  $M20 \times 80$  bolts of 10.9 class spaced in three rows of two bolts each, as depicted in Fig. 2. It was assumed that in the zone directly adjacent to the beam end plate, at the height of 500 mm, measured from the top, the original column flange was replaced by one 30 mm thick, regardless of the joint considered. This allowed for elimination of the influence of this flange on the joint rigidity, observed and quantified in numerical simulations described in this paper. These simulations were performed for four joints of identical geometry, depicted in Fig. 1, but differing in the end-plate thickness. In the joint of the type A this thickness was equal to 20 mm resulting in relatively rigid plate resisting deformation even when subjected to relatively large loads. In the joint of the types B, C and D the end-plate thickness was equal to 10 mm, 8 mm and 6 mm, respectively.

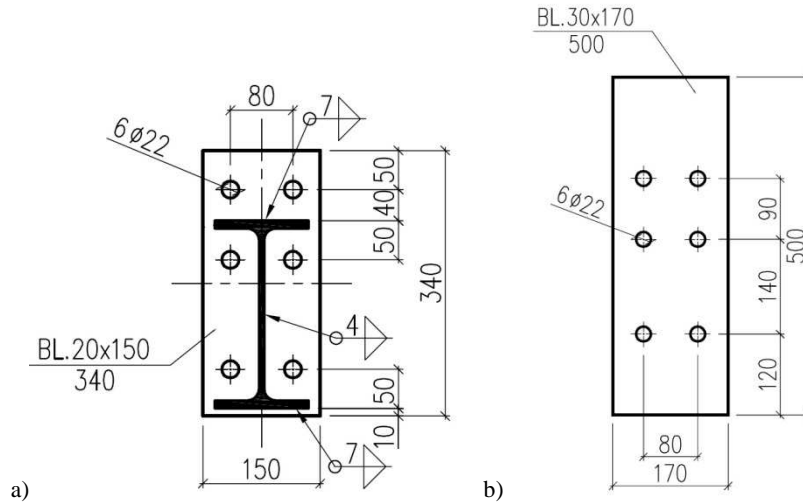


Fig. 2. Bolt location in the joints simulated in present paper and application of fillet welds: a) beam side view towards the end plate, b) column flange view towards the joint (replaced flange part only)

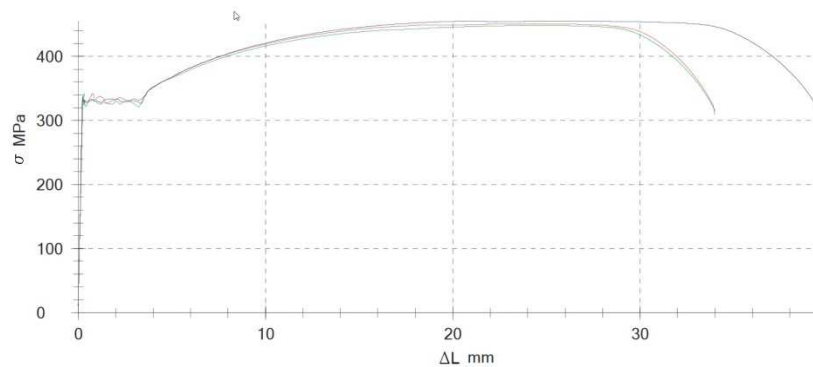


Fig. 3. Independently obtained stress – strain relationship for the structural steel of which all the structural components of joints simulated in present paper have been made

All the components of joints simulated in present paper have been made of structural steel characterized by the  $\sigma - \varepsilon$  relationship determined experimentally on three specimens subjected to the uniaxial tension test. The following authoritative average values of material data have been determined:

- for the conventional yield point –  $R_{p,0.2} = 328.9$  MPa ,
- for the ultimate strength –  $R_m = 451.5$  MPa ,
- for the longitudinal modulus of elasticity –  $E_a = 205.2$  GPa ,
- for the limit elongation: in the case of fivefold sample  $A_{5,65} = 30.6\%$  , and in the case of tenfold sample  $A_{11,2} = 23.6\%$  .

The selection and calibration of the numerical model parameters listed above have been made by the authors with the intent to verify the assumptions and results of experiments conducted at the Cracow University of Technology by another research team. Detailed elaboration of the results obtained in this experiment is still in preparation. In this research the initial imperfections of the end plate not adhering to the column flange are additionally introduced. The assessment of the influence of these imperfections and various methods of their correction on the real rigidity and bearing capacity of the considered joint is the main goal of that analysis.

## **2. Characteristics of the numerical model applied**

The numerical model developed within the Abaqus [1] computational environment has been applied in order to simulate the behavior of the four joint types of the same geometry, but differing in the end-plate thickness as described above, when subjected to external loads. Eight node brick type C3D8R finite elements with reduced integration and hourglass control have been applied. The total number of degrees of freedom was equal to 403350 – for the model with endplate 20 mm thick, 415392 – for the model with endplate 10 mm thick, 420246 – for the model with end-plate 8 mm thick and 418041 – for the model with end-plate 6 mm thick. The external load has been applied as the vertical traction applied to the cylindrical spacer at the end of beam. The complex contact interactions have been modeled by the contact pairs between the respective interacting surfaces, in a manner analogous to that used in the paper [2]. The „surface-to-surface” contact type has been used throughout the analysis, with friction coefficient  $\mu=0.50$ . Each bolt with nut has been modeled as a single unit, while spacers have been modeled independently. The following contact pairs have been created: bolt head – end-plate, bolt shank – end-plate bolt hole, nut – spacer, spacer – column flange, bolt shank – column head bolt hole, end-plate – column flange. The scheme of assumed numerical model is depicted in Fig. 4.

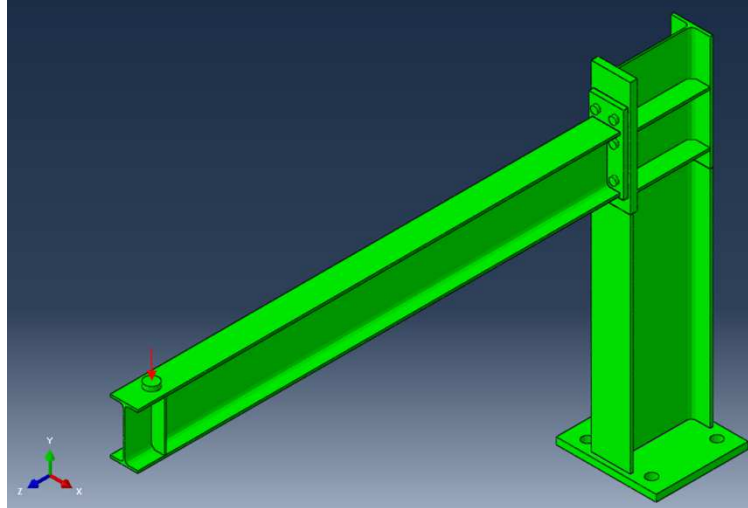


Fig. 4. Numerical model applied to simulate the behavior of joints analyzed in this paper when subjected to external loads

### 3. The joint destruction forecast depending on the end plate thickness applied

The simulations performed visualized the differences in deformation modes of both constituting components of each node as well as whole surroundings of joint area at limit loads. Observation of differences in the deformation of the end-plate for end-plates substantially differing in rigidity was especially important for the authors. The destruction mode of the A type joint, having the end plate 20 mm thick is depicted in detail in Fig. 5. One may easily observe that this end-plate is so rigid that even when a relatively large bending moment is applied to the joint, deformation of the end-plate is hardly visible even at the ultimate limit state. This suggests the relatively large probability that the joint would fail due to the destruction of the highly stressed bolts located at the external edge of end-plate without any interaction with the relatively undeformed plate, such as, for instance, the lever action amplifying the tensile force in these bolts. The simulation performed by the authors indicated completely different destruction mode of the joint determining its bearing capacity. The limit state was determined by the yielding and deformation of the bottom, compressed, beam flange (Fig. 5), while the bolts remained undamaged. Such behavior should be associated with relatively stringent limitation of effective rotation angle and thus in practical terms deformation corresponding to the nominally rigid work regimen.

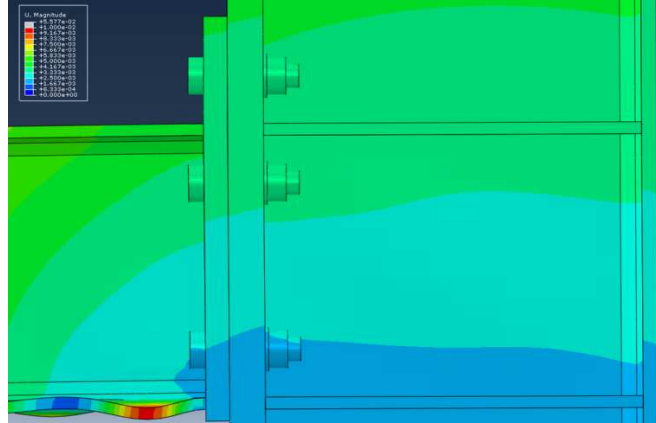


Fig. 5. Ultimate limit state of the A type joint considered here, equipped with 20 mm thick end-plate, attained via yielding of the bottom, compressed, beam flange. The deformation of the beam end-plate in the tensile zone of the joint is hardly visible. The bolts remain undamaged

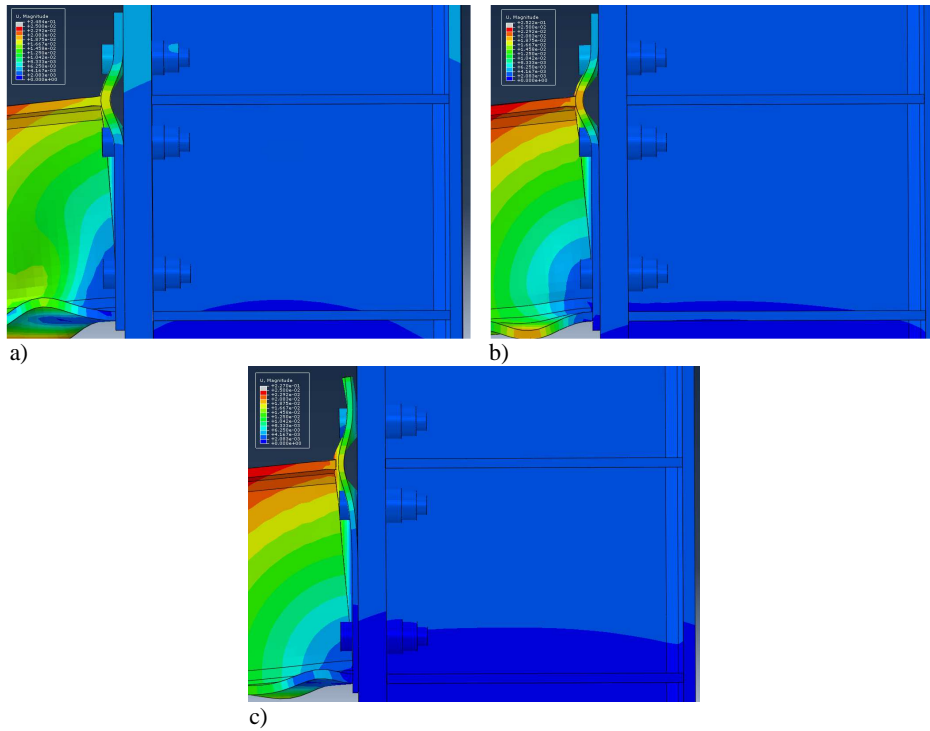


Fig. 6. Joint destruction mode for joints equipped with thin end-plate realized via large deformation of this plate in the tensile zone of the joint, accompanied by the deformation of the compressed bottom flange of the beam: a) B type joint – end-plate 10 mm thick, b) C type joint – end-plate 8 mm thick, c) D type joint – end-plate 6 mm thick

The numerically simulated destruction mode of the joints belonging to the types B, C and D, equipped with relatively thin end-plate, is fundamentally different. The bearing capacity of the whole joint is, to the increasing extent, determined by the deformation of the end-plate in the tensile zone accompanied by the deformation of the bottom, compressed, beam flange (Fig. 6). The maximum displacement of the end-plate face is here always observed at the level of the beam top flange, as this flange, subjected to tension, „pulls” behind the very thin end-plate, susceptible to this type of action in the zone located between the two top rows of bolts, stabilizing its location. It should be noted, however, that this „pulling” action of beam is the strongest in the web plane of the beam and is noticeably weaker outside of its flanges at the distance to the web. This difference, under favorable circumstances, may lead to additional deformations of the end-plate, observed in the plane perpendicular to the frame plane. However, in general due to the substantial resistance to deplanation of the hot rolled beam section, this phenomenon plays secondary, and thus negligible role. Interestingly, with decreasing thickness of the end-plate the deformation associated with top, tensioned, beam flange tends to play increasingly dominant role, while the influence of the compressed bottom flange gradually diminishes.

Detailed analysis of equivalent Huber – von Mises stress distributions on both sides of the end-plate (view towards the column and view towards the beam) yields additional interesting information – Figs. 7–10. The thinner the end-plate the more it deforms. Thus the zones of the highest stresses in the thin plates are usually isolated and localized around the bolt holes. This is the direct result of reaction to the dominating interaction between the plate and bolts prestressing the joint. The more distant surroundings of the bolt holes relatively weakly contribute to the transfer of loads. However, if the end-plate is sufficiently thick the redistribution of equivalent stresses seems to be more pronounced and this in turn makes the cooperation of adjacent regions more efficient. Thence in such situations the highest equivalent stresses do not concentrate around bolt holes but become more pronounced in the adjacent areas as well. This in turn results in grouping of formerly isolated stress concentration zones into much larger areas, and subsequently in relocation of these zones to the area directly affected by the action of top, tensioned, beam flange. This relocation proves that when a thicker plate is applied at the joint the „pulling” of the end-plate by the tensioned beam flange becomes dominant in the general balance of actions, while the action of bolts, dominant in the thin plates substantially loses in importance.

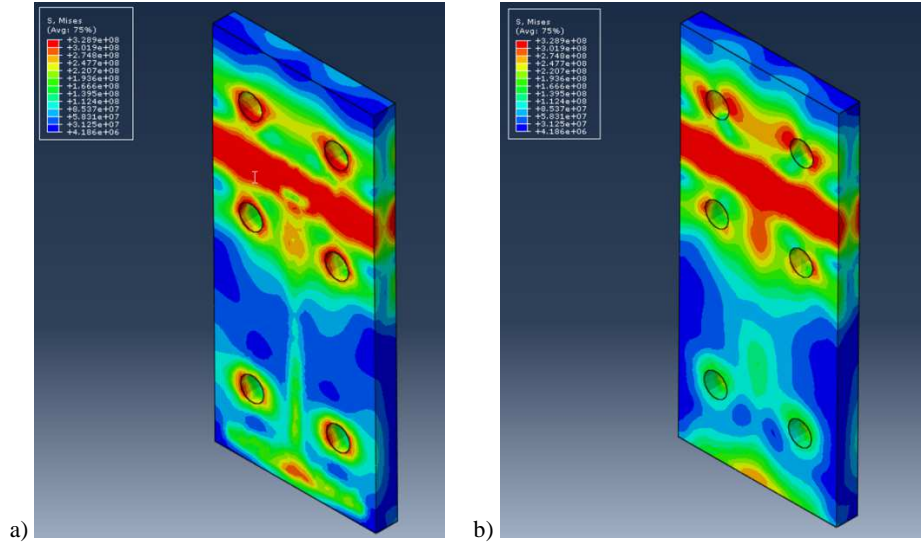


Fig. 7. Distribution of equivalent Huber – von Mises stresses in the end-plate of the A type joint, 20 mm thick: a) view towards the column flange, b) view towards the beam

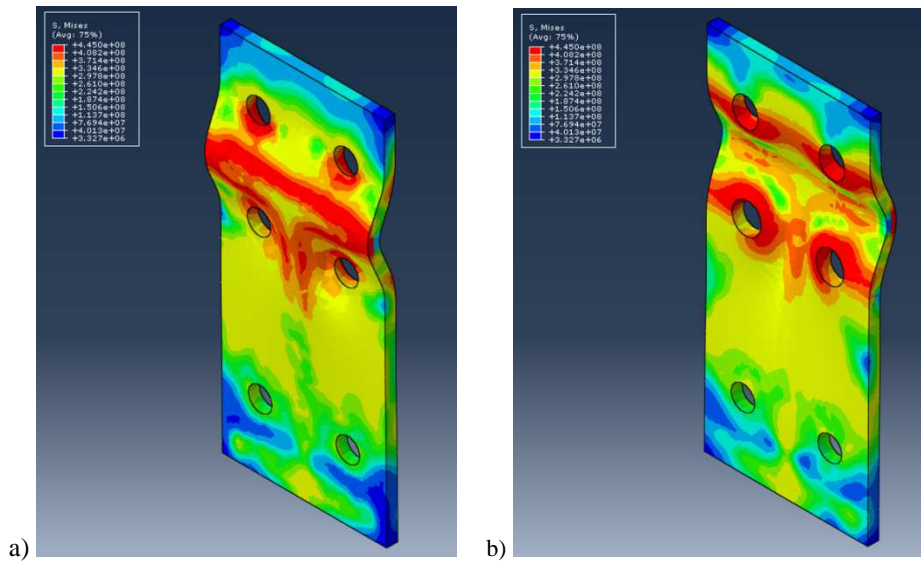


Fig. 8. Distribution of equivalent Huber – von Mises stresses in the end-plate of the B type joint, 10 mm thick: a) view towards the column flange, b) view towards the beam

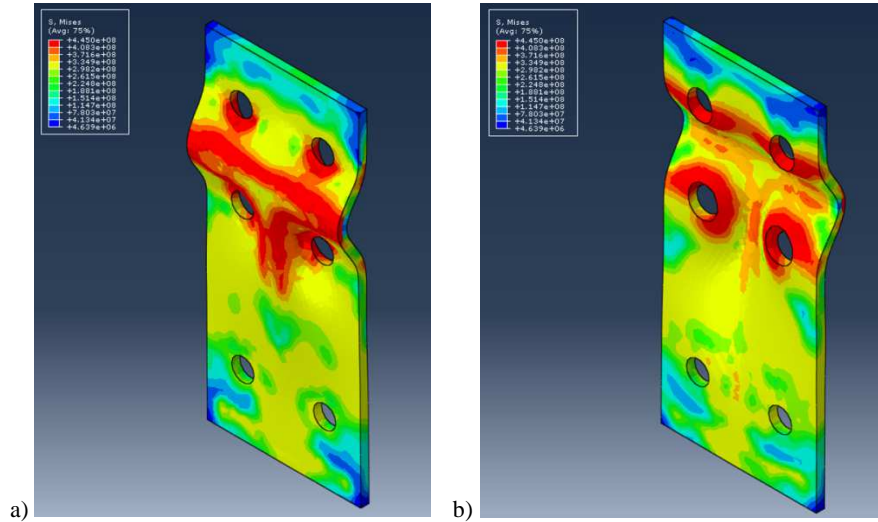


Fig. 9. Distribution of equivalent Huber – von Mises stresses in the end-plate of the C type joint, 8 mm thick: a) view towards the column flange, b) view towards the beam

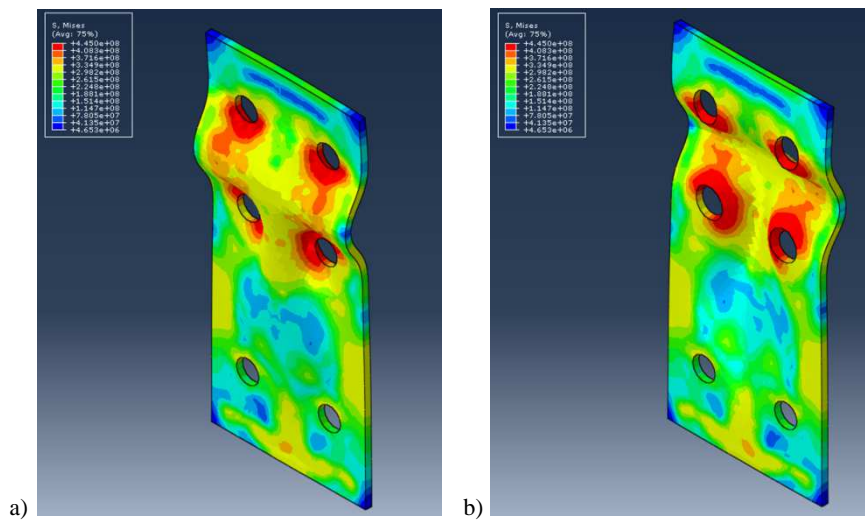


Fig. 10. Distribution of equivalent Huber – von Mises stresses in the end-plate of an A type joint, 6 mm thick: a) view towards the column flange, b) view towards the beam

#### 4. Evaluation of modeled joint rigidity

Performed numerical simulations allowed for the determination of the  $M-\varphi$  relationship for each of the joints considered, quantifying the interdependence between the bending moment applied to the joint and the increase in the rotation angle measured between the beam axis and the column axis, related to the

initially straight angle between those two structural component axes. The increase in the rotation angle has been measured in the frame plane, determined before the deformation, thus all the out of plane displacements occurring during the deformation process have been disregarded. No imperfections have been assumed in simulated joint geometry nor in simulated loads. The authoritative  $M-\varphi$  characteristics, a result of current simulation are depicted in Fig. 11. These characteristics, from left to right, pertain to the joints with decreasing rigidity (i.e. A, B, C and D). The borderlines between the zones qualifying the joint as rigid (when the condition  $S_{j,ini} \geq 25 \left( \frac{E_a I_b}{L_b} \right)$  is satisfied), semi rigid and fully flexible (when the condition  $S_{j,ini} \leq 0.5 \left( \frac{E_a I_b}{L_b} \right)$  is satisfied), as recommended in the code PN-EN 1993-1-8 [3] for sway frames, are depicted in Fig. 11 with straight continuous lines. The borderlines have been determined under the assumption that the considered frame represents one half of a typical sway portal frame. This means that the authoritative equivalent beam length was assumed as  $L_b = 2 \times 2.0 \text{ m} = 4.0 \text{ m}$ .

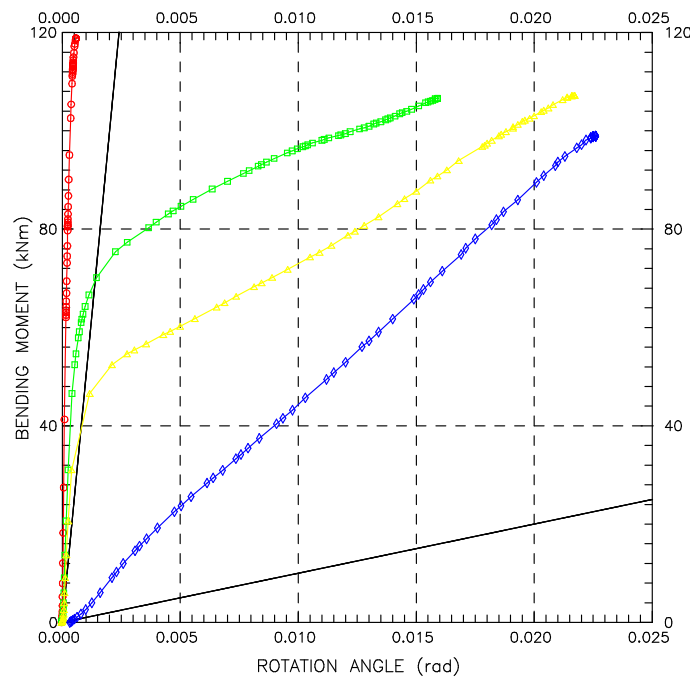


Fig. 11. Resultant  $M-\varphi$  characteristics obtained for the joints analyzed in present paper. The relations presented, from left to right, pertain to the joints of type A, B, C and D. Thus decreasing end-plate rigidity is accompanied by decreasing joint rigidity

It is clearly visible in Fig. 11 that the deformation of A type joint when subjected to load is qualitatively different than the deformation of B and C type joints. In turn the joints of these two types deform in a manner substantially different than the D type joint. Should the joints analyzed in present paper be qualified based on the initial rigidity  $S_{j,ini}$ , the first three types (i.e. A, B and C) would be assigned to the fully rigid group. In reality, however, the joints belonging to the types B and C attain the full bearing capacity at the relatively large value of rotation angle  $\varphi$ , while the limit value of the same angle in the case of A type joint is much smaller, in general negligibly small. One should also note the qualitatively different behavior of D type joint when subjected to loads. The joint of this type, based on the results of performed simulations is qualified as typical flexible one. Its characteristic is at the same time very close to linear in the whole deformation range, in which it is able to safely resist the loads applied to it. Its initial rigidity, even at the very low values of bending moment applied, is very low, as its value is incomparable with the values determined for other joint types considered here.

Relations depicted in Fig. 11 allow for the determination of bearing capacity of analyzed joints. This proved to be relatively similar for all considered joints. This means that the change in end plate thickness, even so drastic as considered here, exerts unequivocal and clear influence on the resultant joint rigidity. The influence on the bearing capacity, however, is much more subtle.

## 5. Concluding remarks

It was shown in the paper that the numerical simulation especially on performed on the sufficiently complex computational models may constitute an efficient and effective tool allowing for determination of joint rigidity and bearing capacity, relatively reliable and unequivocal in interpretation. The authors' experience seems to indicate that the  $M-\varphi$  curves – a result of such analysis tend to indicate that the initial rigidity of the considered joints is much higher than the corresponding rigidity determined for the same joints using the classical analytical component method. This conclusion is not surprising. It only confirms the earlier findings reported for instance in [4]. In the bibliography on the subject one may find as well the opinions, that the numerical models may overestimate the joint rigidity, with respect to values arrived at via experiment. This conclusion may hardly be generalized and should be verified by individualized and sufficiently detailed comparisons. However, one should always keep in mind that that every estimate of joint rigidity determined by numerical simulation is highly sensitive to many details preset during the development of numerical model (c.f. for instance [5]). Therefore the validation of results obtained by the authors and presented in this paper, even if only via the application of different computational environment [6] would be highly desirable.

## References

- [1] Abaqus 6.14: Abaqus/CAE user's guide, Dassault Systèmes, 2014.
- [2] Górnik G., Ślęczka L.: Degradation of structural properties in steel joints butt joint loaded in a non monotonic manner, *Inżynieria i Budownictwo*, 2/2018, pp. 91–94 (in Polish).
- [3] PN-EN 1993-1-8: Eurocode 3 – Design of steel structures, Part 1-8: Design of joints.
- [4] Jabłońska-Krysiewicz A.: Finite element modeling of the behaviour of steel end-plate connections, *Czasopismo Inżynierii Ładowej, Środowiska i Architektury – Journal of Civil Engineering, Environment and Architecture, JCEEA*, vol. XXXII, z. 62, 3/II/2015, pp. 173–184, DOI:10.7862/rb.2015.148.
- [5] Czaja J., Śliwa R.: Modelling of screw joints with its experimental verification, *Archives of Metallurgy and Materials*, vol. 52, issue 2, 2007, pp. 267–276.
- [6] Maślak M., Pazdanowski M., Woźniczka P.: Numerical validations of selected computer programs in nonlinear analysis of steel frame exposed to fire, *AIP Conference Proceedings* 1922, 150007-1-150007-9, Published by AIP Publishing, 2018.

*Przesłano do redakcji: 01.05.2018 r.*

*Przyjęto do druku: 15.06.2018 r.*

Tomasz SIWOWSKI<sup>1</sup>  
Maciej KULPA<sup>2</sup>

## FATIGUE TESTS OF WELDED JOINTS IN STEEL ORTHOTROPIC BRIDGE DECK

The procedure supported by testing has been used for the fatigue assessment of the existing steel bridge with the orthotropic deck, built in the early 80's of the XX century. The main goal was to check if the remaining fatigue life of the existing steel deck is at least 25 years, without the need of extensive repair or strengthening. The assessment comprised the fatigue calculation according to European codes with the use of updated values for material resistance. In order to obtain the updated information on material resistance the fatigue testing was carried out and the actual fatigue resistance  $\Delta\sigma_c$  was applied in damage accumulation calculation. The fatigue tests were carried out for two most critical deck details. Test specimens were cut out of the existing deck at the locations where the preliminary analysis showed the possible highest stress ranges. The assessment based on the actual material resistance revealed that the bridge deck had got very long service life. The main results of the fatigue assessment of orthotropic steel deck supported by testing have been presented in the paper.

**Keywords:** welded connections, orthotropic deck, fatigue testing, service life

### 1. Introduction

Steel bridges with orthotropic decks have been built worldwide over the past 60 years due to their advantages, such as high carrying capacity, low weight, rapid construction and life-cycle economy [10]. However, the detailing of the welded connections and the execution of welding was not always carried out in the most optimal way. This has resulted in fatigue cracks in orthotropic decks during their service life. Nowadays, due to the higher wheel loads and the increased traffic, steel bridges with orthotropic decks are more subject to fatigue loading than in the past. A number of these bridges have suffered fatigue cracks. Although cracks are found at many deck locations, they usually do not threaten the performance of the bridge immediately [3]. Repairs, however, generate additional expenses as bridge decks are large areas thus include many spots to be repaired.

---

<sup>1</sup> Corresponding author: Tomasz Siwowski, Rzeszow University of Technology, ul. Poznańska 2, siwowski@prz.edu.pl

<sup>2</sup> Maciej Kulpa, Rzeszow University of Technology, ul. Poznańska 2, kulpa@prz.edu.pl

Steel bridges with orthotropic decks have been built in Poland since early 70's of the XXth century. One of the biggest is the Grot-Rowecki Bridge across the Vistula River in Warsaw, built in 1981. The bridge is a key element of the traffic network of Poland. It is the busiest Polish bridge located along the strategic DK-8 national road. Several years ago the decision was made to alter the Warsaw section of the DK-8 into S-8 expressway, which caused the modernization (widening and strengthening) of the bridge was required. Before the final technical solutions were approved, the comprehensive evaluation of the technical condition had been carried out by Rzeszow University of Technology (RUT). One of the most important part of this evaluation was the thorough fatigue assessment of the orthotropic steel deck. The main goal of that assessment was to check if the remaining fatigue life of the existing deck would be at least 25 years without the need of extensive repair or strengthening.

In case of the existing steel bridges with orthotropic decks there are numerous approaches how to estimate their remaining fatigue life [1], [2], [5]. A classification system of assessment levels is presented in the joint JRC-ECCS report [4], which offers the recommendations to provide technical insight on the way the existing steel structures could be assessed. For the fatigue assessment of existing welded structures the detail categories  $\Delta\sigma_C$  given in [7] should be used, if the actual weld geometry is close to the ones produced today by manual arc welding. If not, or to make this procedure more reliable the specific fatigue tests need to be carried out. The procedure supported by testing has been used for the fatigue assessment of the existing steel bridge with the orthotropic deck. The fatigue tests were carried out for deck's critical details (welds). Test specimens were cut out of the existing orthotropic deck where the preliminary analysis showed the possible highest stress ranges. The updated information on material resistance was used and the actual fatigue resistance  $\Delta\sigma_C$  was applied in fatigue assessment according to recommendations [4]. The main results of fatigue assessment along with fatigue test results have been presented in the paper.

## 2. Bridge description

The Grot-Rowecki Bridge is one of the first Polish biggest steel bridges equipped in an orthotropic steel deck, very modern in those days. It has the total length of 646 m and consists of two parallel and independent steel box structures. The bridge superstructure is a seven-span continuous beam with the span lengths of  $3 \times 75 + 2 \times 90 + 120 + 60$  m. The two biggest spans located directly over the river bed have the one-box cross-section (Fig. 1a), the remaining spans are two-girder plated structures with the constant depth of 4.1 m of all girders. It is the widest bridge in Warsaw ( $2 \times 18.5$  m), located along the north by-pass of the city, and hosts 4 traffic lanes of  $3 \times 3.5$  m + 3.0 m and one sidewalk of 1.6 m.



Fig. 1. The Grot-Rowecki Bridge: general view of box girders (left), the orthotropic deck (right)

The orthotropic bridge deck consists of steel plates stiffened with longitudinal trapezoidal closed stiffeners and T-shaped cross-beams (Fig. 1b). The thickness of the deck plate varies from 12 mm in the middle to 28 mm in the support regions of the spans. The trapezoidal stiffeners are made of cold-formed 8-mm plates and continuously go through the webs of cross-beams. The axial distance of the stiffeners is 600 mm and their depth is 178 mm. The cross-beams are made up of 12-mm web with the depth of 850 mm and bottom flange with  $20 \times 400$  mm cross-section. They are placed every 2 500 mm along the bridge. The whole steel superstructure was completely welded and is made of 18G2A steel grade (S-355 according to current codes).

The technical state of the orthotropic deck of Grot-Rowecki Bridge after 30 years of service was described in [11]. In the bridge supervisions conducted during last years the special attention was paid to the orthotropic deck in particular. However, no serious damages were observed in this bridge. Recently, the visual inspection of the deck structure has been also carried out by the RUT as a part of the preliminary evaluation before fatigue assessment.

### 3. Selection of fatigue – prone welds

In order to identify the welded connections which are critical in terms of fatigue, apart from the visual inspection of the deck structure, the calculations were conducted and the critical regions were chosen for preliminary evaluation of the deck (Fig. 2). For the calculation of stress ranges in the chosen details, the part of the orthotropic deck with the length of 13.0 m was modelled, comprising 5 spans of longitudinal stiffeners supported on 6 cross-beams. A beam and shell elements in FEM *Sofistik*-code environment were used for deck modelling. Using 3-D structural model of the orthotropic deck, the inner forces and corresponding maximum and minimum stresses in all relevant details were calculated and followed by establishing stress ranges applied for the fatigue evaluation [9].

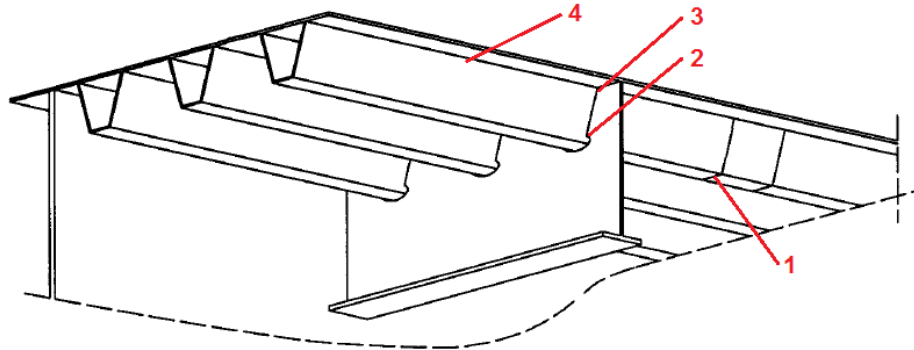


Fig. 2. Critical welds of the deck chosen for preliminary evaluation

The Fatigue Load Model No. 3 (FLM 3) according to [10] was used to generate stress ranges in the details under consideration. Equivalent damage coefficients  $\lambda_1 - \lambda_4$  according to [8] for the bridge were determined. For welded joints in the orthotropic deck the values of  $\Delta\sigma_C$  were applied according to [7]. Fatigue safety coefficient  $\gamma_{Ff} = 1.0$  according to [6] and partial factor  $\gamma_{Mf} = 1.15$  for high consequences of failure according to [7] were also applied. The fatigue assessment was undertaken using damage tolerant method.

Table 1 shows the fatigue safety calculations ( $\mu_{fat}$ ) for selected critical details (Fig. 2). This way two critical details of the deck were determined with the fatigue safety level  $\mu_{fat} < 1.0$ : the fillet weld connecting the deck to trapezoidal stiffener (detail no. 1 in Fig. 2) and the splice joint in stiffener, full penetration butt weld with steel backing plate (detail no. 4 in Fig. 2).

Table 1. Fatigue safety calculations ( $\Delta\sigma_{E,2}$ ,  $\mu_{fat}$ ) for selected critical welds

Detail	$\Delta\sigma_p$	$\lambda$	$\Delta\sigma_{E,2}$	$\Delta\sigma_C$	$\mu_{fat}$	Fatigue safety $\mu_{fat} > 1,0$
1	57.2	1.31	74.9	71	0.70	no – check level 2
2	33.4		43.8	80	1.35	yes
3						yes
4	40.0		52.4	50	0.71	no – check level 2

Once the critical construction details were found, the detailed investigation of the remaining fatigue life supported by testing could be done. Because the actual weld geometry is not the same to the ones produced today and to make the assessment procedure more reliable, the fatigue tests were decided to be carried out. On the other side, a more refined load model, composed of the different types of lorries crossing the bridge, was applied in the further calculation. The Fatigue Load Model No. 4 (FML 4) given in [6] and adjusted to the actual bridge service situation was taken into consideration [9].

#### 4. Fatigue testing

For the reliable fatigue assessment of existing welded structures the detail categories  $\Delta\sigma_c$  given in [7] should be determined by means of the specific fatigue tests. In our case the fatigue tests were carried out for both critical details (no. 1 and no. 4). Test specimens were cut out of the existing orthotropic deck (Fig. 3).

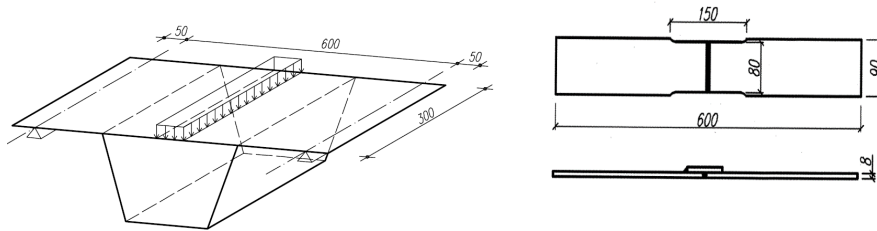


Fig. 3. Fatigue test specimens: weld no. 1 (left), weld no. 4 (right)

Detail no. 1 was the fillet weld connecting the deck slab to the trapezoidal stiffener (Fig. 2). In this case the fatigue assessment is based on the direct stress range from bending of the deck plate. Therefore the main point of interest was the fatigue strength of the deck plate under the bending stresses imposed by wheel loading. Testing was carried out on full-scale one-stiffener specimens, consisted of a 300-mm-long single stiffener with accompanying part of the deck plate 700 mm wide (Fig. 3a). Twelve test specimens were cut out of three different parts of the deck, located on three relevant spans of the bridge and along the slow lanes of the deck.

The test involved one mode of fatigue loading at the frequency of 5 Hz, i.e. on the deck at the stiffener centre-line, with the specimen supported symmetrically (Fig. 4a). Using the test specimen and the loading shown in Figure 4a the approximation of the actual loading conditions was achieved. The load value  $F$  and relevant stresses in the vicinity of fillet weld was evaluated



Fig. 4. Detail no.1 under testing: loading scheme (left), typical fatigue failure (right)

on the basis of the FEM calculations using the numerical model of specimen validated against the strain measurement done on the actual bridge deck before fatigue specimens were cut out. The stress ratio at the weld toe in the deck plate was assumed as  $R = 0.1$  with constant amplitude loading.

The series of 6 specimens was tested at the stress ranges  $\Delta\sigma$  between 160 and 220 MPa. All specimens failed in the weld as a result of fatigue crack propagation from the weld root through the stiffener (Fig. 4b). It was induced by the transverse bending of the deck plate. The results of the tests of a fillet weld connecting the deck plate to the trapezoidal stiffener are shown in Table 2.

Table 2. Results of fatigue testing of the detail no. 1

No.	$\Delta\sigma$ [MPa]	$F_{min}$ [kN]	$F_{max}$ [kN]	$\Delta F$ [kN]	Number of cycles $N$
1	160	1.09	10.9	9.8	2,763,055
2	170	1.16	11.58	10.42	1,652,000
3	180	1.22	12.25	11.02	2,233,811
4	190	1.29	12.93	11.64	1,313,332
5	200	1.36	13.61	12.25	889,523
6	220	1.49	14.97	13.48	636,615

Detail no. 4 was the splice joint in a stiffener, full penetration butt weld with steel backing plate (Fig. 2). In this case the fatigue assessment is based on the direct stress range  $\Delta\sigma$  in the stiffener. Testing was carried out on small strip specimens cut out of the full-scale splice joint. This was a tensile fatigue test on a butt-jointed plate,  $600 \times 90 \times 12$  mm thick (Fig. 3b). These test specimens were cut out of four different parts of the deck, located on four relevant spans of the bridge and along the slow lanes of the deck.

The small strip specimens were loaded in tension at a frequency of 5 Hz. The stress ratio at the weld in the stiffener bottom plate was assumed as  $R = 0.1$  with constant amplitude loading. The series of 7 specimens was tested at the stress ranges  $\Delta\sigma$  between 120 and 200 MPa. Most specimens failed in the weld as a result of fatigue crack propagation from the weld root through the plate (Fig. 5b). One run-out was observed at  $\Delta\sigma = 120$  MPa. The results of the tests on a penetration butt weld with steel backing plate in stiffener are shown in Table 3.



Fig. 5. Detail no. 1 under testing: loading scheme (left), typical fatigue failure (right)

Table 3. Results of fatigue testing of the detail no. 4

No.	$\Delta\sigma$ [MPa]	$\sigma_{min}$ [MPa]	$\sigma_{max}$ [MPa]	Number of cycles $N$
1	120	13.3	133.3	5,000,000
2	125	13.85	138.85	2,029,651
3	130	14.4	144.4	753,060
4	140	15.6	155.6	593,422
5	160	17.8	177.8	209,464
6	180	20	200	567,058
7	200	22.2	222.2	44,414

The fatigue results are presented in S-N diagrams including the current relevant classification according to [7] (Fig. 6). Since the test data were used to determine the appropriate detail category for a particular construction detail, the value of the stress range  $\Delta\sigma_C$  corresponding to the value of  $N_C = 2$  million cycles was calculated for a 75% confidence level of 95% probability of survival for  $\log N$ . For details no. 1 and no. 4 the stress ranges were established experimentally as  $\Delta\sigma_C = 158.8$  MPa and  $\Delta\sigma_C = 101.0$  MPa, respectively.

## 5. Deck's service life estimation

The damage accumulation calculation for two welds took into account updated values for loads and resistance. For critical construction details the stress ranges  $\Delta\sigma_i$  resulting from crossing the bridge by each lorry of FLM 4 were calculated, using the refined 3-D model of the deck [9].

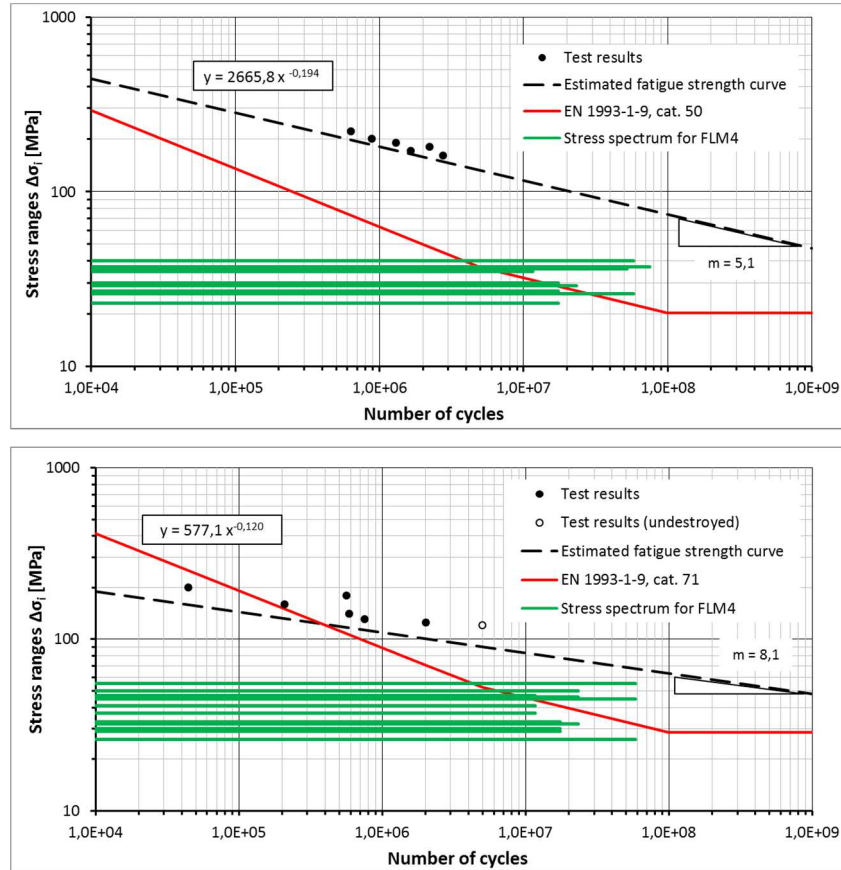


Fig. 6. S-N diagram for the detail no. 1 (top) and no. 4 (bottom) against the relevant curves [7]

The number of cycles occurring at each stress range magnitude  $\gamma_{Ff} \Delta\sigma_i$  of a stress spectrum was calculated on the basis of estimated  $N_{obs}$  of the FML4. Thus the stress history for the selected deck details was established. The number  $N_{Ri}$  was determined using updated material resistance information, i.e. the actual S-N curves based on fatigue testing (Fig. 6). In Table 4 the service life estimation for the detail no. 1 was shown, including 33 years of up-to-date service and additional 25 years required by the road administration. The damage accumulation calculation accounts the curve established with fatigue testing and – for comparison – the S-N curve according to [7]. The practically unlimited service lives for both deck details were obtained:  $7.80E+02$  and  $1.80E+02$  years for detail no. 1 and no. 4 respectively. However, using the standard S-N curve according to [7] in both cases the service life of the deck was exhausted. Thus the fatigue calculation clearly revealed the influence of the updated information on material resistance on the final fatigue assessment result.

Table 4. Damage accumulation calculation for the detail no. 4 and the time period of 33 years

Stress ranges $\Delta\sigma_i$	Number of cycles in a year $n_i$	Service life estimation			
		According to [8]		Based on fatigue tests	
		Endurance $N_i$	$n_i / N_i$	Endurance $N_i$	$n_i / N_i$
		(a)	(b)	(c)	(a) / (c)
2	2.00E+06	$\infty$	0	1.11E+16	1.80E-10
5	3.00E+05	$\infty$	0	9.89E+13	3.03E-09
7	1.30E+06	$\infty$	0	1.75E+13	7.45E-08
10	1.00E+06	$\infty$	0	2.78E+12	3.60E-07
23	3.00E+05	2.62E+07	1.15E-02	3.79E+10	7.91E-06
26	1.00E+06	1.42E+07	7.04E-02	2.02E+10	4.96E-05
27	3.00E+05	1.18E+07	2.54E-02	1.66E+10	1.81E-05
29	4.00E+05	8.24E+06	4.85E-02	1.15E+10	3.48E-05
30	3.00E+05	6.95E+06	4.32E-02	9.64E+09	3.11E-05
35	2.00E+05	3.83E+06	5.22E-02	4.36E+09	4.59E-05
36	9.00E+05	3.52E+06	2.56E-01	3.77E+09	2.39E-04
37	1.30E+06	3.25E+06	4.00E-01	3.27E+09	3.97E-04
40	1.00E+06	2.57E+06	3.89E-01	2.19E+09	4.57E-04
Linear damage cummulation in a year: $D_d = \sum n_i / N_i$			1.30E+00		1.28E-03
Fatigue life (in years): $T_s = 1 / D_d$			7.72E-01		7.80E+02
Remaining fatigue life (in years) after 33 years of service			exhausted		747

The damage accumulation calculation revealed that the most critical details of the deck had got very long service life in terms of fatigue ( $D_d \ll 1.0$ ). It means that in these details fatigue cracks could not be initiated and propagated in the assumed time of service.

## 6. Conclusions

The applied approach of fatigue assessment of the existing orthotropic deck was supported by testing and follows the principles and application rules in the Eurocodes. The calculation and fatigue testing were performed for two welds, which were estimated to be the most critical for fatigue according to preliminary evaluation. However, the detailed assessment showed that the remaining fatigue life of the welds under consideration is practically unlimited. As there are several uncertainties in the applied procedure for the fatigue assessment [4], some further measures were necessary. Since quantitative investigation using NDT (magnetic particle inspection as well as ultrasonic testing) revealed that no cracks were found, the adapted final solution could have resulted in no further measures. Thus the orthotropic deck of the Grot-Rowecki Bridge was considered safe with the required remaining life of at least 25 years.

## References

- [1] Aygül M., Al-Emrani M., Urushadze S.: Modelling and fatigue life assessment of orthotropic bridge deck details using FEM, *International Journal of Fatigue*, vol. 40, no. 7, 2012, pp. 129–142.
- [2] Battista R.C., Pfeil M.S., Carvalho E.M.L.: Fatigue life estimates for a slender orthotropic steel deck, *Journal of Constructional Steel Research*, vol. 64, no. 1, 2008, pp. 134–143.
- [3] Kolstein M.H.: Fatigue classification of welded joints in orthotropic steel bridge decks, Delft University of Technology, Delft, The Netherlands, 2007.
- [4] JRC Scientific and Technical Reports: Assessment of existing steel structures: recommendations for estimation of remaining fatigue life, Report No. 43401, Joint Research Centre, European Commission, Luxembourg, 2008.
- [5] Maljaars J., Dooren F., Kolstein H.: Fatigue assessment for deck plates in orthotropic bridge decks, *Steel Construction*, vol. 5, no. 2, 2012, pp. 93–100.
- [6] PN-EN 1991-2. Eurocode 1: Actions on structures. Part 2: Traffic loads on bridges. The Polish Committee for Standardization, Warsaw, 2003.
- [7] PN-EN 1993-1-9. Eurocode 3: Design of steel structures. Part 1-9: Fatigue. The Polish Committee for Standardization, Warsaw, 2005.
- [8] PN-EN 1993-2. Eurocode 3: Design of steel structures. Part 2: Steel bridges. The Polish Committee for Standardization, Warsaw, 2006.
- [9] Siwowski T., Kozłowski A., Kulpa M.: Fatigue assessment of orthotropic steel deck in existing road bridge. Proceedings of SBIC-2015 – the International Symposium on Steel Bridges: Innovation & New Challenges, Istanbul, Turkey, 2015.
- [10] Troitsky M.S.: Orthotropic bridges – theory and design, James F. Lincoln Arc Welding Foundation, Cleveland, USA, 1987.
- [11] Zobel H., Karwowski W., Mossakowski P., Wróbel M.: Pomosty ortotropowe niektórych mostów drogowych po wieloletniej eksploatacji, *Inżynieria i Budownictwo*, vol. 65, nr 6, 2009, pp. 306–311.

*Przesłano do redakcji: 04.05.2018 r.*

*Przyjęto do druku: 15.06.2018 r.*

Piotr MILEWSKI<sup>1</sup>  
Mirosław BRONIEWICZ<sup>2</sup>

## RESISTANCE OF THE WELDS IN CHS JOINTS WITH THE RIB PLATES

With regard to the calculation of welds' resistance in connections between hollow sections in EN 1993-1-8, very general information is given without any indication of specific calculation procedures. These recommendations are basically as follows: the resistance of the welds must have the value of the cross-section and assessment of the welds' resistance based on the effective lengths is allowed in cases when forces in the braces are smaller than the resistance of the joint, but the detailed method is not specified. The objective of this paper is to present the most up-to-date information for the design of welds for overlap joints with reinforcing rib plates. The article presents the FEM analysis of the welds in the intermediate joint with the rib in a truss made of circular hollow sections. The conclusions from the analysis were presented.

**Keywords:** trusses, hollow sections, K joint with the ribs, welds, FEM analysis

### 1. Introduction

#### 1.1. Welded joints made of hollow sections

Welded joints of trusses made of hollow sections with the reinforcing rib plates between braces occur mainly in assembly joints of chords (Fig. 1) and in support joints (Fig. 2) [1]. Similar solutions are also found in the case of design of overlap joints when there is little overlap of braces ( $\lambda_{ov} < 25\%$ ). For executive reasons, joints with rib plates are used in the case of technological difficulties in the proper execution of welds on covered sections of joining members or in order to avoid welding accumulation. The ribs are also used in K type intermediate joints of lattice systems when it is necessary to attach an additional structural element to the joint (Fig. 3).

---

<sup>1</sup> Corresponding author: Piotr Milewski, Białystok University of Technology, ul. Wiejska 45A, milewski.piotr@o2.pl, praca badawcza MB/WBiIS/5/16

<sup>2</sup> Mirosław Broniewicz, Białystok University of Technology, ul. Wiejska 45A, m.broniewicz@pb.edu.pl

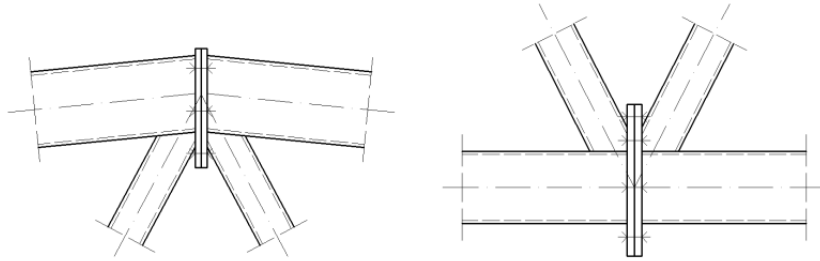


Fig. 1. Midspan assembly joints

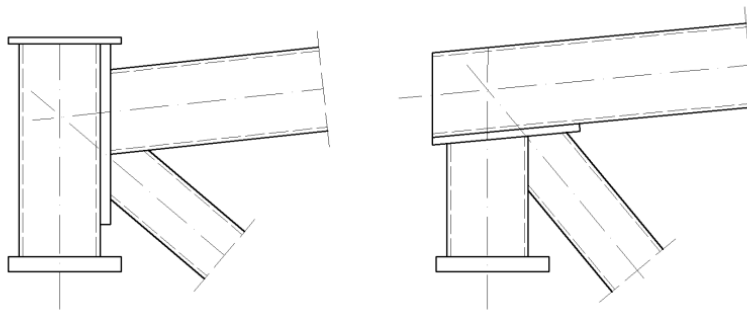


Fig. 2. Support of a truss on an outer column

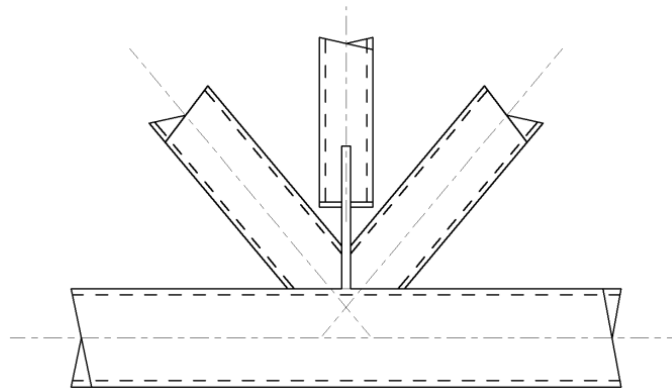


Fig. 3. Joint with the head rib and an additional post

## 1.2. Assessment of the resistance of fillet welds

The principles for the assessment of the joints capacity made of hollow sections are given in PN-EN 1993-1-8 [2], in many monographs [3], [4] and CIDECT guides. To assess the capacity of joints with the ribs, the formulas given in PN-EN 1993-1-8 [2] can be used, referring to K joints with mutual overlap of the braces [4]. However, the calculation of welds resistance in welded

joints of members in lattice girders made of hollow sections has been treated in the PN-EN 1993-1-8 [2] very generally without providing detailed calculation guidelines. The procedure for assessing the capacity of T, Y and X joints as well as K and N joints with the gap was presented by Bródka and Broniewicz in publications [5] and [6]. Calculation of the resistance of welded K and N overlap joints made of rectangular and square hollow sections are given in the publication [7].

In all examined joints fillet welds with effective lengths calculated on the basis of experimental research were used. The assessment method presented in Annex K to the pre-standard EN 1993-1-1 [7] has been adopted as the basis for assessing the effective lengths of welds, with respect to gap joints made of rectangular hollow sections. It is stated that in the case of K and N joints at the angle of inclination of the braces  $\theta_i \leq 50^\circ$ , both transverse welds are effective in transferring of stresses and the total length of welds is  $l_w = 2(h_i / \sin \theta_i + b_i)$ , while in the case  $\theta_i \leq 60^\circ$  the transverse weld located on the acute angle does not participate in the stress transfer and  $l_w = 2h_i / \sin \theta_i + b_i$ .

According to the standard PN-EN 1993-1-8 [2], design effective lengths should be used in cases of welded joints made of fillet or groove welds when the forces in the braces are smaller than the capacity of the joints due to occurrence of general instability of members or unification their cross-sections. In such cases it is uneconomic to use the standard criterion so that the design resistance of the weld per unit length of the circumference of the brace is not less than the design resistance of the cross-section of this brace per unit of its circumference. In addition, it may be difficult to properly position of the welds with the required thickness, especially on sections of the inclined member at an obtuse angle.

The presented indications cannot be extended to the assessment of the resistance of welds in the joints with the rib plate, as the cutting of the ends of the joined sections is different, so the effective lengths and often the shapes of fillet or groove welds are different. The rules for calculating the capacity of such connections are presented in [9].

### 1.3. Welded joints with the rib plate made of circular hollow sections

In welded trusses joints made of hollow circular sections between the brace members and chords, depending on the location of the weld on the circumference of the member butt welds, fillet welds or groove welds are designed. In the case of using circular hollow sections at the contact points of the brace with the upper wall of the chord, fillet or butt welds are used, with the appropriate method of beveling of the walls of the circular member, while at the contact points of the brace with the side wall of the chord the groove welds are used. In the case of rectangular hollow sections, when the width of the brace is smaller than the width of the chord, fillet welds are used, or butt welds when the width of the brace is equal to the width of the chord.

In the paper [1], it was pointed out that the formulas, given in PN-EN 1993-1-8 [2], referring to assessing of the capacity of joints with mutual overlapping of the brace members, can be used to assess capacity of such joints with a rib plate. The evaluation of the resistance of fillet welds laid in connection of the braces with the rib plate is different due to the different way of cutting the ends of joined members. The effective lengths of the welds and the shapes of fillet or groove welds are also different.

Fig. 4 shows the intermediate welded K-joint of the bottom truss chord made of circular hollow sections with the same diameter of the brace members. Due to the low overlap value of the braces, in order to avoid welds along the spatial curve, which imitates the contact of the brace with the chord, a rib plate has been used.

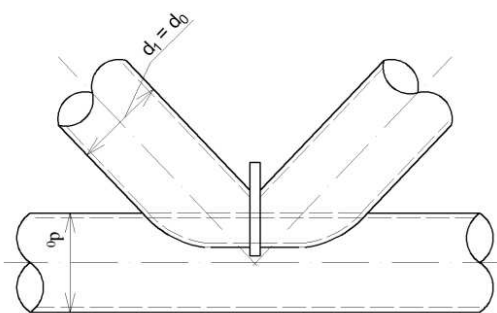


Fig. 4. Joint made of circular hollow sections with a reinforcing rib plate

Preparing the ends of circular members according to a specific spatial curve, ensuring proper matching of connecting elements is possible using modern, numerically controlled cutting machines. Making the right welded joints requires chamfering of walls with different angle of inclination. The spatial shape of the joint, as well as the variability of the type of weld in its length and its cross-section, make it difficult to assess the capacity of such welds. The thickness of such welds should be determined in accordance with their shapes, usually treated them as fillet or groove welds.

An exemplary arrangement of welds in the connection of braces with a chord in a K-joint with the rib plate made of circular hollow sections, at the inclination angle of the braces to the chord  $\theta \leq 50^\circ$  is shown in Fig. 5.

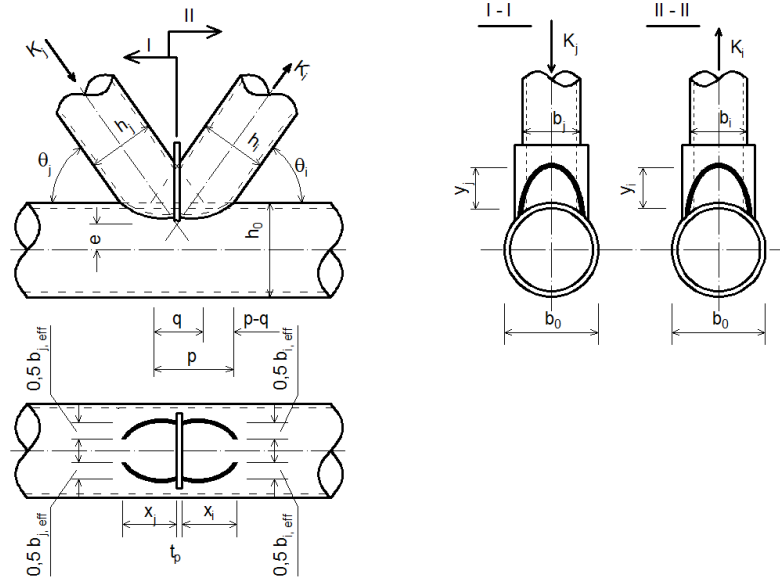


Fig. 5. Welds layout in circular hollow section overlap joint with reinforcing rib plate

An analytical method for determining the effective lengths of welds of such a joint is presented in the publication [8]. The values of mutual overlapping of braces  $q$  and  $p$  were evaluated in accordance with PN-EN 1993-1-8 [2]. The rib plate is connected to both the braces and the chord and participates in transferring forces from the braces to the chord. In order to determine the capacity of welded joints between the braces and the chord and the rib plate, the thickness of individual weld sections and their effective lengths  $x_j$ ,  $x_i$ ,  $y_j$ ,  $y_i$ ,  $b_{j,eff}$  and  $b_{i,eff}$  were determined. The values of  $x_j$ ,  $x_i$  are the effective lengths of welds connecting the braces with the chord, while the values  $y_j$ ,  $y_i$  are the effective lengths of welds connecting the braces to the rib plate.

The effective lengths of welds depend on the susceptibility of the connected member walls. Welds are loaded with components of forces occurring in braces parallel and perpendicular to the plane of the chord and the rib. Stresses in welds  $\sigma'$  and  $\sigma''$  are calculated taking into account the load direction, parallel or perpendicular to cross-section of the weld.

## 2. Description of the K-type CHS joint with the rib plate FEM analysis

### 2.1. Assumptions adopted for the joint analysis

The intermediate K-type joint with the rib plate made of circular hollow sections was analyzed. In order to obtain different angles of braces inclination, the lattice girder with the same span of 12.0 m was varied in terms of heights,

which were successively 1.70 m, 1.40 m and 1.10 m. Corresponding angles of braces inclination to the bottom chord were  $60^\circ$ ,  $54^\circ$ ,  $48^\circ$ . The truss was loaded with concentrated forces from the standard loads (dead, snow, wind loads) in the joints of the top chord. As the sections of the top and bottom chord, circular hollow sections RO 88,9 $\times$ 5 mm were assumed, while as the braces RO 57 $\times$ 4 mm. The thickness of the rib plate was taken equal to 5 mm. The girder schema for variant I is shown in Fig. 6. The joint adopted for analysis is marked with the letter "A". The joint model, which was used for the FEM analysis is shown in Fig. 7.

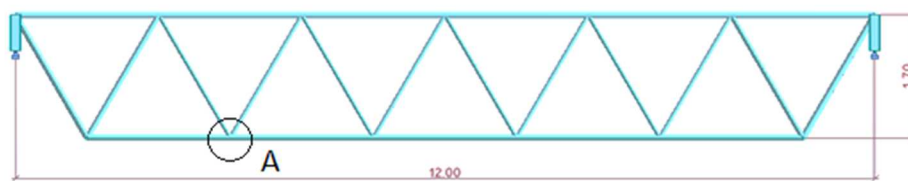


Fig. 6. Analyzed truss and the designation of the analyzed joint

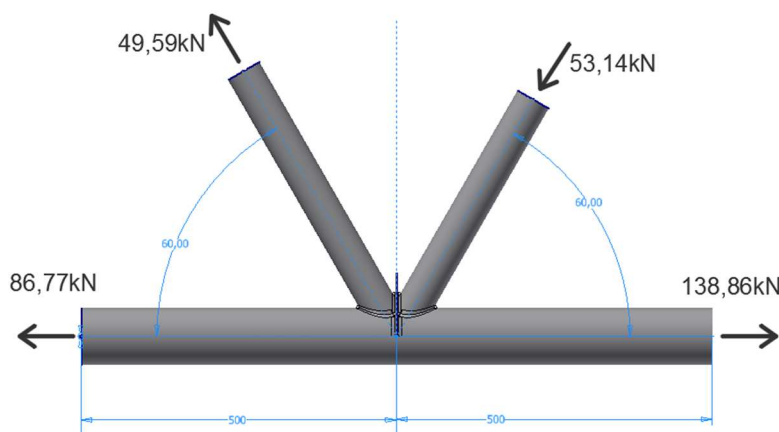


Fig. 7. Analyzed joint modeled in the FEM analysis program

The same material parameters were adopted for each joint. Both truss chords, braces, ribs and welds were modeled from S235 steel, which has a yield strength of 235 MPa and Young's modulus of 210 000 MPa. The material was defined as Bilinear Isotropic Hardening"

The mesh density of the analyzed joint was 5 mm, while in order to achieve more accurate results, the mesh was thickened around to 2 mm near the welds. In order to facilitate computer analysis, three solids of welds were modeled which were not connected to each other. At the same time, their length is as large as possible.

Additionally, in order to obtain a more accurate image of stresses not only outside the joint, but also inside it, it was decided to cut the joint along the axis of symmetry of the bottom chord in the plane of the truss. The model of the joint together with the mesh of finite elements and the solids of the welds is shown in Fig. 8. The main object of the analysis was the weld connecting the brace with the bottom chord. In addition to the three height variants of the truss, each joint was modeled with three variants of weld thickness successively: 4 mm, 3 mm, 2 mm. In the model connections between the bottom chord and braces and the rib was defined as sliding with a coefficient of friction of 0.15, while the remaining connections, between welds and individual elements, were defined as bonded.

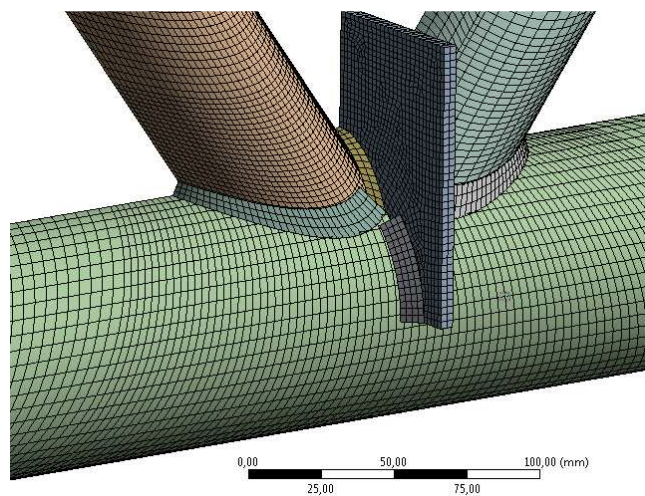


Fig. 8. View of the meshed joint with the welds

Computer analysis was carried out in a program using FEM type analysis. After the joints modeling, they were loaded with concentrated forces occurring in a given truss joint. In the figures below (Fig. 9 to 14) the results of von Mises

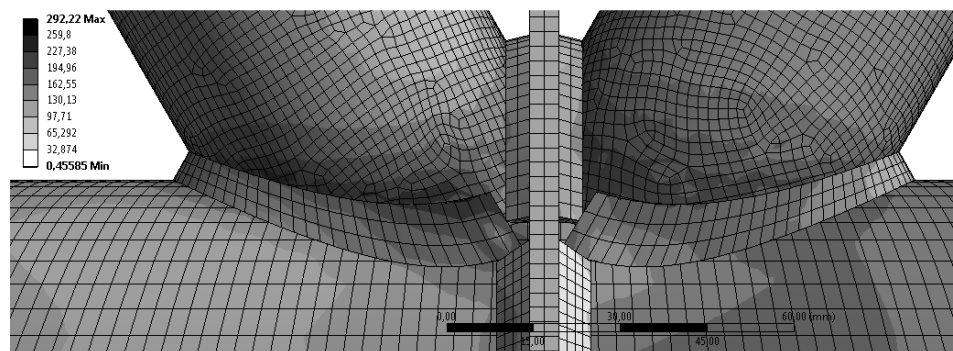


Fig. 9. Stress in the joint for the angle of  $60^\circ$  and welds 4 mm

stresses for the truss of 60° and 48°, as well as for the thickness of welds 4 mm and 2 mm were presented.

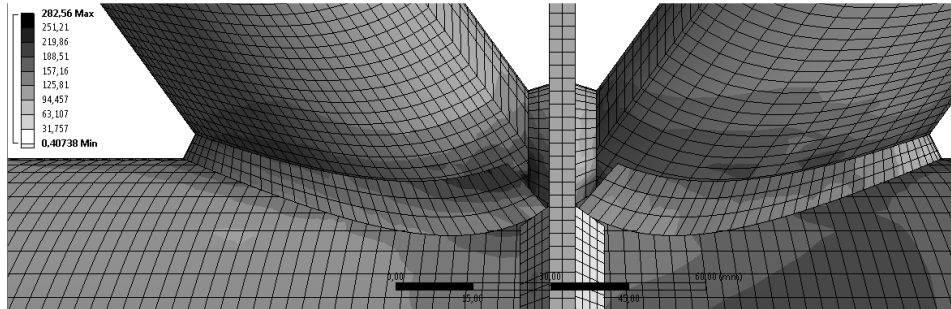


Fig. 10. Stress in the joint for the angle of 54° and welds 4 mm

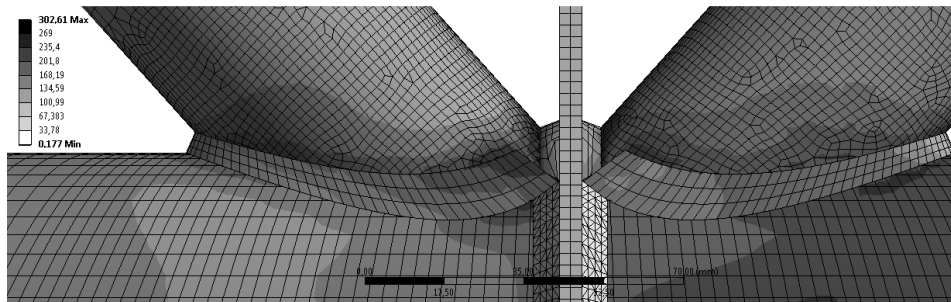


Fig. 11. Stress in the joint for the angle of 48° and welds 4 mm

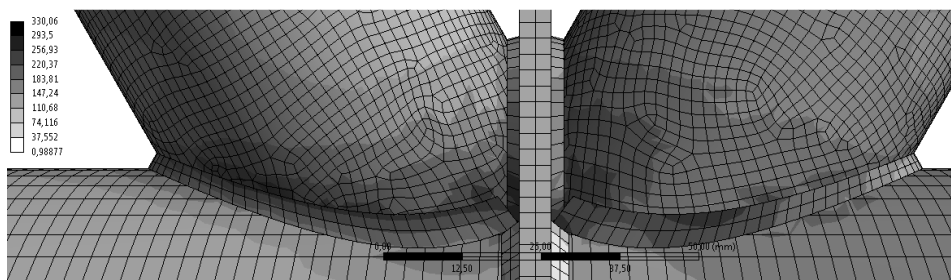


Fig. 12. Stress in the joint for the angle of 60° and welds 2 mm

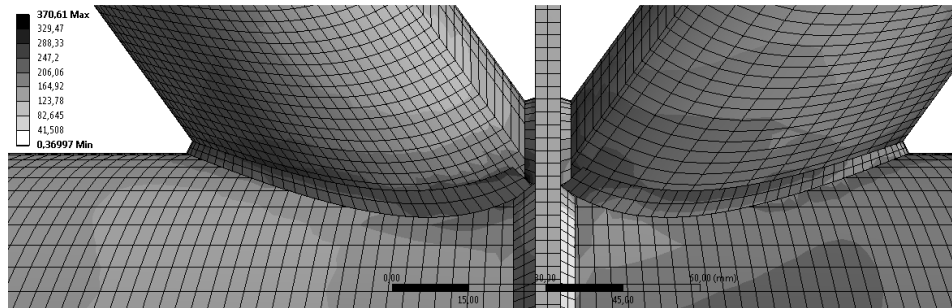


Fig. 13. Stress in the joint for the angle of  $54^\circ$  and welds 2 mm

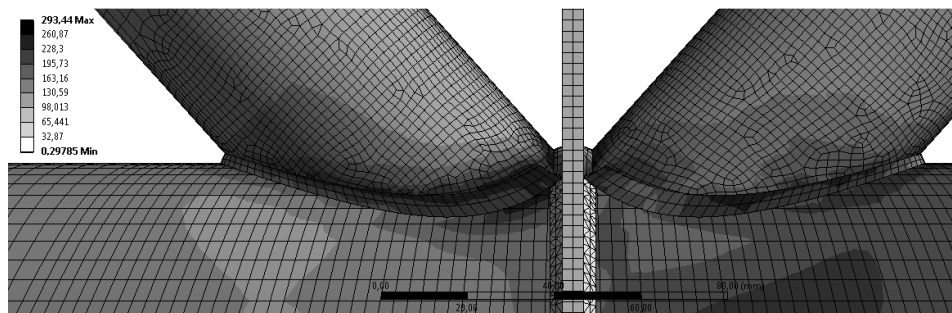


Fig. 14. Stress in the joints for the angle of  $48^\circ$  and welds 2 mm

### 3. Conclusions

After analyzing the test results, it can be concluded that the distribution of stresses in the welds connecting the braces with the chord varies and depends on the angle of inclination of the braces in relation to the chord and the thickness of the weld. In the case of an angle  $\theta \leq 60^\circ$ , the greatest stresses in the welds connecting the brace with the chord can be observed in the groove weld located on the side of the obtuse angle, near the place of the rib plate. Stress values decrease in the longitudinal weld together with the distance from the rib plate, in order to reach its minimum on the opposite side of the brace, i.e. in the transverse weld on the side of the acute angle. A smaller variation in the stress values in both transverse joints occurs in the case of angle  $\theta \leq 48^\circ$ . The transverse weld located on the side of the acute angle more effectively transfers stresses from the brace to the chord.

This is especially evident in the case of welds with a thickness of 2 mm because a greater role in the transfer of stresses play horizontal welds connecting the brace with the chord. Increasing the thickness of welds to 4 mm disturbs slightly the described stress distribution in the welds, causing that the greater part of the transferred force falls on the vertical welds connecting the brace with the rib.

If the brace is compressed, it can be observed that the maximum stresses in the longitudinal welds are shifted towards its central part. However in the case of tension brace the largest stresses can be observed in close proximity to the rib plate.

These analyses indicate that not all welds joining the brace members to the chords carry the load in the same way. On the basis of computer analyzes it is impossible to determine exactly which sections of welds are fully effective and which transfer only a small load. This is especially difficult in the case of longitudinal welds. However, the calculations indicate that the standard assessment of stresses in welds of hollow section joints is only approximate and does not fully reflect the actual distribution of stresses in the welds, which confirms the earlier studies of Packer and Henderson. To verify these calculations, experimental tests should be carried out on real truss joints. However, the analysis will confirm that the recommendations given in the literature regarding the calculation of welds' resistance can be optimized and new computational solutions can be introduced, which however, are impossible to propose at the current stage of research.

## References

- [1] Bródka J. Design of joints with the rib plate made of hollow sections. Capacity of joints. II International Polish-Ukrainian Scientific-Technical Conference "Current Problems of Metal Structures". Book of the Conference. Gdansk, 27-28 November 2014 (in polish).
- [2] EN 1993-1-8: 2008 Eurokod 3: Design of steel structures - Part 1-8: Designing of joints.
- [3] Packer J. A., Henderson J. E.: Hollow Structural Section Connections and Trusses – A Design Guide. Second Edition. Canadian Institute of Steel Construction. Toronto 1997.
- [4] Bródka J., Broniewicz M.: Steel structures made of hollow sections. Vol. 1. PWT. Rzeszów 2017 (in polish).
- [5] Bródka J., Broniewicz M.: Calculation of welded joints of trusses made of rectangular hollow sections. – Steel Structures, 2002, No 4 (in polish).
- [6] Bródka J., Broniewicz M.: Assessment of the welded joint resistance according to EN 1993-1-8: 2009. – Steel Structure, 2007, No 1 (in polish).
- [7] Bródka J., Broniewicz M.: Calculation of welding trusses overlap joints made of rectangular hollow sections. – Archives of Civil Engineering, 2013, No 4.
- [8] ENV 1993-1-1. Eurocode 3: Design of steel structures. Part 1-1. General rules and rules for buildings. Annex K. Hollow section lattice girder connections. CEN. Brussels. 1994.
- [9] Bródka J., Broniewicz M.: Hollow section overlap joints with reinforcing rib plate in structural applications. Lambert Academic Publishing. 2016.

*Przesłano do redakcji: 25.04.2018 r.*

*Przyjęto do druku: 15.06.2018 r.*

Jerzy K. SZLENDAK<sup>1</sup>  
Adrian SZPYRKA<sup>2</sup>

## RESISTANCE OF TENSION BRACE IN PLUG & PLAY N SHAPE RHS TRUSS CONNECTION

The paper presents concept of RHS truss with N-shape connections in the plug & play form, made in non-welded technology. The procedure of calculating the resistance of tension brace truss connection was presented, using the component method. The results of obtained resistance of joint was compared with the tension bracing RHS strut resistance and the usefulness of the concept considered was determined.

**Keywords:** steel truss N shape RHS joints, non-welded plug & play connections

### 1. Introduction

The subject of the paper is a new plug & play connection in application to a steel truss made of rectangular hollow section (RHS). The resistance of such a joint was the subject of previous works [2 and 3]. In this paper, a study was carried out on the resistance modified in relation to the tension brace shown in [2].

The use of modern 3D laser cutting technology enables easy and precise cutting in steel elements, here closed RHS profiles, of openings of any and often very complex shapes.

It was an inspiration to develop plug & play non-welded joints. Tests of this type of joints were previously presented in [2 and 3], where forces were transferred only by bearing and shearing stresses in the elements in contact with each other, the key (bracing elements) and the lock (holes in the truss chord). For this purpose, a "lock" was made in the truss chord, in which a "key" strut was inserted. A tension brace made of double plate bar is attached to the chord. It covering the chord on both sides and it is fixed to the chord with a bolt. This solution led to a quick ovalization of the hole in the RHS profile of the chord. To remedy this, a steel square bar was placed under the chord, see Fig. 1 [5].

---

<sup>1</sup> Corresponding author: Department of Building Structures and Architecture, Faculty of Civil and Environmental Engineering, Białystok University of Technology, tel. 603641235; e-mail: jerzy.szlendak@gmail.com

<sup>2</sup> Department of Building Structures, Faculty of Civil Engineering and Architecture, Rzeszów University of Technology, tel. 692160551; e-mail: adrianszp@gmail.com

This bar has significantly reduced the ovalization of the hole in the side walls of the chord, because the load is also transferred by the stress to the lower RHS chord face plate with a much larger contact area than previously.

The combination of this type eliminates the need for welds in the joint. The publications [3 and 4] present the results of experimental research, as well as the theoretical estimation of the resistance capacity of T-shape truss joints, made of RHS profiles, in non-welded technology in the plug & play form [3]. The theoretical resistance, calculated by means of a developed yield lines model with experimental studies, was also compared [4].

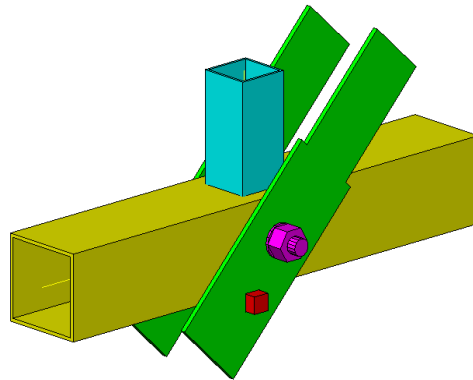


Fig. 1. Plug & play N-shape connection, 3D model [5]

In this paper, a modified concept of connecting the tension brace to the chord in the N-shape connection was considered. The tension brace is made not from flat bars as before [5], but from the RHS profile with special "teeth" and meshes against the chord walls. A "lock" is made in the truss chord, which allows inserting a "key" or a tension brace into it. The vertical strut is also inserted in the "lock" made in the chord, but after the tension brace is mounted, which causes it to jam in the connection. The combination of this type eliminates the need to use welds to connect the bracing with the chord. In concept No. I, Fig. 2, the resistance of the lock was small. So, this was improved by developing concept no. II, where the surface of the "teeth" was changed, which allowed the increase of the resistance of the connection. The scheme of such a solution is shown in Fig.3.

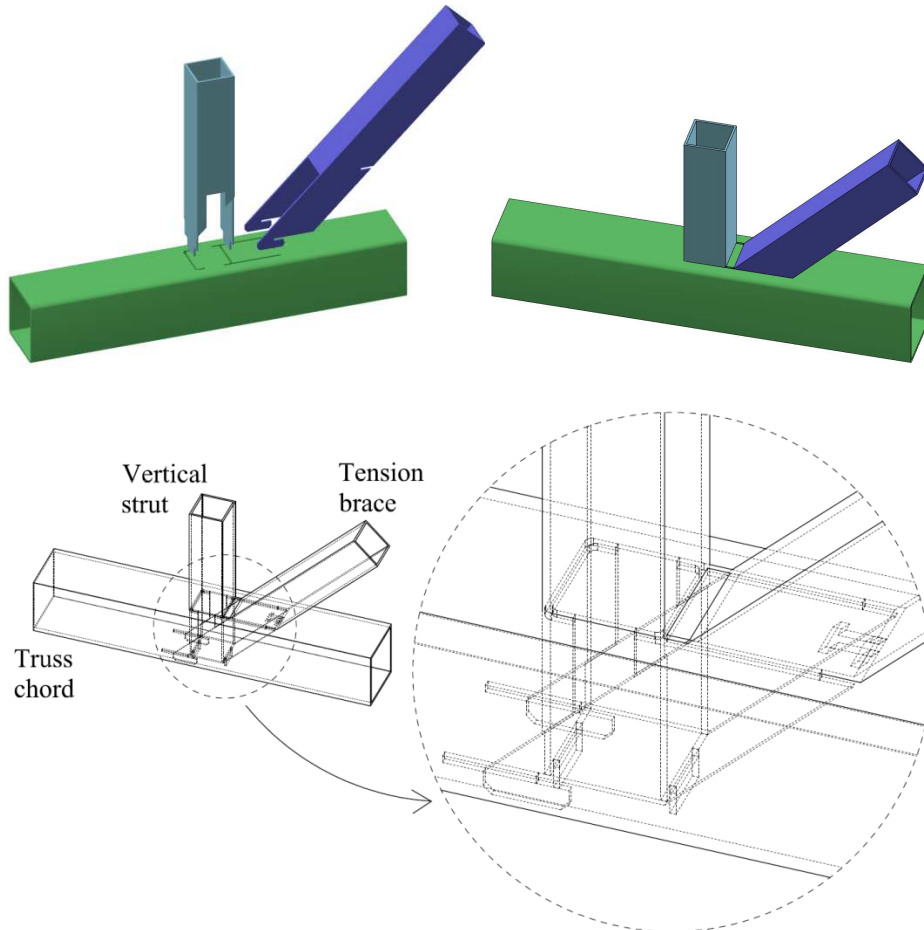


Fig. 2. Concept no. I –plug & play N-shape connection, 3D model

Structures made in non-welded technology can be used successfully in construction, for example for production facilities, warehouses, etc. Easy transport of this type of construction in single elements allows for the construction of permanent or temporary halls. Due to the lack of permanent connections between the elements, such structure can be dismantled and reassembled elsewhere.

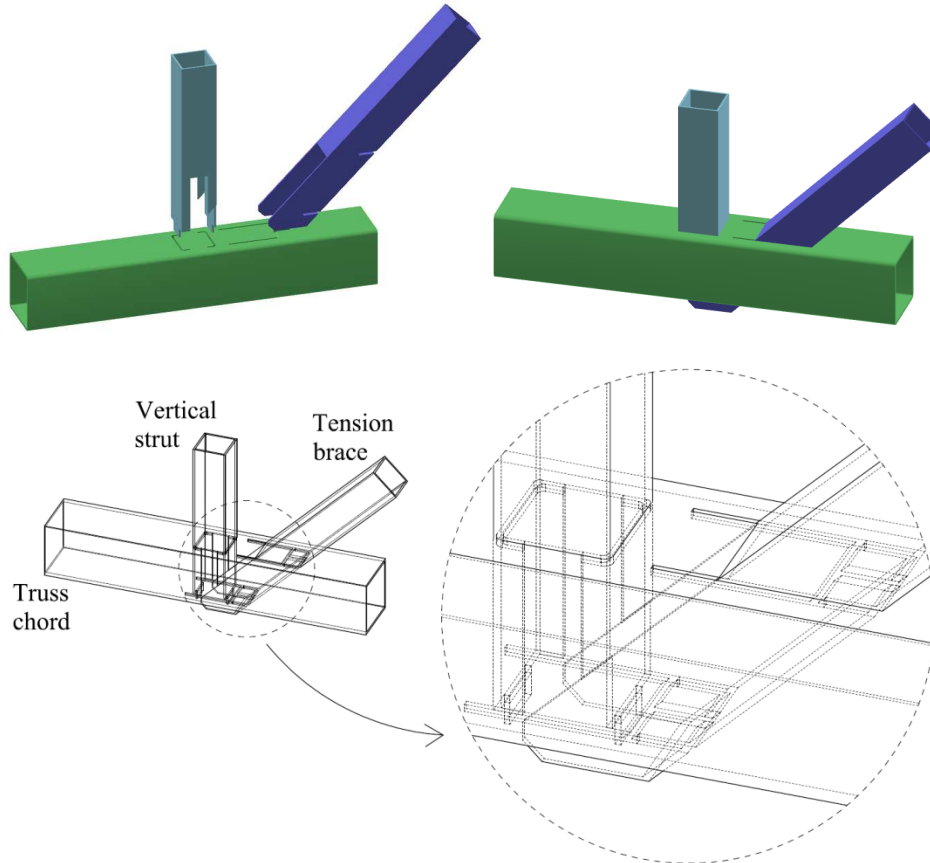


Fig. 3. Concept no II – plug & play N-shape connection, 3D model

## 2. Theoretical estimation of the resistance of tension brace

The resistance of the tension brace connection with the chord was calculated using the component method. The theoretical model of failure was presented (model I - upper connection, model II - lower connection). The tension brace loaded with axial force  $N$ , distributed over the horizontal  $N_x$  and vertical  $N_z$  components, the load diagram and the theoretical plane of failure was shown in Figure 4. Also, the 3D model of the tested tension brace made of RHS where the contact of individual planes surfaces is indicated, is shown in this Fig. It is assumed that the element is deformation resistant (compact).

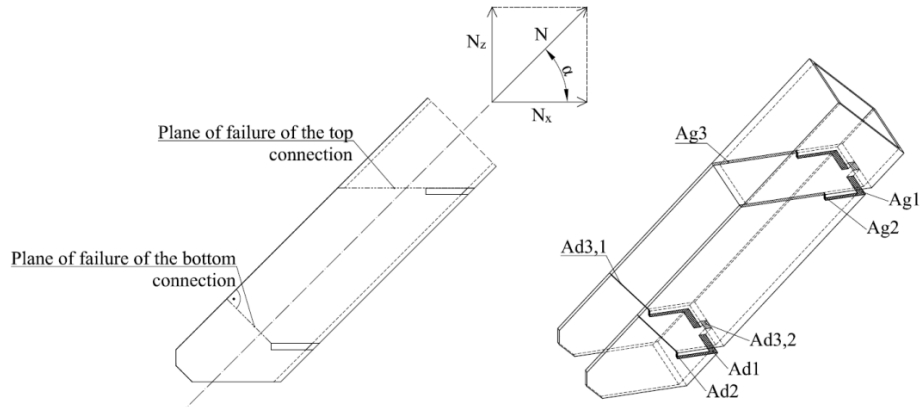


Fig. 4. Tension brace side view and 3D view, where:  $A_{g1}$ ,  $A_{d1}$  – stress area perpendicular to  $N_z$  force,  $A_{g2}$ ,  $A_{d2}$  – stress area perpendicular to  $N_x$  force,  $A_{g3}$  – area of failure of the top connection,  $A_{d3,1}$  – area of failure of the bottom connection (subjected to tension),  $A_{d3,2}$  – area of failure of the bottom connection (subjected to shear and tension)

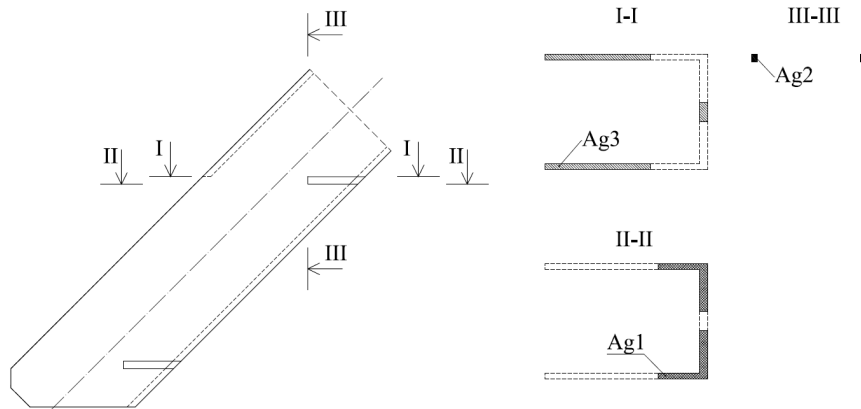


Fig. 5. Tension brace view – top connection

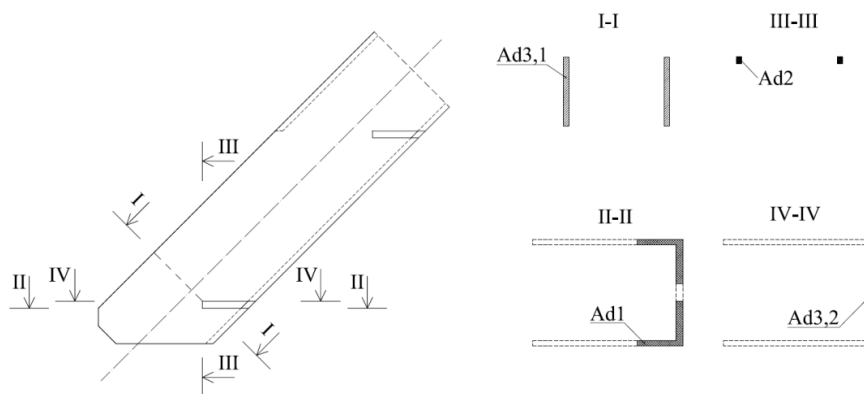


Fig. 6. Tension brace view – bottom connection

## 2.1. Model I – tension brace top connection

### 2.1.1. Resistance of connection („teeth”) to Hertz contact stress

$$f_{dbH} = 3.6 \times f_d \quad (1)$$

where:  $f_{dbH}$  – resistance of connection (Hertz contact stress),  
 $f_d$  – design resistance of steel according to PN-B-90-03200.

So, the force on the stress surface is estimated as

$$N_{z(x),g} = \frac{f_{dbH} \times A_{g1}(A_{g2})}{\gamma} \quad (2)$$

where:  $A_{g1}$  – stress area perpendicular to the direction of  $N_z$  force,  
 $A_{g2}$  – stress area perpendicular to the direction of  $N_x$  force,  
 $\gamma$  – safety factor.

The resistance of the connection is calculated as bellow

$$\frac{N_z(N_x)}{N_{z(x),g}} \leq 1.0 \quad (3)$$

### 2.1.2. Block tearing

Resistance of the connection subjected to shear and tension is equal

$$\frac{N_x}{\frac{1}{\sqrt{3}} \times \frac{f_y \times A_{g3}}{\gamma}} + \frac{N_z}{\frac{f_u \times A_{g3}}{\gamma}} \leq 1.0 \rightarrow N \leq \frac{1}{\frac{\cos \alpha}{\frac{1}{\sqrt{3}} \times \frac{f_y \times A_{g3}}{\gamma}} + \frac{\sin \alpha}{\frac{f_u \times A_{g3}}{\gamma}}} \quad (4)$$

where:  $f_y$  – yield strength of steel,  
 $f_u$  – tensile strength of steel,  
 $\gamma$  – safety factor.

## 2.2. Model II – tension brace bottom connection

### 2.2.1. Resistance of connection („teeth”) to Hertz contact stress

Proceedings is analogous to the procedure in pt. 2.1.1.

### 2.2.2. Block tearing

The condition of resistance of the connection subjected to shear and tension is analogous to the procedure in pt. 2.1.2.

Tensile strength of the connection is calculated as bellow

$$N_{u,Rd} = \frac{A_{d3,1} \times f_u}{\gamma} \quad (5)$$

where:  $A_{d3,1}$  – area of the connection subjected to tension,  
 $f_u$  – tensile strength of steel,  
 $\gamma$  – safety factor.

Condition for the resistance of the connection subject to tension

$$\frac{N}{N_{u,Rd}} \leq 1.0 \rightarrow N \leq N_{u,Rd} \quad (6)$$

So, the total resistance of the bottom connection to block tearing

$$N \leq \frac{1}{\frac{\cos \alpha}{\frac{1}{\sqrt{3}} \times \frac{f_y \times A_{g3}}{\gamma}} + \frac{\sin \alpha}{\frac{f_u \times A_{g3}}{\gamma}}} + \frac{A_{d3,1} \times f_u}{\gamma} \quad (7)$$

where:  $f_y$  – yield strength of steel,  
 $f_u$  – tensile strength of steel,  
 $\gamma$  – safety factor,  
 $\alpha$  – the inclination angle of the tension brace to the horizontal surface

### 2.3. Resistance of the connection

The connection resistance is equal to the sum of the resistance on the top and bottom connection, both on the x and z direction

$$N_{z(x),gd} = N_{z(x),g} + N_{z(x),d} \quad (8)$$

where:  $N_{z(x),g}$  – resistance of top connection,  
 $N_{z(x),d}$  – resistance of bottom connection.

### 2.4. Tension brace resistance [1]

$$N_{pl,Rd} = \frac{A \times f_y}{\gamma_{M0}} \quad (9)$$

where:  $A$  – tension brace cross-section area,  
 $\gamma_{M0}$  – safety factor.

### 3. Resistance calculations

The resistance of connection between the tension brace and the chord was compared with the resistance of the bracing profile RHS in order to assess the efficiency of such connection. The cross-section of the profiles and their properties is presented below. Due to the lack of experimental research and reliable other data, a safety factor was assumed ( $\gamma = 1.0$ ).

Table 1. Data of the considered tension brace

Concept	Geometric dimensions [mm]		Yield strength [MPa]	Design resistance of steel [MPa]	Tensile strength [kN]	$\alpha$ [°]
	b×h	t				
II	60×60	3	355	305	235	45

Results of the theoretical resistance of the components and the tension brace strut are shown in Table 2.

Table 2. Results of resistance of particular components of the tension brace

Resistance condition	Symbol	Resistance [kN]
Block tearing connection	A	198.4
Stress on x direction	B	61.3
Stress on z direction	C	849
Resistance of the tension brace strut	D	235

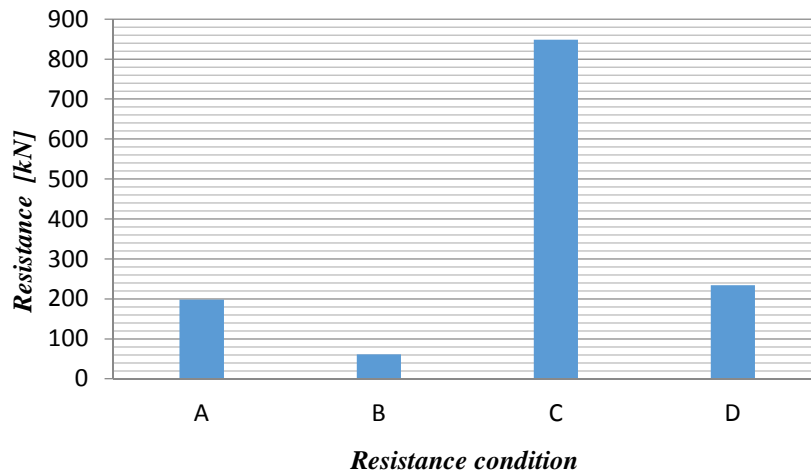


Fig. 7. Diagram of the resistance of the individual components of the tension brace connection

The connection is characterized by a high resistance to stress in the z-direction (C) equal to 849 kN, due to the large contact area to the chord. However, the resistance in the x-direction (B) is only 61.3 kN, due to the small wall thickness of RHS member, what decides about too small contact area. The resistance for block tearing (A) is satisfactory and it is equal to 198.4 kN (sum bottom and top resistance of connection).

#### 4. Summary

Follow the performed above calculations, it can be concluded that:

- it is possible to eliminate the welding of the bracing connections with the chord,
- resistance of the tension brace connection with the chord is highly variable depending on the resistance of the individual components,
- the connection under consideration is characterized by a high resistance to stress in the z-direction, due to the large contact area to the chord. However, the resistance in the x-direction is only 26% of the resistance of the tension brace. Another weak component was the top connection with the chord, where the resistance for block tearing is only 32% of the resistance of the tension brace.

Generally, after carrying out the above analyzes, the authors concluded that presented here connection between the tension brace and the chord does not offer great possibilities to obtain a significant resistance in the x-direction (B), comparable to the resistance of the tension brace. For that much bigger wall thickness of RHS members is needed, which is not necessary for the resistance of chord and branch members.

So, the summarized conclusions from the advantages, and especially the disadvantages of the presented here N-shape connection, leads to a new solution of such joints, characterized by a much higher resistance of the contact stress area. The results of the research of these new innovative connections will be presented in the subsequent works of the authors.

***Acknowledgements:** The author gratefully acknowledges The National Centre for Research and Development (NCBiR) research project N R040008 06, PR/WBiI/1/09/NCBR. Studies were carried out within the framework of statutory research work S/WBiIS/2/2012 at the Bialystok University of Technology, and financed by funds for science provided by the Ministry of Science and Higher Education, Poland.*

#### References

- [1] PN-EN 1993-1-1:2006 Eurocode 3: Design of steel structures – Part 1-1: General rules and rules for buildings.
- [2] Szlendak J.K. RHS trusses and frames completed without welding with branch-chord clock laser made joints, National Centre for Research and Development (NCBiR) research project N R04 0008 06, PR/WBiIS/1/09/NCBR, Poland, 2009.

- 
- [3] Szlendak J.K., Oponowicz P.L. Behaviour of one and double side non-welded T RHS compression truss joints, 7<sup>th</sup> International Conference on Steel & Aluminium Structures, Kuching, Sarawak, Malaysia, 13-15 July 2011.
- [4] Szlendak J.K., Oponowicz P.L. Experimental tests and numerical models of one and double side non-welded T RHS truss joints, 11<sup>th</sup> International Conference "Modern Building Materials, Structures and Technique, Vilnius, 16-17 May 2013.
- [5] Szlendak J.K., Oponowicz P.L. Nośność węzłów kratownicowych typu N z rur prostokątnych w połączeniach bezspoinowych, w formie klucz-zamek. Wydawnictwo Uczelniane Politechniki Lubelskiej, 2013.

*Przesłano do redakcji: 12.04.2018 r.*

*Przyjęto do druku: 15.06.2018 r.*

Jan ZAMOROWSKI<sup>1</sup>  
Grzegorz GREMZA<sup>2</sup>

## ON THE DESIGN OF A STEEL END-PLATE BEAM-TO-COLUMN BOLTED JOINT ACCORDING TO PN-EN 1993-1-8

Considering joints with unstiffened columns, the load capacity of an inner bolt-row being a part of bolts group defined by a flange capacity is directly proportional to a distance between bolts. In turn, a flexibility of the column flange in the inner bolt-row area depends not only on that distance but also on a flexibility of other basic joint components. Hence, that situation may occur, when internal forces in inner bolt-row will be greater than its capacity estimated as an equivalent of T-stub. This possibility has been taken into account in the standard [3] – see the rule in the point 6.2.4.2 (3). In practice, this rule is not implemented in calculations of this kind of joints. In this work, a simplified algorithm of these joints calculation as well as an example, where the need for force reduction in the inner bolt-row to the value of bolt resistance has occurred, were presented. Moreover, the influence of the aforementioned reduction on the joint stiffness was estimated.

**Keywords:** component method, equivalent T-stub, joint capacity and stiffness

### 1. Introduction

In available publications in the field of bolted end-plate beam-to-column joints calculation, e.g. [1], [2], it is recognized that the load capacity of analysed joint is sufficient, if the condition  $M_{j.Ed} < M_{j.Rd}$ , introduced in point 6.2.7(1) of standard [3] is fulfilled, what may result from the general rule contained in the point 6.1.3 (4) of this standard. However, in specific provisions concerning the capacity of an equivalent of T-stub in tension zone – see point 6.2.4.2(3) – additional requirements regarding the values of forces in each bolt-rows and in groups of these rows are introduced.

---

<sup>1</sup> Corresponding author: Jan Zamorowski, University of Bielsko-Biala, Faculty of Materials, Civil and Environmental Engineering, ul. Willowa 2, 43-360 Bielsko-Biała; tel. +48609654098; Zamski@interia.pl

<sup>2</sup> Grzegorz Gremza, Silesian University of Technology in Gliwice, Department of Building Structures, ul. Akademicka 5, 44-100 Gliwice; tel. +48662349538; GGRE@interia.pl

It is required that:

- a) forces transferred by each bolt-row should not exceed the design resistance determined considering only that individual bolt-row, and,
- b) the total force of each bolt-rows group, comprised two or more adjacent bolt-rows within the same bolt-group, should not exceed the design resistance of that group of bolt-rows.

These provisions indicate the necessity of estimation the values of forces in individual bolt rows and groups of rows, in order to compare them with the resistances of these rows and groups of rows. If the forces in some rows or group of rows would be greater than their load capacity, the load capacity of the joint should be reduced.

Such a case may occur in joint of a beam with an unstiffened column (Fig. 1a), when the load capacity of these joint is determined by the resistance of the column flange in tension zone.

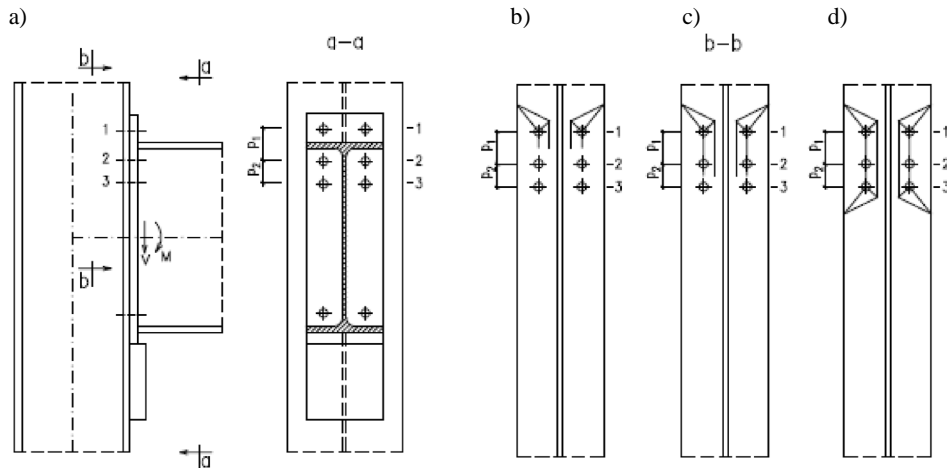


Fig. 1. Joint of a beam with an unstiffened column; a) side view and section a-a, b), c) and d) yield lines of a column flange

According to the standard [3], the model of the destruction of the unstiffened column flange is assumed analogously to the model of equivalent T-stub, considering the individual bolt rows and groups of these rows. Bolt rows are numbered starting from the most distant one from the centre of compression. In case of unstiffened column flange, only one group of bolts with the 1<sup>st</sup> and next rows may occur, while in case of the end plate – two groups, one group above a beam flange and the second one under that flange. Thus, in a column with an unstiffened web, group of rows 1-2, 1-2-3 or 1-2-3-4 may occur, if the fourth row is present, while group 2-3 or 2-3-4 does not occur. However, such groups appear for the modelling of end-plate with one row of bolts placed above a beam flange.

The yield lines for an equivalent of T-stub flange of the column for the non-circular mechanism of failure is presented in Fig. 1d. If a group of bolts,

consisted of rows 1-2 in joint with three rows is considered (see Fig. 1c), the length of the equivalent of T-stub is bigger only by  $(p_1 + p_2)/2$  from the effective length for row 1 of this group. Thus, there is a big difference of the effective length values for bolts in row 1 and 2 from a group of rows (compare Fig. 1b and 1c). Analysis of these lengths indicates that the design resistance capacity of the inner bolt rows of the bolt group is much smaller than design resistance of the end bolt-row and is directly proportional to the effective length of the inner row. In turn, the distribution of forces for individual bolt rows is dependent on the stiffness of all components of the joint - see Fig. 2, on which only the stiffness coefficients relevant to the rotational stiffness of the joint are shown.

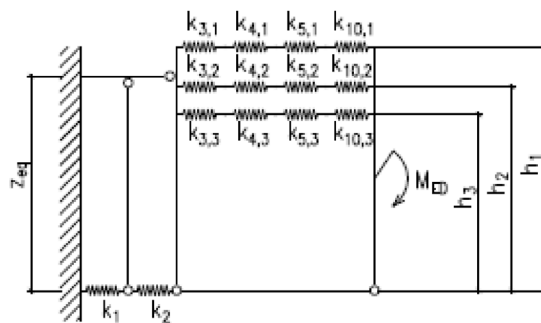


Fig. 2. Component model of joint with marking as in [N1]

For instance, decreasing of the effective length of an unstiffened column flange in bending in the area of row 2 by 50% will also decrease the load capacity of this flange by 50%, but decreasing of the connection stiffness in that area does not exceed a dozen or so percent. This is due to the fact that the flexibility of a joint in the area of the bolt-row 2 is the sum of the flexibility of the joint components: column web in tension, column flange in bending, end-plate in bending, bolts in tension and, in addition, a beam web flexibility in the tensile zone, which was omitted in the algorithm of the stiffness of joints calculation given in standard [3] as a negligible value. It can, therefore, be concluded that when the effective length of the column flange in bending in the area of the inner rows is changed, the redistribution of internal forces in the connection will be different than the variation of the load capacity of these rows, which means that the internal bolts may be overloaded.

The presented analysis indicates that checking the condition of the joint load capacity in accordance with 6.2.7.1(1) in [3]:  $M_{j,Ed} < M_{j,Rd}$  where  $M_{j,Rd}$  – load capacity according to 6.2.7.2 may not be sufficient. So, in order to ensure the load-bearing capacity of individual bolt rows, it is necessary to fulfill the conditions contained in point 6.2.4.2(3) of standards [3].

In the paper, the algorithm for calculating of an end-plate joint between a beam and unstiffened column with three rows of bolts, with an indication of what components should be considered for individual rows of bolts and groups of rows, will be presented. In that algorithm, the requirements listed in point 6.2.4.2 (3)

of standards [3] will be taken into account. This algorithm will be supplemented with a numerical example, in which there will be a need to reduce the load capacity of the joint due to the need to ensure the safety of bolt group 1-2.

The influence of earlier plasticization of the T-stub flange (at lower values of the bending moment in the frame girder) on the rotational stiffness of the joint will also be assessed.

## 2. Algorithm of beam-to-column joint load capacity estimating

Analyzed joint consists of compression zone, shear zone and tension zone. The load-bearing capacity of the tension zone is not greater than the minimum load capacity of the compression and shearing zones. According to [3], in the compression zone are located: column web, web and flange of a frame girder (beam) or flange and web of a haunch, and the shear zone consists of a web of a column. In the tension zone is located: column web, column flange, end-plate with bolts and web of the frame girder. In general, the way of estimation the joint load capacity according to the standard involves determining the minimum design resistance of the joint parts in tension and in shear and then determining the minimum design resistance of each bolt-row as individual as well as a part of a group of them. Next, the sum of obtained design resistances in the rows from 1 to  $r$  is compared with the minimum load capacity of the joint parts in tension zone and in the compression zone. If this sum is greater than the minimum load capacity of the tension zone and compression zone, the load capacity of the row  $r$  is reduced. The second stage is to determine the load capacity of the joint according to the standard formula (6.23) [3]. In the third stage, the values of forces in each bolt rows are determined, e.g. by use of the elastic model as in Fig. 2. Then, the obtained values of forces are compared in individual bolt rows and in bolt-row groups. In the case when the forces in the rows or groups of rows are greater than their design resistances, the calculated load capacity of the joint is proportionally reduced.

Details of the algorithm are given in Table 1.

Table 1. Details of algorithm of beam-to-column joint calculation

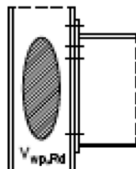
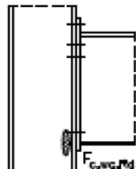
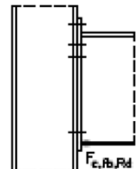
Design resistance of basic components in compression and shear			
	Column web panel in shear	Column web in transverse compression	Beam flange and web in compression
$F_{c,v,min,Rd} =$ $\min \begin{cases} V_{wp,Rd} / \beta \\ F_{c,wc,Rd} \\ F_{c,fb,Rd} \end{cases}$			
	$V_{wp,Rd} / \beta$ acc. 6.2.6.1	$F_{c,wc,Rd}$ acc. 6.2.6.2	$F_{c,fb,Rd}$ acc. 6.2.6.7

Table 1. (cont.) Details of algorithm of beam-to-column joint calculation

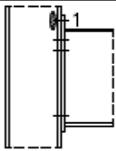
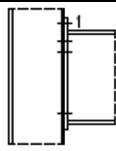
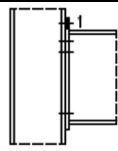
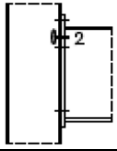
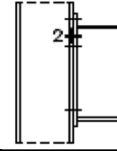
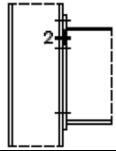
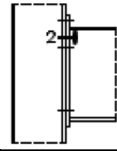
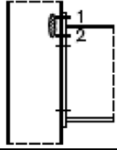
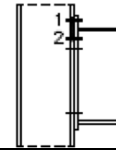
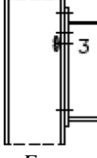
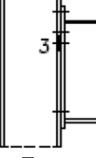
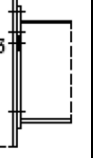
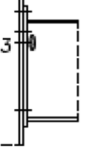
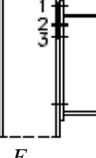
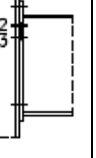
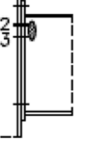
Algorithm of the design resistance of the bolt-row 1 determination				
$F_{t1,Rd} = \min \begin{cases} F_{t1,wc,Rd} \\ F_{t1,fc,Rd} \\ F_{t1,ep,Rd} \end{cases}$ acc. 6.2.7.2(6)	Column web in transverse tension	Column flange in transverse bending	End-plate in bending	
				
	$F_{t1,wc,Rd}$ acc. 6.2.6.3	$F_{t1,fc,Rd}$ acc. 6.2.6.4	$F_{t1,ep,Rd}$ acc. 6.2.6.5	
Limiting the design resistance due to the compression and shear of the joint parts, acc. 6.2.7.2(7)				
$F_{t1,Rd} \leq F_{c,v,min,Rd}$				
Design resistance of individual bolt-row 2				
$F_{t2,Rd,ind} = \min \begin{cases} F_{t2,wc,Rd} \\ F_{t2,fc,Rd} \\ F_{t2,ep,Rd} \\ F_{t2,wb,Rd} \end{cases}$ acc. 6.2.7.2(6)	Column web in transverse tension	Column flange in transverse bending	End-plate in bending	Beam web in tension
				
	$F_{t2,wc,Rd}$ acc. 6.2.6.3	$F_{t2,fc,Rd}$ acc. 6.2.6.4	$F_{t2,ep,Rd}$ acc. 6.2.6.5	$F_{t2,wb,Rd}$ acc. 6.2.6.8
Limiting the design resistance due to compression and shear of the joint parts				
$F_{t2,Rd,ind} \leq F_{c,v,min,Rd} - F_{t1,Rd}$				
Design resistance of row 2 as a part of group of bolt rows 1-2				
$F_{t1-2,Rd} = \min \begin{cases} F_{t1-2,wc,Rd} \\ F_{t1-2,fc,Rd} \end{cases}$	Column web in transverse tension		Column flange in transverse bending	
				
	$F_{t1-2,wc,Rd}$ acc. 6.2.6.3		$F_{t1-2,fc,Rd}$ acc. 6.2.6.4	
Limiting the design resistance of the bolt-row due to design resistance of the group of bolt-rows according to 6.2.7.2(8): $F_{t2,Rd} = \min(F_{t2,Rd,ind}, F_{t2,Rd,group})$ , where $F_{t2,Rd,group} = F_{t1-2,Rd} - F_{t1,Rd}$ .				
If in connections exposed to dynamic actions and vibrations $F_{t1,Rd} > 1.9F_{t2,Rd}$				
then $F_{t2,Rd} \leq F_{t1,Rd} \cdot h_2 / h_1$ - acc. 6.2.7.2 (9) +NA.5.				

Table 1. (cont.) Details of algorithm of beam-to-column joint calculation

Design resistance of individual bolt-row 3				
$F_{t3,Rd,ind}$ $= \min \begin{cases} F_{t3,wc,Rd} \\ F_{t3,fc,Rd} \\ F_{t3,ep,Rd} \\ F_{t3,wb,Rd} \end{cases}$	Column web in transverse tension	Column flange in transverse bending	End-plate in bending	Beam web in tension
	 $F_{t3,wc,Rd}$ acc. 6.2.6.3	 $F_{t3,fc,Rd}$ acc. 6.2.6.4	 $F_{t3,ep,Rd}$ acc. 6.2.6.5	 $F_{t3,wb,Rd}$ acc. 6.2.6.8
Limiting of the bolt-row resistance due to components in bending and shear $F_{t3,Rd} \leq F_{c,v,min,Rd} - (F_{t1,Rd} + F_{t2,Rd})$ - acc. 6.2.7.2(7).				
Design resistance of row 3 as a part of group of rows 1 – 3 and 2 – 3				
$F_{t1-3,Rd} =$ $\min \begin{cases} F_{t1-3,wc,Rd} \\ F_{t1-3,fc,Rd} \end{cases}$ $F_{t2-3,Rd} =$ $\min \begin{cases} F_{t2-3,ep,Rd} \\ F_{t2-3,wb,Rd} \end{cases}$	Column web in transverse tension	Column flange in transverse bending	End-plate in bending	Beam web in tension
	 $F_{t1-3,wc,Rd}$ acc. 6.2.6.3	 $F_{t1-3,fc,Rd}$ acc. 6.2.6.4	 $F_{t2-3,ep,Rd}$ acc. 6.2.6.5	 $F_{t2-3,wb,Rd}$ acc. 6.2.6.8
Limiting of resistance due to resistance of the group of rows – acc. 6.2.7.2(8) $F_{t3,Rd} = \min(F_{t3,Rd,ind}, F_{t3,Rd,group,c}, F_{t3,Rd,group,b})$ , where $F_{t3,Rd,group,c} = F_{t1-3,Rd} - (F_{t1,Rd} + F_{t2,Rd})$ , $F_{t3,Rd,group,b} = F_{t2-3,Rd} - F_{t2,Rd}$ .				
If in connections exposed to dynamic actions and vibrations $F_{t3,Rd} > 1.9F_{tx,Rd}$ , where $x = 1.2$ to $F_{t3,Rd} \leq F_{tx,Rd} \cdot h_3 / h_x$ - acc. 6.2.7.2 (9) +NA.5.				
Design bending resistance $M_{j,Rd}$ acc. to formula (6.25)				
Stiffness coefficients of the joint basic components – acc. to point 6.3.				
Values of forces in each bolt-row ( $N_{i,Ed}$ ) may be calculated e.g. using the model shown in Fig. 2.				
The requirements contained in point 6.2.4.2(3) a), omitted in algorithms: If $N_{i,Ed} > F_{ti,Rd,ind}$ , then $w_i = F_{ti,Rd,ind} / N_{i,Ed}$ for $i = 1, 2, 3$				
The requirements contained in point. 6.2.4.2(3) b), omitted in algorithms If $\sum_{i=1}^r N_{i,Rd} > F_{t1-r,Rd}$ , then $w_{r+2} = F_{t1-r,Rd} / \sum_{i=1}^r N_{i,Rd}$ for $r = 2, 3$ - for group of column flange. If $\sum_{i=2}^3 N_{i,Rd} > F_{t2-3,Rd}$ , then $w_6 = F_{t2-3,Rd} / \sum_{i=2}^3 N_{i,Rd}$ - for end-plate				
If $w_i < 1.0$ , then $w_{min} = \min(w_i)$ for $i = 1$ , by 1, to 6 and $M_{j,Rd,red} = w_{min} \cdot M_{j,Rd}$ .				

### 3. Calculation example

As an example, a joint in frame that was made of S235 steel, with end-plate bolted connection category E between IPE 500 and column HE 300 B with geometrical characteristics as in Fig. 3, was selected.

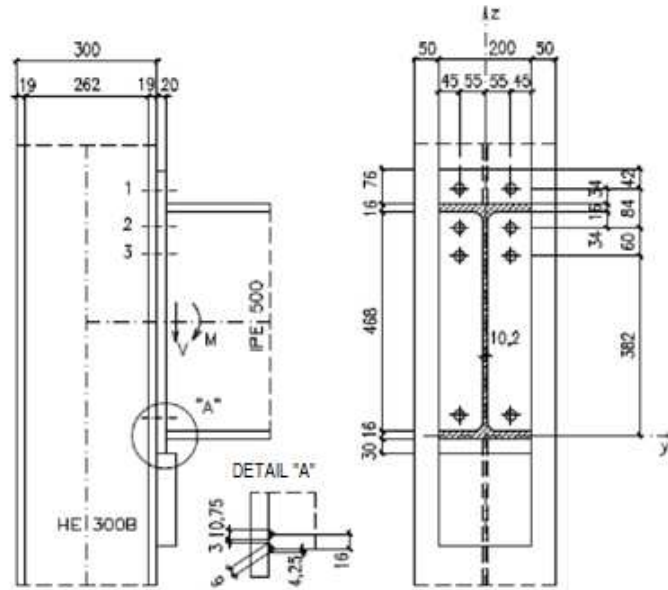


Fig. 3. Analyzed beam-to column joint with bolts M20-10.9

The obtained results of calculations are presented in Table 2.

Table 2. Design resistance of a joint without reduction resulting from the rule in point 6.2.4.2 (3)

Design resistance of joint basic components in compression and in shear			
$F_{c,v,min,Rd} = \min \begin{cases} V_{wp,Rd} / \beta \\ F_{c,wc,Rd} \\ F_{c,fb,Rd} \end{cases}$ $= 579.4 \text{ kN}$	Column web panel in shear	Column web in transverse compression	Beam flange and web in compression
	579.4 kN	588.1 kN	1 068 kN
	$V_{wp,Rd} / \beta$	$F_{c,wc,Rd}$	$F_{c,fb,Rd}$
Algorithm of the design resistance of the bolt-row 1 determination			
$F_{t1,Rd} = \min \begin{cases} F_{t1,wc,Rd} \\ F_{t1,fc,Rd} \\ F_{t1,ep,Rd} \end{cases}$ $= 264.3 \text{ kN}$	Column web in transverse tension	Column flange in transverse bending	End-plate in bending
	411.0 kN	266.5 kN	264.3 kN
	$F_{t1,wc,Rd}$	$F_{t1,fc,Rd}$	$F_{t1,ep,Rd}$
There is no need to limit the resistance due to joint components in bending and shear $F_{t1,Rd} = 264.3 \text{ kN} < F_{c,v,min,Rd} = 579.4 \text{ kN}$			

Table 2. (cont.) Resistance of a joint without reduction resulting from the rule in point 6.2.4.2 (3)

Design resistance of individual bolt-row 2				
$F_{t2,Rd,ind} = \min \begin{cases} F_{t2,wc,Rd} \\ F_{t2,fc,Rd} \\ F_{t2,ep,Rd} \\ F_{t2,wb,Rd} \end{cases}$ $= 266.5 \text{ kN}$	Column web in transverse tension	Column flange in transverse bending	End-plate in bending	Beam web in tension
	411.0 kN	266.5 kN	323.1 kN	624.2 kN
	$F_{t2,wc,Rd}$	$F_{t2,fc,Rd}$	$F_{t2,ep,Rd}$	$F_{t2,wb,Rd}$
There is no need to limit the load capacity due to joint components in bending and shear				
$F_{t2,Rd,ind} = 266.5 \text{ kN} \leq 579.4 - 264.3 = 315.1 \text{ kN}$				
Resistance of row 2 as a part of a the group of rows 1-2				
$F_{t1-2,Rd} = \min \begin{cases} F_{t1-2,wc,Rd} \\ F_{t1-2,fc,Rd} \end{cases}$ $= 348.5 \text{ kN}$	Column web in transverse tension	Column flange in transverse bending		
	506.6 kN	348.5 kN		
	$F_{t1-2,wc,Rd}$	$F_{t1-2,fc,Rd}$		
Limiting of the row resistance due to the resistance of the group of rows:				
$F_{t2,Rd,group} = 348.5 - 264.3 = 84.2 \text{ kN}$ , $F_{t2,Rd} = \min(266.5, 84.2) = 84.2 \text{ kN}$				
Connection is not exposed to dynamic actions and vibrations.				
Design resistance of individual row 3				
$F_{t3,Rd,ind} = \min \begin{cases} F_{t3,wc,Rd} \\ F_{t3,fc,Rd} \\ F_{t3,ep,Rd} \\ F_{t3,wb,Rd} \end{cases}$ $= 266.5 \text{ kN}$	Column web in transverse tension	Column flange in transverse bending	End-plate in bending	Beam web in tension
	411.0 kN	266.5 kN	303.7 kN	537.6 kN
	$F_{t3,wc,Rd}$	$F_{t3,fc,Rd}$	$F_{t3,ep,Rd}$	$F_{t3,wb,Rd}$
Limiting of the resistance due to components in bending and shear:				
$F_{t3,Rd} \leq 579.4 - (264.3 + 84.2) = 230.9 \text{ kN}$ , hence $F_{t3,Rd} = 230.9 \text{ kN}$ .				
Design resistance of row 3 as a part of group 1 – 3 and 2 – 3				
$F_{t1-3,Rd} = \min \begin{cases} F_{t1-3,wc,Rd} \\ F_{t1-3,fc,Rd} \end{cases}$ $= 569.2 \text{ kN}$	Column web in transverse tension	Column flange in transverse bending	End-plate in bending	Beam web in tension
	688.1 kN	569.2	538.0 kN	768.0 kN
$F_{t2-3,Rd} = \min \begin{cases} F_{t2-3,ep,Rd} \\ F_{t2-3,wb,Rd} \end{cases}$ $= 538.0 \text{ kN}$	$F_{t1-3,wc,Rd}$	$F_{t1-3,fc,Rd}$	$F_{t2-3,ep,Rd}$	$F_{t2-3,wb,Rd}$
Limiting of the resistance due to the resistance of group of row – acc. 6.2.7.2(8)				
$F_{t3,Rd,group,c} = 569.2 - (364.3 + 84.2) = 220.7 \text{ kN}$ , $F_{t3,Rd,group,b} = 538.0 - 84.2 = 453.8 \text{ kN}$				
$F_{t3,Rd} = \min(230.9, 220.7, 453.8) = 220.7 \text{ kN}$				
Design resistance of a joint in bending				
$M_{j,Rd} = \sum_r F_{tr,Rd} \cdot h_r = 264.3 \cdot 0.526 + 84.2 \cdot 0.442 + 220.7 \cdot 0.382 = 260.54 \text{ kNm}$				

Table 2. (cont.) Resistance of a joint without reduction resulting from the rule in point 6.2.4.2 (3)

Stiffness coefficient of the basic joint components				
Component	Stiffness coefficient	Bolt-row		
		1	2	3
Column web in transverse tension	$k_3 \cdot 10^3$ [m]	4.620	2,116	4.267
Column flange in transverse bending	$k_4 \cdot 10^3$ [m]	44.683	20.466	41.272
Beam web in tension	$k_5 \cdot 10^3$ [m]	25.129	17.328	13.810
Bolts in tension	$k_{10} \cdot 10^3$ [m]	6.374	6.374	6.374
The effective stiffness coefficient	$k_{eff. r} \cdot 10^3$ [m]	2.296	1.359	2.050
The equivalent lever arm	$z_{eq}$ [m]	0.463		
Column web panel in shear	$k_1 \cdot 10^3$ [m]	3.894		
Column web in compression	$k_2 \cdot 10^3$ [m]	8.655		
Bolt forces calculated according to the model as in Fig. 2 for $M_{Ed} = M_{j,Rd} = 260,5$ kN and design resistances of bolts				
Bolt-rows	Force [kN]	Design resistance [kN]	$w_i$	
1	173.9	264.3		
2	247.7	266.5		
3	155.9	230.9		
1-2	173.9+247.7 = 421.6	348.5	0.827	
1-3	421.6+155.9 = 577.5	569.2	0.986	
2-3	247.7+155.9 = 403.6	538.0		
$w_{min} = 0.827$				
$M_{j,Rd,red} = 0.827 \cdot 260.5 = 215.5$ kNm				

Using the standard formula (6.27) in [3], the effect of the joint load capacity reduction on its stiffness  $S_j$  was evaluated. The stiffness ratio  $\mu$  given in formulas (6.28a) and (6.28b) was taken into account. Obtained results in the form of the  $M - \phi$  relationship, where  $\phi = M/S_j$  is shown in Fig. 4.

After load capacity reduction, a secant stiffness  $S_j$  of analysed joint under load  $M = 2/3 M_{j,Rd}$  is equal to 60% of its stiffness calculated without that reduction.

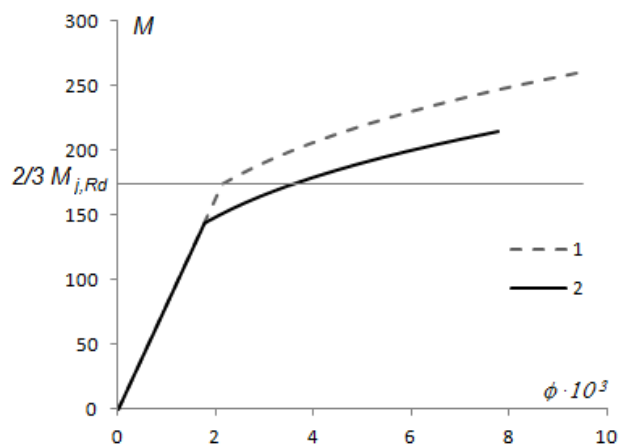


Fig. 4. Relationship  $M - \phi$ : 1 – for  $M_{j,Rd}$ , 2 – for  $M_{j,Rd,red}$

#### 4. Concluding remarks

In this work, the algorithm for calculating of a joint between the beam and unstiffened column with end-plate and three rows of bolts, with an indication on the components for each row of bolts and groups of bolt rows which should be considered, was described. In this regard, many available examples are not in compliance with the requirements contained in [3]. In such a joint, other groups of bolt rows for the column flange than for the end-plate should be considered. According to the standard [3], groups of rows starting from the row most distant from the compression zone are taken into account. Therefore, in a flange of an unstiffened column the groups of rows 1-2, 1-2-3, etc. may occur, whereas in extended end-plate it would be the row of bolt placed above upper flange of a beam and group of rows 2-3. So, in the case of an unstiffened column flange, the group of bolt rows 2-3 cannot be considered. Such a group will occur only in a joint with a stiffened column.

A calculation example of a beam-to-column joint was also presented. It was demonstrated that in joint under the load equal to load capacity  $M_{j,Rd}$  derived from the formula (6.25) in [3] it may happen, that the load capacity of the column flange is exceeded in the area of the group of bolt rows 1-2. For this reason, the reduction of this capacity is necessary as follows from the point 6.2.4.2 (3) in the standard [3].

In the presented example, forces in each bolt rows were estimated on the basis of a linear model using stiffness coefficients adopted in the standard [3]. This way of calculation may be easily applied by a designer. In order to better understanding of the state of forces and deformations in a joint of a beam with an unstiffened column, it would be advisable to make a model of a joint by using the finite element method and to determine the values of these forces using elastic, elastically plastic and plastic models, e.g. as in [4]. These analyses would allow estimating the accuracy of simplified models and their suitability for design purposes.

#### References

- [1] Kozłowski A., Pisarek Z., Wierzbicki S.: Projektowanie doczołowych połączeń śrubowych według PN-EN 1993-1-1 i PN-EN 1993-1-8. Inżynieria i Budownictwo 4/2009, s. 103–204.
- [2] CSI Hellas: Dimensioning of Metallic Connections per EC3. Manual of Analysis and verification examples. Analysis reference and verification. Sparta, Greece 2007.
- [3] PN-EN 1993-1-8: 2006+AC: 2009+Ap1:2010 Eurocode 3: Design of Steel Structures, Part 1.8: Design of joints.
- [4] Butterworth J.: Finite Element Analysis of Structural Steelwork. Beam to Column Bolted Connections. Constructional Research Unit, School of Science & Technology, University of Teesside.

*Przesłano do redakcji: 12.04.2018 r.*

*Przyjęto do druku: 15.06.2018 r.*

Zdzisław PISAREK<sup>1</sup>

## APPROXIMATED METHOD FOR DETERMINING MOMENT RESISTANCE AND STIFFNESS OF BOLTED BEAM TO COLUMN JOINTS MADE WITH ANGLE WEB AND FLANGE CLEATS

Bolted beam to column joints with angle cleats are often used in braced and unbraced steel frame structures. It is related to their simple technology which does not require expensive welding process. Works on the estimation of moment resistance and stiffness of such connections were already carried out in the 1930s. However, the lack of appropriate computational tools forced researchers to introduce simplifications and some assumptions in determining the strength of a joint in a complex load condition. Currently, computing techniques allow for taking into account the actual resistance and stiffness of connections at the stage of global static analysis of the structure. Advanced computer methods as well as applied analytical models allow for a fairly precise determination of the parameters of this type of joints. However, these methods, due to their complexity, are quite time-consuming and labor-intensive, and they are suitable for verification of resistance of the connection or analysis of the structure in the final design phase. The paper presents simplified formulas for calculating the moment resistance and rotational stiffness of the beams to column joints with the use of angle sections connecting both the flanges and the web of the beam. An outline of the component method for determining the moment resistance and stiffness of such connections is also presented. The analysis of the influence of individual components of the joint on its global resistance and stiffness was conducted. The presented formulas, developed on the basis of the component method, preferred by Eurocode 3, can be used in the preliminary determination of the characteristics of the joints, used in the global structure analysis.

**Keywords:** bolted joint with angle web and flange cleats, moment resistance, stiffness, joint characteristics, simplified formula, component method

### 1. Introduction

Bolted beam to column joints with angle cleats (Fig. 1) are often used in steel frame structures. It is related to their simple technology (fast assembly, lack of the expensive welding processes), and the possibility of easy rectification of executive deviations.

---

<sup>1</sup> Corresponding author: Zdzisław Pisarek, Rzeszow University of Technology, The Faculty of Civil and Environmental Engineering and Architecture, ul. Poznańska 2, 35-959 Rzeszów; tel. 178651615; pisarzd@prz.edu.pl

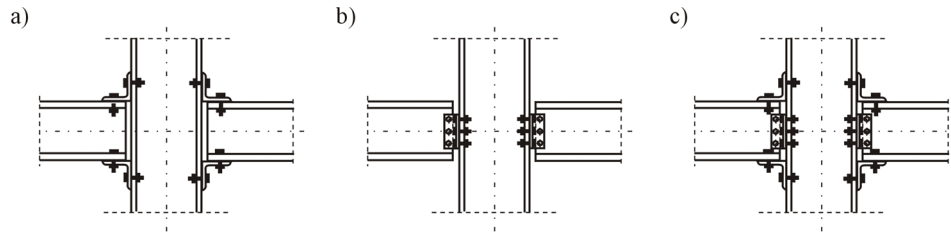


Fig. 1. Angle cleats joint; a) flange angle cleats connection, b) web angle cleats connection, c) flange and web angle cleats connection

Connections of this type are widely used in the USA and Great Britain [1–4] as a natural transition from riveted joints. Angle cleats are also often used to reinforce joints in existing structures, especially in places where welded processes are avoided due to fire reasons. Beam to column joints with using angle cleats connecting the beam web are treated as nominally pinned connections, transferring only shear force from the beam to the column [5]. The bending moment created as a result of the eccentric application of this force, causing twisting angles, due to the small value was neglected. Similarly, in bolted beam to column joints using the web and flange angle cleats, it is assumed that the bending moment carries the angle cleats connecting flanges of the beam, whereas the angle cleat connecting the beam web only transmit shear force.

Experimental tests show that the moment resistance of the joint using angle cleats connecting both the flanges and beam web is greater by several dozen percent in relation to the same joint using only angle cleats connecting only the beam flanges [6] (Fig. 2).

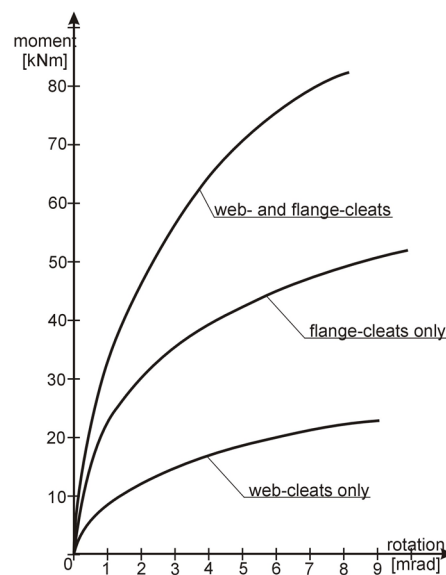


Fig. 2. Moment rotation characteristics for angle cleats joint, based on [6]

## 2. Moment resistance bolted joints with angle web and flange cleats

The analytical model for calculation characteristics of the joints, introduced in [7], is based on the component method. In this method, the whole connection is composed of basic components. Moment resistance of the joint is based on the lowest resistance of the joint components. In the case of a joint using angle flange cleats only, only the compression zone relative to the bottom angle cleat, the shear zone relating to the column web panel and the tension zone relating to the upper beam angle cleat are distinguished [8]. In the case of connection using angle cleats connecting the flanges and web of the beam, the bolt rows joining the beam web are considered as successive bolt rows in the tensile zone [9]. In addition, some basic components are considered for the individual bolt row and as part of the group of the bolt rows. The list of basic components for individual bolt row is shown in figures 3 and 4.

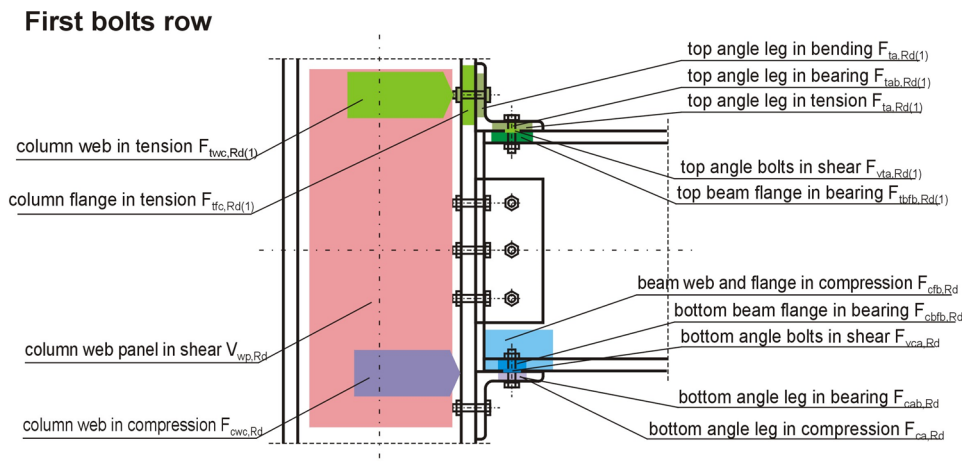
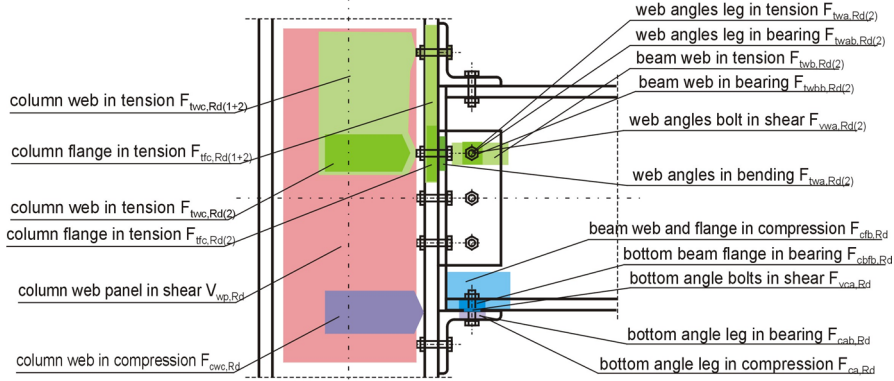


Fig. 3. The basic components of the joint refer to the first bolt row (bolts connecting the column flange with the top angle)

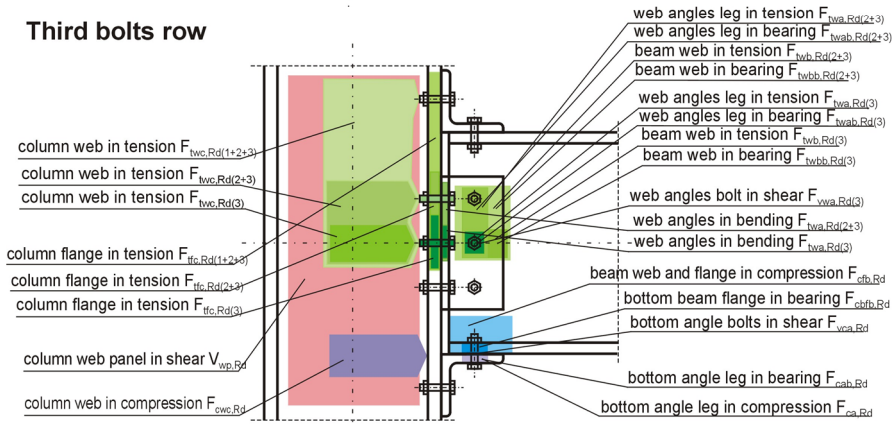
The design resistance of most components can be calculated according to the principles presented in Eurocode [7]. Only, due to the dependence of the collapse mechanism of the web angle cleats from its height, the strength of the angle web cleats in bending are not directly presented in the Standard.

Angle flange cleats in bending can be treated as single T-stubs (Fig. 5). The T-stub should be considered for each individual bolt row as well as for the group of bolt rows. In each case, three possible types of failure are considered.

**Second bolts row**



**Third bolts row**



**Fourth bolts row**

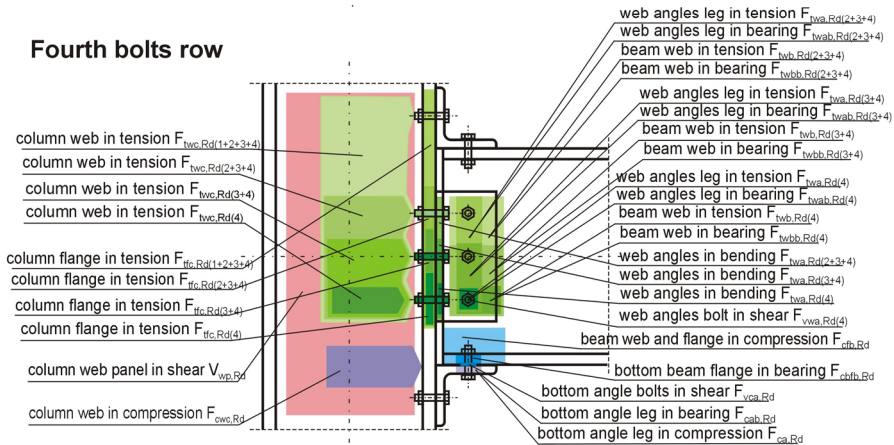


Fig. 4. The basic components of the joint refer to the second, third and fourth bolt row (bolts connecting the column flange with the angle web cleats)

With reference to the equivalent T-stub failing with complete yielding mode, the resistance of the single bolt row correspondingly assumes that the resistance of a couple web angles is equivalent, for each bolt row with the parameter  $m'_i$  (Fig. 5) [9].

$$m'_i = \frac{3}{2} \frac{t_{wa}}{\left[ \left( \frac{m_{max} \cdot h_i}{t_{wa} \cdot l_{wa}} \right)^2 + 3 \right]^{\frac{1}{2}} - \frac{m_{max} \cdot h_i}{t_{wa} \cdot l_{wa}}} \quad (1)$$

where:  $t_{wa}$  – thickness of legs of the angle web cleats,  
 $m_{max}$  – maximum distance between angle leg and bolt axis,  
 $l_{wa}$  – height of angle web cleats,  
 $h_i$  – lever arm i-bolt row.

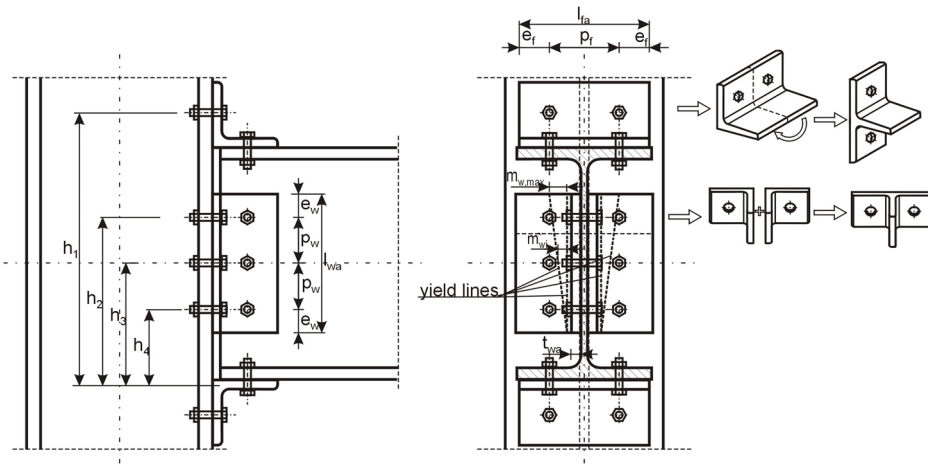


Fig. 5. Method of determining the parameters of the T-stub of the angle web cleats

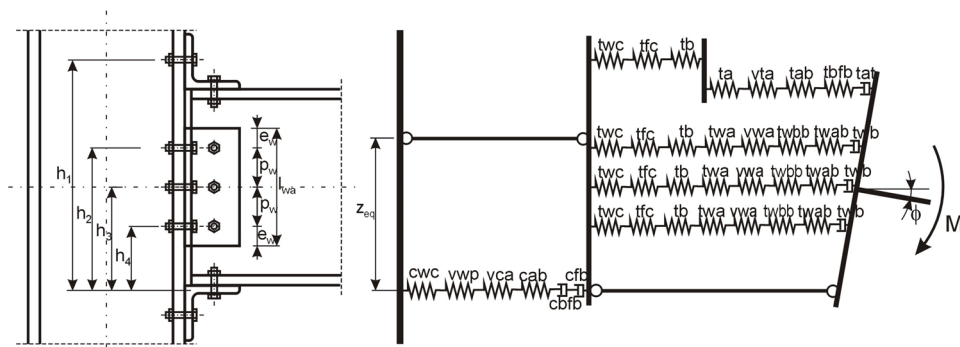


Fig. 6. Mechanical model for evaluating initial stiffness of joint with flange and web angle cleats

The initial stiffness of the joint is calculated on the basis of the mechanical model. This procedure is able to account for all sources of deformations, including the angle cleats, bolts, beam and column components. Mechanical model to determine the initial stiffness of the joint with angle web and flange cleats is presented in figure 6.

### 3. Worked example

For the performance of the procedure, was presented a worked example. This example illustrated beam to column joint with use angle web and flange cleats (Fig. 7).

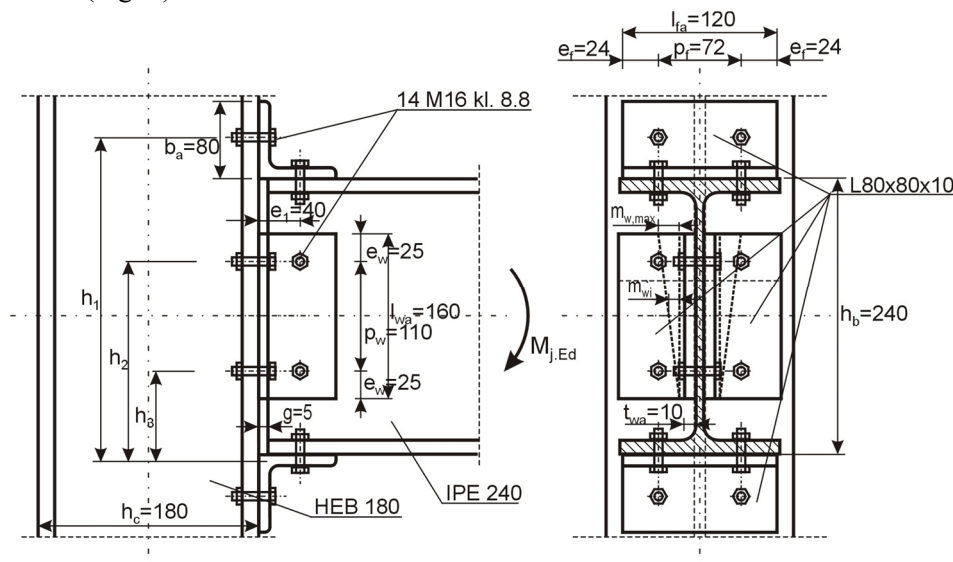


Fig. 7. Geometrical details of joint for calculation example

Basic data:

Steel grade S275  $f_y = 275 \text{ N/mm}^2$ ,  $f_u = 430 \text{ N/mm}^2$ ,  $\varepsilon = 0,92$

Beam IPE 240:  $W_{y,pl} = 367 \cdot 10^3 \text{ mm}^3$ ,  $A_b = 39,1 \cdot 10^2 \text{ mm}^2$ ,  
 $h_b = 240 \text{ mm}$ ,  $b_b = 120 \text{ mm}$ ,  $t_{fb} = 9,8 \text{ mm}$ ,  
 $t_{wb} = 6,2 \text{ mm}$ ,  $r_b = 15 \text{ mm}$ .

Column HEB 180:  $W_{y,pl} = 481,4 \cdot 10^3 \text{ mm}^3$ ,  $A_c = 65,3 \cdot 10^2 \text{ mm}^2$ ,  
 $h_c = 180 \text{ mm}$ ,  $b_c = 180 \text{ mm}$ ,  $t_{fc} = 14,0 \text{ mm}$ ,  
 $t_{wc} = 8,5 \text{ mm}$ ,  $r_c = 15 \text{ mm}$ .

Angle cleats L80x80x10:  $b_a = 80 \text{ mm}$ ,  $t_a = 10 \text{ mm}$ ,  $r_a = 10,0 \text{ mm}$ .

Bolts M16 class 8.8:  $A_{v,b} = 201 \text{ mm}^2$ ,  $A_{s,b} = 157 \text{ mm}^2$ .

Beam and column sections are in class 1.

**Design moment resistance of the joint.**

## • Column web panel in shear

For single-sided joint, the design plastic shear resistance of unstiffened column web is obtained from:

$$V_{wp,Rd} = \frac{0,9 \cdot f_{y,wc} \cdot A_{vc}}{\sqrt{3} \cdot \gamma_{M0}} = \frac{0,9 \cdot 275 \cdot 2029}{\sqrt{3} \cdot 1,0} = 289932 N = 289,9 kN \quad (2)$$

where

$$A_{vc} = A_c - 2 \cdot b_c \cdot t_{fc} + (t_{wc} + 2 \cdot r_c) \cdot t_{fc} = 65,3 \cdot 10^2 - 2 \cdot 180 \cdot 14,0 + (8,5 + 2 \cdot 15) \cdot 14,0 = 2029 \text{ mm}^2 \quad (3)$$

## • Column web panel in compression

$$F_{cwc,Rd} = \frac{\omega \cdot k_{wc} \cdot b_{eff,c,wc} \cdot t_{wc} \cdot f_{ywc}}{\gamma_{M0}} \text{ and } F_{cwc,Rd} \leq \frac{\omega \cdot k_{wc} \cdot \rho \cdot b_{eff,c,wc} \cdot t_{wc} \cdot f_{ywc}}{\gamma_{M0}} \quad (4)$$

effective width of column web in compression:

$$b_{eff,c,wc} = 2 \cdot t_a + 0,6 \cdot r_a + 5 \cdot (t_{fc} + s) = 2 \cdot 10,0 + 0,6 \cdot 10,0 + 5 \cdot (14,0 + 15,0) = 171 \text{ mm} \quad (5)$$

Transformation parameter, for single-sided joint is equal  $\beta = 1,0$ , and reduction factor for  $\beta = 1,0$  is  $\omega = \omega_1$

$$\omega_1 = \frac{1}{\sqrt{1 + 1,3 \cdot \left(\frac{b_{eff,c,wc} \cdot t_{wc}}{A_{vc}}\right)^2}} = \frac{1}{\sqrt{1 + 1,3 \cdot \left(\frac{171 \cdot 8,5}{2029}\right)^2}} = 0,774 \quad (6)$$

If the maximum longitudinal compressive stress in column  $\sigma_{com,Ed}$  not exceed  $0,7 \cdot f_{y,wd}$ , then reduction factor  $k_{wc}$  can be adopted as 1, then:

$$F_{cwc,Rd} = \frac{0,774 \cdot 1,0 \cdot 171 \cdot 8,5 \cdot 275}{1,0} = 309377 N = 309,4 kN \quad (7)$$

The reduction factor for web panel buckling  $\rho$ , is depending on the web slenderness:

$$\bar{\lambda}_p = 0,932 \cdot \sqrt{\frac{b_{eff,c,wc} \cdot d_{wc} \cdot f_{ywc}}{E \cdot t_{wc}^2}} = 0,932 \cdot \sqrt{\frac{171 \cdot 122 \cdot 275}{210 \cdot 10^3 \cdot 8,5^2}} = 0,573 \quad (8)$$

where:

$$d_{wc} = h_c - 2 \cdot (t_{fc} + r_c) = 180 - 2 \cdot (14,0 + 15,0) = 122 \text{ mm} \quad (9)$$

if  $\bar{\lambda}_p \leq 0,72$  then  $\rho = 1$ , and finally:  $F_{cwc,Rd} = 309,4 kN$

- Beam flange and web in compression

$$F_{cfb,Rd} = \frac{M_{b,Rd}}{h_b - t_{fb}} = \frac{100,9 \cdot 10^6}{240 - 9,8} = 438423 \text{ N} = 438,4 \text{ kN} \quad (10)$$

$$\text{with } M_{b,Rd} = M_{pl,Rd} = \frac{W_{y,pl} \cdot f_y}{\gamma_{M0}} = \frac{367 \cdot 10^3 \cdot 275}{1,0} = 100,9 \cdot 10^6 \text{ Nmm}$$

- Bottom angle leg in compression

$$F_{ca,Rd} = \frac{l_{fa} \cdot t_{fa} \cdot f_{ya}}{\gamma_{M0}} \text{ and } F_{ca,Rd} \leq \frac{\rho \cdot l_{fa} \cdot t_{fa} \cdot f_{ya}}{\gamma_{M0}} \quad (11)$$

The reduction factor for angle leg buckling  $\rho$ , is depending on the slenderness:

$$\bar{\lambda}_p = 0,932 \cdot \sqrt{\frac{l_{fa} \cdot b_a \cdot f_{ya}}{E \cdot t_{fa}^2}} = 0,932 \cdot \sqrt{\frac{120 \cdot 80 \cdot 275}{210 \cdot 10^3 \cdot 10^2}} = 0,330 \quad (12)$$

if  $\bar{\lambda}_p \leq 0,72$  then  $\rho = 1$ , and:

$$F_{ca,Rd} = \frac{120 \cdot 10,0 \cdot 275}{1,0} = 330000 \text{ N} = 330,0 \text{ kN} \quad (13)$$

- Bolts in bottom angle leg in bearing

$$F_{cab,Rd} = 2 \cdot \frac{k_1 \cdot \alpha_b \cdot f_u \cdot d \cdot t_{fa}}{\gamma_{M2}} = 2 \cdot \frac{2,03 \cdot 0,741 \cdot 430 \cdot 16 \cdot 10,0}{1,25} = 165586 \text{ N} = 165,6 \text{ kN} \quad (14)$$

$$\text{where } k_1 = \min \left\{ \begin{array}{l} 2,8 \cdot \frac{e_f}{d_0} - 1,7 = 2,8 \cdot \frac{24}{18} - 1,7 = 2,03 \\ 2,5 \end{array} \right. = 2,03$$

$$\alpha_b = \min \left\{ \begin{array}{l} \alpha_d = \frac{e_f}{3 \cdot d_0} = \frac{40}{3 \cdot 18} = 0,741 \\ \frac{f_{ub}}{f_{ua}} = \frac{800}{430} = 1,86 \\ 1,0 \end{array} \right. = 0,741$$

- Bolts in bottom beam flange in bearing

$$F_{cbfb,Rd} = 2 \cdot \frac{k_1 \cdot \alpha_b \cdot f_u \cdot d \cdot t_{fb}}{\gamma_{M2}} = 2 \cdot \frac{2,03 \cdot 1,0 \cdot 430 \cdot 16 \cdot 9,8}{1,25} = 218993 \text{ N} = 219,0 \text{ kN} \quad (15)$$

$$\text{where } k_1 = \min \left\{ \begin{array}{l} 2,8 \cdot \frac{e_f}{d_0} - 1,7 = 2,8 \cdot \frac{24}{18} - 1,7 = 2,03 \\ 2,5 \end{array} \right. = 2,03$$

$$\alpha_b = \min \left\{ \begin{array}{l} \alpha_d = \frac{e}{3 \cdot d_0} = \frac{\infty}{3 \cdot 18} = \infty \\ \frac{f_{ub}}{f_{ua}} = \frac{800}{430} = 1,86 \\ 1,0 \end{array} \right. = 1,0$$

- Bolts in shear

Shear plane passes through the unthreaded portion of the bolt

$$F_{vca,Rd} = 2 \cdot \frac{\alpha_v \cdot f_{ub} \cdot A_{v,b}}{\gamma_{M2}} = 2 \cdot \frac{0,6 \cdot 800 \cdot 201}{1,25} = 154368 \text{ N} = 154,4 \text{ kN} \quad (16)$$

- Column flange in bending

Tension resistance of the bolt:

$$F_{t,Rd} = \min \left\{ \begin{array}{l} F_{t,Rd} = \frac{0,9 \cdot f_{ub} \cdot A_{s,b}}{\gamma_{M2}} = \frac{0,9 \cdot 800 \cdot 157}{1,25} = 90432 \\ B_{p,Rd} = \frac{0,6 \cdot \pi \cdot d_m \cdot t_a \cdot f_u}{\gamma_{M2}} = \frac{0,6 \cdot \pi \cdot 24 \cdot 10,0 \cdot 430}{1,25} = 155622 \end{array} \right. = 90432 \text{ N} = 90,4 \text{ kN} \quad (17)$$

$$\text{Parameter } m = \frac{(p_f - t_{wc} - 2 \cdot 0,8 \cdot r_c)}{2} = \frac{(72 - 8,5 - 2 \cdot 0,8 \cdot 15)}{2} = 19,75 \text{ mm, and}$$

$$e = \frac{b_c - p_f}{2} = \frac{180 - 72}{2} = 54 \text{ mm, but } e \leq 1,25 \cdot m = 1,25 \cdot 19,75 = 24,7 \text{ mm}$$

Effective length of equivalent T-stub:

$$\text{- Circular patterns: } l_{eff,cp} = 2 \cdot \pi \cdot m = 2 \cdot \pi \cdot 19,75 = 124 \text{ mm}$$

$$\text{- Non - circular patterns: } l_{eff,nc} = 4 \cdot m + 1,25 \cdot e = 4 \cdot 19,75 + 1,25 \cdot 24,7 = 109,9 \text{ mm,}$$

$$M_{pl,Rd} = \frac{0,25 \cdot l_{eff,nc} \cdot t_{fc}^2 \cdot f_y}{\gamma_{M0}} = \frac{0,25 \cdot 109,9 \cdot 14,0^2 \cdot 275}{1,0} = 1480902 \text{ Nmm}$$

The resistance of the column flange in bending is taken as minimum values from three modes of failure.

$$F_{tfc,Rd} = \min \left\{ \begin{array}{l} \frac{4 \cdot M_{pl,Rd}}{m} = \frac{4 \cdot 1480902}{19,75} = 299930 \\ \frac{2 \cdot M_{pl,Rd} + n \cdot \sum F_{t,Rd}}{m+n} = \frac{2 \cdot 1480902 + 24,7 \cdot 2 \cdot 90432}{19,75 + 24,7} = 167135 \\ \sum F_{t,Rd} = 2 \cdot 90432 = 180864 \end{array} \right. = 167,1 \text{ kN} \quad (18)$$

- Column web panel in tension

$$F_{twc,Rd} = \frac{\omega \cdot b_{eff,t,wc} \cdot t_{wc} \cdot f_{ywc}}{\gamma_{M0}} = \frac{0,774 \cdot 109,9 \cdot 8,5 \cdot 275}{1,0} = 198834 \text{ N} = 198,8 \text{ kN} \quad (19)$$

- Bolts in top angle leg in bearing

$$F_{tab,Rd} = 2 \cdot \frac{k_1 \cdot \alpha_b \cdot f_u \cdot d \cdot t_{fa}}{\gamma_{M2}} = 2 \cdot \frac{2,03 \cdot 0,741 \cdot 430 \cdot 16 \cdot 10,0}{1,25} = 165586 \text{ N} = 165,6 \text{ kN} \quad (20)$$

$$\text{where } \alpha_b = \min \begin{cases} \alpha_d = \frac{e_2}{3 \cdot d_0} = \frac{40}{3 \cdot 18} = 0,741 \\ \frac{f_{ub}}{f_{ua}} = \frac{800}{430} = 1,86 \\ 1,0 \end{cases} = 0,741$$

- Bolts in top beam flange in bearing

$$F_{tbf,Rd} = 2 \cdot \frac{k_1 \cdot \alpha_b \cdot f_u \cdot d \cdot t_{fb}}{\gamma_{M2}} = 2 \cdot \frac{2,03 \cdot 0,648 \cdot 430 \cdot 16 \cdot 9,8}{1,25} = 141908 \text{ N} = 141,9 \text{ kN} \quad (21)$$

$$\text{where } \alpha_b = \min \begin{cases} \alpha_d = \frac{e_f - g}{3 \cdot d_0} = \frac{40 - 5}{3 \cdot 18} = 0,648 \\ \frac{f_{ub}}{f_{ua}} = \frac{800}{430} = 1,86 \\ 1,0 \end{cases} = 0,648$$

- Bolts in shear

Shear resistance of the bolts in top flange is the same as in the bottom flange:

$$F_{vta,Rd} = F_{vca,Rd} = 154,4 \text{ kN}$$

- Angle cleat in bending

The effective length of the angle flange cleats is taken as half of width of the cleats, then  $l_{eff} = 60 \text{ mm}$ , value  $m$  for large gap  $m = e_1 - 0,5 \cdot t_a = 40 - 0,5 \cdot 10,0 = 35 \text{ mm}$ , and  $e = 40 \text{ mm}$

$$M_{pl,Rd} = \frac{0,25 \cdot l_{eff} \cdot t_a^2 \cdot f_y}{\gamma_{M0}} = \frac{0,25 \cdot 60 \cdot 10,0^2 \cdot 275}{1,0} = 412500 \text{ Nmm}$$

$$F_{ta,Rd} = \min \begin{cases} \frac{4 \cdot M_{pl,Rd}}{m} = \frac{4 \cdot 412500}{35} = 47142 \\ \frac{2 \cdot M_{pl,Rd} + n \cdot \sum F_{t,Rd}}{m+n} = \frac{2 \cdot 412500 + 40 \cdot 2 \cdot 90432}{35+40} = 107461 \\ \sum F_{t,Rd} = 2 \cdot 90432 = 180864 \end{cases} = 47,1 \text{ kN} \quad (22)$$

- Angle cleat in tension

$$F_{ta,Rd} = \min \begin{cases} \frac{l_{fa} \cdot t_a \cdot f_{ya}}{\gamma_{M0}} = \frac{120 \cdot 10,0 \cdot 275}{1,0} = 330000 \\ \frac{(l_{fa} - 2 \cdot d_0) \cdot t_a \cdot f_{ua}}{\gamma_{M2}} = \frac{(120 - 2 \cdot 18) \cdot 10,0 \cdot 430}{1,1} = 328364 \end{cases} = 328,4 \text{ kN} \quad (23)$$

Finally, the design resistance of the first bolt row:

$$F_{1,Rd} = \min(V_{wp,Rd}, F_{cwc,Rd}, F_{cfb,Rd}, F_{ca,Rd}, F_{cab,Rd}, F_{cbfb,Rd}, F_{vca,Rd}, F_{tfc,Rd}, F_{twc,Rd}, F_{tab,Rd}, F_{tbf,Rd}, F_{vta,Rd}, F_{ta,Rd}, F_{ta,Rd})$$

$$F_{1,Rd} = \min(289,9; 309,4; 438,4; 330,0; 165,6; 219,0; 154,4; 167,1; 198,8; 165,6; 141,9; 154,4; 47,1; 328,4) = 47,1 \text{ kN}$$

Second bolt row:

- Column flange in bending for first and second bolt rows

Effective length of equivalent T-stub:

- Circular patterns:

$$l_{eff,cp} = 2 \cdot \pi \cdot m + 2 \cdot p_1 = 2 \cdot \pi \cdot 19,75 + 2 \cdot 105 = 334 \text{ mm}$$

- Non – circular patterns:

$$l_{eff,nc} = 4 \cdot m + 1,25 \cdot e + p_1 = 4 \cdot 19,75 + 1,25 \cdot 24,7 + 105 = 214,9 \text{ mm}$$

$$\text{where } p_1 = \frac{h_b}{2} + e_1 - \frac{p_w}{2} = \frac{240}{2} + 40 - \frac{110}{2} = 105 \text{ mm}$$

$$M_{pl,Rd} = \frac{0,25 \cdot l_{eff,nc} \cdot t_{fc}^2 \cdot f_y}{\gamma_{M0}} = \frac{0,25 \cdot 214,9 \cdot 14,0^2 \cdot 275}{1,0} = 2895778 \text{ Nmm}$$

The resistance of the column flange in bending is taken as minimum values from three modes of failure.

$$F_{tfc(1+2),Rd} = \min \left\{ \begin{array}{l} \frac{4 \cdot M_{pl,Rd}}{m} = \frac{4 \cdot 2895778}{19,75} = 586487 \\ \frac{2 \cdot M_{pl,Rd} + n \cdot \sum F_{t,Rd}}{m+n} = \frac{2 \cdot 2895778 + 24,7 \cdot 4 \cdot 90432}{19,75 + 24,7} = 331299 = \\ \sum F_{t,Rd} = 4 \cdot 90432 = 361728 \end{array} \right. = 331,3 \text{ kN} \quad (24)$$

- Column web panel in tension

$$F_{twc(1+2),Rd} = \frac{\omega \cdot b_{eff,t,wc} \cdot t_{wc} \cdot f_{ywc}}{\gamma_{M0}} = \frac{0,774 \cdot 214,9 \cdot 8,5 \cdot 275}{1,0} = 388802 \text{ N} = 388,8 \text{ kN} \quad (25)$$

- Bolts in web angle leg in bearing

$$F_{twab,Rd} = \frac{k_1 \cdot \alpha_b \cdot f_u \cdot d \cdot 2 \cdot t_{fa}}{\gamma_{M2}} = \frac{2,19 \cdot 0,741 \cdot 430 \cdot 16 \cdot 2 \cdot 10,0}{1,25} = 178637 \text{ N} = 178,6 \text{ kN} \quad (26)$$

$$\text{where } k_1 = \min \left\{ \begin{array}{l} 2,8 \cdot \frac{e_w}{d_0} - 1,7 = 2,8 \cdot \frac{25}{18} - 1,7 = 2,19 \\ 2,5 \end{array} \right. = 2,19$$

$$\alpha_b = \min \left\{ \begin{array}{l} \alpha_d = \frac{e_2}{3 \cdot d_0} = \frac{40}{3 \cdot 18} = 0,741 \\ \frac{f_{ub}}{f_{ua}} = \frac{800}{430} = 1,86 \\ 1,0 \end{array} \right. = 0,741$$

- Bolts in beam web in bearing

$$F_{twbb,Rd} = \frac{k_1 \cdot \alpha_b \cdot f_u \cdot d \cdot t_{wb}}{\gamma_{M2}} = \frac{2,5 \cdot 0,648 \cdot 430 \cdot 16 \cdot 6,2}{1,25} = 55282 \text{ N} = 55,3 \text{ kN} \quad (27)$$

$$\text{where } k_1 = \min \left\{ \begin{array}{l} 2,8 \cdot \frac{h_b - p_w}{2 \cdot d_0} - 1,7 = 2,8 \cdot \frac{240 - 110}{2 \cdot 18} - 1,7 = 8,4 \\ 2,5 \end{array} \right. = 2,5$$

$$\alpha_b = \min \left\{ \begin{array}{l} \alpha_d = \frac{e_1 - g}{3 \cdot d_0} = \frac{40 - 5}{3 \cdot 18} = 0,648 \\ \frac{f_{ub}}{f_{ua}} = \frac{800}{430} = 1,86 \\ 1,0 \end{array} \right. = 0,648$$

- Bolts in shear.

Shear resistance of the bolt in web is the same as in the flange:

$$F_{vwa,Rd} = F_{vca,Rd} = 154,4 \text{ kN}$$

- Angle cleat in bending

Value of  $m$  for large gap  $m_{w,max} = e_1 - 0,5 \cdot t_a = 40 - 0,5 \cdot 10,0 = 35 \text{ mm}$ , and  $e = 40 \text{ mm}$ .

$$m_2 = \frac{3}{2} \frac{t_{wa}}{\left[ \left( \frac{m_{max} \cdot h_2}{t_{wa} \cdot t_{wa}} \right)^2 + 3 \right]^{\frac{1}{2}} - \frac{m_{max} \cdot h_2}{t_{wa} \cdot t_{wa}}} = \frac{3}{2} \frac{10,0}{\left[ \left( \frac{35,0 \cdot 180}{10,0 \cdot 160} \right)^2 + 3 \right]^{\frac{1}{2}} - \frac{35,0 \cdot 180}{10,0 \cdot 160}} = 9,57 \text{ mm} \quad (28)$$

$$\text{where } h_2 = \frac{(h_b + p_w + t_a)}{2} = \frac{(240 + 110 + 10,0)}{2} = 180 \text{ mm}$$

Effective length of equivalent T-stub:

- Circular patterns:

$$l_{eff,cp} = \min \left\{ \begin{array}{l} 2 \cdot \pi \cdot m_2 = 2 \cdot \pi \cdot 9,57 = 60,1 \\ \pi \cdot m_2 + 2 \cdot e_w = \pi \cdot 9,57 + 2 \cdot 25 = 80,0 \end{array} \right. = 60,1 \text{ mm}$$

- Non – circular patterns:

$$l_{eff,nc} = \min \left\{ \begin{array}{l} 4 \cdot m_2 + 1,25 \cdot e = 4 \cdot 9,57 + 1,25 \cdot 12,0 = 53,3 \\ 2 \cdot m_2 + 0,625 \cdot e + e_w = 2 \cdot 9,57 + 0,625 \cdot 12,0 + 25 = 51,6 \end{array} \right. = 51,6 \text{ mm}$$

$$M_{pl,Rd} = \frac{0,25 \cdot l_{eff} \cdot t_a^2 \cdot f_y}{\gamma_{M0}} = \frac{0,25 \cdot 51,6 \cdot 10,0^2 \cdot 275}{1,0} = 354750 \text{ Nmm}$$

$$F_{twa,Rd} = \min \left\{ \begin{array}{l} \frac{4 \cdot M_{pl,Rd}}{m_2} = \frac{4 \cdot 354750}{9,57} = 148276 \\ \frac{2 \cdot M_{pl,Rd} + n \cdot \sum F_{t,Rd}}{m+n} = \frac{2 \cdot 354750 + 12,0 \cdot 2 \cdot 90432}{9,57 + 12,0} = 133513 = \\ \sum F_{t,Rd} = 2 \cdot 90432 = 180864 \end{array} \right. = 133,5 \text{ kN} \quad (29)$$

- Angle web cleats in tension

$$F_{twa,Rd} = \frac{l_{eff} \cdot 2 \cdot t_a \cdot f_{ya}}{\gamma_{M0}} = \frac{51,6 \cdot 2 \cdot 10,0 \cdot 275}{1,0} = 283800 \text{ N} = 283,8 \text{ kN} \quad (30)$$

- Beam web in tension

$$F_{twb,Rd} = \frac{l_{eff} \cdot t_{wb} \cdot f_{yb}}{\gamma_{M0}} = \frac{51,6 \cdot 6,2 \cdot 275}{1,0} = 87978 \text{ N} = 88,0 \text{ kN} \quad (31)$$

Finally, the design resistance of the second bolt row:

$$F_{2,Rd} = \min (V_{wp,Rd} \cdot F_{1,Rd}; F_{cwc,Rd} \cdot F_{1,Rd}; F_{cfb,Rd} \cdot F_{1,Rd}; F_{ca,Rd} \cdot F_{1,Rd}; F_{cab,Rd} \cdot F_{1,Rd}; \\ F_{cbfb,Rd} \cdot F_{1,Rd}; F_{vca,Rd} \cdot F_{1,Rd}; F_{tfc,Rd}; F_{tfc,Rd(1+2)} \cdot F_{1,Rd}; F_{twc,Rd}; F_{twc,Rd(1+2)} \cdot F_{1,Rd}; \\ F_{twab,Rd}; F_{twbb,Rd}; F_{twa,Rd}; F_{twb,Rd}; F_{twa,Rd}; F_{vwa,Rd})$$

$$F_{1,Rd} = \min (289,9-47,1; 309,4-47,1; 438,4-47,1; 330,0-47,1; 165,6-47,1; \\ 219,0-47,1; 154,4-47,1; 167,1; 331,3-47,1; 198,8; 388,8-47,1; 178,6; \\ 55,3; 133,5; 88,0; 283,8; 154,4) = 55,3 \text{ kN}$$

Third bolt row:

- Column flange in bending for first, second and third bolt rows

Effective length of equivalent T-stub:

- Circular patterns:

$$l_{eff,cp} = 2 \cdot \pi \cdot m + 2 \cdot (p_1 + p_w) = 2 \cdot \pi \cdot 19,75 + 2 \cdot (105 + 110) = 554 \text{ mm}$$

- Non – circular patterns:

$$l_{eff,nc} = 4 \cdot m + 1,25 \cdot e + p_1 + p_w = 4 \cdot 19,75 + 1,25 \cdot 24,7 + 105 + 110 = 324,9 \text{ mm}$$

$$M_{pl,Rd} = \frac{0,25 \cdot l_{eff,nc} \cdot t_{fc}^2 \cdot f_y}{\gamma_{M0}} = \frac{0,25 \cdot 324,9 \cdot 14,0^2 \cdot 275}{1,0} = 4378028 \text{ Nmm}$$

The resistance of the column flange in bending is taken as minimum values from three modes of failure.

$$F_{tfc(1+2+3),Rd} = \min \left\{ \begin{array}{l} \frac{4 \cdot M_{pl,Rd}}{m} = \frac{4 \cdot 4378028}{19,75} = 886689 \\ \frac{2 \cdot M_{pl,Rd} + n \cdot \sum F_{t,Rd}}{m+n} = \frac{2 \cdot 4378028 + 24,7 \cdot 6 \cdot 90432}{19,75 + 24,7} = 498494 = \\ \sum F_{t,Rd} = 6 \cdot 90432 = 542592 \end{array} \right. = 498,5 \text{ kN} \quad (32)$$

- Column flange in bending for second and third bolt rows

Effective length of equivalent T-stub:

- Circular patterns:

$$l_{eff,cp} = 2 \cdot \pi \cdot m + 2 \cdot p_w = 2 \cdot \pi \cdot 19,75 + 2 \cdot 110 = 344 \text{ mm}$$

- Non – circular patterns:

$$l_{eff,nc} = 4 \cdot m + 1,25 \cdot e + p_w = 4 \cdot 19,75 + 1,25 \cdot 24,7 + 110 = 219,9 \text{ mm}$$

$$M_{pl,Rd} = \frac{0,25 \cdot l_{eff,nc} \cdot t_{fc}^2 \cdot f_y}{\gamma_{M0}} = \frac{0,25 \cdot 219,9 \cdot 14,0^2 \cdot 275}{1,0} = 2963152 \text{ Nmm}$$

The resistance of the column flange in bending is taken as minimum values from three modes of failure.

$$F_{tfc(1+2),Rd} = \min \left\{ \begin{array}{l} \frac{4 \cdot M_{pl,Rd}}{m} = \frac{4 \cdot 2963152}{19,75} = 600132 \\ \frac{2 \cdot M_{pl,Rd} + n \cdot \sum F_{t,Rd}}{m+n} = \frac{2 \cdot 2963152 + 24,7 \cdot 4 \cdot 90432}{19,75 + 24,7} = 334330 \\ \sum F_{t,Rd} = 4 \cdot 90432 = 361728 \end{array} \right. = 334,3 \text{ kN} \quad (33)$$

- Column web panel in tension for first, second and third bolt rows

$$F_{twc(1+2+3),Rd} = \frac{\omega \cdot b_{eff,t,wc} \cdot t_{wc} \cdot f_{ywc}}{\gamma_{M0}} = \frac{0,774 \cdot 324,9 \cdot 8,5 \cdot 275}{1,0} = 587817 \text{ N} = 587,8 \text{ kN} \quad (34)$$

- Column web panel in tension for second and third bolt rows

$$F_{twc(2+3),Rd} = \frac{\omega \cdot b_{eff,t,wc} \cdot t_{wc} \cdot f_{ywc}}{\gamma_{M0}} = \frac{0,774 \cdot 219,9 \cdot 8,5 \cdot 275}{1,0} = 397849 \text{ N} = 397,8 \text{ kN} \quad (35)$$

- Angle cleat in bending

$$m_3 = \frac{3}{2} \frac{t_{wa}}{\left[ \left( \frac{m_{max} \cdot h_3}{t_{wa} \cdot l_{wa}} \right)^2 + 3 \right]^{\frac{1}{2}} - \frac{m_{max} \cdot h_3}{t_{wa} \cdot l_{wa}}} = \frac{3}{2} \frac{10,0}{\left[ \left( \frac{35,0 \cdot 70}{10,0 \cdot 160} \right)^2 + 3 \right]^{\frac{1}{2}} - \frac{35,0 \cdot 70}{10,0 \cdot 160}} = 4,87 \text{ mm} \quad (36)$$

$$\text{where } h_3 = \frac{(h_b - p_w + t_a)}{2} = \frac{(240 - 110 + 10,0)}{2} = 70 \text{ mm}$$

Effective length of equivalent T-stub:

- Circular patterns:

$$l_{eff,cp} = \min \left\{ \begin{array}{l} 2 \cdot \pi \cdot m_3 = 2 \cdot \pi \cdot 4,87 = 30,6 \\ \pi \cdot m_3 + 2 \cdot e_w = \pi \cdot 4,87 + 2 \cdot 25 = 65,3 \end{array} \right. = 30,6 \text{ mm}$$

- Non – circular patterns:

$$\begin{aligned}
 l_{eff,nc} &= \\
 &= \min \left\{ \begin{array}{l} 4 \cdot m_3 + 1,25 \cdot e = 4 \cdot 4,87 + 1,25 \cdot 6,09 = 27,1 \\ 2 \cdot m_3 + 0,625 \cdot e + e_w = 2 \cdot 4,87 + 0,625 \cdot 6,09 + 25 = 38,5 \end{array} \right. = \\
 &= 27,1 \text{ mm}
 \end{aligned}$$

$$M_{pl,Rd} = \frac{0,25 \cdot l_{eff} \cdot t_a^2 \cdot f_y}{\gamma_{M0}} = \frac{0,25 \cdot 27,1 \cdot 10,0^2 \cdot 275}{1,0} = 186312 \text{ Nmm}$$

$$\begin{aligned}
 F_{twa,Rd} &= \min \left\{ \begin{array}{l} \frac{4 \cdot M_{pl,Rd}}{m_3} = \frac{4 \cdot 186312}{4,87} = 153029 \\ \frac{2 \cdot M_{pl,Rd} + n \cdot \sum F_{t,Rd}}{m+n} = \frac{2 \cdot 186312 + 6,09 \cdot 2 \cdot 90432}{4,87 + 6,09} = 134497 \\ \sum F_{t,Rd} = 2 \cdot 90432 = 180864 \end{array} \right. = \\
 &= 134,5 \text{ kN} \quad (37)
 \end{aligned}$$

• Angle web cleats in tension

$$F_{twa,Rd} = \frac{l_{eff} \cdot 2 \cdot t_a \cdot f_{ya}}{\gamma_{M0}} = \frac{27,1 \cdot 2 \cdot 10,0 \cdot 275}{1,0} = 149050 \text{ N} = 149,0 \text{ kN} \quad (38)$$

• Beam web in tension

$$F_{twb,Rd} = \frac{l_{eff} \cdot t_{wb} \cdot f_{yb}}{\gamma_{M0}} = \frac{27,1 \cdot 6,2 \cdot 275}{1,0} = 46205 \text{ N} = 46,2 \text{ kN} \quad (39)$$

Due to the fact that  $\sum l_{eff} = 51,6 + 27,1 = 78,7 \text{ mm} < p_w = 110 \text{ mm}$ , the resistance of the components for the group of bolts is greater than for individual bolts, so it can be omitted in the calculations. The shear and bearing resistance of the bolts for third bolt row are the same as for the second bolt row.

Finally, the design resistance of the third bolt row:

$$\begin{aligned}
 F_{3,Rd} &= \min (V_{wp,Rd} - F_{1,Rd} - F_{2,Rd}; F_{cwc,Rd} - F_{1,Rd} - F_{2,Rd}; F_{cfb,Rd} - F_{1,Rd} - F_{2,Rd}; F_{ca,Rd} - \\
 &F_{1,Rd} - F_{2,Rd}; F_{cab,Rd} - F_{1,Rd} - F_{2,Rd}; F_{cbfb,Rd} - F_{1,Rd} - F_{2,Rd}; F_{vca,Rd} - F_{1,Rd} - F_{2,Rd}; \\
 &F_{ffc,Rd(3)}; F_{ffc,Rd(1+2+3)} - F_{1,Rd} - F_{2,Rd}; F_{ffc,Rd(2+3)} - F_{2,Rd}; F_{twc,Rd(3)}; F_{twc,Rd(1+2+3)} - \\
 &F_{1,Rd} - F_{2,Rd}; F_{twc,Rd(2+3)} - F_{2,Rd}; F_{twab,Rd}; F_{twbb,Rd}; F_{twa,Rd}; F_{twb,Rd}; F_{twa,Rd}; \\
 &F_{vwa,Rd})
 \end{aligned}$$

$$\begin{aligned}
 F_{3,Rd} &= \min (289,9-47,1-55,3; 309,4-47,1-55,3; 438,4-47,1-55,3; 330,0-47,1- \\
 &55,3; 165,6-47,1-55,3; 219,0-47,1-55,3; 154,4-47,1-55,3; 167,1; \\
 &498,5-47,1-55,3; 334,3-55,3; 198,8; 587,8-47,1-55,3; 397,8-55,3; \\
 &178,6; 55,3; 134,5; 46,2; 149,0; 154,4) = 46,2 \text{ kN}
 \end{aligned}$$

Moment resistance of the joint:

$$\begin{aligned} M_{j,Rd} &= \sum h_r \cdot F_{r,Rd} = 285 \cdot 47,1 + 180 \cdot 55,3 + 70 \cdot 46,2 = \\ &= 26600 \text{ kNm} = 26,6 \text{ kNm}. \end{aligned} \quad (40)$$

### Rotational stiffness of the joint.

- Column web panel in shear

$$k_{vwp} = \frac{0,38 \cdot A_{vc}}{\beta \cdot h_1} = \frac{0,38 \cdot 2029}{1,0 \cdot 285} = 2,71 \text{ mm} \quad (41)$$

- Column web panel in compression

$$k_{cwc} = \frac{0,7 \cdot b_{eff} \cdot t_{wc}}{d_{wc}} = \frac{0,7 \cdot 171 \cdot 8,5}{122} = 8,34 \text{ mm} \quad (42)$$

- Bolts in bottom flange in shear

$$k_{vca} = \frac{16 \cdot n_b \cdot d^2 \cdot f_{ub}}{E \cdot d_{M16}} = \frac{16 \cdot 1 \cdot 16^2 \cdot 800}{210 \cdot 10^3 \cdot 16} = 0,98 \text{ mm} \quad (43)$$

- Bolts in bottom angle cleat in bearing

$$k_{cab} = \frac{24 \cdot n_b \cdot k_b \cdot k_t \cdot d \cdot f_u}{E} = \frac{24 \cdot 1 \cdot 1,25 \cdot 0,938 \cdot 16 \cdot 430}{210 \cdot 10^3} = 0,92 \text{ mm} \quad (44)$$

$$\text{where } k_b = 1,25, \text{ and } k_t = \frac{1,5 \cdot t_a}{d_{M16}} = \frac{1,5 \cdot 10,0}{16} = 0,938 < 2,5$$

- Column web panel in tension

$$k_{twc} = \frac{0,7 \cdot l_{eff} \cdot t_{wc}}{d_{wc}} = \frac{0,7 \cdot 109,9 \cdot 8,5}{122} = 5,36 \text{ mm} \quad (45)$$

- Column flange in bending

$$k_{tfc} = \frac{0,9 \cdot l_{eff} \cdot t_{fc}^3}{m^3} = \frac{0,9 \cdot 109,9 \cdot 14,0^3}{19,75^3} = 35,23 \text{ mm} \quad (46)$$

- Bolts in tension

$$k_{tb} = \frac{1,6 \cdot A_{sb}}{L_b} = \frac{1,6 \cdot 157}{42,4} = 5,92 \text{ mm} \quad (47)$$

$$\text{where } L_b = t_{fc} + t_a + 2 \cdot t_w + 0,5 \cdot (k + t_n) = 14,0 + 10,0 + 2 \cdot 3,0 + 0,5 \cdot (10,0 + 14,8) = 42,4 \text{ mm}$$

For first bolt row

- Top angle cleat in bending

$$k_{ta} = \frac{0,9 \cdot l_{eff} \cdot t_a^3}{m^3} = \frac{0,9 \cdot 60 \cdot 10,0^3}{35^3} = 1,26 \text{ mm} \quad (48)$$

- Bolts in top angle cleat in bearing

$$k_{tab} = \frac{24 \cdot n_b \cdot k_b \cdot k_t \cdot d \cdot f_u}{E} = \frac{24 \cdot 1 \cdot 1,125 \cdot 0,938 \cdot 16 \cdot 430}{210 \cdot 10^3} = 0,83 \text{ mm} \quad (49)$$

where  $k_b = \frac{0,25 \cdot e_2}{d} + 0,5 = \frac{0,25 \cdot 40}{16} + 0,5 = 1,125 < 1,25$ ,  
and  $k_t = \frac{1,5 \cdot t_a}{d_{M16}} = \frac{1,5 \cdot 10,0}{16} = 0,938 < 2,5$

- Bolts in top beam flange in bearing

$$k_{tbf b} = \frac{24 \cdot n_b \cdot k_b \cdot k_t \cdot d \cdot f_u}{E} = \frac{24 \cdot 1 \cdot 1,047 \cdot 0,919 \cdot 16 \cdot 430}{210 \cdot 10^3} = 0,76 \text{ mm} \quad (50)$$

where  $k_b = \frac{0,25 \cdot e_2}{d} + 0,5 = \frac{0,25 \cdot 35}{16} + 0,5 = 1,047 < 1,25$ ,  
and  $k_t = \frac{1,5 \cdot t_{fb}}{d_{M16}} = \frac{1,5 \cdot 9,8}{16} = 0,919 < 2,5$

For second bolt row

- Web angle cleats in bending

$$k_{twa} = \frac{0,9 \cdot l_{eff} \cdot t_a^3}{m^3} = \frac{0,9 \cdot 51,6 \cdot 10,0^3}{9,57^3} = 52,99 \text{ mm} \quad (51)$$

- Bolts in beam web in bearing

$$k_{twbb} = \frac{24 \cdot n_b \cdot k_b \cdot k_t \cdot d \cdot f_u}{E} = \frac{24 \cdot 0,5 \cdot 1,047 \cdot 0,581 \cdot 16 \cdot 430}{210 \cdot 10^3} = 0,24 \text{ mm} \quad (52)$$

where  $k_b = 1,047$ , and  $k_t = \frac{1,5 \cdot t_{wb}}{d_{M16}} = \frac{1,5 \cdot 6,2}{16} = 0,581 < 2,5$

For third bolt row

- Web angle cleats in bending

$$k_{twa} = \frac{0,9 \cdot l_{eff} \cdot t_a^3}{m^3} = \frac{0,9 \cdot 27,1 \cdot 10,0^3}{4,87^3} = 211,17 \text{ mm} \quad (53)$$

Shear and bearing resistance are the same as for previous bolt rows.

Effective stiffness coefficient for first bolt row

$$k_{eff1} = \frac{1}{\sum \frac{1}{k_{i,1}}} = \frac{1}{\frac{1}{k_{twc}} + \frac{1}{k_{tfc}} + \frac{1}{k_{tb}} + \frac{1}{k_{ta}} + \frac{1}{k_{vta}} + \frac{1}{k_{tab}} + \frac{1}{k_{tbf b}}} =$$

$$= \frac{1}{\frac{1}{5,36} + \frac{1}{35,23} + \frac{1}{5,92} + \frac{1}{1,26} + \frac{1}{0,98} + \frac{1}{0,83} + \frac{1}{0,76}} = 0,21 \text{ mm} \quad (54)$$

Effective lever arm for first bolt row

$$h_{eff1} = \frac{k_{eff,c} \cdot h_1^2 + k_{eff,a} \cdot (h_b + t_a/2)^2}{k_{eff,c} \cdot h_1 + k_{eff,a} \cdot (h_b + t_a/2)} = \frac{2,07 \cdot 285^2 + 0,23 \cdot (240 + 10,0/2)^2}{2,07 \cdot 285 + 0,23 \cdot (240 + 10,0/2)} =$$

$$= 281,5 \text{ mm} \quad (55)$$

$$\text{where } k_{eff,c} = \frac{1}{\frac{1}{k_{twc}} + \frac{1}{k_{tfc}} + \frac{1}{k_{tb}}} = \frac{1}{\frac{1}{5,36} + \frac{1}{7,88} + \frac{1}{5,92}} = 2,07 \text{ mm, and}$$

$$k_{eff,a} = \frac{1}{\frac{1}{k_{ta}} + \frac{1}{k_{vta}} + \frac{1}{k_{tab}} + \frac{1}{k_{tbfb}}} = \frac{1}{\frac{1}{1,26} + \frac{1}{0,98} + \frac{1}{0,83} + \frac{1}{0,76}} = 0,23 \text{ mm}$$

Effective stiffness coefficient for second bolt row

$$k_{eff2} = \frac{1}{\sum \frac{1}{k_{i,2}}} = \frac{1}{\frac{1}{k_{twc}} + \frac{1}{k_{tfc}} + \frac{1}{k_{tb}} + \frac{1}{k_{twa}} + \frac{1}{k_{vwa}} + \frac{1}{k_{twbb}} + \frac{1}{k_{twab}}} =$$

$$= \frac{1}{\frac{1}{5,36} + \frac{1}{7,88} + \frac{1}{5,92} + \frac{1}{52,99} + \frac{1}{0,98} + \frac{1}{0,24} + \frac{1}{0,83}} = 0,15 \text{ mm} \quad (56)$$

Effective stiffness coefficient for third bolt row

$$k_{eff3} = \frac{1}{\sum \frac{1}{k_{i,3}}} = \frac{1}{\frac{1}{k_{twc}} + \frac{1}{k_{tfc}} + \frac{1}{k_{tb}} + \frac{1}{k_{twa}} + \frac{1}{k_{vwa}} + \frac{1}{k_{twbb}} + \frac{1}{k_{twab}}} =$$

$$= \frac{1}{\frac{1}{5,36} + \frac{1}{7,88} + \frac{1}{5,92} + \frac{1}{211,17} + \frac{1}{0,98} + \frac{1}{0,24} + \frac{1}{0,83}} = 0,15 \text{ mm} \quad (57)$$

Equivalent lever arm

$$z_{eq} = \frac{\sum k_{eff,i} h_i^2}{\sum k_{eff,i} h_i} = \frac{0,21 \cdot 281,5^2 + 0,15 \cdot 180^2 + 0,15 \cdot 70^2}{0,21 \cdot 281,5 + 0,15 \cdot 180 + 0,15 \cdot 70} = 230,1 \text{ mm} \quad (58)$$

Equivalent stiffness coefficient

$$k_{eq} = \frac{\sum k_{eff,i} h_i}{z_{eq}} = \frac{0,21 \cdot 281,5 + 0,15 \cdot 180 + 0,15 \cdot 70}{230,1} = 0,42 \text{ mm} \quad (59)$$

Finally, stiffness of the joint is equal:

$$S_j = \frac{E \cdot z_{eq}^2}{\mu \cdot \sum \frac{1}{k_i}} = \frac{E \cdot z_{eq}^2}{\mu \cdot \left( \frac{1}{k_{cwc}} + \frac{1}{k_{vwp}} + \frac{1}{k_{vca}} + \frac{1}{k_{cab}} + \frac{1}{k_{eq}} \right)} = \frac{210 \cdot 10^3 \cdot 230,1^2}{1,0 \cdot \left( \frac{1}{8,34} + \frac{1}{2,71} + \frac{1}{0,98} + \frac{1}{0,92} + \frac{1}{0,42} \right)} =$$

$$= 34233,9 \cdot 10^6 \frac{\text{Nmm}}{\text{rad}} = 34233,9 \text{ kNm/rad.} \quad (60)$$

#### 4. Proposed estimation of the resistance and stiffness of the joint

As can see in the example, the procedure of the calculating of moment resistance and initial stiffness of the connection is labor-intensive and complicated. Therefore, this method is used to check the characteristics of existing connections or in computer programs. In the initial phase, designers need fast and approximated methods to estimate the resistance and stiffness of the joints. In such cases polynomial approximation functions are often used.

Design procedure shown that the moment resistance and initial stiffness are depend on many different parameters both dependent and independent in relation to himself. The influence of some of these parameters on the resistance and the

stiffness of the connection is very similar to the joints with only flange angle cleats introduced in [8].

In the case of joints with web and flange angle cleats, one of the additional parameters is the length of the angle web cleat  $l_{wa}$ . The influence of length of the angle web cleat on the resistance and the stiffness of the connection are introduced on Fig. 8 and 9.

After analyzing dozens of different configurations of beam to column joints with use of angle web and flange cleats was ascertained that on the resistance and the stiffness the greatest influence had: the height of the beam  $h_b$ , the depth of the column  $h_c$ , the length of flange of the angle cleats  $b_a$ , the diameter of the bolts  $d$ , length of the angle web cleat  $l_{wa}$ , and geometric dimensions which usually are variable dependent from the elements of the connection.

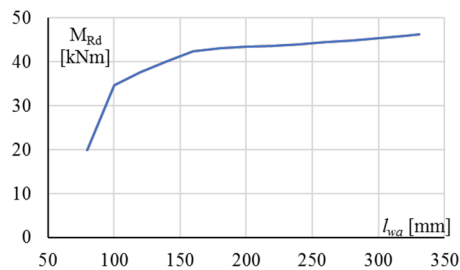


Fig. 8. Influence of length of the angle web cleat  $l_{wa}$  on moment resistance of the joint

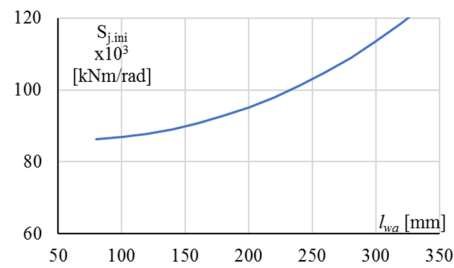


Fig. 9. Influence of length of the angle web cleat  $l_{wa}$  on initial stiffness of the joint

For further analysis, typical design assumptions and constant values of the following parameters were established:

- steel grade for all elements S275,
- bolts grade 8.8,
- bolts diameter for web and angle cleats is the same,
- column with HEB - section,
- beam with IPE - section,
- angle cleats and web cleats are made of the same sections,
- thickness of the angle leg is means thickness of accepted angle section,
- angle flange cleats length is equal to width of column flange,
- the spacing of the bolts is depended on connected elements according to constructional recommendations,
- edge distance for angle web cleat is equal  $1,2 \cdot d_0$ .
- gap  $g$  is equal 5 mm.

As a variable parameters, the following joint properties were analyzed:

- beam height  $x_1 = h_b$  in range (200 ÷ 450) [mm],
- column depth  $x_2 = h_c$  in range (100 ÷ 300) [mm],
- length of flange of the angle cleats  $x_3 = b_a$  in range (60 ÷ 200) [mm],

- bolt diameter  $x_4 = d$  in range ( 10 ÷ 24) [mm], and
- length of the angle web cleat  $x_5 = l_{wa}$  in range (4,6· $d_0$  ÷  $d_b$ ) [mm].

To finding of the approximation function of was applied the theory of the planning of the experiment [10], and the computer simulation. For determine of characteristics of the joins, was adopted a plan the experiment of Hartley PS/DS-P:Ha5 based at the range of variation on the hypercube, with the arrangement showing in table 1.

Table 1. Planning of experiment for determination of the resistance and stiffness of the joint

	$\hat{x}_1$	$\hat{x}_2$	$\hat{x}_3$	$\hat{x}_4$	$\hat{x}_5$	$x_1:$ $h_b$	$x_2:$ $h_c$	$x_3:$ $b_a$	$x_4:$ $d$	$x_5:$ $l_{wa}$	$M_R$ [kN·m]	$S_{f,ini}$ [kN·m/rad]
1	+1	+1	+1	+1	+1	450	300	200	24	379	103,18	145239
2	-1	-1	+1	+1	+1	200	100	200	24	159	-	-
3	-1	+1	-1	-1	-1	200	300	60	10	51	8,08	58962
4	+1	-1	-1	-1	-1	450	100	60	10	51	22,65	126819
5	-1	+1	-1	+1	+1	200	300	60	24	159	3,43	20213
6	+1	-1	-1	+1	+1	450	100	60	24	379	39,82	109450
7	+1	+1	+1	-1	-1	450	300	200	10	51	33,78	117502
8	-1	-1	+1	-1	-1	200	100	200	10	51	17,84	79079
9	-1	+1	+1	+1	-1	200	300	200	24	120	16,41	16098
10	+1	-1	+1	+1	-1	450	100	200	24	120	63,40	109376
11	+1	+1	-1	-1	+1	450	300	60	10	379	27,13	131015
12	-1	-1	-1	-1	+1	200	100	60	10	159	11,06	42265
13	-1	+1	+1	-1	+1	200	300	200	10	159	18,09	40379
14	+1	-1	+1	-1	+1	450	100	200	10	379	33,78	100128
15	+1	+1	-1	+1	-1	450	300	60	24	120	22,85	116191
16	-1	-1	-1	+1	-1	200	100	60	24	120	3,43	28869
17	+1	0	0	0	0	450	200	130	16	233	73,84	73177
18	-1	0	0	0	0	200	200	130	16	120	15,79	24590
19	0	+1	0	0	0	330	300	130	16	177	54,32	40224
20	0	-1	0	0	0	330	100	130	16	177	41,18	53243
21	0	0	+1	0	0	330	200	200	16	177	63,68	44586
22	0	0	-1	0	0	330	200	60	16	177	25,36	60854
23	0	0	0	+1	0	330	200	130	24	195	83,11	37264
24	0	0	0	-1	0	330	200	130	10	161	23,90	78301
25	0	0	0	0	+1	330	200	130	16	271	55,61	47523
26	0	0	0	0	-1	330	200	130	16	83	50,85	67749
27	0	0	0	0	0	330	200	130	16	177	53,23	47109

After analyzing with the overlay SOLVER of several variants of the approximation function, the function giving the least square error was chose. The resistance of the bolted beam to column joint with the use of angle web flange cleats can be obtain from:

$$M_{Rd} = 4,885 \cdot 10^{-3} \cdot h_b^{0,636} \cdot h_c^{0,048} \cdot b_a^{0,508} \cdot d^{0,534} \cdot l_{wa}^{0,222} \quad (61)$$

The stiffness of the unstiffened joint can be obtained from:

$$S_{j,ini} = 4,528 \cdot 10^{-5} \cdot h_b^{3,529} \cdot h_c^{0,105} \cdot b_a^{-0,088} \cdot d^{-0,075} \cdot l_{wa}^{-0,031} + 30139 \quad (62)$$

where:  $M_{Rd}$  – in [kNm],  $S_{j,ini}$  - in [kNm/rad], and  $h_b, h_c, b_a, l_{wa}, d$  - in [mm].

The equations (55) and (56) refer to one-sided connections of the beam to the unstiffened column. In the initial stage of the designing they can also be used for other similar types of joints. After the achievement of calculations was observed that in the investigated range of joints, the stiffening of the column has not influence on the resistance of the joint, and only enlarges his stiffness. The increase of stiffness of the joint, caused by the ribbing of the column, does not exceed several dozen percent. So, it can be omitted in the preliminary analysis of the joint. In case of two-sided joints, their resistance is the same as the moment resistance of the cantilever joints. The initial stiffnes of two-sided stiffened joints is such alone as stiffness of the stiffened cantilever joints. In case of two-sided not stiffened joints the stiffness is comparable with the arithmetic mean of the stiffness of cantilever stiffened and unstiffened joints.

## 5. Conclusion

The knowledge of the moment resistance and the initial stiffness of the joint has a basic meaning in the initial stage of the designing, for choice of the suitable method of analysis of the construction. Proposed in this paper, an approximation formulas allowed on the preliminary estimation of the joint characteristics, without the necessity of the usage of arduousness calculations according to the procedure presented in [7].

Comparing results received according to the exact standard method, and calculations by means of simplified formulas, differences did not exceed a dozen percent.

For worked example introduced in the Section 3, from approximate formulas the moment resistance amounts 25,7 [kNm] (26,6 [kNm]), and the initial stiffness 39 394 [kNm/rad] (34 234 [kNm/rad]).

## References

- [1] Altman W. G., Azizinamini A., Bardburn J. H., Radziminski J. B.: Moment-rotation characteristics of semi-rigid steel beam-column connections. Civil Engineering Department, University of South Carolina, 1982.
- [2] American Institute of Steel Construction, 'Steel construction manual', 13th edition, 2005.
- [3] Gambhir L.M. Fundamentals of Structural Steel Design. Tata McGraw-Hill Education, New Delhi, 2013.
- [4] Baker J.F. The steel skeleton. Volume 1. Elastic behavior and design. Cambridge University Press. 1963.

- 
- [5] Robustness. Chapter 4 in: Steel Buildings in Europe. Multi-Storey Steel Buildings. Part 5. Joint Design. [http://sections.arcelormittal.com/fileadmin/redaction/4-Library/4-SBE/EN/MSB05\\_Joint\\_Design.pdf](http://sections.arcelormittal.com/fileadmin/redaction/4-Library/4-SBE/EN/MSB05_Joint_Design.pdf). (dostęp: 12.03.2017).
- [6] Beaufoy, Leroy A., Moharram A.: Derived moment-angle curves for web cleat connections. IABSE Congress Report. <http://doi.org/10.5169/seals-4002> (dostęp: 4.04.2017).
- [7] EN 1993-1-8: 2006 Eurocode 3: Design of steel structures – Part 1-8: Design of joints.
- [8] Pisarek Z.: Resistance and stiffness of the beam to column joints with angle flange cleats. Scientific Papers of Rzeszow University of Technology – Civil and Environmental Engineering. vol. 256, no 50. 2008, pp. 219–228.
- [9] Faella C., Piluso V., Rizzano G.: Structural Steel Semirigid Connections: Theory, Design and Software. CRC Press. 2000.
- [10] Polański Z.: Planowanie doświadczalne w technice. PWN Warszawa 1984 (in polish).

*Przesłano do redakcji: 24.04.2018 r.*

*Przyjęto do druku: 15.06.2018 r.*

Krzysztof OSTROWSKI  
Aleksander KOZŁOWSKI

## CREDIBILITY OF FEM ANALYSIS IN THE T-STUB MODELLING

The paper presents the results of a comparative analysis between numerical calculations of T-stubs of the 3<sup>rd</sup> stage of FEM models hierarchical validation and the results of laboratory tests. The procedure for the development of the material characteristics used in numerical calculations of FEM models is presented. The scope of this article allows determining the non-linear characteristics of the T-stub which maps the work of the end-plate joint of the beam to the column in the tensile zone. The results of laboratory tests of a series of T-stubs made of rolled profiles (HEB240, HEA240) and of welded profiles (thickness of end-plate:  $t_p = 12$  mm and  $t_p = 20$  mm) have been presented. The principles of shaping the geometrical features of the FEM model of end-plate joints of the T-stub type are given, with particular emphasis on the shaping of the bolt with a thread. The impact of the bolt thread on the accuracy of the obtained results was assessed. The criterion of reliability of the obtained results with respect to the maximum force in the bolt obtained on the basis of laboratory tests in the axial tensile test of the bolts in the configuration: bolt - washer - nut was formulated.

**Keywords:** T-stub, rotation capacity, material ductility, multistage hierarchical validation, FEM modelling

### 1. Introduction

For a relatively long time, traditional steel connections have been considered as a fully rigid or ideally hinged, regardless of their actual behavior. This assumption considerably simplified the calculation process and the expense of unoptimized projects and higher production costs borne to produce construction elements [1], [2]. Principles for the assessment of the structural elements behavior have well-established methodology, allowing to determine all the instability effects and to assess the safety of local systems as well as the whole structural system [3]. In the case of joints, a similar level of knowledge and the applied methodology is not available, in particular in the area of response surface prediction of rotation angle defined in the form of the joint rotation curve  $M-\phi$ .

---

<sup>1</sup> Corresponding author: Krzysztof Ostrowski, MTA Engineering Ltd., ul. Poniatowskiego 14, 35-026 Rzeszów, krzysztof.ostrowski@mta-online.net

<sup>2</sup> Aleksander Kozłowski, Rzeszow University of Technology, ul. Poznańska 2, kozlowsk@prz.edu.pl

The behavior of steel structure joints is very complicated and requires consideration of many occurring phenomena including material nonlinearities, contact surface nonlinearities, local geometrical imperfections, as well as complex configurations of joints geometry. The difficulties we encounter in creating analytical models describing the joints' behavior in the full scope of their deformability is caused by the compilation of factors having their basis in the phase shift of the plastic deformations initiation of individual joint components. There is an equilibrium path for each element that is part of the joint, which has its own non-linear force-strain characteristics ( $F-\Delta$ ) [3], [4]. This relationship causes that the behavior of the joint subjected to load in the form of bending moment is also characterized by non-linear behavior.

This non-linearity occurs because a joint is a collection of several components which interact differently at different levels of applied loads. Each non-linearity regulates the behavior of the joint and is at the same time an obstacle to the systematic and theoretical solution to this problem [5]. Analysis of this complex behavior has a usually approximate character with the use of drastic simplifications. The tests (both laboratory and numerical) are often carried out in order to obtain an actual answer, which is then modeled by approximating the solution by means of mathematical formulas, having reference to the main properties of the joint structure.

During the last decades, different approaches have been applied in the area of assessment of the steel joints behavior. Extensive literature studies present a well-developed methodology of experimental research [6], [7], [8] and developed empirical [9], [10], analytical [11, 12], numerical [13], [14], [15], [16], [17] and mechanical models [18]. After the introduction of semi-rigid connections concept, many researchers have focused their efforts on accurately predicting parameters such as initial stiffness ( $S_{j,ini}$ ), moment resistance ( $M_{j,Rd}$ ) and rotation capacity of joints ( $\phi_{cu}$ ), to obtain the actual response surface of rotation angle of joint  $M-\phi$ . Numerous research works dedicated to estimate the strength and stiffness of T-stubs connections (Zoetemeijer [19], Yee and Melchers [20]) contributed to the creation of a new trend in the analysis of the behavior of the bolted connections, where a particular example of this approach is the so-called component method, which was actually adopted as a calculation procedure in well-known regulatory standards, such as Eurocode 3 [5, 21]. Component method included in PN-EN 1993-1-8 [22] is used to determine the moment resistance and stiffness of joints. The wide application of the component method in the design of joints was possible due to the development of mechanical and spring models, supporting the development of analytical and empirical models. The basic principle of these models is to divide the connection into simpler components for which the moment-rotation relation ( $M-\phi$ ) of the whole bolted connection is determined by assembling all individual responses of its components in a spring system.

However, the procedures of the component method do not precisely define the rules for determining the rotation capacity of joints in the full range of

deformability. In a relatively large number of laboratory tests conducted as part of the research work on the behavior of joints, the maximum rotation angle ( $\phi_{cu}$ ) was not focused on. In these tests, the initial zone of deformation of the joint was analyzed, which was associated with the determination of its initial stiffness  $S_{j,ini}$ . The second determined test parameter was the limit resistance of joint  $M_R$ .

In addition to many advantages, the basic disadvantage of laboratory tests is the time and cost of their execution. For this reason, the use of numerical analyzes to simulate the behavior of joints, becomes a routine activity in research processes. The FEM analyzes reduce research costs, provide much more information about the state of strain and stress of the tested objects, which is not possible to achieve in such a wide range by performing traditional destructive laboratory tests. It should be noted that in case of using numerical analyzes, the results of such analysis may be subjected to a relatively large error in the absence of proper verification and validation of numerical models. In the article, the authors presented the extended results of 3<sup>rd</sup> stage of multistage hierarchical validation of FEM models, as a continuation of the validation process of FEM models, for the needs of rotation capacity prediction of joints [23].

## **2. The necessity of validation for the needs of the correct FEM modeling**

The development of computer technology, whose dynamic growth has been recorded since the 80s of the last century, allowed to develop computational methods using the finite element method to the level where the complicated effects of the examined objects can be calculated on PCs. Previously, it was possible to do only in computing centers. It is assumed that the results obtained in numerical analyses using the finite element method can be considered reliable if they are comparable with the results of experimental research or other known precise solutions.

In each FEM analysis, the accuracy of the model is evaluated. Relevant regulations including the formalization of validation and verification procedures were developed by the American National Institute of Standards [24]. The evaluation of the accuracy of the FEM model should precede every more serious FEM analysis [25]. The verification process is an evaluation of the accuracy of the solution in the FEM calculation model compared to known solutions, e.g. analytical solutions. In the validation process, the computational accuracy of simulated solutions is evaluated by comparison with experimental results. The validation should be performed gradually, i.e. at the level of the material model, set of fasteners, subassemblies and structure fragments. In the literature it has been called as a hierarchical validation [24]. The validation is an iterative process, and the final result in the form of proper material characteristics and a calculation model is a set of requirements that should be met in a computational model that maps the analyzed real model (Fig. 1). The validation must evaluate the

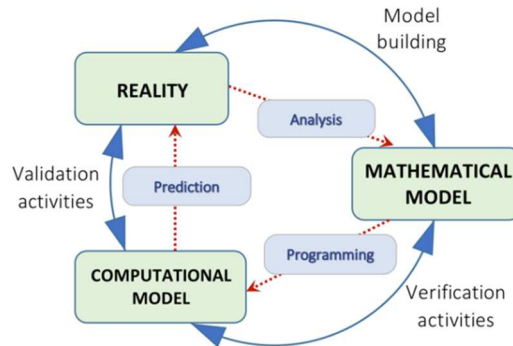


Fig. 1. Diagram of the verification and validation interaction circle in the numerical modeling process (on the basis of [24])

predictive ability of the FEM model in its physical aspect and should take into account any uncertainties that arise from both the results of the numerical simulation and the experimental data.

The hierarchical validation of FEM models used in the analysis of the joints behavior in the full range of deformations was carried out as part of the work [23], [26] in the following four stages:

I Stage – tensile test of steel and bolt specimens (Fig. 2a),

II Stage – bolt tensile in the configuration: bolt – washer – nut (Fig. 2b),

III Stage – tensile test of the T-stubs (Fig. 2c),

IV Stage – test beam to column connection in the configuration of frame (Fig. 2d).

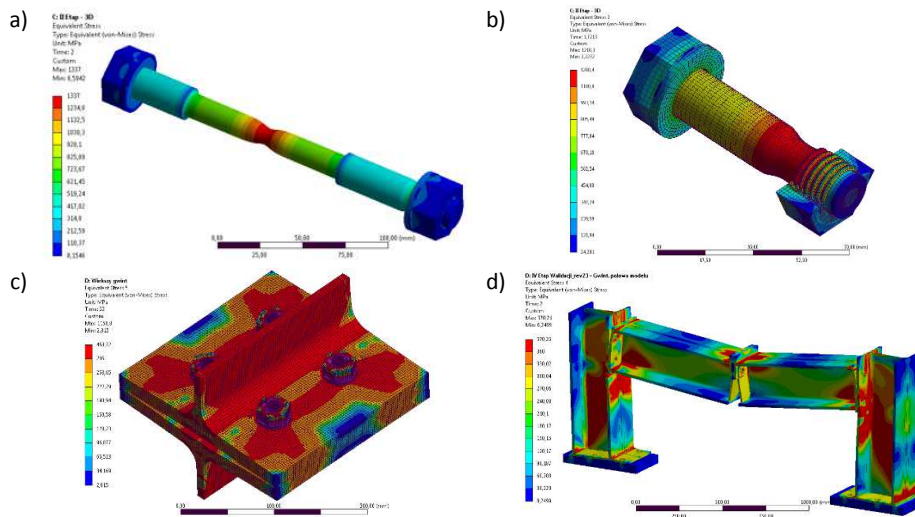


Fig. 2. Multistage Hierarchical Validation of FEM models: a) I stage: the tests of material of steel samples; b) II stage: the tests of fasteners in the configuration of bolt-washer-nut; c) III stage: the tests of T-stubs; d) IV stage: the joint tests in the configuration of frame

In Fig. 3 FEM models used in the process of hierarchical validation were presented. Introduced 4-stage process of model adjustment in the scope of material characteristics describing the properties of the used materials and geometrical features assumes the analysis of the models with different levels of complexity. Such an attitude enables to obtain the required level of detailing which is needed to obtain results convergent with the results of laboratory tests. Material characteristics which do not have logarithmic strain are a kind of reliability guarantor of optimized object due to the fact, that in such cases the analysis always proves earlier achievement of the tolerable stress and strain state. The only characteristic which complies with the requirements for accurate strain mapping of the tested object is the stress - strain characteristic referring to cross section momentary areas, which are real stresses in the deformed section. The adjustment process is obtained as a result of modification of the curve  $\sigma$ - $\varepsilon$  to such a form by which the acceptable compatibility between results and laboratory tests is achieved.

$$\sigma_{\text{true}} = \sigma(1 + \varepsilon) \quad (1)$$

$$\varepsilon_{\text{true}} = \ln(1 + \varepsilon) \quad (2)$$

The area for which the characteristic stress – strain is known is determined by the formula (1) and (2). The modification of the curve can be made only in the unknown scope of material behavior, that is from the moment of creating the necking in the tested material sample, for which it is impossible to determine the stress - strain relation based on the analytical relations available in the literature. The value of the maximal stress  $\sigma_u$  is determined on the basis of the force value in the tensile test before failure referred to deformed cross-section area of the sample A after failure. The maximal value of the strain  $\varepsilon_u$  corresponding to maximal stress  $\sigma_u$  is determined in iterative manner by increasing deformation  $\varepsilon_u$  to such values at which the best adjustment of the actual response curve  $\sigma$ - $\varepsilon$  is obtained.

### 3. Laboratory tests of T-stubs

Research program of the 3<sup>rd</sup> validation stage, included the tensile test of 12 T-stub connections. The study included performing the tests of 4 series T-stub connections with division into rolled and welded profiles.

T-stubs from rolled profiles:

- series H01 – T-stub of profile HEA 240, steel: S235 – 3 samples,
- series B01 – T-stub of profile HEB 240, steel: S355 – 3 samples.

Welded T-stubs:

- series SP01 – welded T-stub: end-plate 20 mm, steel S355 – 3 samples,
- series SP02 – welded T-stub: end-plate 12 mm, steel S235 – 3 samples.

The range of the tested T-stubs was constructed in such a way that, in the tested models, we obtain the 1<sup>st</sup> and 2<sup>nd</sup> failure mode according to the classification

included in the standard [5]. In numerical models of tested objects, geometry projection has been made based on exact measurement of the elements subjected to tensile test. During the sample measurement, significant geometrical imperfections of the profiles have been found. Deviations dispersion in thickness of the flanges for HEB 240 (series B01) was in the range  $16.35 \div 17.84$  mm and it was the highest from all tested series. After measuring the fasteners sets, some dimension deviations with respect to nominal dimensions were also noted (ISO 4014). These deviations were introduced to the FEM model.

In sample A, series H01, a strain gauge system was used to measure strains at predefined characteristic points. The location of the strain gauges is shown in Fig. 3c. In order to measure the strains in the bolts, a system of strain gauges arranged on the periphery of the bolt shank was used in a radial system with a  $120^\circ$  offset (Fig. 4a). All tested samples were attached in an auxiliary holder,

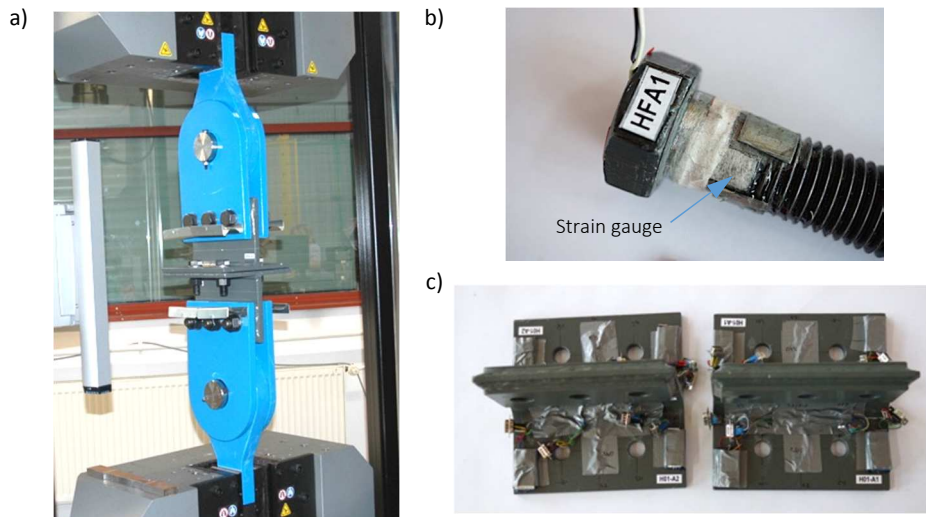


Fig. 3. Sample H01: a) sample of series H01 in a testing machine after damage; b) location of strain gauge in the bolt; c) location of strain gauge in the sample of series H01

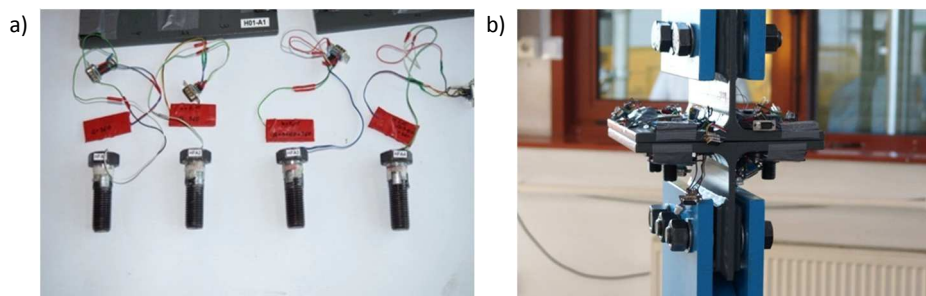


Fig. 4. Measuring system: a) set of fasteners with a strain gauge system; b) sample of series H01 before damage

which ensured the axial introduction of force in the test sample (Fig. 3a). Measurement of deformations of the examined joints was made by means of an optical extensometer, measuring the distance increment between 2 points applied to the side surface of the centre of the tested samples.

The distance between the points was about 100 mm. In order to eliminate the clearances in contact, the prestressing of the bolts with a force of  $F = 50$  kN has been introduced (Fig. 6c). Due to geometrical imperfection in tested samples in each series the differences in the response curve  $F-\Delta$  were noticed (Fig. 5a and Fig. 5b).

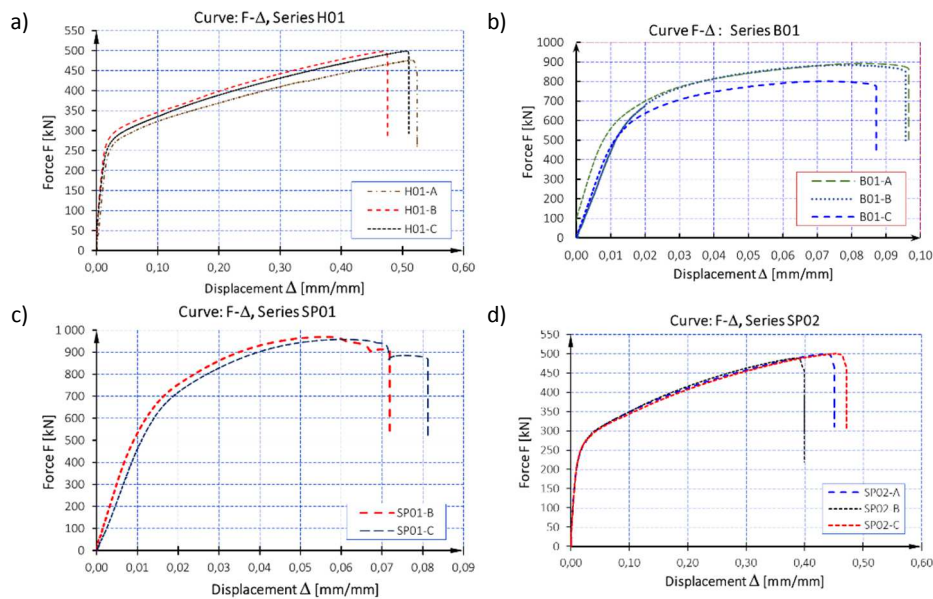


Fig. 5. The results of tensile test: a) series H01; b) series B01; c) series SP01; d) series SP02

#### 4. Description of the numerical model

For the creation of the numerical model 3-dimensional finite elements type Tet10, Hex20, Pyr5, Hex8 and Wed6 were used (Fig 6a). The multi-linear material model defined on the basis of the 1st scope of hierarchical validation (Fig. 7a and Fig. 7b) was used. The contacts between particular elements of joint were created as nonlinear with the friction factor assumed for the surface in a natural condition with the value of  $\mu=0.2$ . A reduction in contact stiffness has been introduced with each subsequent iteration. For all contacts in the model, an augmented Lagrange contact formulation was applied [27]. Contact surfaces were introduced in the areas of contact between: end plates, washer – end-plate, washer – nut and washer – head of the bolt. Additionally, radial surface contacts between bolt hole and bolt shank and thread were introduced in the model (Fig. 9a).

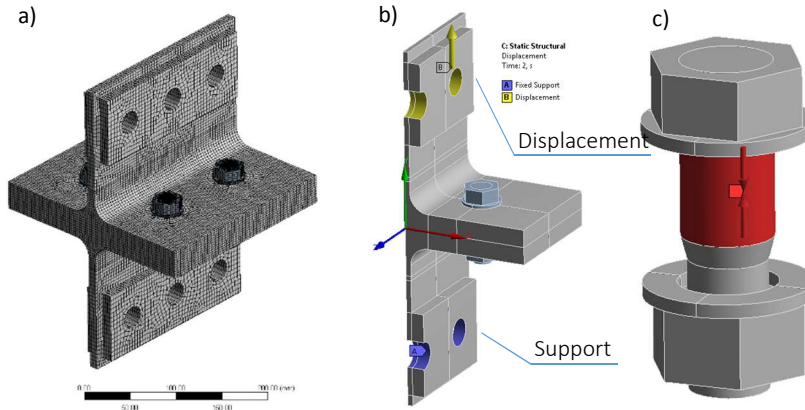


Fig. 6. FEM model: a) 3D view (meshing); b) model 3D of T-stub in double symmetry; c) location of a prestressing force application

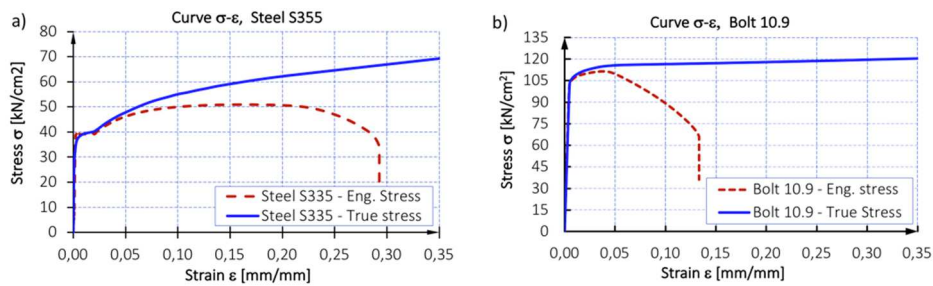


Fig. 7. Material characteristic: a) steel S355; b) bolt grade 10.9 (ISO 4014)

A specific type of contact surface which has been introduced into the FEM model is shown in Fig. 9c. The last from mentioned contacts create boundary conditions to support the bolt that rests on the inner surface of the plate's hole caused by a large joint gap. In the initial stage of joint deformation, the side surface of the washer and the upper surface of the plate have no contact, but with a large gap in the joint they interact between each other, and plate surface is the support for the lateral surface of washer. Introducing such contact surface is dictated by possible occurrence of non-coinciding the FEM model caused by penetrating objects.

In the model of washer, three layers of finite elements and the division into 48 elements were introduced. In the area where the thread connects to the nut, mesh density was increased to the size of 1 mm. In end-plate five layers of finite elements were introduced. The corresponding density of the mesh in this area greatly helps to achieve convergence of the FEM model. In summary, a well-elaborated meshing model is a necessary condition to obtain the correct deformation of particular elements of the analyzed joint.

In order to increase the calculation efficiency, a double symmetry was introduced to the computational model with respect to the center planes of the system, as illustrated in Fig. 6b. In order to evaluate the impact of the thread in the bolt 2 computational models were prepared. In the first model the bolts with modeled metric thread were used (Fig. 8a), in the second one the bolt without thread was used. In this model the nut was permanently connected with the bolt shank (Fig. 8b).

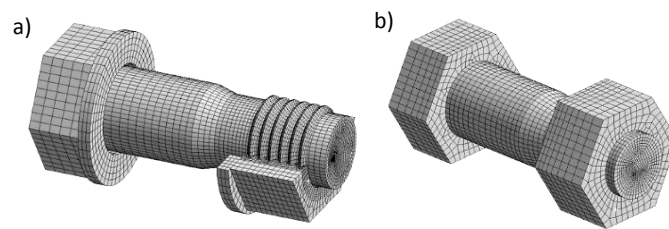


Fig. 8. FEM model of bolt: a) Bolt with thread; b) Bolt without thread

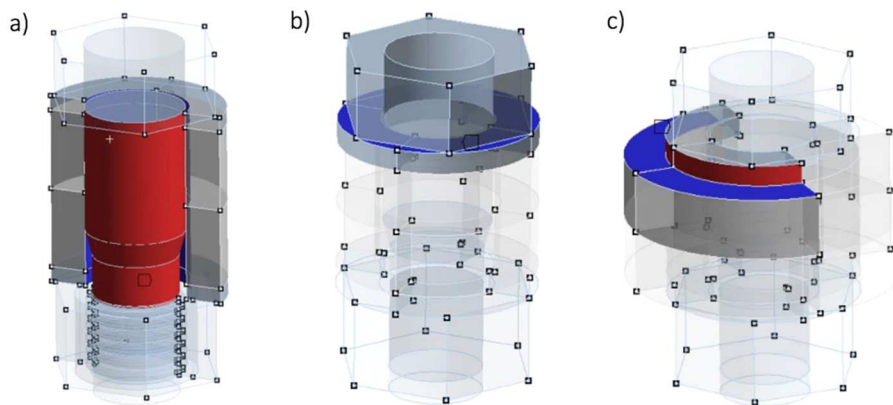


Fig. 9. Contacts: a) radial contact: bolt – end-plate b) anti-slip contact: bolt – washer; c) contact between end plate and external surface of washer

The FEM models were loaded in the same method, as was the case in laboratory tests, by introducing a displacement load. In models with thin end-plates (series: H01 and SP02) the load was applied in 150 steps. In the B01 and SP01 series, the load was applied in 50 steps. Locations of the applied loading are shown in Fig. 6b. The numerical calculations of the analysed objects were performed using the material characteristics shown in Fig. 7.

## 5. Results comparison and summary

The T-stubs research program presented in the paper, used for the needs of the 3<sup>rd</sup> stage of multi-stage hierarchical validation of FEM models, provides a wide range of information needed to geometric discretization of analysed objects in

numerical analysis. Available tools in Ansys software, allow to obtain many interesting results that are only obtainable in the case of advanced numerical analysis performing. If during the creation of the numerical model in a sufficiently accurate manner the geometrical and material imperfections are mapped, then as a result we can obtain not only the deformation state of the tested object (Fig. 10), but also a reliable result of the force distribution (Fig. 11) and distribution of stresses (Fig. 12) in the analysed objects.

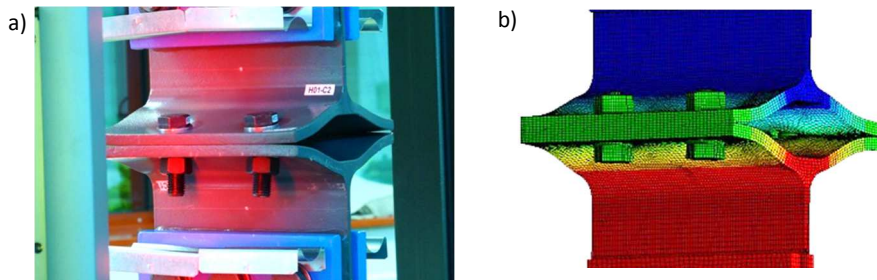


Fig. 10. Comparative analysis: a) laboratory test: sample H01 – type C; b) FEM analysis – sample series H01

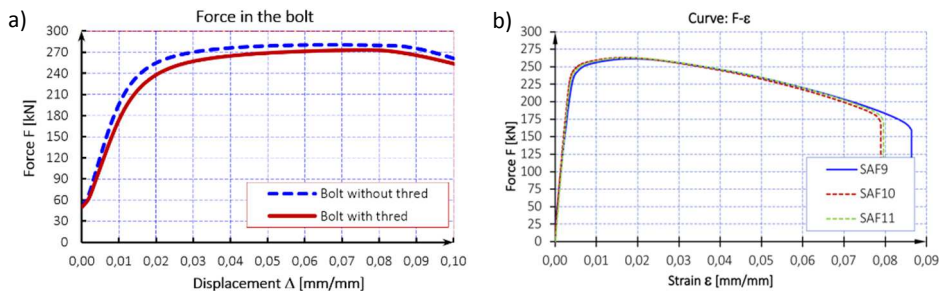


Fig. 11. Distribution of forces in the bolt: a) response curve  $F-\Delta$  - T-stub connection: series B01, HEB 240, steel grade: S355, the forces in the bolt with thread and without thread; b) response curve  $F-\varepsilon$  – 2nd stage of hierarchical validation

One of the most important results obtained in the analysis is the value of the maximum force in the bolt, which is comparable to the value of force in the bolt obtained in the laboratory test in the 2<sup>nd</sup> stage of validation [23]. The maximum bolt force in the laboratory test was  $F_{\text{bolt,lab}} = 263.18$  kN (Fig. 10b – SAF10) and it is most approximate to the results obtained in numerical analysis in a bolt in set with inserted thread (Fig. 8a). The results presented in Fig. 8a and Fig. 8b indicate that bolt without thread achieves an earlier deformation achievement, at which the bolt achieves the maximum value of force. The value of the force in the bolt obtained in the set with the thread is smaller in relation to the value of the force in the bolt in the set without a thread and is  $F_{\text{thread}} = 273.11$  kN.

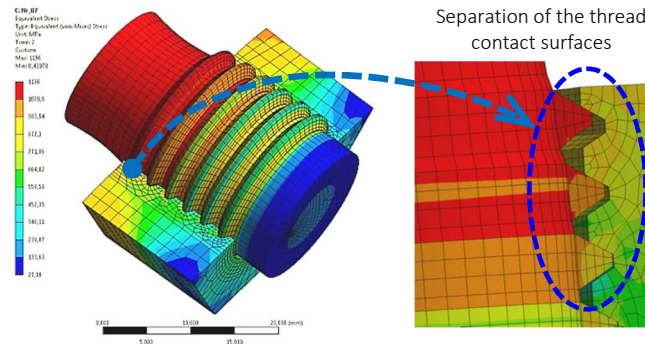


Fig. 12. Separation of the thread contact surfaces between the bolt and the nut

In the analyzed connection it was observed characteristic effect of the increase in the effective length of the thread. After reaching the plastic stress, a neck is formed in the area of the thread, which with its range reaches up to one-third the height of the nut (Fig. 12). This effect will not occur in the case of bolt modeling, in which the bolt is connected to the nut (Fig. 8b). Introduced to the FEM analysis model of the bolt with thread is dedicated to case studies where there is the need for accurate assessment of the forces distribution in the analyzed model.

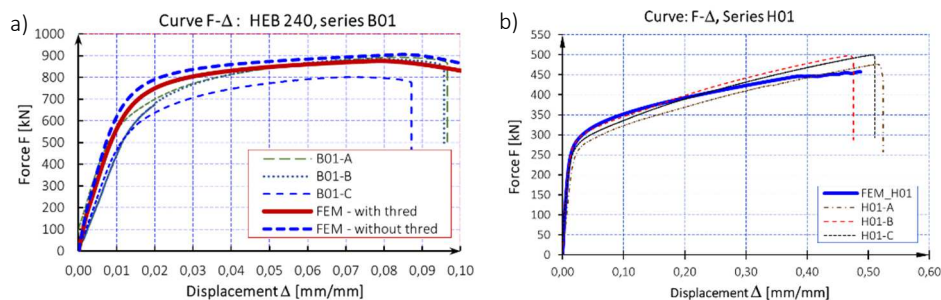


Fig. 13. The results comparison of the numerical analysis with the results of laboratory tests:  
a) Sample of series B01; b) Sample of series H01

Relationship of loading  $F$  and relative change in the distance between reference points are shown in Fig. 13.

Determination of the force distribution in the bolt in laboratory conditions of the separate structure elements testing (joints, frames etc.) is quite troublesome and possible only in a certain range of stress and strain. The available research instruments are well suited for elastic stress and leave a free, unexplored space for analysis of the force distribution in the bolt in range of plastic deformation.

The analysis of end-plate bolted connections deformations defined in the T-stub form is usually performed assuming the possibility of occurrence of three plastic hinges (two in the front panel: the first in the bolt area, the second in the connection of end-plate with the web panel, the third plastic hinge in the bolt).

In the case under study (Fig. 13b), a fourth plastic hinge is formed in the web panel. Fig. 14 shows the progress development of plastic zones for the five load phases defined in the form of displacement. In the first phase, the plastic zones have developed in the face of end-plate (Fig. 14a), in the 2nd phase the plastic zones start to develop in the region of the web panel in the bolt axis (Fig. 14b), in the next phase the plastic zones (in the bolt axis) merge into one the compact zone and this state is maintained until the end of the test (Fig. 14c, Fig. 14d, Fig. 14e).

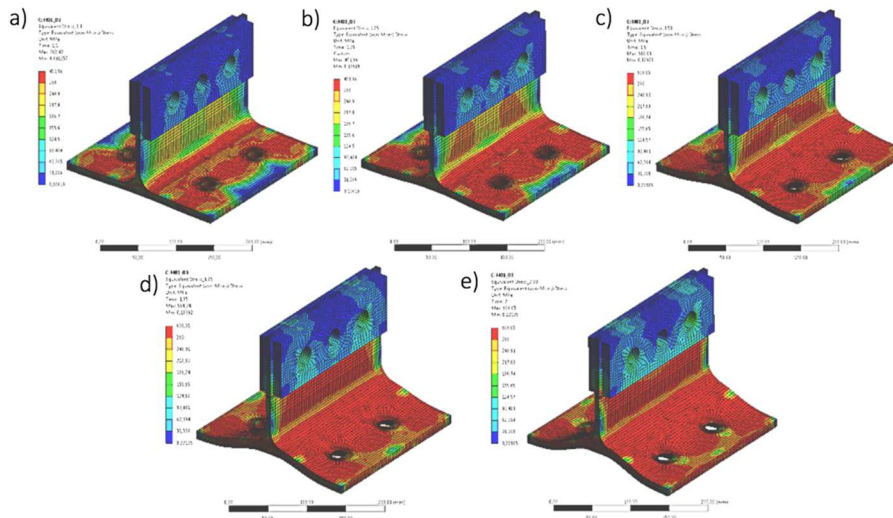


Fig. 14. Development of plastic zones: a) displacement  $\Delta = 5$  mm; b) displacement  $\Delta = 12.5$  mm; c) displacement  $\Delta = 25$  mm; d) displacement  $\Delta = 37.5$  mm; e) displacement  $\Delta = 50$  mm

This irregularity in the behaviour of the web panel is caused by the membrane effect which results from the low stiffness of the end-plate. The confirmation of this phenomenon is the distribution of von Mises stresses depicted in Fig. 15, along a path located in the bolt axis on the upper surface of the end-plate. There

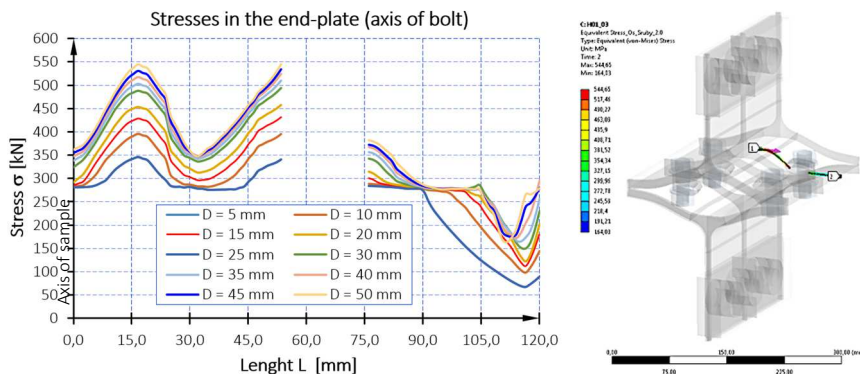


Fig. 15. Distribution of stresses in the end-plate along a path located in the axis of the bolt

was a significant decrease of stresses in relation to stress at the point of the bolt fixing and at the point where the end-plate connects to the web panel. This effect of the variable redistribution of deformations is a particular obstacle to the regular analytical description of the connection behaviour in the case where the web panel is the weakest link in the chain.

Conducting a multistage hierarchical validation is a prerequisite for obtaining reliable results of the FEM analysis of the examined objects. This is particularly important in relation to the structure and its parts subjected to large deformations. Introduction of material characteristics as a result of the process of tuning the FEM models implemented as part of the validation allows to analyze the behavior of joints subjected to significant deformations, close to the state of exhaustion of the structural capacity for load transfer.

Finite element method is an alternative approach in the predicting behavior of the T-stub type connections. Based on the results obtained in the numerical calculations, we encounter relatively large difficulties in formulating the analytical relationship describing the state of the joint's behavior, similarly in the case of laboratory tests. However, using numerical analyzes, it is much easier to obtain enough data for the behavioral assessment when statistical methods are used for this purpose.

## References

- [1] K. Ostrowski, "Experience in structures designing according to European standards," *Journal of Civil Engineering, Environment and Architecture*, vol. 58, no. 3/I, pp. 203–214, 2011.
- [2] K. Weynand, J. P. Jaspart, and M. Steenhuis, "Economy studies of steel building frames with semirigid joints," *Journal of Constructional Steel Research*, vol. 46, no. 1, p. 85, 1998/04/01 1998.
- [3] U. Kuhlmann and A. Fürch, "Rotation capacity of steel joints (second draft)," in *COST C1 – Working Group Meeting*, Helsinki, 1997.
- [4] U. Kuhlmann and A. Fürch, "Rotation capacity of steel joints," in *COST Project C1 – Working Group Meeting*, Clermont-Ferrand, 1996.
- [5] M. E. Lemonis and C. J. Gantes, "Incremental modeling of T-stub connections," *Journal of Mechanics of Materials and Structures*, vol. 1, no. 7, pp. 1135–1159, 2006. *Journal of Mechanics of Materials and Structures*.
- [6] L. Massimo, R. Gianvittorio, S. Aldina, and S. da Silva Luis, "Experimental analysis and mechanical modeling of T-stubs with four bolts per row," *Journal of Constructional Steel Research*, vol. 101, pp. 158–174, 2014.
- [7] A. M. Girão Coelho, F. S. K. Bijlaard, and L. Simões da Silva, "Experimental assessment of the ductility of extended end plate connections," *Engineering Structures*, vol. 26, pp. 1185–1206, 2004.
- [8] Y. Shi, G. Shi, and Y. Wang, "Experimental and theoretical analysis of the moment–rotation behaviour of stiffened extended end-plate connections," *Journal of Constructional Steel Research*, vol. 63, no. 9, pp. 1279–1293, 9// 2007.
- [9] G. L. Kulak, J. W. Fisher, and J. H. Struik, "Guide to Design Criteria for Bolted and Riveted Joints Second Edition," 2001.

- [10] H. Agerskov, "Analysis of bolted connections subject to prying," *Journal of the Structural Division*, pp. 2145–2163, November/January 1977.
- [11] V. Piluso, C. Faella, and G. Rizzano, "Ultimate behavior of bolted T-stubs. I: Theoretical model," *Journal of Structural Engineering*, vol. 127, no. 6, pp. 686–693, 2001.
- [12] V. Piluso, C. Faella, and G. Rizzano, "Structural Semi-Rigid Connections: Theory, Design and Software," ed: Boca Raton (USA): CRC Press, 2000.
- [13] A. M. Girão Coelho and L. Simões da Silva, "Numerical evaluation of the ductility of a bolted T-stub connection," in *Advances in Steel Structures (ICASS '02)* Oxford: Elsevier, 2002, pp. 277–284.
- [14] A. Girão Coelho, "Rotation capacity of partial strength steel joints with three-dimensional finite element approach," *Computers and Structures*, vol. 116, pp. 88–97, 2013.
- [15] K. Ostrowski and A. Kozłowski, "FEM based assessment of the rotation capacity of bolted joints," in *Recent Progress in Steel and Composite Structures: Proceedings of the XIII International Conference on Metal Structures (ICMS2016, Zielona Góra, Poland, 15-17 June 2016)*, 2016, p. 479: CRC Press.
- [16] K. Ostrowski and A. Kozłowski, "The influence of end-plate joints stiffening on the rotation capacity," *ce/papers*, vol. 1, no. 2–3, pp. 381–388, 2017. *ce/papers*.
- [17] K. Ostrowski, "Finite element analysis of the rotation capacity of beam-to-column end-plate bolted joints," ed: Eurosteel, 2014.
- [18] J.-P. Jaspart, "Etude de la semi-rigidité des noeuds poutre-colonne et son influence sur la résistance et la stabilité des ossatures en acier," Université de Liège, Belgique, 1991.
- [19] P. Zoetemeijer, "A Design Method for the Tension Side of Statically Loaded, Bolted Beam-to-Column Connections," (in en), 1974.
- [20] B. Yoke, L. Yee, and R. E. Melchers, "Moment-rotation curves for bolted connections," *Journal of Structural Engineering*, vol. 112, pp. 615–635, 1986.
- [21] *DD ENV 1993-1-1:1992, Eurocode 3: Design of steel structures – Part 1.1: General rules and rules for buildings*, 1992.
- [22] *EN 1993-1-8:2005 (E), Eurocode 3: Design of steel structures – Part 1-8: Design of joints*, 2005.
- [23] K. Ostrowski and A. Kozłowski, "Hierarchical validation of FEM models," in *XIV International Scientific Conference Rzeszów–Lwów–Koszyce*. Rzeszów, 2015.
- [24] L. E. Schwer, "Verification and validation in computational solid mechanics and the ASME Standards Committee," *WIT Transactions on the Built Environment*, vol. 84, 2005.
- [25] F. Wald, L. Gödrich, M. Kurejková, L. Šabatka, J. Kabeláč, and D. Kojala, "Validation and verification in design of structural steel connections," *ce/papers*, vol. 1, no. 2–3, pp. 143–152, 2017.
- [26] K. Ostrowski and A. Kozłowski, "Experimental study of the portal frame for the validation of FEM model of beam to column joint (in Polish)" *Czasopismo Inżynierii Łądowej, Środowiska i Architektury – Journal of Civil Engineering, Environment and Architecture*, JCEEA. T. XXXIV, Z. 64 (3/I/17), pp. 437–446, 2017, DOI:10.7862/rb.2017.136.
- [27] A. Mijar and J. Arora, "An augmented Lagrangian optimization method for contact analysis problems, 1: formulation and algorithm," *Structural and Multidisciplinary Optimization*, vol. 28, no. 2–3, pp. 99–112, 2004.

Przesłano do redakcji: 10.05.2018 r.

Przyjęto do druku: 15.06.2018 r.

## Informacje dodatkowe

1. Lista recenzentów współpracujących będzie opublikowana w czwartym numerze *Czasopisma Inżynierii Lądowej, Środowiska i Architektury*: 64(4/17) oraz na stronie internetowej:  
[www.oficyna.prz.edu.pl/pl/zeszyty-naukowe/czasopismo-inzynierii-ladowej-s/](http://www.oficyna.prz.edu.pl/pl/zeszyty-naukowe/czasopismo-inzynierii-ladowej-s/)  
(dotychczasowa nazwa: *Zeszyty Naukowe Politechniki Rzeszowskiej, Budownictwo i Inżynieria Środowiska*), strona internetowa:  
[www.oficyna.prz.edu.pl/pl/zeszyty-naukowe/budownictwo-i/](http://www.oficyna.prz.edu.pl/pl/zeszyty-naukowe/budownictwo-i/)
2. Zasady recenzowania są udostępnione na stronie internetowej:  
[www.oficyna.prz.edu.pl/zasady-recenzowania/](http://www.oficyna.prz.edu.pl/zasady-recenzowania/)
3. Informacje dla autorów artykułów są udostępnione na stronie internetowej:  
[oficyna.prz.edu.pl/informacje-dla-autorów/](http://oficyna.prz.edu.pl/informacje-dla-autorow/)
4. Formularz recenzji jest udostępniony na stronie internetowej:  
[www.oficyna.prz.edu.pl/pl/zeszyty-naukowe/czasopismo-inzynierii-ladowej-s/](http://www.oficyna.prz.edu.pl/pl/zeszyty-naukowe/czasopismo-inzynierii-ladowej-s/)
5. Instrukcja dla autorów omawiająca szczegółowo strukturę artykułu, jego układ, sposób przygotowywania materiału ilustracyjnego i piśmiennictwa jest zamieszczona na stronie internetowej:  
[www.oficyna.prz.edu.pl/pl/instrukcja-dla-autorów/](http://www.oficyna.prz.edu.pl/pl/instrukcja-dla-autorow/)  
oraz  
[www.oficyna.prz.edu.pl/pl/zeszyty-naukowe/czasopismo-inzynierii-ladowej-s/](http://www.oficyna.prz.edu.pl/pl/zeszyty-naukowe/czasopismo-inzynierii-ladowej-s/) w zakładce „Instrukcja dla autorów”
6. Dane kontaktowe do redakcji czasopisma, adresy pocztowe i e-mail do przesyłania artykułów oraz dane kontaktowe do wydawcy są podane na stronie internetowej (Komitet Redakcyjny):  
[www.oficyna.prz.edu.pl/pl/zeszyty-naukowe/czasopismo-inzynierii-ladowej-s/](http://www.oficyna.prz.edu.pl/pl/zeszyty-naukowe/czasopismo-inzynierii-ladowej-s/)

Zasady recenzowania, informacje dla autorów, formularz recenzji, instrukcja dla autorów i dane kontaktowe do redakcji czasopisma i wydawcy będą również opublikowane w czwartym numerze *Czasopisma Inżynierii Lądowej, Środowiska i Architektury*, z. 65 (4/2018).

Ark. wyd. 13,46. Ark. druk. 14,75.

Oddano do druku we wrześniu 2018 r. Wydrukowano we wrześniu 2018 r.

Zakład Poligrafii Politechniki Rzeszowskiej, al. Powstańców Warszawy 12, 35-959 Rzeszów

Zam. nr 82/18